HYDROGENOLYSIS OF SMALL PARAFFINS

OVER RUTHENIUM

HYDROGENOLYSIS OF SOME SMALL PARAFFINIC HYDROCARBONS OVER SUPPORTED RUTHENIUM

By

JOHN CHRISTOPHER KEMPLING, B.E.Sc.

A Thesis

Submitted to the Faculty of Graduate Studies

in Partial Fulfilment of the Requirements

for the Degree

Doctor of Philosophy

McMaster University

January, 1971

DOCTOR OF PHILOSOPHY (1971) McMASTER UNIVERSITY
(Chemical Engineering) Hamilton, Ontario.

TITLE: Hydrogenolysis of Some Small Paraffinic Hydrocarbons over Supported Ruthenium

AUTHOR: John Christopher Kempling, B.E.Sc. (University of Western Ontario)

SUPERVISOR: Professor R. B. Anderson

NUMBER OF PAGES: 277, xiv

SCOPE AND CONTENTS:

The hydrogenolysis reactions of a series of small paraffinic hydrocarbons (propane, n-butane, isobutane, isopentane, and neopentane) were examined using a continuous stirred-tank catalytic reactor. The catalyst was 0.5 weight percent ruthenium supported on γ-alumina.

The reaction orders with respect to hydrocarbon and hydrogen and the activation energies were determined for the reaction of each hydrocarbon. The order of reactivity was also examined.

The product distributions from each hydrocarbon were measured over a wide range of conversion (5 to 80%) and several temperatures. Reaction networks proposing reversible adsorption-desorption of the hydrocarbons and irreversible rupture of the carbon-carbon bonds in the surface species were applied to these data.

Some conclusions were made concerning the mechanism of hydrogenolysis and the rate-limiting step.

ACKNOWLEDGEMENTS

The author is deeply indebted to his research director, Professor R. B. Anderson, who proposed and guided this project. The many helpful suggestions concerning the method of analysis of the experimental data were particularly appreciated.

The author also wishes to acknowledge the contributions of his wife who was instrumental in preparing the thesis and whose encouragement over the years was greatly valued.

Many fellow students were involved in this work including Dr. J. Freel who assisted in the adsorption measurements, H. C. Chen who helped with the electron probe studies, and A. J. Orlickas who contributed much to the statistical treatment of the data.

Financial assistance provided by the National Research Council of Canada was also gratefully accepted.

TABLE OF CONTENTS

LIST OF FIGURES

LIST OF TABLES

Chapter 1

INTRODUCTION

1.1 General

The term hydrogenolysis refers to a group of catalytic reactions involving bond rupture by interaction with hydrogen. The bond types usually considered include carbon-carbon, carbon-nitrogen, carbon-oxygen, and carbon-halogen (1); the present work is limited to the breaking of carbon-carbon bonds in saturated aliphatic hydrocarbons. The hydrogenolysis of ethane (2) and of small hydrocarbon rings (3) have been reported in great detail but there have been comparatively few investigations related to the reaction of larger alkanes.

The purpose of this investigation was to determine the kinetics for hydrogenolysis of some small aliphatic hydrocarbons and to gain an insight into the nature of the mechanism by examination of both the rates of reaction and the product distributions. A series of hydrocarbons, i.e., propane, n-butane, isobutane, isopentane, and neopentane, were examined in an attempt to provide an overall picture of the hydrocracking reactions in which the experimental evidence for each compound was consistent with the data for the other compounds.

The transition metals, especially those in Group VIII of the periodic table, have commonly been used as catalysts for hydrogenolysis reactions either in the form of metal films or supported on an inert carrier. Supported metals are of interest because of their vast

commercial importance. The catalyst used in these studies was 0.5 weight percent ruthenium impregnated on γ-alumina; ruthenium is one of the most active elements for the hydrogenolysis of ethane (4).

A continuous stirred-tank catalytic reactor (5) was used because it lent itself to simple and direct analysis. The reactor had an ideal flow pattern (thoroughly mixed) and operated under steady state conditions, thereby yielding differential data, i.e., data occurring at one level of concentration and temperature. This type of data is amenable to direct analysis and does not require integration or differentiation techniques to test rate equations or reaction networks. Moreover, the reactor operated over a wide range of integral conversions; this minimized the effect of effluent analysis errors and allowed a wider range of conditions to be examined.

1.2 Hydrogenolysis of Hydrocarbons

There are several stages in the interaction of a paraffin with hydrogen over a catalytic surface. Initially, the hydrocarbon chemisorbs dissociatively (6, 7), i.e., with the loss of hydrogen atoms, to form a radical which is probably held to the surface by multipoint adsorption (8). At elevated temperatures, carbon-carbon bonds rupture in the presence of hydrogen to create smaller adsorbed fragments which can subsequently desorb with the addition of hydrogen. The hydrogen also adsorbs dissociatively to form hydrogen atoms and may compete for adsorption sites with the hydrocarbon species (9).

Catalytic hydrogenolysis of paraffins was first studied by Taylor et al.(10, 11, 12). For the reaction of ethane on nickel and

cobalt, and propane on nickel,some unusual phenomena were observed, particularly a strong inverse dependence of the reaction rate on hydrogen pressure and a large activation energy. A summary of their results appears in Table 1-1. An examination of deuterium exchange reactions over the same catalysts revealed that methane, ethane, and propane exchange their hydrogen at temperatures much lower than those required to break the carbon-carbon bonds. These workers concluded that the adsorption-desorption reactions are much faster than the surface cracking reaction and that the latter reaction is therefore the rate-limiting step. Reversible poisoning of the catalyst by carbon deposition was also noted for hydrogen to hydrocarbon ratios less than 1:1.

Further experimentation at a later date by Kemball and Taylor (13) gave slightly different results when an excess of hydrogen was used for cracking ethane over nickel. With hydrogen to ethane molar ratios between 1 and 8, the hydrogen and ethane orders were -1.2 and 0.7, respectively, and the activation energy was 52 kcal. per mole. More recent studies by Shephard (14), and Anderson and Avery (15) have confirmed this change in activation energy. For propane hydrogenolysis over nickel, the activation energy increased from 41 to 50 kcal. per mole with an increase in hydrogen pressure and for butane cracking over palladium, the change was from 13 to 38 kcal. per mole.

The first mechanistic interpretation of this reaction appeared in a paper by Cimino, Boudart, and Taylor (16). According to their analysis, the initial step involves the dissociative adsorption of the hydrocarbon to form an unsaturated surface species.

TABLE 1-1

Hydrogenolysis Data, Taylor et al. (1936-39)

Hydrocarbon	Catalyst	Temp. (°C)	E	M	N	Reference
Ethane	Nickel	165	43	-	-2.5	10
Ethane	Cobalt	250	30	-	-1	12
Propane	Nickel	155	34	0.9	-2.6	11

E: activation energy (kcal. per mole)

M: reaction order with respect to hydrocarbon

N: reaction order with respect to hydrogen

$$C_nH_{2n+2} \longrightarrow C_nH_x^* + aH_2 \qquad (1\text{-}1)$$

In this case, $C_nH_x^*$ represents the adsorbed radical and "a" is equal to $(2n + 2 - x)/2$. The surface species interacts with hydrogen, resulting in the rupture of a carbon-carbon bond.

$$H_2 + C_nH_x^* \longrightarrow C_{n-m}H_y^* + C_mH_z^* \qquad (1\text{-}2)$$

The resultant adsorbed fragments combine with hydrogen to form saturated products. Since the exchange of hydrocarbons with deuterium usually occurs at temperatures much lower than those required for hydrogenolysis (17, 18), Reaction 1-2 is the rate-limiting step; Reaction 1-1 can therefore be assumed to be at equilibrium.

If the adsorption equilibrium is described by a Langmuir expression (19), the fraction of the surface covered by $C_nH_x^*$ will be

$$\theta = \frac{K(P_c/P_H^a)}{1 + K(P_c/P_H^a)} \qquad (1\text{-}3)$$

where: θ - fractional surface coverage

K - equilibrium constant

P_c, P_H - partial pressure of hydrocarbon and hydrogen

Because the reaction is limited by the interaction of the adsorbed hydrocarbon with hydrogen, the overall rate is given by the expression:

$$R = k'P_H\theta \qquad (1\text{-}4)$$

where: R - overall rate of hydrogenolysis

k' - rate constant

Over a restricted range of pressures, Equation 1-3 can be approximated by

$$\theta \propto K^n (P_c / P_H^a)^n \qquad (1\text{-}5)$$

where "n" has some value between zero and unity. By substituting this expression in Equation 1-4, the overall rate equation becomes

$$R = k\, P_c^n\, P_H^{1-na} \qquad (1\text{-}6)$$

This final equation indicates that the hydrogen order is negative when the product "na" is greater than unity. This is often the case because the adsorbed hydrocarbon is highly unsaturated ($a > 1$) but relatively weakly adsorbed ($n \simeq 1$). The calculation of "a" from the experimental values of the hydrogen and hydrocarbon exponents reveals the degree of unsaturation of the adsorbed hydrocarbon. For the reaction of ethane over ruthenium (4), the calculated value of "a" is 3, i.e., the surface radical is acetylenic in nature.

This mechanism has been criticised because it does not allow for the competitive adsorption of hydrogen (9) or the reaction products (14). However, the inclusion of these effects would not greatly alter the development of the equations or the conclusions drawn from them (20) and despite these deficiencies, the mechanism has been widely used because of its ability to explain the strong inhibitory effect of hydrogen on the reaction rate.

In cases where the adsorption-desorption reactions are not in equilibrium, the derived rate equation will not apply; this has been

claimed for ethane hydrogenolysis over cobalt (21) and iron (22). Application of Equation 1-6 to data for the reaction over cobalt produces a hydrogen exponent varying from -1 to 0 with increasing temperature and over iron the hydrogen order is positive. Deuterium exchange reactions demonstrate that dissociative adsorption is slow over these metals. With cobalt, the formation of deuteroethanes occurs simultaneously with hydrogenolysis and with iron the exchange reaction is not observed even at temperatures where hydrogenolysis occurs readily (17). The desorption of methane may also be the rate-limiting step, as reported for the hydrocracking of ethane over nickel at low pressures (6,8).

The study of hydrogenolysis reactions has been principally concerned with the cracking of ethane over various metal catalysts. Sinfelt et al. have examined all of the metals in Group VIII and also copper and rhenium supported on silica (22, 23, 24, 4, 25). Table 1-2 is a summary of their kinetic parameters, including the activation energy, the experimental order with respect to hydrogen and ethane, the calculated degree of unsaturation of the adsorbed hydrocarbon, and an approximate specific activity (based on a platinum activity of unity) for reaction at 205°C, and hydrogen and ethane partial pressures of 0.2 and 0.03 atm., respectively. The catalytic properties of these elements are a function of their position within the periodic table, as is demonstrated by Figure 1-1 (2). Proceeding across a period in the direction of decreasing atomic number the hydrogen exponent becomes less negative, and the ethane exponent and activation energy decrease. The behavior of copper is significantly different from the other elements.

TABLE 1-2

Hydrogenolysis of Ethane on Group VIII Metals

All catalysts were 10% metal supported on silica.

$$r = Ae^{-\frac{E}{RT}} P_H^N P_E^M$$

Metal	Temp. (°C)	E	M	N	a	Standard Activity	Ref.
Iron	270	—	0.6	0.5	1	10^4	22
Cobalt	219	30	1.0	-0.8	2	5×10^4	23
Nickel	177	41	1.0	-2.4	3	10^6	24
Copper	330	21	1.0	-0.4	1	10^3	24
Ruthenium	188	32	0.8	-1.3	3	5×10^6	4
Rhodium	214	42	0.8	-2.2	3	10^5	4
Palladium	354	58	0.9	-2.5	3	1	4
Rhenium	250	31	0.5	0.3	1	10^5	25
Osmium	152	35	0.6	-1.2	3	10^8	22
Iridium	210	36	0.7	-1.6	3	10^5	4
Platinum	360	54	0.9	-2.5	3	1	24

E: activation energy (kcal. per mole)

M: ethane order

N: hydrogen order

a: calculated number of hydrogen molecules lost on adsorption of hydrocarbon (Equation 1-6)

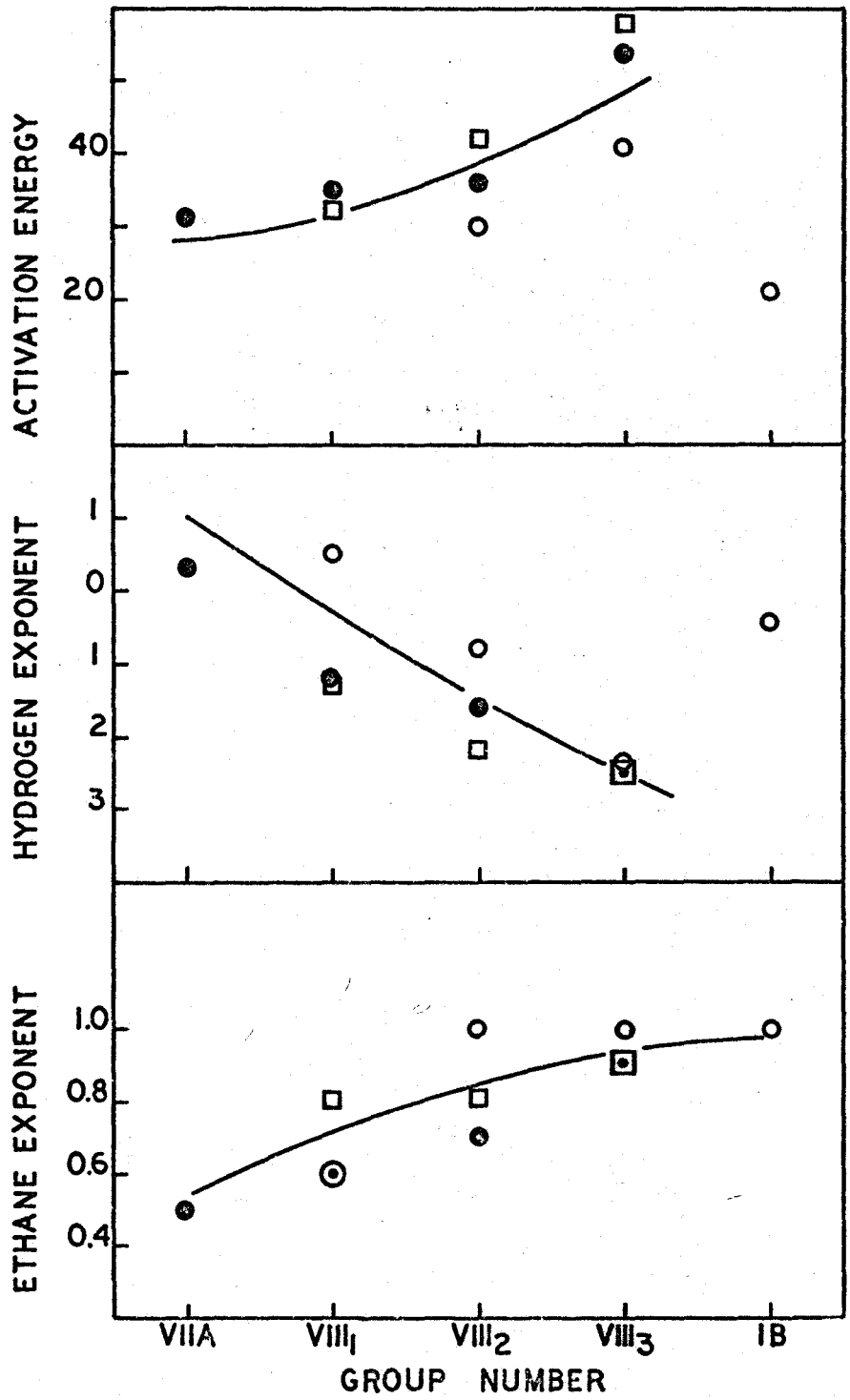

Figure 1-1: Periodic Variation of Kinetic Parameters for Ethane Hydrogenolysis

○ 1st transition period, □ 2nd transition period, ◉ 3rd transition period

Sinfelt related the catalytic activity to the percentage d-character of the metallic bond (2), which is a measure of the strength of the bond. There is a close parallel between change in catalytic activity and in percentage d-character from one metal to another.

An increase in activation energy has been observed to occur in conjunction with an increase in the degree of unsaturation of the adsorbed species (20). This was interpreted by proposing that the adsorption of the hydrocarbon is endothermic and that the degree of endothermicity increases with unsaturation.

Ethane hydrogenolysis has also been used to examine the effects of the support material and the state of metal dispersion on the catalytic properties of the metal. The effect of the carrier has been determined using nickel (26), platinum (27), and cobalt (23) supported on silica, alumina, silica-alumina, and carbon. Metals supported on silica and alumina had approximately equal activities but on silica-alumina and carbon the activities were lower by a factor of fifty. With nickel supported on silica and silica-alumina an increase in specific activity was observed as the metal concentration increased from 1 to 10% (28). But for a series of rhodium-silica catalysts (0.1 to 100% rhodium), a maximum specific activity was noted for crystallite sizes about 10 to 50 Å (29). Catalysts with 10% nickel showed constant specific activity when the surface area was increased from 4 to 14 square meters per gram by preheating in air (30); however, when the crystallite size was varied by sintering at various temperatures (370 - 700°C) in flowing hydrogen, the specific activity decreased by a factor of twenty (31).

More recently, the hydrogenolysis of ethane was examined with a "Carberry" reactor similar to the one used in this experimental study. For the reaction over nickel, the hydrogen and ethane orders were -2 and 1 and the activation energy was 46 kcal. per mole (32). Over ruthenium supported on alumina, the reaction was first order in ethane, -2 order in hydrogen, and had an activation energy of 42 kcal. per mole (33). These results are similar to those previously reported using a differential reactor (4, 28).

Supported nickel (14, 11) and ruthenium (33), and nickel, rhodium, and platinum films (6) have been used as catalysts for propane hydrogenolysis. Over films at low pressures (50 torr), the products are nearly equal amounts of methane and ethane. The kinetic parameters for the reaction of propane over supported metals are summarized in Table 1-3. The orders with respect to hydrogen and the hydrocarbon are similar to those for ethane cracking, thereby suggesting a common intermediate. Over supported nickel catalysts, the following two overall reactions are operative (14):

$$C_3H_8 + H_2 \longrightarrow CH_4 + C_2H_6 \qquad (1\text{-}7)$$

$$C_3H_8 + 2H_2 \longrightarrow 3CH_4 \qquad (1\text{-}8)$$

For Reaction 1-8 to occur, both carbon-carbon bonds must break. The fraction of propane reacting via Reaction 1-8 increases from 0.3 at 200°C to 0.9 at 300°C; a lower concentration of hydrogen also favours this reaction.

Few papers have reported the hydrogenolysis of alkanes larger than propane. Anderson and Baker (6) studied the product distribution

TABLE 1-3

Kinetics of Propane Hydrogenolysis

Metal	Support	Activation Energy (kcal./mole)	Propane Order	Hydrogen Order	% Methane Produced	Reference
Ni	Kieselguhr	34	0.9	-2.6	60	11
Ni	Al_2O_3	50	1	-2	variable	14
Ru	Al_2O_3	36	1.0	-1.5	52	33

from the hydrogenolysis of n-butane, isobutane, neopentane, and neohexane. Over nickel, methane is formed extensively with only small amounts of products with higher carbon number; over rhodium and platinum, the production of methane is less dominant. In general, they observed that the rate of cracking increases with increasing number of carbons in the hydrocarbon.

The reaction of ethane, n-butane, isobutane, isopentane, and neopentane have been investigated over platinum and palladium (15). The ethane hydrogenolysis rate is markedly lower than the other hydrocarbons and has a correspondingly high activation energy. Over palladium, isomerization of the butanes and pentanes accounts for only 3% of the reaction but over platinum, isomerization is substantial (up to 50%). Because the activation energy for the isomerization and hydrogenolysis reactions are identical over platinum, a common intermediate is likely (34). The initial distribution of cracking products from all these hydrocarbons is consistent with the rupture of only one carbon-carbon bond during the residence of a molecule on the surface and the product distributions are also independent of temperature and hydrogen to hydrocarbon ratio.

For the reaction of neopentane (35), simultaneous isomerization occurs over platinum, gold, and iridium and in each of these cases the activation energy for hydrogenolysis and isomerization are nearly equal. Over ruthenium, the hydrogenolysis reaction occurs readily with an activation energy of 36 kcal. per mole.

The hydrogenolysis of n-pentane on nickel catalysts for pressures up to 50 atm. yields product distributions which change widely with hydrogen pressure and reaction temperature (36). At lower hydrogen pressures and higher temperatures, methane is formed as a predominant product but with higher pressures and lower temperatures equal amounts of n-butane and methane are produced. However, all of these product distribution results are consistent with the rupture of only terminal carbon-carbon bonds in the chain.

1.3 The Reactor

In any experimental study of chemical kinetics, it is necessary to insure that the information acquired accurately represents the selectivity and activity of the catalyst. Complications due to mass and heat transfer limitations should be minimized by designing for the virtual elimination of all concentration and temperature gradients. Large gas velocities, small catalyst particles, and low reaction rates can be used to obtain adequate physical transport rates.

The catalyst bed should be isothermal because reaction rates are strongly dependent on temperature in a nonlinear manner and an attempt to account for temperature gradients can lead to large uncertainties. A well-characterized flow pattern is also necessary in order to relate the experimental measurements to reaction rate. The more easily handled flow types are plug flow (fixed-bed reactor) and perfectly mixed (static or continuous flow stirred-tank reactor). The equations for determining reaction rates from these systems can be derived from a simple mass balance around the reactor (37).

There are also concentration and temperature gradients associated with the catalyst particles. The flow of fluid past a pellet sets up a thin boundary layer in which the transport mechanism varies from molecular diffusion near the surface to turbulent mixing in the free stream. The interparticle transport rate across this film is related to the Reynolds number of the flowing fluid and can be increased by increasing the flow rate. For reaction within a porous medium, intraparticle transfer (diffusion through the pores) is also important. This process is usually described in terms of the Thiele modulus and an effectiveness factor (38). To insure negligible concentration and temperature gradients in the vicinity of the particle, i.e., a surface concentration and temperature equal to those in the bulk phase, interparticle and intraparticle transfer rates must be rapid compared to the reaction rate and heat generation rate.

There are many different types of small experimental reactors including both static and flow, integral and differential reactors (37). Carberry stated that "the ideal reactor is one which operates isothermally over a wide range of conversions in the steady state with respect to the catalyst and reactants under clearly defined residence time conditions while facilitating direct rate law determinations" (5). The continuous perfectly stirred-tank catalytic reactor (5, 39, 40, 33, 32, 41), exhibits many of these advantages. A schematic diagram of this type of reactor is located in Figure 1-2. The catalyst is placed in an assembly attached to a stirrer and rotated rapidly through the fluid, thereby producing perfect mixing in the bulk phase and enhancing the

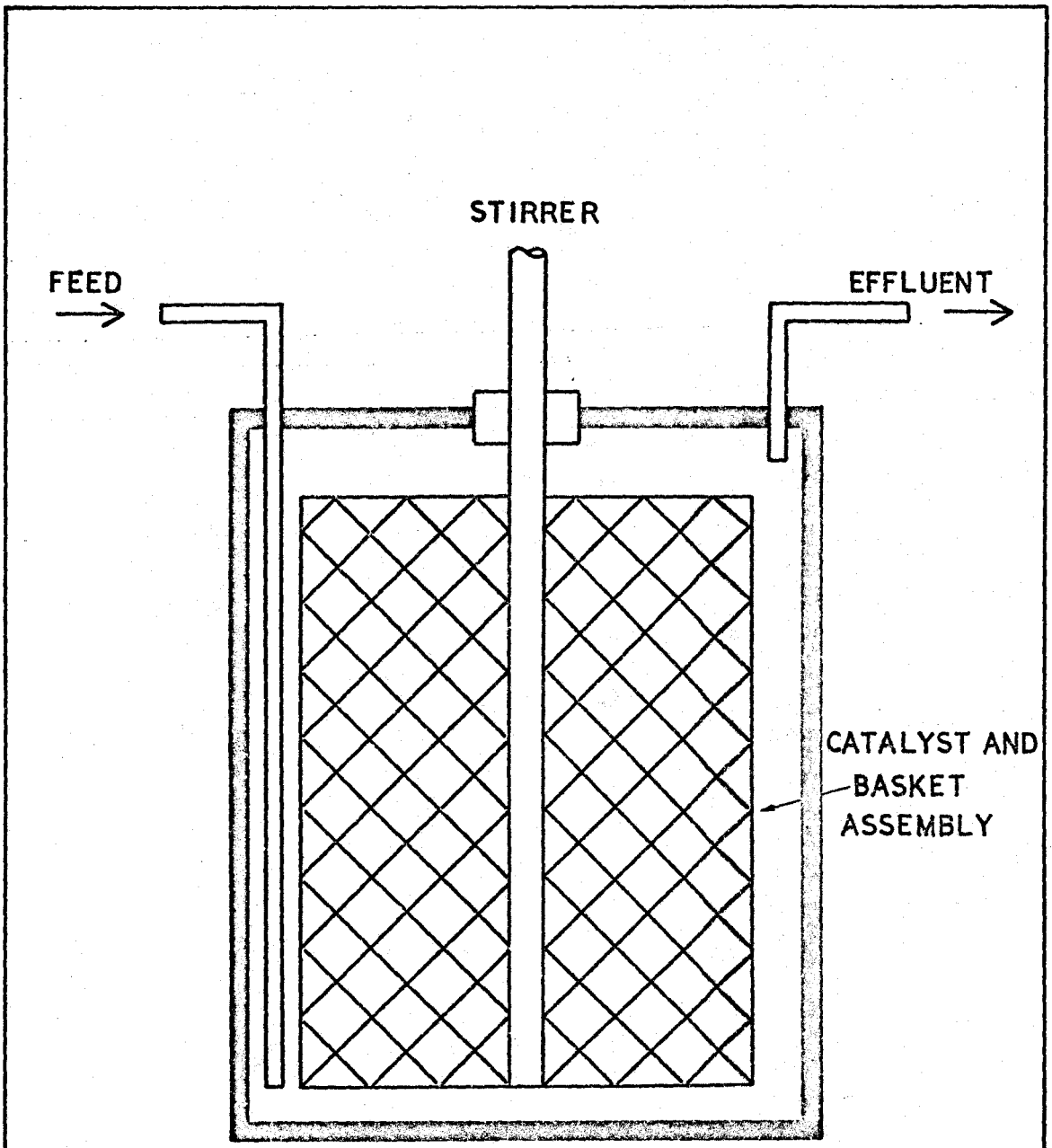

Figure 1-2: Carberry Reactor

interparticle mass and heat transfer rates. The reactants flow continuously through the reactor and the reactor contents attain a steady state composition after a number of residence times at one feed condition. Large conversion levels can be tolerated in this unit and since finite conversions are involved effluent analysis errors are minimized.

The data acquired from this type of reactor are differential in nature - they occur at one level of concentration and temperature. For each experiment one value of reaction rate and product distribution are obtained corresponding to the reactor conditions. The rate of reaction can be determined from the effluent flow rate and concentration according to the following equation:

$$r_i = \frac{X_i Q_i}{W} \qquad (1\text{-}9)$$

where: r - reaction rate

X - fractional conversion of reactant

Q - molar feed rate of reactant

W - weight of catalyst

Empirical or theoretically derived rate equations can be examined by direct application of these data.

The Carberry reactor has a number of undesirable features. The large void volume makes it unattractive for studies in which homogeneous reaction rates are appreciable. Because the effluent concentration cannot easily be set at any predetermined level, operation is difficult in cases where catalyst deactivation is rapid or for experimental programs in

which exact replicate experiments are necessary. There are also many operational problems associated with this system including construction of effective agitator seals to prevent leakage and bearings which will run at high speeds over a long period of time without contaminating the catalyst.

The continuous stirred-tank catalytic reactor has been employed for kinetic studies. Data reported for the oxidation of carbon monoxide on supported palladium are consistent with previous results on evaporated films and wires (39). Also, observations for the hydrocracking of ethane on nickel (32), and ethane and propane on ruthenium (33) are similar to those reported for supported metals in a differential reactor (4, 28). These studies demonstrate the ability of this type of reactor to produce accurate kinetic data.

1.4 Analysis of Reaction Networks

The analysis of reaction networks by fitting data to rate equations is essential for both the elucidation of mechanisms, and the optimal design and operation of chemical reactors. Because the present understanding of heterogeneous reactions precludes a complete description of the mechanism, it is necessary to resort to an approximation of the process which often involves many assumptions concerning the nature of the surface and the adsorbed species. The equations, or mathematical models, generally used can be separated into two broad classifications. First, there are power-function models, which are similar to

$$r = k P_A^a P_B^b \qquad (1\text{-}10)$$

and second, there are Hougen-Watson models possessing a general functional form

$$r = \frac{k P_A P_B}{(1 + K_A P_A + K_B P_B)^n} \qquad (1\text{-}11)$$

The first type of equation is more empirical, although it could result from the simplification of a more complex equation with mechanistic significance (see Equations 1-3 and 1-6). This equation directly utilizes the concept of reaction order. The second type of equation is usually derived from a specific reaction mechanism, assuming the existence of a single rate-determining step such as adsorption, surface reaction, or desorption.

In most applications, the analysis should proceed as far towards the theoretical extreme as the experimental data permit. This approach affords some insight into the reaction mechanism and aids in making extrapolations outside the experimental region more reliable (42). However, within the criteria of adequate data representation, an attempt should be made to select a model with the minimum number of parameters. Kinetic data for heterogeneous systems often contain so much error that the use of mathematical forms more complicated than Equation 1-10 is unwarranted. It has also been asserted that, due to the theoretical inadequacies of the Langmuir adsorption isotherm, the Hougen-Watson type of equation is valid only in a qualitative manner (43), and that much of the observed fitting of data can be explained by the great flexibility of the equations arising from the abundance of parameters. Despite these limitations, this type of mechanistic equation is used because

it often leads to some understanding of the reaction mechanism and catalyst behavior (44, 45).

The problem of examining rate equations can be divided into three sections, (a) the identification of the best model, (b) the estimation of the parameters (rate constants, activation energy, etc.) in a model, and (c) the interpretation of the parameters with respect to the reaction mechanism. The first of these involves some type of discrimination technique while the second usually includes linear or nonlinear regression analysis. These statistical methods have been described numerous times in the literature (46, 47, 48, 49, 50, 42) and the pertinent procedures are considered in detail in Appendix B.

Obviously inadequate models can be eliminated by plotting the reaction rate data against the corresponding independent variables such as composition. The data are then fitted to the remaining equations by some test such as a minimum sum of squares between the predicted and observed rates. The criteria for model rejection are (a) a lack of fit as evidenced by an excessively large residual mean square or correlation of the error with a dependent or independent variable and (b) unacceptable characteristics of the estimated parameters such as negative rate constants or adsorption coefficients. Very frequently, more than one equation is plausible. The reaction mechanism is only unambiguously proven when all other possible mechanisms have been rejected due to some incompatibility with the experimental observations. Since no investigation can examine all possibilities, the investigator is usually satisfied with an adequate representation of the data over the experimental range considered.

The estimation of the best parameter values for any particular model is essentially a determination of the values which minimize some appropriate measure of the error between the observed and predicted variable. In the least-squares approach, the sum of squares of the errors is minimized. For linear equations, a general theory has been developed and by means of a single matrix inversion it is possible to solve for the best parameter estimates (46). Unfortunately, few kinetic models occur in the linear form and the parameter values must then be estimated by some numerical technique such as direct-search methods (47). Both linear and nonlinear methods have been used in this study.

Chapter 2

EXAMINATION OF THE CATALYST

2.1 Introduction

The physical properties of a catalyst are important in determining its chemical activity and usefulness for both laboratory and industrial applications. The following sections are a summary of the investigations completed to describe the catalyst itself.

The catalyst was a commercial preparation (courtesy of Engelhard Industries, Inc.) consisting of a nominal 0.5 weight percent ruthenium impregnated on γ-alumina. This catalyst was in the form of 3.2- by 3.2-mm. cylindrical pellets with the ruthenium impregnated only on the outer shell of the pellet. The outer shell appeared dark black while the inner section of the pellet was white and by optical examination the thickness of the dark layer was estimated to be approximately 0.2 mm.

2.2 Adsorption Studies

2.2.1 General

A conventional glass vacuum system (37) was used to measure adsorption isotherms by standard volumetric techniques. The Pyrex sample cell was fitted with two stopcocks to permit the flow of hydrogen over the sample during reductions. The catalyst sample was evacuated at room temperature for one hour, then reduced in flowing hydrogen at 350°C and atmospheric pressure for twelve hours (the same conditions as were used for reducing catalyst for kinetic experiments), evacuated at 350°C for

one hour, and cooled to room temperature.

2.2.2 Nitrogen Adsorption

A nitrogen adsorption isotherm was determined at 77°K over a range of relative pressures from 0.1 to 1.0. The data were taken in two stages due to the high pore volume, first a lower range ($0.1 < p/p_o < 0.45$) for the BET calculations and then the upper range to determine the pore volume. The data appear in Table 2-1 and Figure 2-1. The resultant Type II (51) isotherm is similar to those reported by De Boer and Lippens (52) for microcrystalline boehmite.

The BET equation (53) was used to determine the surface area by examining the data between 0.1 and 0.3 relative pressure.

$$\frac{x}{V(1-x)} = \frac{1}{V_m C} + \frac{(C-1)}{V_m C} x \qquad (2\text{-}1)$$

where: x - relative pressure

V - volume adsorbed

V_m - volume corresponding to a monolayer

C - constant

A plot of the group of variables, $x/V(1-x)$, against the relative pressure is linear as shown in Figure 2-2. The monolayer volume was estimated to be 20.1 cc. (STP) per gram. If the density of the physically adsorbed layer is equal to that of the liquid phase, each molecule of adsorbate will cover 16.3 square angstroms of surface (54). The corresponding specific surface area was therefore 87.8 square meters per gram of catalyst.

TABLE 2-1

Nitrogen Isotherm

Adsorption		Desorption	
Volume $\left[\frac{\text{cc. (STP)}}{\text{g. catalyst}}\right]$	Relative Pressure	Volume $\left[\frac{\text{cc. (STP)}}{\text{g. catalyst}}\right]$	Relative Pressure
20.0	0.102	20.0	0.102
20.9	0.111	22.5	0.156
21.2	0.119	23.6	0.182
21.4	0.125	24.2	0.205
24.9	0.223	24.9	0.223
25.3	0.237	25.4	0.236
28.5	0.308	28.7	0.306
29.6	0.356	29.9	0.355
32.8	0.452	33.9	0.456
34.1	0.456	45.4	0.523
35.1	0.473	67.0	0.691
40.2	0.563	85.0	0.748
43.0	0.599	90.9	0.771
42.8	0.601	115.3	0.817
46.5	0.637	128.0	0.851
50.8	0.676	151.5	0.964
56.0	0.720		
76.1	0.789		
105.9	0.857		
119.8	0.885		
151.4	0.967		
158.9	0.987		
190.7	1.00		

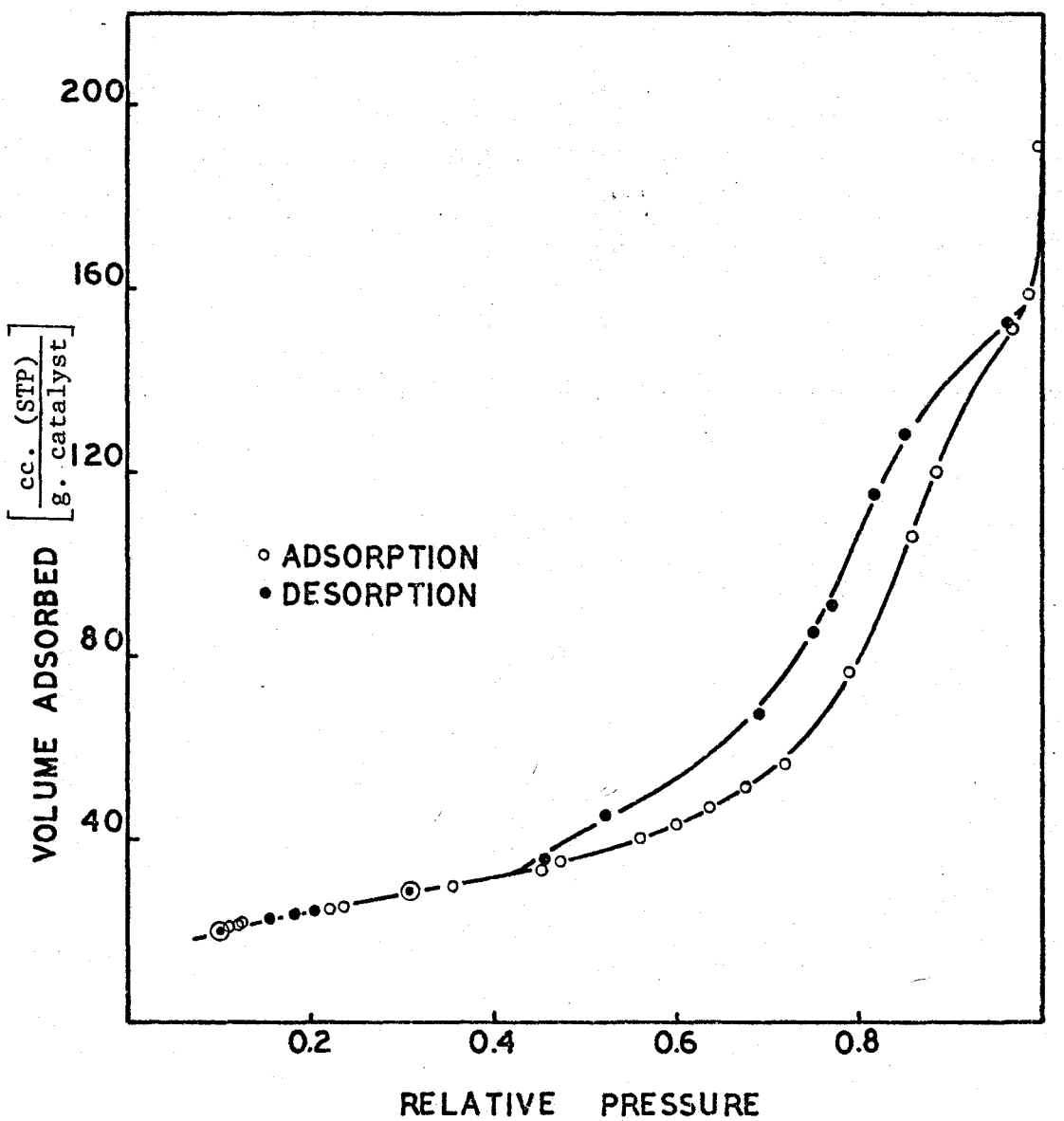

Figure 2-1: Nitrogen Isotherm

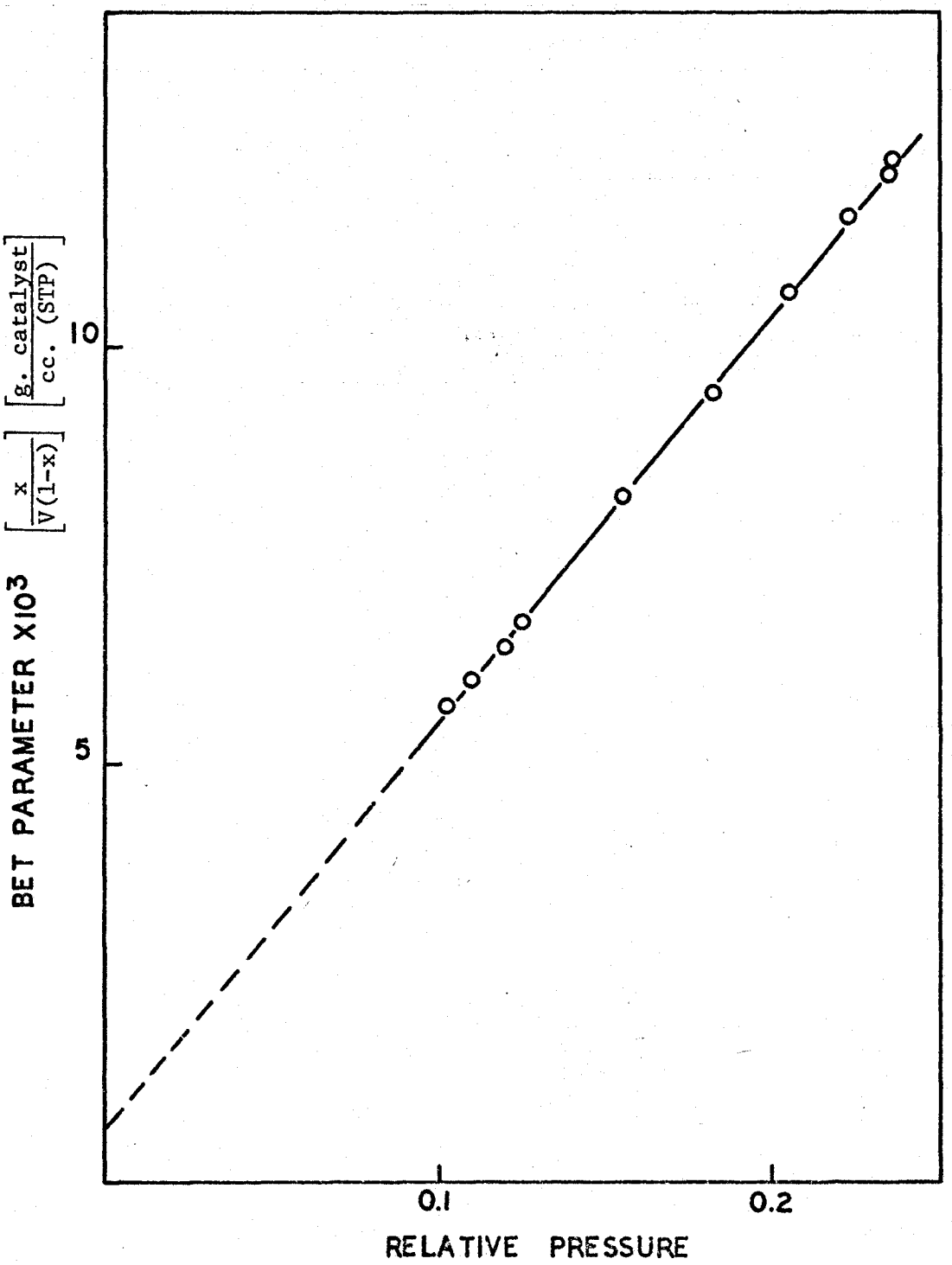

Figure 2-2: BET Plot for Ruthenium on Alumina

The total amount adsorbed at saturation (relative pressure of unity) was approximately 180 cc. (STP) per gram. From this, the pore volume of the catalyst was calculated to be 0.27 cc. per gram and the corresponding pellet porosity was 0.5. An average pore radius can be determined from the following equation (55):

$$\bar{r} = 2Vp/S \qquad (2\text{-}2)$$

where: $\bar{r}$ - average pore radius

Vp - pore volume

S - surface area

This equation assumes that the pores are cylindrical and uniform (37). The average pore radius was 60 Å.

Lippens and De Boer suggested an alternate method of examining physical adsorption data (56). By plotting the volume adsorbed as a function of the thickness of the adsorbed layer, as determined from a universal isotherm, a straight line is obtained as long as the multilayer is formed unhindered. This line must pass through the origin and its slope is a measure of the surface area according to the following equation:

$$S_t = 15.47\ V/t \qquad (2\text{-}3)$$

where: S_t - surface area

V - volume adsorbed

t - thickness of adsorbed layer

At higher relative pressures, deviations occur. Capillary condensation causes the slope of the plot to increase due to increased adsorption but

eventually the surface area in the pores is no longer accessible and the slope decreases.

The volume adsorbed was obtained as a function of relative pressure but with the aid of a correlation between the film thickness and relative pressure (57), this was transformed to a function of the thickness of the adsorbed layer (Figure 2-3). The area calculated using the linear section of the curve was 84.2 square meters per gram (within 5% of the BET value). Capillary condensation commenced at approximately the same place as hysteresis (a relative pressure of 0.4 or a film thickness of 6 Å).

Pore distributions can be calculated from the adsorption isotherm (58, 59) assuming that pore condensation occurs due to surface tension effects similar to those in the liquid phase, i.e., the Kelvin equation may be applied to the meniscus of the gas-adsorbed layer interface (55). These calculations were performed using a computer program developed by Shaw (60) which assumes cylindrical pores and uses the film thickness and condensation data of De Boer (59). The frequency distribution for pore radius appears in Figure 2-4 and the results from adsorption and desorption data were in good agreement showing maxima at about 50 Å.

The calculations also yielded cumulative estimates of the surface area and pore volume (61) and these compared favourably (Table 2-2) with the values previously determined using other methods. This is a good check of the validity of the pore distribution calculation procedure.

Table 2-2 summarizes the information obtained from the nitrogen adsorption isotherm.

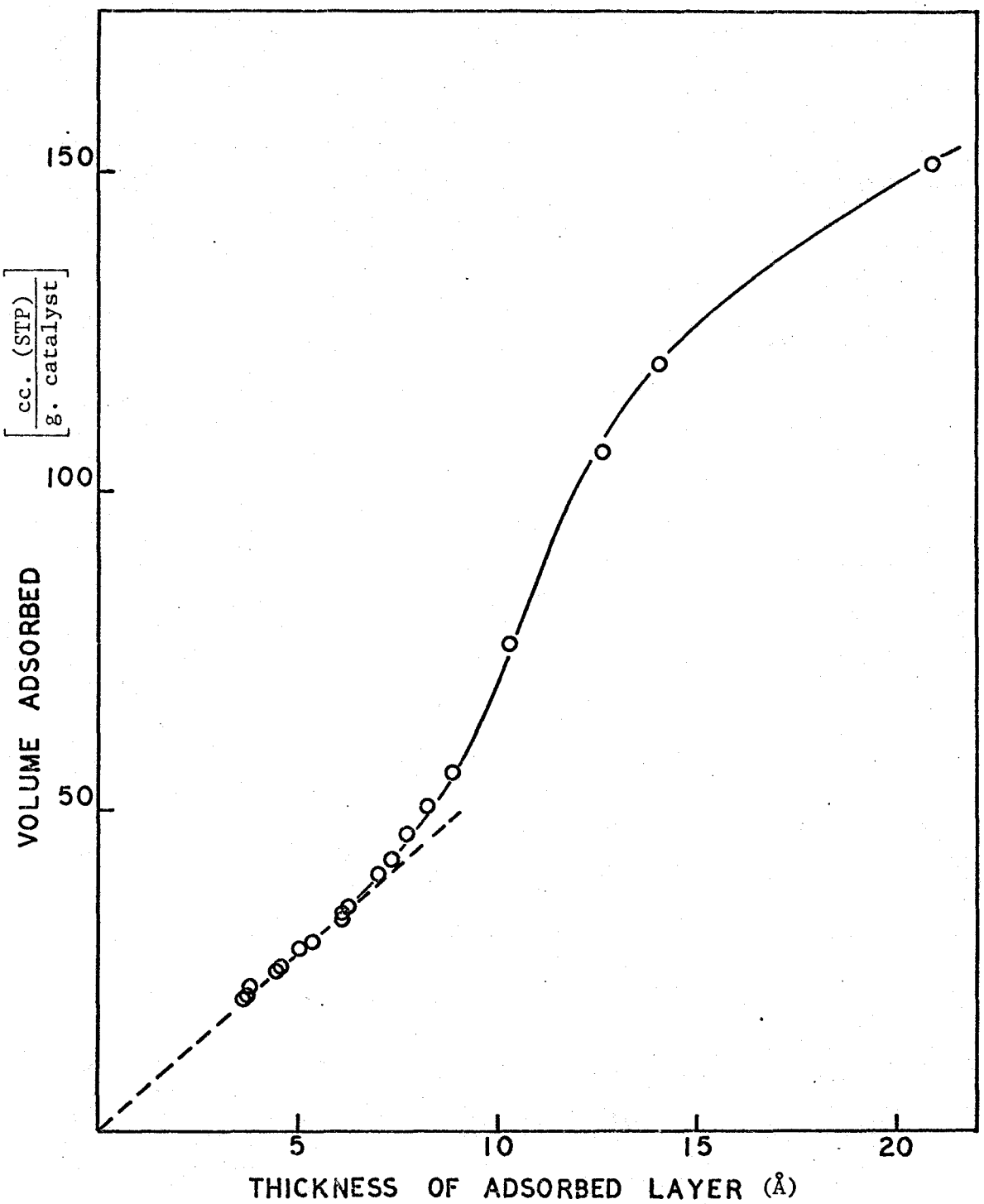

Figure 2-3: Volume Adsorbed versus Thickness of the Adsorbed Layer (Adsorption Data)

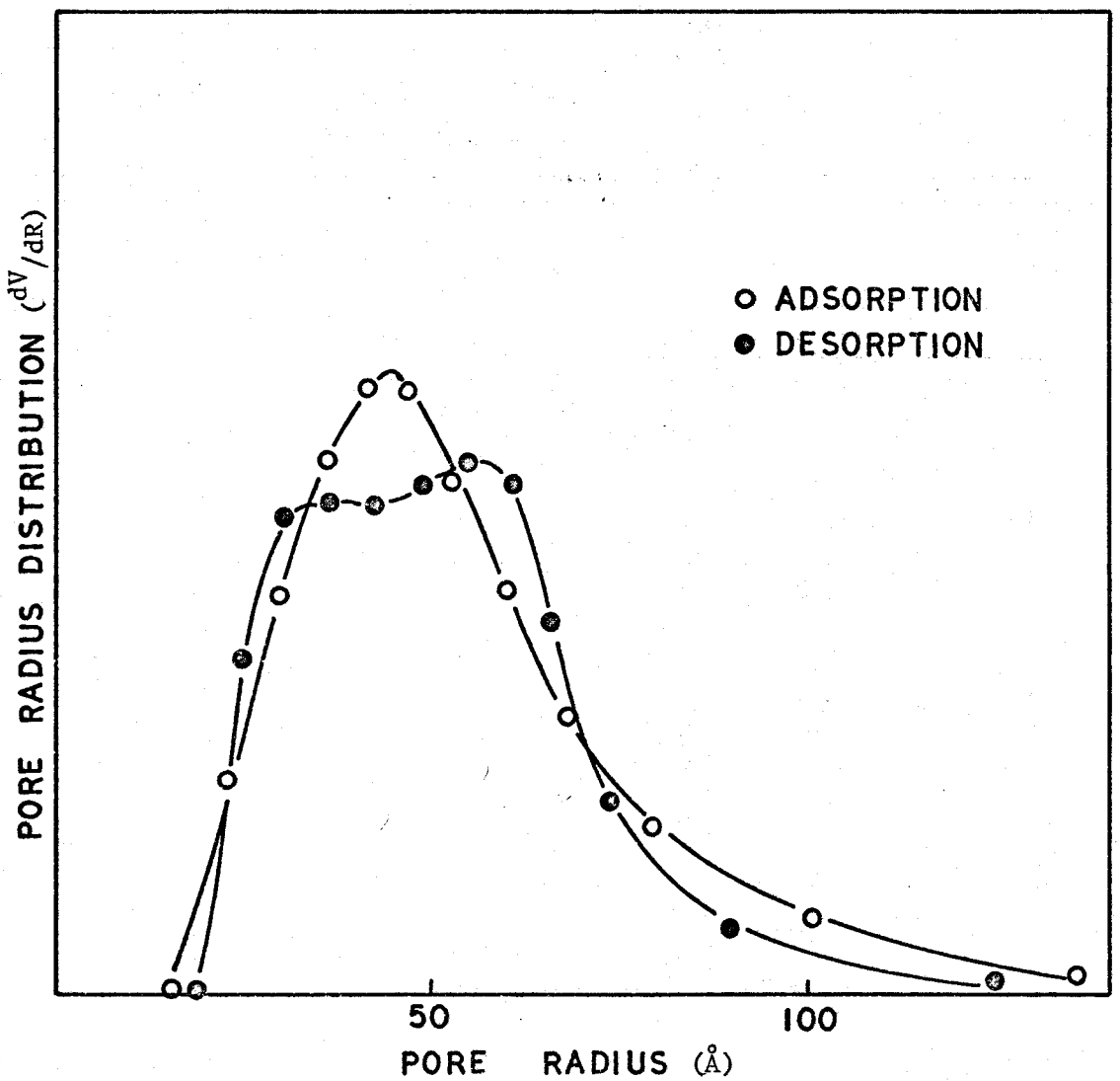

Figure 2-4: Pore Size Distribution

TABLE 2-2

Summary of Catalyst Properties Determined from Nitrogen Adsorption Isotherm

Calculation Method	Surface Area (m^2/g.)	Pore Volume (cc. (STP)/g.)	"Average" Pore Radius (Å)
Saturation (x=1)	-	180	-
BET Method	87.8	-	-
Equation 2-2	-	-	60
Universal Thickness Isotherm	84.2	-	-
Pore Distribution			
(i) Adsorption	92.5	175	50
(ii) Desorption	97.7	175	50

2.2.3 Surface Area of Ruthenium Metal

The surface area of supported metals can be estimated from the chemisorption of a gas, such as hydrogen, which selectively adsorbs on the metal but not on the support (4, 62, 63). However, when the metal concentration is very small, a significant amount of the adsorbate may become weakly associated with the support (29). In this case, two consecutive adsorption experiments can be performed separated by a brief evacuation period; the difference between the two isotherms is the amount which is chemisorbed (62). It is reasonable to expect that hydrogen chemisorbs dissociatively on ruthenium with one hydrogen atom adsorbed per surface metal atom and therefore the number of surface atoms is directly related to the volume chemisorbed at saturation. Sinfelt and Yates (4) estimated 7.6 square angstroms for the area occupied by one surface metal atom.

Two hydrogen adsorption experiments were performed at 20°C and pressures up to 200 torr. The time required for equilibration at one pressure was about 45 minutes. The sample was evacuated at 20°C for one-half hour between the two experiments and a good vacuum was obtained.

The isotherms appear in Figure 2-5. The observed monolayer volume was 0.20 cc. (STP) per gram catalyst. The corresponding ruthenium surface area was 0.82 square meters per gram of catalyst or approximately 160 square meters per gram of ruthenium. These values are similar to those reported for finely dispersed rhodium metal on silica (29). The average crystallite size was calculated assuming cubic crystallites of length 1, using the geometrical relationship:

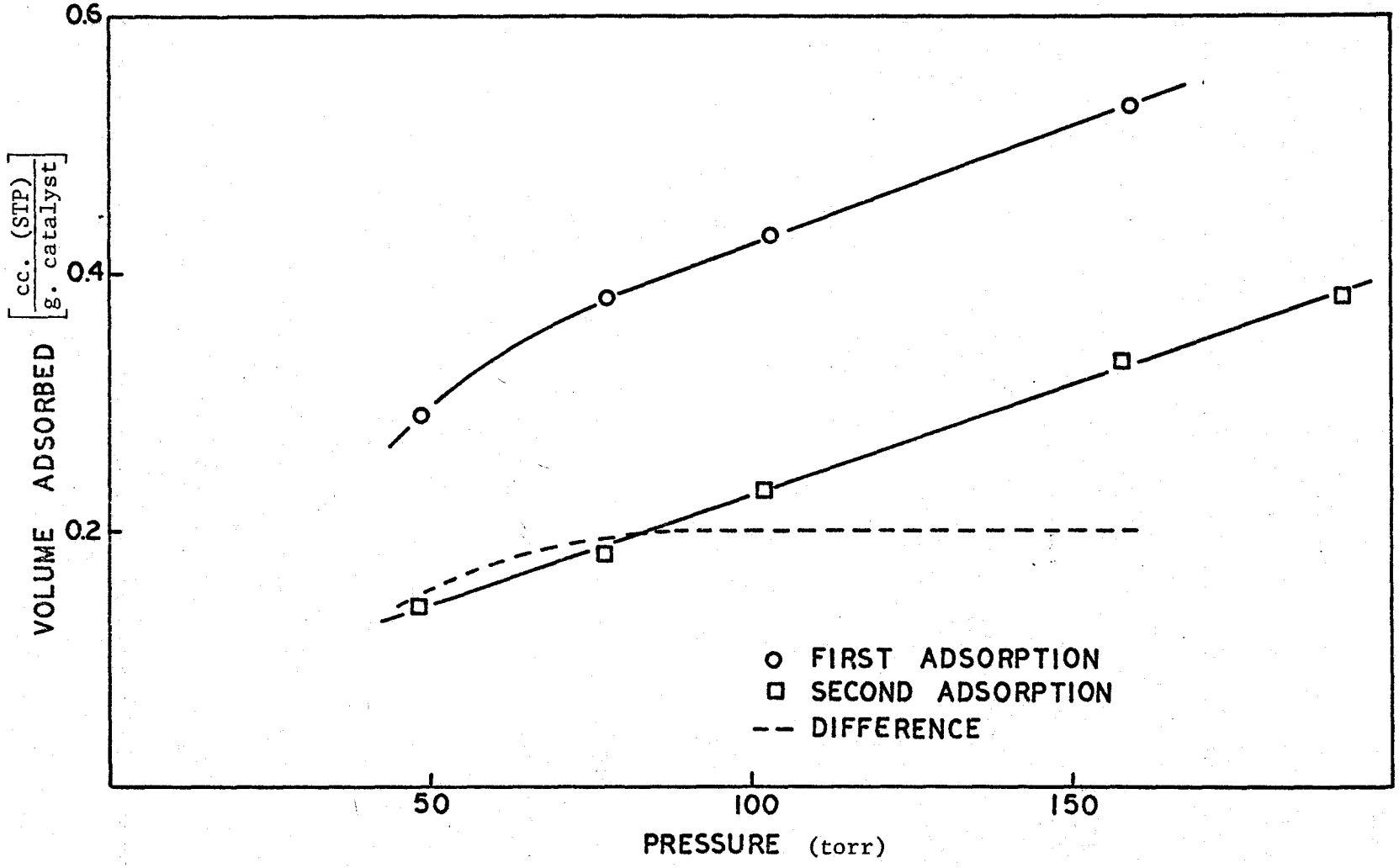

Figure 2-5: Hydrogen Adsorption

$$l = \frac{6}{Sd} \qquad (2\text{-}4)$$

where: S - surface area per gram of ruthenium

d - density of ruthenium

The density of ruthenium is 11.9 grams per cc. (64) and the concentration of ruthenium was assumed to be 0.4 weight percent. The calculated average crystallite length was about 25 Å.

2.3 Electron Microprobe Analysis

The distribution of ruthenium metal throughout the catalyst pellets is required to calculate the effects of pore diffusion on the reaction kinetics. An electron probe microanalyser was used to determine this concentration profile.

Standard metallographic procedures were used for mounting pellets in bakelite and polishing them to obtain a smooth cross-sectional area for analysis. Due to the original porosity and softness of the pellet, the surface was not as smooth as a polished metal; however, carefully polished pellets gave reproducible results. Good conduction of electrons away from the probe impact area is essential to avoid over-heating or "hot spot" formation and to remove the negative charge. Specimens were found to be sufficiently conducting after vacuum deposition of a 1000 angstrom layer of carbon.

An Acton electron probe microanalyser (fixed angle of take off of 18°) was used with mica diffraction crystals to obtain the ruthenium $L\alpha_1$ and $L\alpha_2$ lines. Other pertinent operating conditions are listed in Table 2-3.

TABLE 2-3

Operating Conditions of Electron Probe Microanalyser

Beam Voltage	25 kv.
Beam Current	150 μa.
Specimen Current	300 na.
Counter	# 3
Column Window	open
Diffraction Crystal	mica
Ruthenium Lines	$L\alpha_1$, $L\alpha_2$

To test for the presence of ruthenium, the detector system was scanned across the position at which x-rays from ruthenium would be expected. This was repeated with the electron beam incident on a number of different positions in the pellet. Typical results for the two distinct regions are shown in Figure 2-6. The expected maximum intensity position was an angular setting of 121.8. These results definitely show that ruthenium was present in the outer shell of the pellet but not in the center region.

The second experiment consisted of scanning across the pellet with the detector set at the optimum angular position. Figure 2-7 shows a typical response of signal intensity to the distance from the outside edge. The pellet diameter was 3400 microns; the ruthenium concentration dropped to zero within a few hundred microns of the surface. A sample of pure ruthenium metal, polished and mounted in a similar manner, was used as a standard and all signal intensities were taken in ratio to the intensity for the pure metal. The noise level in the particle was determined by averaging a number of signal intensity measurements taken on the interior of the pellet where no ruthenium was previously detected. This noise level was then subtracted from the total signal to get the ruthenium signal.

A total of ten scans were made over two pellets at different positions. All of the responses were similar in form but differed slightly in numerical value. Due to the softness of the catalyst, the polished surface of the pellet was rough causing low readings due to adsorption of the x-rays. A few readings with abnormally low responses

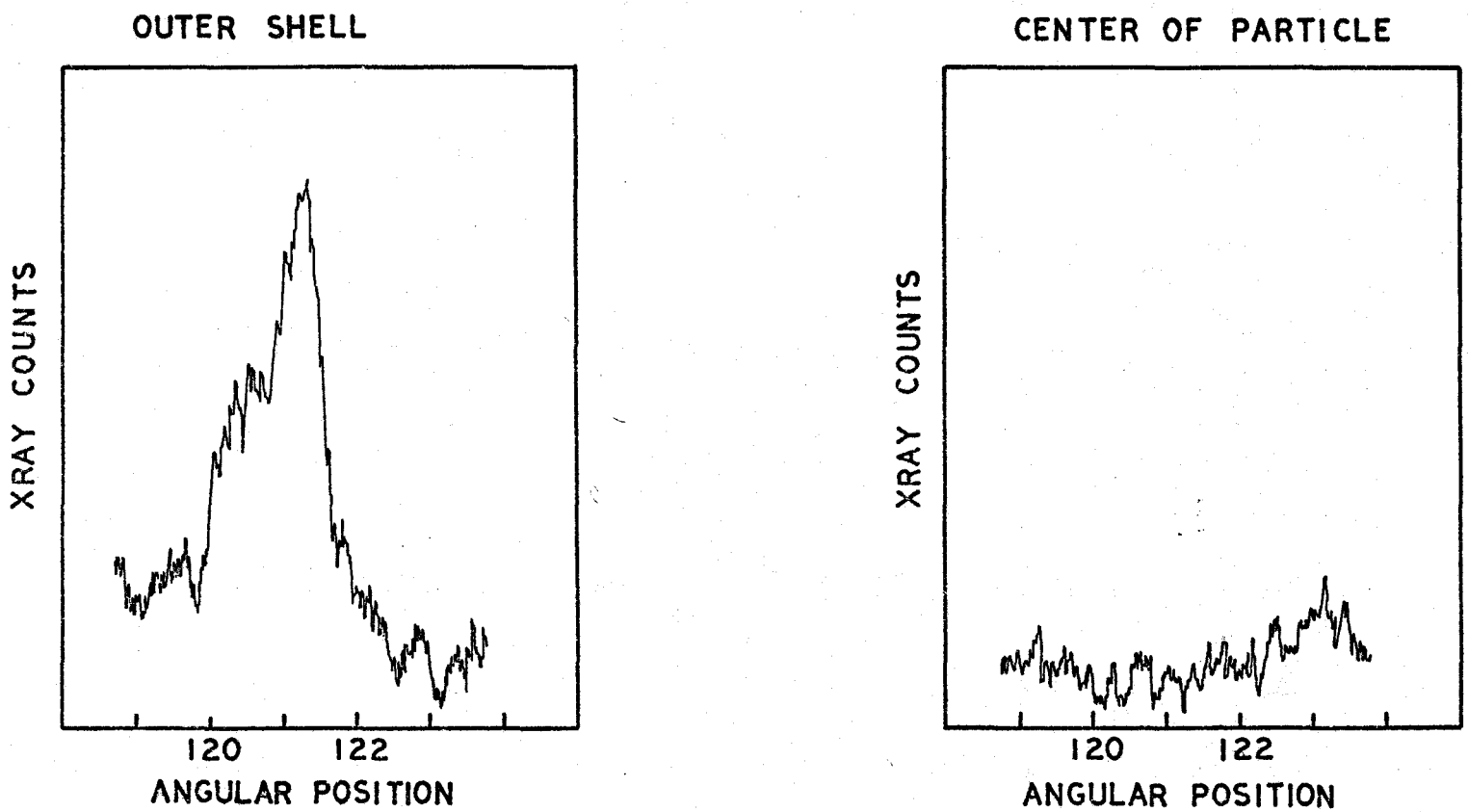

Figure 2-6: Electron Probe Analysis - Varying Detector Position

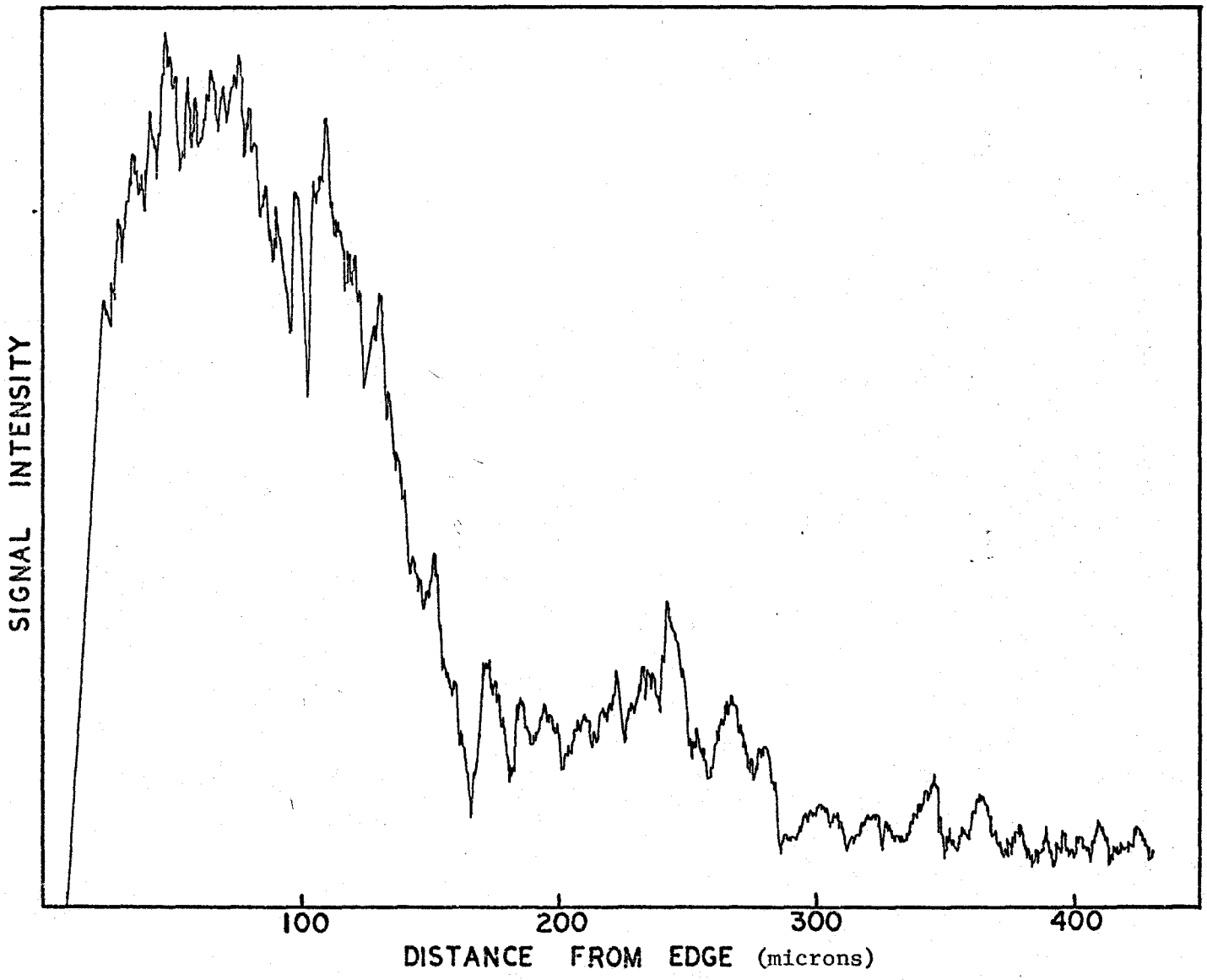

Figure 2-7: Variation of the X-ray Count with Position in the Catalyst Pellet

were discarded, and the rest of the values were averaged to produce a representative response for one scan across the pellet exterior.

In order to convert this type of data into concentrations of ruthenium, a number of corrections were made. The total signal correction can be divided into three separate factors: atomic number correction, absorption, and fluoresence. These corrections were made using the method outlined in the manual "The Electron Probe Microanalyser" (65).

Table 2-4 lists the average signal intensity ratios and the corresponding concentrations as a function of position within the pellet; these data are plotted in Figure 2-8.

Integration of this concentration curve over the whole pellet resulted in an average ruthenium concentration of 0.4 weight %. The nominal value for the catalyst is 0.5%.

TABLE 2-4

Data from Electron Probe Experiments

Position from Edge (microns)	Signal Intensity Ratio X100	Weight Percent Ruthenium
0	0.89	1.5
17	1.28	2.2
35	1.04	1.8
52	1.06	1.9
70	0.89	1.5
87	0.85	1.5
104	0.46	0.8
122	0.32	0.6
139	0.23	0.4
157	0.09	0.2
174	0.01	0.0
191	0.02	0.1
209	0.02	0.1
226	0.02	0.1
244	0.04	0.1
261	0.0	0.0
278	0.03	0.1
295	0.01	0.0
313	0.02	0.1
330	0.01	0.0
340	0.0	0.0
365	0.05	0.1

Background Noise Level:

Pellet # 1: 366 ± 15 counts
Pellet # 2: 363 ± 30 counts

Pure ruthenium response: 39,700 ± 2,000 counts

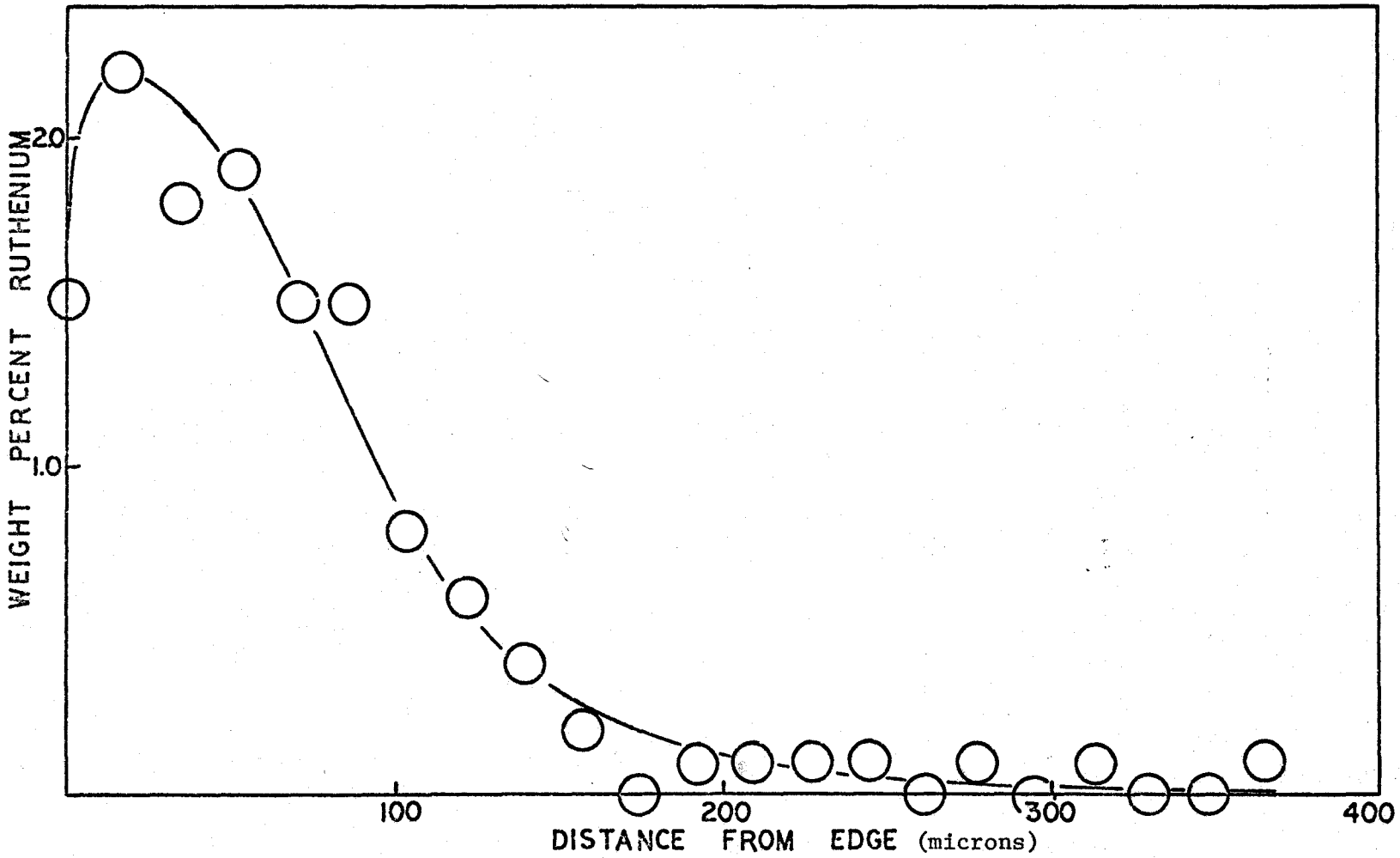

Figure 2-8: Ruthenium Concentration Gradient

Chapter 3

EXPERIMENTAL EQUIPMENT

3.1 Materials

A commercial catalyst (courtesy of Engelhard Industries, Inc.) consisting of a nominal 0.5 weight percent ruthenium impregnated on alumina was used. This catalyst has been thoroughly described in the previous section.

The hydrogen and hydrocarbon gases (propane, n-butane, isobutane, and neopentane) were purchased from the Matheson Co. The hydrogen (nominal purity 99.95% minimum) was further purified with a Deoxo unit to remove trace quantities of oxygen and then dried over 5A molecular sieve. Gas chromatographic analyses of the hydrocarbons showed only trace impurities in the propane, 0.25% isobutane impurity in the n-butane, 0.2% n-butane in the isobutane, and 0.1% n-butane in the neopentane. These gases were used directly.

The isopentane was purchased as a liquid from Distillation Prod. Inc. and originally contained 5% n-butane and n-pentane. After treatment with 5A molecular sieve which adsorbed the straight chain hydrocarbons, chromatographic analysis of the vapour in equilibrium with the liquid showed an impurity of only 0.08% n-butane and 0.1% n-pentane. The liquid was stored with molecular sieve during usage to ensure that the above purity was maintained.

3.2 Flow System

The apparatus used for the kinetic experiments was a continuous flow system consisting of three individual sections: the feed system, the reactor, and the effluent analysis system. A schematic diagram of this equipment appears in Figure 3-1.

The purpose of the feed system was to mix the hydrogen and hydrocarbon streams in certain definite proportions and to introduce them into the reactor at a given flow rate. Except where otherwise stated the lines were constructed with ¼ inch O.D. copper tubing. The hydrogen gas was passed through a Deoxo purifying unit to remove traces of oxygen and then through three feet of ½ inch O.D. copper tubing packed with 5A molecular sieve to dry it. The gaseous hydrocarbons were fed from their storage cylinders without further purification. Isopentane, a liquid under normal conditions, was vaporized into a hydrogen stream. The isopentane was placed in a gas-washing bottle which was fitted with a fritted disc, and maintained at 0°C by an ice bath to inhibit condensation of isopentane in the lines of the feed system. A hydrogen stream was saturated by bubbling it through the liquid and this mixture was further diluted to the desired concentration by mixing with a separate stream of pure hydrogen.

Both the hydrogen and hydrocarbon flow rates were controlled using fine-metering valves and monitored with capillary-type flowmeters. The manometers were glass U-tubes, three feet in length, with meriam fluid # D-3166 (S.G. = 1.04) as the indicating fluid; the capillary constrictions consisted of one-eighth inch copper tubing which had been

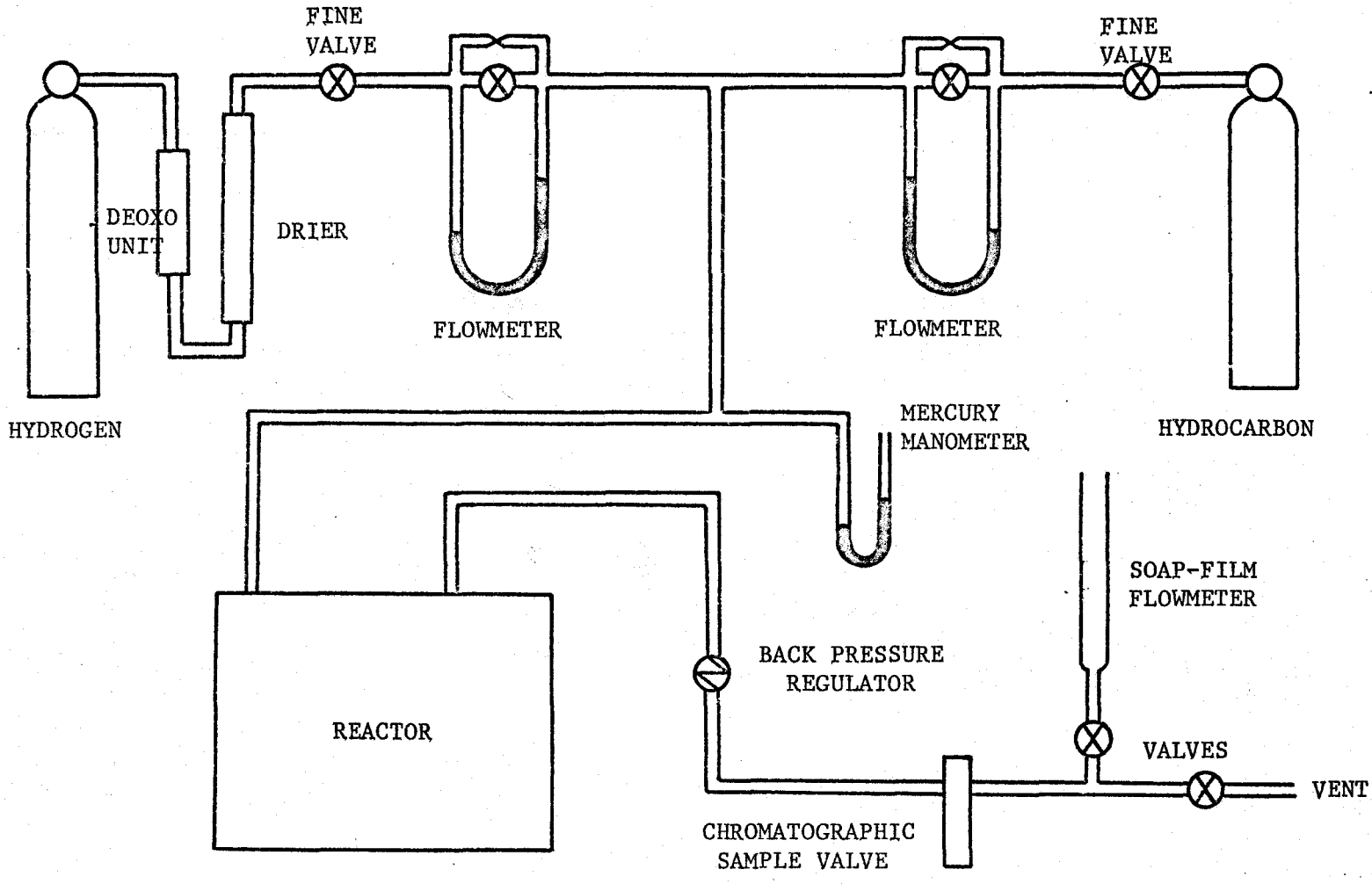

Figure 3-1: Equipment Flowsheet

crimped. Each manometer was fitted with a bypass valve to allow high flow rates for flushing the system. The flowmeters were calibrated for each gas, using a soap-film flowmeter, over the ranges 0 to 5 cc. per sec. and 0 to 15 cc. per sec. for hydrogen and the hydrocarbons, respectively.

The two streams were combined at a ¼ inch tee and then passed into the reactor. A mercury manometer was connected to the feed line just before the reactor to measure the total reactor pressure.

The purpose of the effluent system was to regulate the pressure in the reactor, to measure the total flow of effluent, and to analyse the effluent stream. Directly downstream from the reactor was a variable back-pressure regulator (Brooks Instrument Canada, Kendall Model 10BP) which was capable of controlling the reactor pressure in the range from 0 to 30 psig. for a variable flow rate. Subsequently the effluent was passed through a chromatographic sampling valve (the chromatographic assembly and analysis is described in Appendix A) and a flow measurement system. For all experiments measuring the rate of reaction, the effluent flow rate was measured with a soap-film flowmeter having a volume of 50 ml. so that for typical experiments the film rise time was approximately 15 seconds. When higher flows were required to obtain product distribution data at low conversions, the flow rates were measured with a rotameter.

3.3 The Reactor

The reactor was a converted one-litre Magnedrive packless autoclave (Autoclave Engineers, Inc.) with a magnetic drive action to

rotate the catalyst assembly (Figure 3-2). The external driver magnet and a stainless steel housing surrounded an internal circular magnet encapsulated on a rotor shaft. A strong magnetic field forced the inner shaft to rotate at the same speed (1500 r.p.m.) as the outer housing which was driven by an electric motor. The bearings were graphite and required no lubricant. This design completely sealed the driven shaft within the unit and also prevented contamination of the reactants or catalyst.

The reactor (Figure 3-3) was similar to those described by Carberry (5) and Brisk et al. (40). The body was a stainless steel block with a cylindrical cavity, 3 inches in diameter and 9 inches deep; the head, which was integrally connected to the stirring assembly, was bolted on top. To reduce the "dead" volume, aluminum plugs were placed in the cavity and thus the volume was decreased to 580 ml.

The catalyst was contained in a four-vane basket arrangement supported on the stirrer shaft. Two slightly different assemblies which were similar in overall geometry were used in the course of the experimental program. The first was constructed from four stainless steel wire mesh baskets mounted on a stainless steel tube. This system was difficult to balance and eventually caused excessive bearing wear, thereby making the system inoperative. The second assembly (Figure 3-4) was an aluminum bracket with stainless steel wire mesh bolted on the sides. This arrangement was more symmetrical and therefore not as hard on the bearings. The thickness of each basket was ¼ inch so that only two layers of catalyst pellets were possible. This was to ensure that

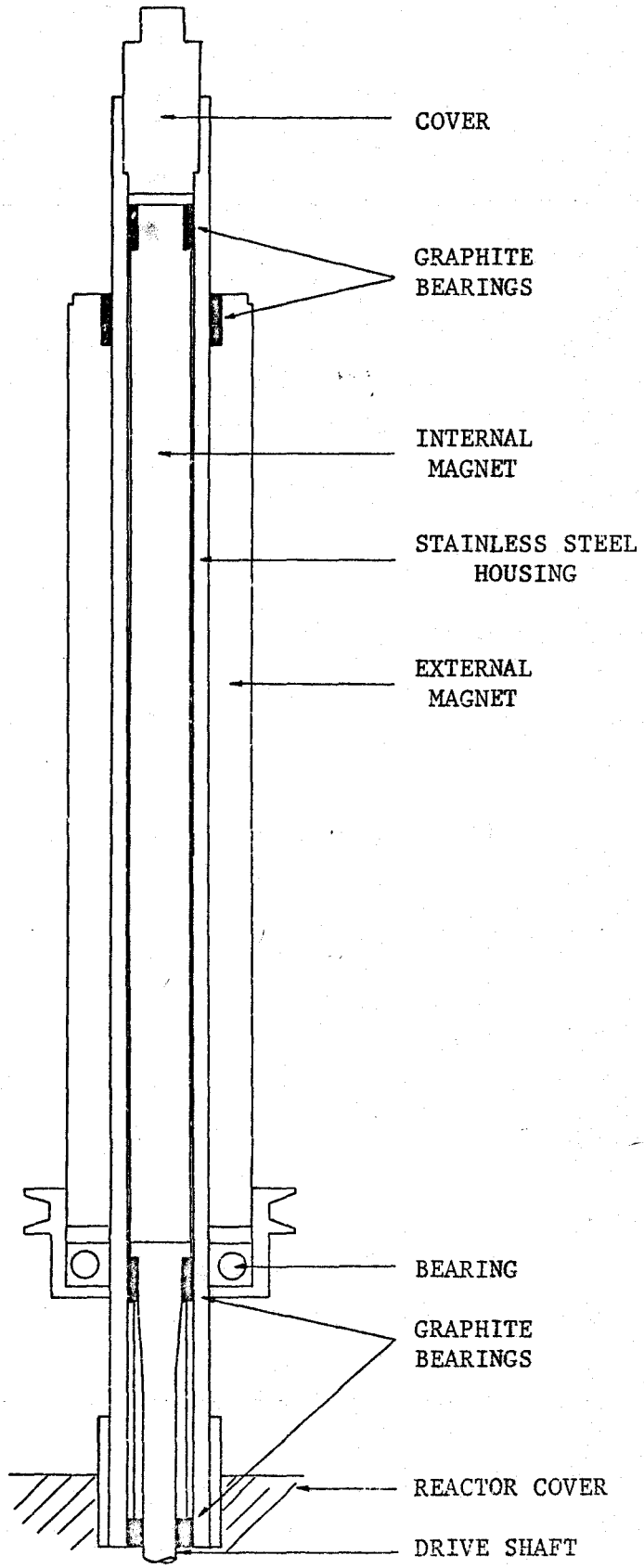

Figure 3-2: Magnedrive Stirring Assembly

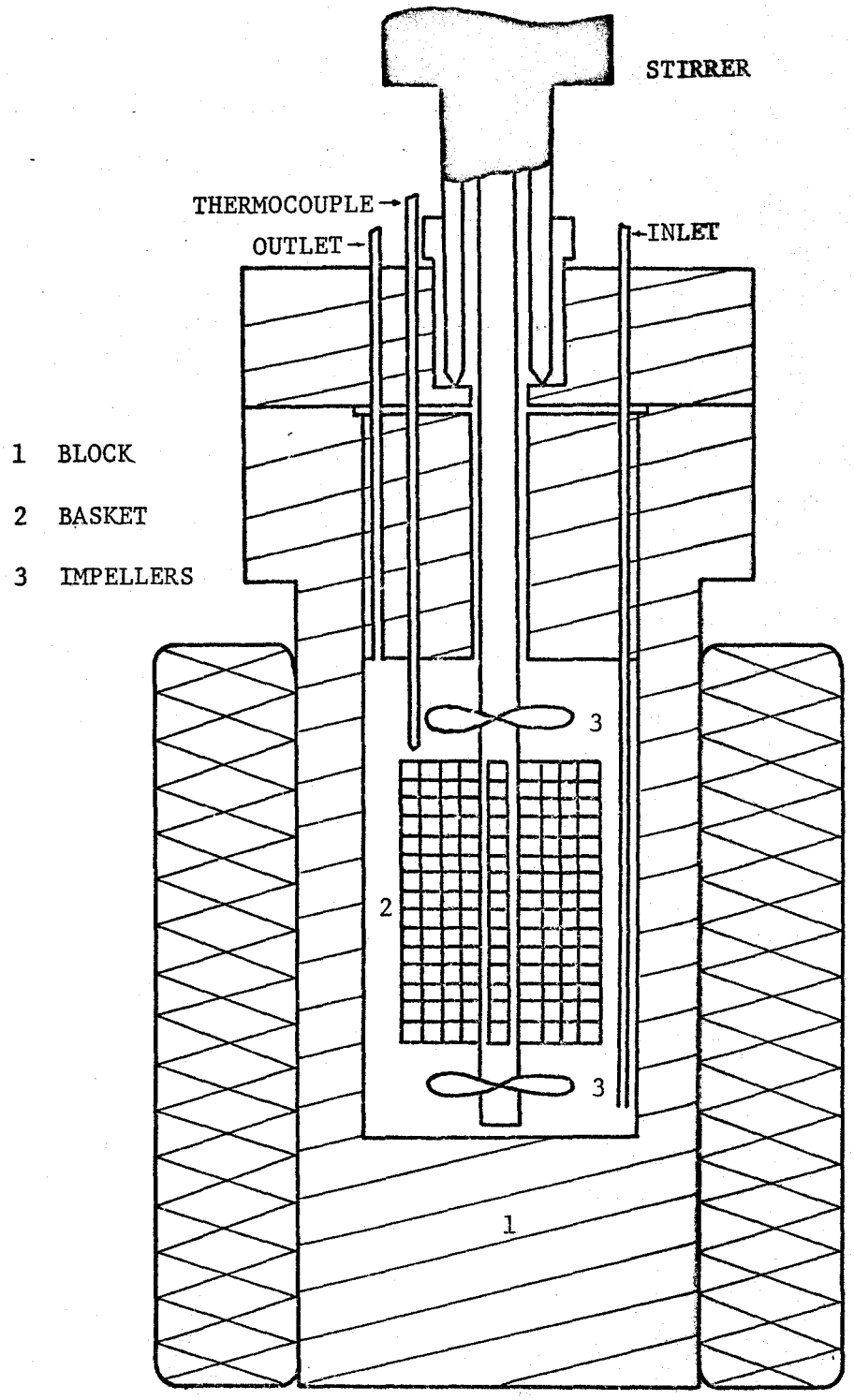

Figure 3-3: Continuous Stirred - Tank Catalytic Reactor

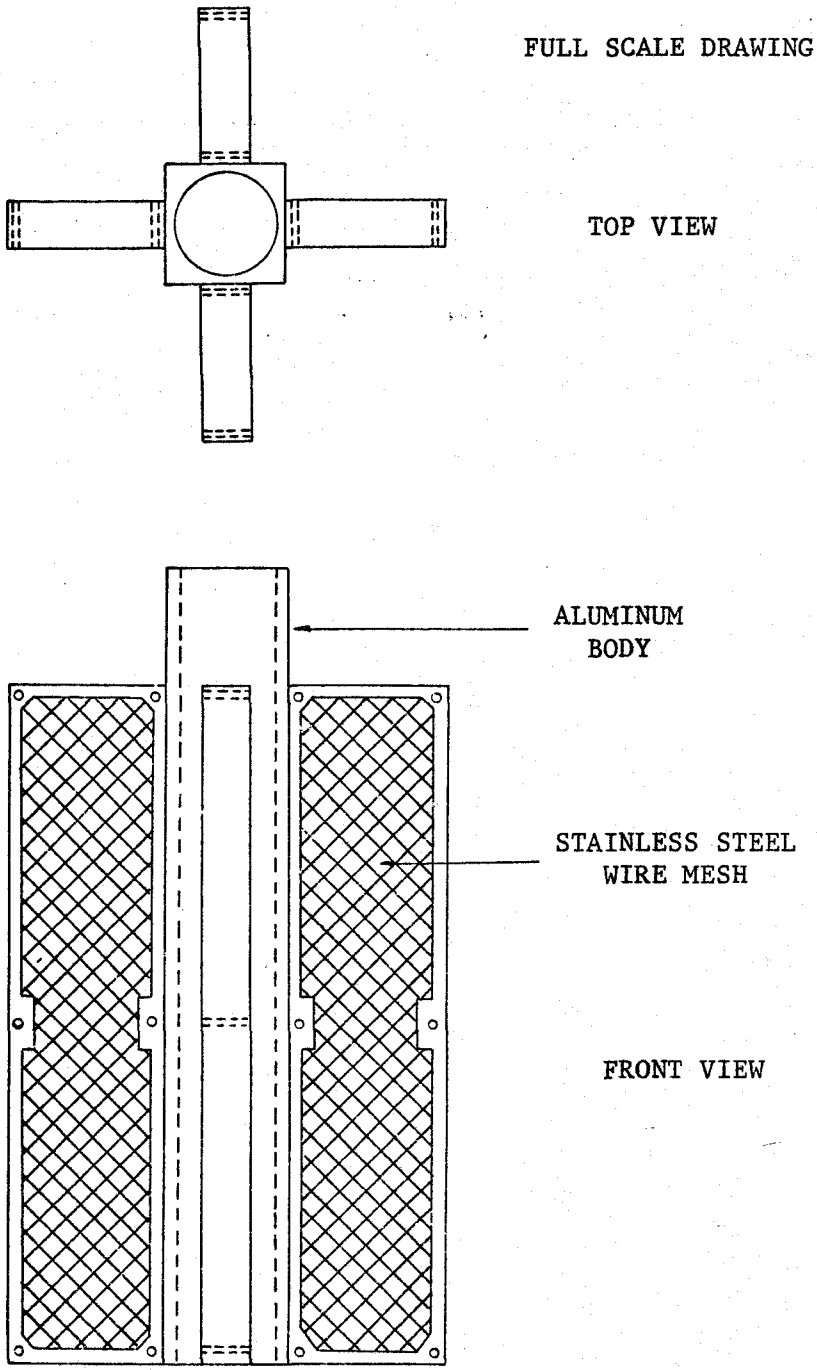

Figure 3-4: Catalyst Basket Assembly

resistance to the flow of gas through the basket would be small. Two impellers, one above and the other below the baskets, were also secured on the stirring shaft to improve mixing. The catalyst charge (40 to 50 grams) was supported on the central shaft and rotated at 1500 r.p.m. during experimental runs.

The inlet was made from one-eighth inch stainless steel tubing which passed down the wall of the reactor to a position slightly above the bottom. The effluent port, also one-eighth inch stainless steel tubing, was located near the top of the reactor.

The heater was a tubular electrical furnace supplied by two variable voltage transformers. The temperature was regulated using an on-off controller which affected only about 10% of the total power and the sensing thermocouple was located in the heating element itself so that temperature lags were minimized. Due to the large thermal capacity of the reactor, it could be maintained isothermal within 0.3°C for the duration of an experiment. The temperature of the reactor was measured using a chromel-alumel thermocouple located in the reacting fluid slightly above the basket (Figure 3-3) and an ice bath was used as the reference junction. A schematic diagram of the electrical system appears in Figure 3-5.

3.4 Operating Procedure

The catalyst was initially reduced in the reactor for twelve hours at 350°C and with a hydrogen flow of about 10 ml. per minute.

A continuous flow system was used in which the feed entered the bottom of the reactor and the exit stream passed from the top over the

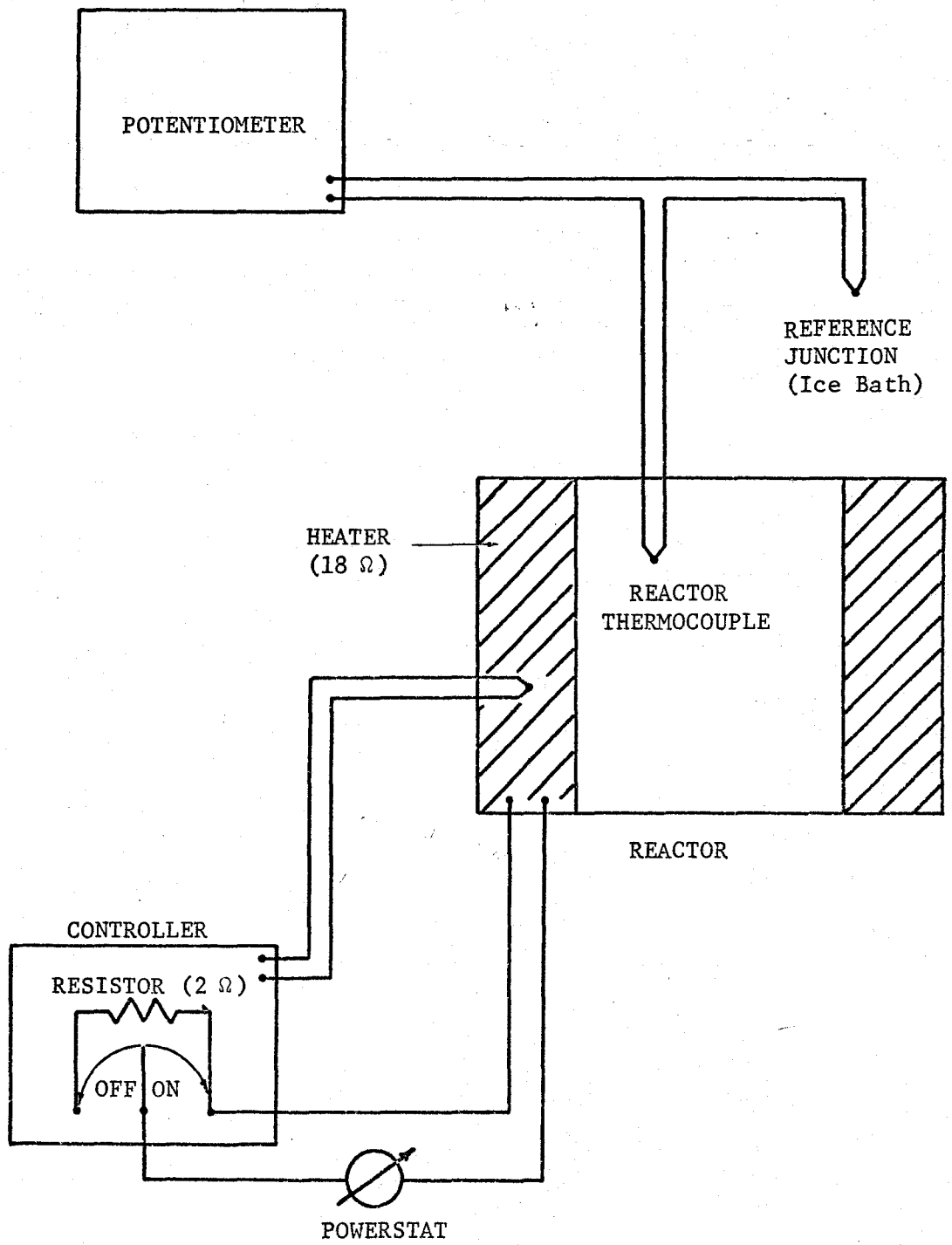

Figure 3-5: Temperature Measurement and Control System

duration of an experiment. The rotation of the catalyst assembly was sufficient to provide mixing of the catalyst plus reactants. An experiment consisted of setting the reactor conditions, allowing sufficient time for steady state to be obtained, and measuring the effluent stream flow rate and composition. Between experiments the reactor temperature was maintained near the operating level and the reactor was purged with hydrogen.

To begin a run the reactor temperature and pressure, and the hydrogen flow rate were set at the desired levels. The stirring mechanism was then activated (1500 r.p.m.) and the hydrocarbon flow was set. These conditions were maintained constant for a time period equivalent to six residence times, after which steady state was assumed to have been obtained. The effluent flow rate was measured using a soap-film flowmeter; the final temperature was recorded and a sample of the effluent was analysed by means of the gas chromatograph. The hydrocarbon flow was discontinued and the hydrogen flow was increased in order to flush the reactor and to prepare it for the next experiment.

For each experiment the total effluent flow rate was compared with the predicted value which would be expected from the sum of the flows monitored on the capillary flowmeters. These values agreed within a few percent (it should be noted that this is an equimolar reaction in which one mole of hydrogen and one mole of hydrocarbon react to produce two moles of smaller hydrocarbons and therefore there is no change in volume on reaction). From the chromatographic analyses it was possible to make a carbon balance and thereby calculate the input

hydrocarbon to hydrogen ratio. These values were compared with the value predicted from a ratio of the monitored inlet feed rates and the agreement was within experimental accuracy (± 3%).

Usually a set of approximately six runs were completed at one time with the first and last ones being at some standard conditions to check the activity.

3.5 Reactor Performance

3.5.1 Mixing Conditions in Bulk Gaseous Phase

The analysis of the experimental data assumed that the bulk gaseous contents were "perfectly" mixed. A sample of the effluent stream was therefore representative of the entire reacting mixture and the overall rate was calculated directly from the effluent concentration and flow rate.

Because the fluid contents were gaseous, the actual mode of mixing was on a microscopic scale and therefore, mixing on a macroscopic scale (mixing of aggregates) was not considered (66). The presence of perfect mixing with respect to concentration precludes any temperature gradients and therefore proof of ideal mixing by examining changes in concentration is sufficient to ensure that there is also ideal mixing with respect to temperature.

Imposition of a pulse of inert tracer on a well-agitated system yields a unique response of tracer concentration versus time in the effluent. The form of this response is described by the following equation (67):

$$C = C^* e^{-t/\tau} \qquad (3\text{-}1)$$

where: C - effluent concentration

C^* - maximum concentration of tracer at t = 0

τ - time constant of reactor

t - time

The dimensionless concentration (C/C^*) is related to dimensionless time (t/τ) through an exponential function and a semilogarithmic plot of these quantities results in a characteristic straight line with a slope -1/2.303. Tajbl et al. (39) have reported this type of study on a Carberry reactor for a wide range of stirring rates and gaseous flow rates. They found that at a stirrer speed of 1600 r.p.m. the reactor was perfectly mixed for flow rates above 2 ml. per second.

The mixing characteristics of the reactor were determined by measuring the response of the system to an impulse (approximately 8 ml.) of nitrogen or n-butane injected into a steadily flowing hydrogen stream at various volumetric flow rates and several stirring rates. The experimental apparatus is shown schematically in Figure 3-6. Hydrogen was allowed to flow through the reactor at the desired flow rate and atmospheric pressure until only hydrogen was present in the effluent. The pulse was then injected using a system of two-way stopcocks and the effluent concentration was measured using a thermal conductivity cell and monitored continuously on a recorder. Butane injections were used when the rotating basket was filled with glass beads (1/8 inch in diameter) because otherwise the butane would physically adsorb on the

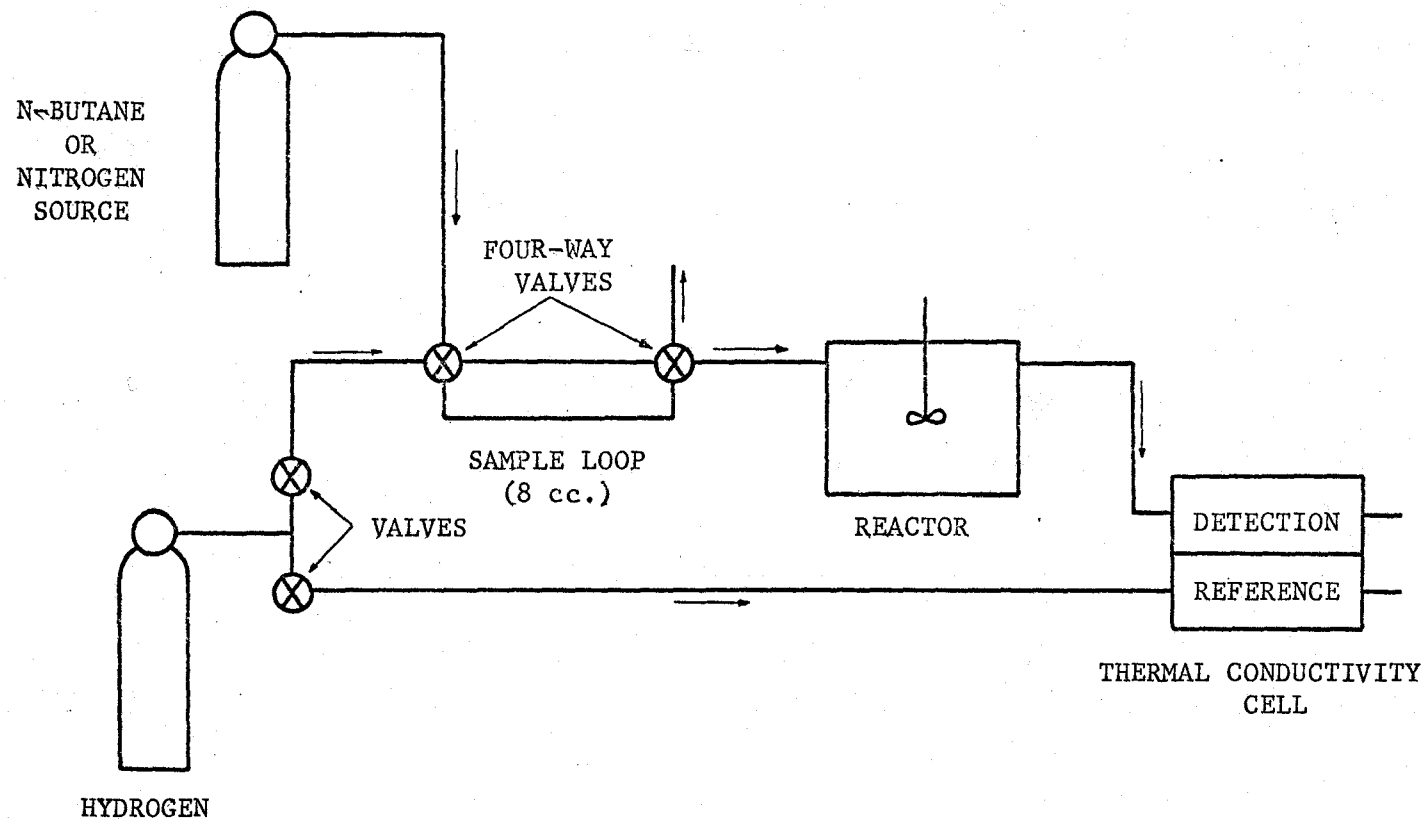

Figure 3-6: Apparatus for Testing Mixing Conditions

catalyst and give spurious results. Nitrogen was used as a pulse when the basket contained catalyst pellets. Stirring speeds of 1500 and 2000 r.p.m. were examined for a range of flow rates from 0.68 to 8.77 ml. per second. The results all showed an exponential decrease in concentration after a sharp increase as would be expected from Equation 3-1. The total reactor volume was estimated from physical dimensions to be 580 ± 20 cc. Using this volume and the flow rate, the elapsed time was transformed to dimensionless time. The corresponding dimensionless concentration was calculated from the concentration response curve.

The data are located in Tables D-18 to D-22 and are plotted in Figure 3-7 along with the theoretical line predicted according to Equation 3-1. These data confirm the assumption that the reactor was perfectly mixed and based on this information, the kinetic experiments were performed at a stirring rate of 1500 r.p.m. and flow rates varying from 0.3 to 10 ml. per second.

3.5.2 Interparticle Mass and Heat Transfer Effects

Fluid passing over catalyst particles creates a thin boundary layer in which the fluid velocity is zero at the solid surface but approaches bulk stream velocity a short distance from the surface. The transport mechanism across this film varies from being essentially molecular diffusion near the surface to turbulent mixing in the bulk fluid phase. Data on mass and heat transfer across boundary layers are commonly expressed in terms of transport coefficients.

$$N_m = k_G a (P_o - P_s) \qquad (3\text{-}2)$$

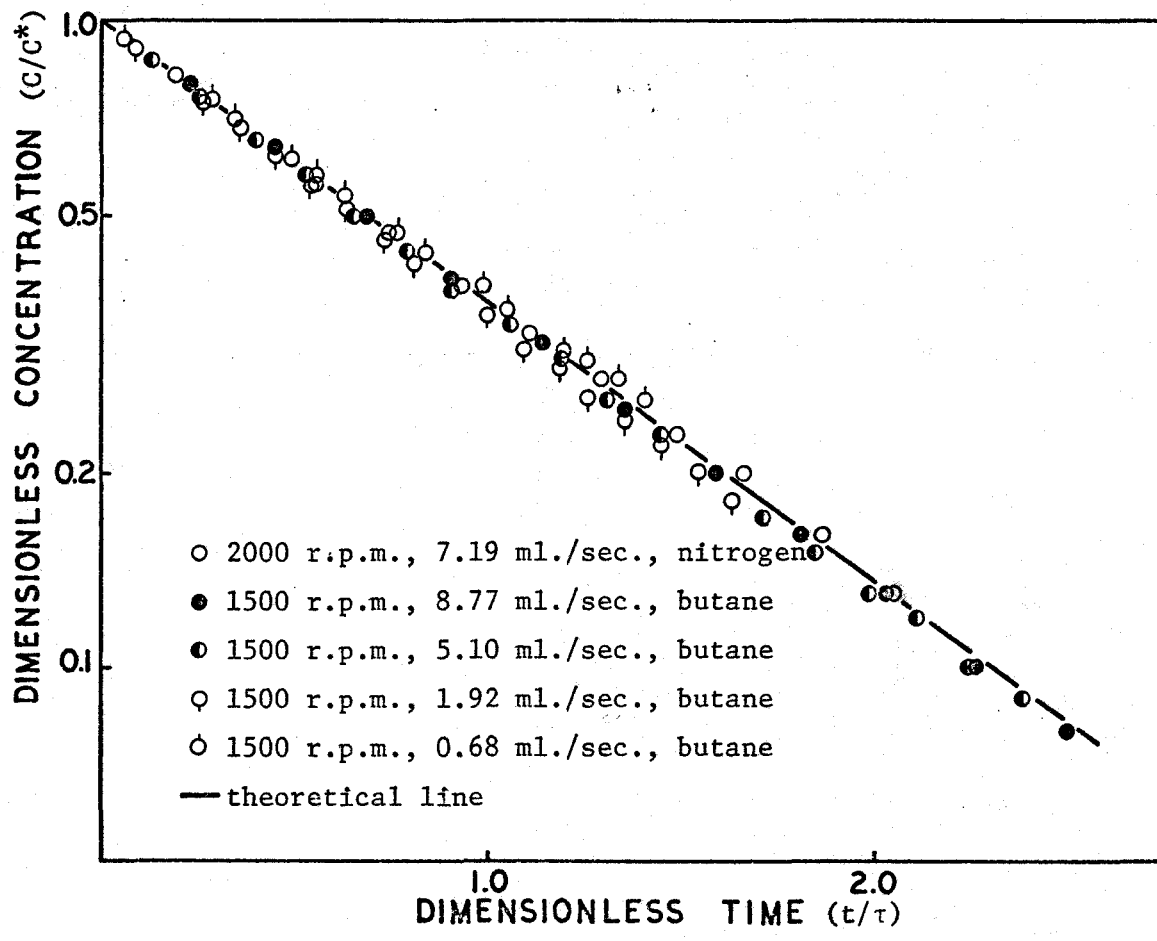

Figure 3-7: Results of Mixing Tests

$$N_H = h\,a\,(T_o - T_s) \qquad (3\text{-}3)$$

where: N_m - mass transfer rate

N_H - heat transfer rate

k_G, h - mass and heat transfer coefficients

a - area available for transfer

P_o, P_s - partial pressure of component in bulk phase and at the surface

T_o, T_s - temperature in bulk phase and at the surface

These transport coefficients are reported as a function of Reynolds number and Schmidt or Prandtl number on j-factor plots; the correlations of De Acetis and Thodos (68) have been used in these computations.

There are two problems specific to this type of reactor in predicting the transfer coefficients. First the particles were located at varying radii from the center of rotation and therefore had different velocities and boundary layer properties depending upon their position. Second, the actual velocity of gas past the catalyst is difficult to estimate because the gas not only passed through the basket, but may also have bypassed it or been dragged along with it. The pellets closest to the center of rotation have been examined because they were subjected to the lowest gas flow rate and therefore the most limiting transport properties. Mass transfer studies on a similar type of reactor (40) have shown an effective gas-velocity factor of approximately 0.5, i.e., the apparent gas velocity past the catalyst pellets was 50% of the velocity of the pellets due to rotation. This factor was used in the following calculations.

The Reynolds number is defined according to the following equation:

$$N_{Re} = \frac{d_p G}{\mu} \qquad (3\text{-}4)$$

where: d_p - equivalent diameter of particle (38)

G - mass flow rate

μ - gaseous viscosity

For a stirring rate of 1500 r.p.m. and pellets ¼ inch from the center of rotation, the pellet velocity is 100 cm. per second. For a 5:1 molar mixture of hydrogen and hydrocarbon the density and viscosity are 3.8×10^{-4} grams per cc. and 10^{-4} poise, respectively. The Reynolds number was calculated to be about 75.

The Schmidt and Prandtl numbers are defined by

$$N_{Sc} = \frac{\mu}{\rho D} \qquad (3\text{-}5)$$

$$N_{Pr} = \frac{C_p \mu}{k} \qquad (3\text{-}6)$$

where: ρ - density

D - diffusivity

C_p - heat capacity

k - thermal conductivity

Using 0.4 square cm. per second, 3.4 cal. per gram per °C, and 5×10^{-4} cal. per second per cm. per °C for diffusivity, heat capacity, and thermal conductivity, the values of Schmidt and Prandtl numbers equal to

0.66 and 0.68 were calculated. From the correlations of De Acetis and Thodos (68), the following values were determined for the transport coefficients:

$$k_G = 3.8 \times 10^{-4} \quad \frac{\text{moles}}{\text{cm}^2 - \text{sec.} - \text{atm.}}$$

$$h = 2.1 \times 10^{-2} \quad \frac{\text{cal.}}{\text{cm}^2 - \text{sec.} - {}^\circ\text{C}}$$

These coefficients were used to calculate the rate of reaction which could be supported under a negligible driving force of concentration and temperature differential between the surface and the bulk gas. Concentration and temperature differentials of 10^{-3} atm. and 0.1 °C have been accepted as negligible. Using Equation 3-2 and a value "a" equal to 10 square cm. per gram, the maximum allowable rate supported by the concentration differential was estimated to be 380×10^{-8} moles per second per gram of catalyst. Using a heat of reaction equal to 20 kcal. per mole of hydrocarbon consumed, the temperature differential was calculated to support a rate of 100×10^{-8} moles per second per gram of catalyst (Equation 3-3).

The kinetic experiments were all performed at rates lower than 50×10^{-8} moles per second per gram of catalyst, a region in which the effects of interparticle concentration and temperature gradients are negligible.

Some kinetic experiments were performed to confirm these calculations. Varying the stirring rate between 1500 and 1900 r.p.m. had no effect on the observed reaction rate for n-butane hydrogenolysis as

TABLE 3-1

Effect of Stirring on Reaction Rate
n-Butane Hydrogenolysis (125°C)

Stirring Rate (r.p.m.)	Reaction Rate $\left[\frac{\text{mole}}{\text{g. catalyst - sec.}}\right]$
1500	26.5×10^{-8}
1900	25.9×10^{-8}
1500	25.7×10^{-8}

shown in Table 3-1. This result can only be explained if interparticle gradients were negligible over the range of stirring rates examined. Similar results have been reported by Tajbl (33) for the hydrogenolysis reaction of ethane over the same catalyst and with rates in the order of 50 x 10^{-8} moles per second per gram of catalyst.

3.5.3 Intraparticle Mass and Heat Transfer

A reaction within a porous medium must occur simultaneously with mass and heat transfer through the pores. This process has been described in the texts of Satterfield and Sherwood (38) and Petersen (69). When pore diffusion is rate limiting, concentration and temperature gradients are established throughout the pellet and the overall reaction rate is different from that which would exist if the conditions within the pellet were the same as in the bulk gaseous phase. The effectiveness factor is defined as the ratio of the reaction rates with and without pore-diffusion limitations. This factor has been correlated against the Thiele modulus by solving the mathematical equations for simultaneous transfer and chemical reaction (69).

Because the calculations for the real system would be prohibitively complex, the following simplifying assumptions were made:

1) the system was isothermal
2) Knudsen diffusion was operative in the pores
3) the active shell of the pellet was considered to approximate a flat plate
4) hydrogen diffused much faster than the hydrocarbons, and therefore there was no concentration gradient with respect to hydrogen

5) the reaction was first order with respect to the hydrocarbon

The effective Knudsen diffusion coefficient can be calculated from the equation (38):

$$D_K = 9700\, r\left[\frac{T}{M}\right]^{\frac{1}{2}}\left[\frac{\theta}{\tau}\right] \qquad (3\text{-}7)$$

where: D_K - effective diffusion coefficient

r - average pore radius

T - temperature

M - hydrocarbon molecular weight

θ - void fraction of catalyst particle

τ - tortuosity factor

Substituting 50 angstroms, 400°K, 60, 0.5, and 2 for the average pore radius, temperature, molecular weight, void fraction, and tortuosity, a value of 3×10^{-3} square cm. per second was calculated for the diffusion coefficient.

The Thiele modulus for the platelet model is given by the equation (38):

$$\phi = L\left[\frac{k_v}{D_K}\right]^{\frac{1}{2}} \qquad (3\text{-}8)$$

where: L - plate thickness (2.2×10^{-2} cm.)

k_v - first order reaction rate constant

The corresponding value for the effectiveness factor is

$$\eta = \frac{\tanh \phi}{\phi} \qquad (3\text{-}9)$$

where: η - effectiveness factor

Table 3-2 contains the values of Thiele modulus and effectiveness factor for different values of the rate constant. The maximum value of the rate constant for which pore diffusion limitations are negligible is unity. This corresponds to an overall rate of 80 x 10^{-8} moles per second per gram of catalyst, for average experimental conditions. The kinetic experiments were all performed in a region of negligible pore diffusion limitations.

The above analysis has assumed that the porous structure was isothermal. Under steady state conditions, diffusion of reactants across a boundary must equal the rate of reaction within the surface and the heat released must all be transferred across the same boundary (70). This relationship is described by the following equation:

$$D_K \frac{dC}{dx} \cdot \Delta H = \lambda \frac{dT}{dx} \qquad (3\text{-}10)$$

Integration yields

$$\Delta T = \frac{(-\Delta H)\, D_K}{\lambda} (C_s - C) \qquad (3\text{-}11)$$

where: ΔT - temperature change

ΔH - enthalpy of reaction

λ - thermal conductivity

C_s, C - concentration at surface and within the pellet

TABLE 3-2

Intraparticle Mass Transfer Effects

Rate Constant k_v (sec.$^{-1}$)	Thiele Modulus ϕ	Effectiveness Factor η
10^{-2}	0.04	1.0
1	0.4	0.95
10^{2}	4	0.25

The maximum temperature rise occurs when all of the reactant is consumed, i.e., C equals zero. This temperature increase was calculated to be 0.3°C in this case. Therefore the assumption of isothermal operation is justified.

3.5.4 Analysis of Transient Response of Carberry Reactor

It has previously been demonstrated that the reactor was ideally mixed. Therefore, at steady state, the concentration and temperature were constant throughout the reactor and invariant with time; however, each experiment had a transient period during which the steady state level was attained. Because the chromatographic analysis was relatively lengthy (requiring up to 30 minutes), the examination of successive samples until constant behavior was observed would have been prohibitively slow. Therefore, sufficient time was allowed for steady state to be obtained (from 10 minutes to 2 hours depending on the feed rate) and then one analysis of the effluent was made. The following are some calculations made in support of this procedure.

If to a stream of hydrogen flowing steadily through the reactor a small step input of hydrocarbon is added, the reactor will approach steady state in a manner determined by the solution of the differential equation for the hydrocarbon mass balance. This equation is comprised of a source term for hydrocarbon (inlet stream), two sink terms (outlet and reaction), and an accumulation term.

The reaction rate was assumed first order in hydrocarbon (2), and the effect of the hydrogen partial pressure was adsorbed into the rate constant.

$$r = kC \tag{3-12}$$

where: r - rate

k - rate constant

C - hydrocarbon concentration

The overall mass balance equation is

$$FC_i - FC - kCV = V\frac{dC}{dt} \tag{3-13}$$

where: F - inlet and outlet flow rate

C_i - inlet concentration of hydrocarbon

C - reactor concentration of hydrocarbon

V - reactor volume

t - time

For a step change in hydrocarbon inlet concentration, the solution to this equation is

$$C = \frac{C^*}{(1 + k\tau)} \left(1 - e^{-t/T}\right) \tag{3-14}$$

where: C^* - size of step change

τ - residence time of reactor (V/F)

T - $\tau/(1 + k\tau)$

The hydrocarbon concentration in the reactor increases until it reaches a steady state value of $C^*/(1 + k\tau)$. For slow reactions, i.e., small values of k, the value of T approaches τ, the time constant for systems

with reaction. However, for fast reactions, the response time approaches $^{1}/k$, and steady state is reached more rapidly than for the case without reaction.

For the conditions under which the Carberry reactor was operated, the average values of k and τ were 0.1 $min.^{-1}$ and 3 min. Substituting these values into Equation 3-14, the calculated fractional responses of the feed hydrocarbon concentration to steady state after 2τ, 3τ, and 4τ are 0.93, 0.98, and 0.995. The response is essentially complete after three residence times.

The approach to steady state of the product concentrations must also be considered. A mass balance on a product is given by

$$- FC' + \nu k C V = V \frac{dC'}{dt} \qquad (3\text{-}15)$$

where: C' - concentration of product in the reactor

ν - stoichiometric number

The solution for the concentration of the product is

$$C' = \frac{C^* k \tau \nu}{(k\tau + 1)} \left[1 - \frac{\tau T}{(\tau - T)} \left(\frac{1}{T} e^{-t/\tau} - \frac{1}{\tau} e^{-t/T} \right) \right] \qquad (3\text{-}16)$$

When the elapsed time is 2τ, 3τ, 4τ, and 5τ, the fractional response of the product concentration to steady state is 0.64, 0.85, 0.94, and 0.98. Therefore, the response for the product essentially reaches its limiting value after five residence times.

An experiment was conducted using a slow flow rate, i.e., a large residence time, to verify these calculations. Two samples were

analysed during the approach to steady state at 2.1τ and 5.6τ. The data are summarized in Table 3-3. The second sample was assumed to be at the steady state value as it was taken after more than five residence times. There is good agreement between the calculated and experimental fractional approaches to equilibrium for the first sample.

On this basis, six residence times were allowed for steady state to be obtained in all kinetic experiments; therefore, any deviation from true steady state was well within the experimental error.

TABLE 3-3

Transient Response of Carberry Reactor

Experimental Conditions:

Hold up time 10.8 min.

Rate Constant ~0.1 min.

Sample Number	Sample Time	Fractional Approach to Steady State			
		Feed Hydrocarbon		Product Hydrocarbon	
		Calc'd	Expt'l	Calc'd	Expt'l
1	2.1τ	0.99	1.0	0.77	0.74
2	5.6τ	1.0	1.0	0.99	1.0

Chapter 4

KINETICS OF HYDROGENOLYSIS REACTIONS OVER RUTHENIUM

4.1 Introduction

For a number of small paraffins including propane, n-butane, isobutane, isopentane, and neopentane, the rates of hydrogenolysis were examined as a function of temperature and composition. The experiments were generally made with excess hydrogen, a total pressure of 800 torr, and temperatures between 85° and 155°C. For n-butane and isopentane, higher total pressures (up to 1500 torr) were also examined to increase the range of experimental concentrations.

The apparatus was such that each experiment afforded one determination of reaction rate corresponding to the reactor temperature and the composition of the gaseous reactants. Because these conditions were invariant with time for all positions within the reactor, the data were differential and could be applied directly to proposed rate equations. The calculation of effluent compositions and reaction rates from raw experimental data is described in Appendix B.1.

The catalyst activity was not constant throughout the experimental program. Due to malfunction of the bearings in the stirrer mechanism, the reactor had to be dismantled occasionally and the catalyst charge was replaced when the system was repaired. The activity of different catalyst batches was not reproducible. Because these changes of catalyst were usually carried out while the area of study was being

shifted from one hydrocarbon to another, there was no effect on the kinetic analysis except that comparisons of rates for different hydrocarbons could not be made directly. The relative hydrogenolysis rates of pairs of hydrocarbons were therefore studied over one catalyst sample (Section 4.7).

In some cases, the activity of the catalyst varied with time as has been reported by Sinfelt and and Yates (4) and, Hahn and Petersen (71); standard experiments were performed intermittently to examine this change. The activity usually remained essentially constant over long periods (four to six weeks) but, when necessary, the observed rates were corrected. Such corrections were normally less than 10 percent.

The data for each hydrocarbon were fitted to a power-function rate equation with an Arrhenius temperature dependence of the rate constant.

$$r = A\, e^{-\frac{E}{RT}}\, P_H^a\, P_{HC}^b \qquad (4\text{-}1)$$

where: r - rate of hydrogenolysis

A - pre-exponential factor

E - activation energy

$(Ae^{-E/RT})$ - rate constant

P_H, P_{HC} - partial pressure of hydrogen and feed hydrocarbon

a, b - reaction orders

Best estimates of the four parameters (A, E, a, and b) were obtained by

linear regression analysis and the reaction orders were used to calculate the degree of unsaturation of the adsorbed hydrocarbon (see Section 1.2). A comparison of the parameter values for each hydrocarbon and a discussion of their significance is included in the summary.

The data were also used to test the mechanistic equation of Cimino et al. (16). Before simplification this equation is

$$r = \frac{A\, e^{-E/RT}\, P_{HC}\, P_H^{\,1-\alpha}}{\left[1 + K\, e^{-\Delta H/RT}\, P_{HC}\, P_H^{\,-\alpha}\right]} \qquad (4\text{-}2)$$

where: A, K - pre-exponential factors

E - apparent activation energy

ΔH - heat of adsorption of hydrocarbon (positive value is endothermic)

α - number of hydrogen molecules lost by hydrocarbon on adsorption

The parameter values were estimated by nonlinear regression analysis.

For the correlation of the n-butane results at different total pressures, a new rate equation was developed because both of the previous equations were inadequate. This equation was derived using the adsorption isotherms of Kemball (9) and is given later in the text.

4.2 Propane

The purpose of the propane experiments was to check the data of Tajbl and to obtain approximately the reactivity for propane hydrogenolysis. Four measurements were taken at a total pressure of 800 torr and 125°C (Table D-1). Unfortunately, the catalyst charge was changed

after the first two experiments. Standard runs with isobutane feed showed that the second catalyst batch had a larger activity by a factor of 1.55 and the rates of the last two experiments were corrected accordingly.

The values of the reaction orders with respect to hydrogen and propane could only be approximated. The data were fitted to the equation

$$r = k P_{C_3} P_H^{-3/2} \qquad (4\text{-}3)$$

where: r - rate of hydrogenolysis

k - rate constant

P_{C_3} - propane partial pressure

P_H - hydrogen partial pressure

by plotting the rate against $(P_{C_3}/P_H^{3/2})$. This rate equation has been proposed by Tajbl (33) for the hydrogenolysis of propane over a similar supported-ruthenium catalyst. Figure 4-1 demonstrates that the data are adequately correlated by this equation.

4.3 n-Butane

The initial data for n-butane hydrogenolysis were obtained over the following range of experimental conditions:

Total Pressure:	800 torr
Temperature:	85°, 100°, 110°, 125°C
Hydrogen Pressure:	350 to 750 torr
Butane Pressure:	10 to 300 torr

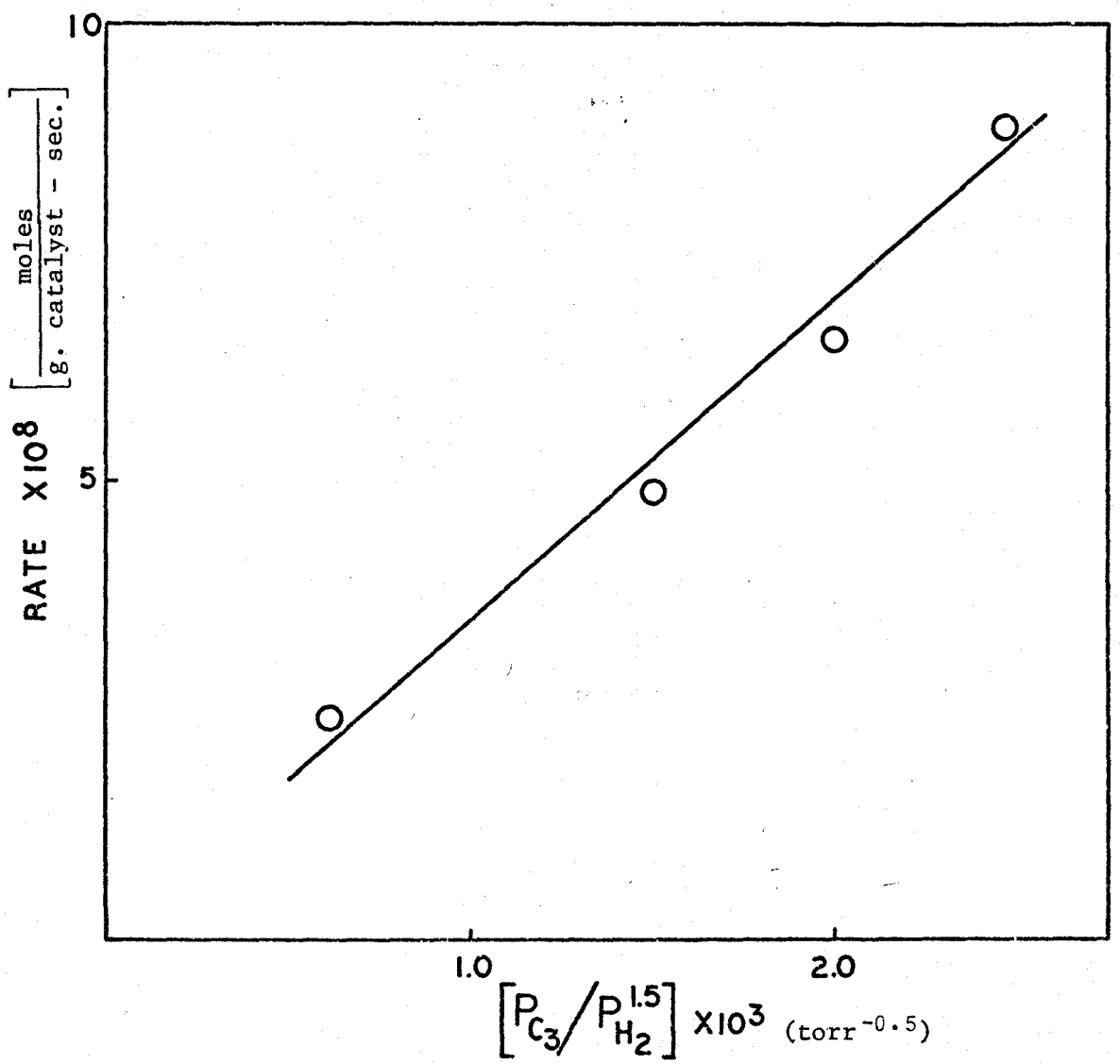

Figure 4-1: Propane Hydrogenolysis Kinetics

Butane Conversion: 5 to 80%

Hydrogen/Hydrocarbon: 11/1 to 1/1

The catalyst activity remained constant throughout the entire period of observation. The results are presented in Table D-2.

The data were fitted to Equation 4-1 by linear least squares analysis. This equation was linearized by taking logarithms and the four parameters and their 95% confidence limits were estimated by the methods outlined in Appendix B.2. Additional terms corresponding to the partial pressures of the reaction products (propane, etc.) were added to Equation 4-1 by raising them to some general exponent in a similar manner to the way in which hydrogen and butane were considered. Since the correlation of the reaction rates was not significantly improved, these terms were neglected.

The results of these calculations are listed in Table 4-1. The butane exponent was positive and slightly less than unity and the hydrogen exponent was negative and large. The overall order of the reaction was also negative. These reaction orders are similar to those which have been reported for ethane and propane hydrogenolysis over ruthenium (4, 33). The activation energy was large; independent experiments measuring rates at nearly the same composition but at different temperatures confirmed this value within ± 2 kcal. per mole. Figure 4-2 is a comparison of the observed and calculated reaction rates.

For each temperature, an average rate constant was calculated using the regressed equation and the experimental data. The results appear in Table 4-2 and are plotted according to the Arrhenius equation

TABLE 4-1

Analysis of n-Butane Rate Data Using Equation 4-1

Number of Observations:	41
Residual Degrees of Freedom:	37
Total Sum of Squares:	19.27
Residual Sum of Squares:	0.038
Residual Root Mean Square:	0.032

Parameter	Estimated Value	95% Confidence Interval
log A	22.17	±0.32 (mole-torr$^{0.44}$/g. catalyst - sec.)
E	48.1	±0.7 (kcal./mole)
a	-1.35	±0.08
b	0.91	±0.04

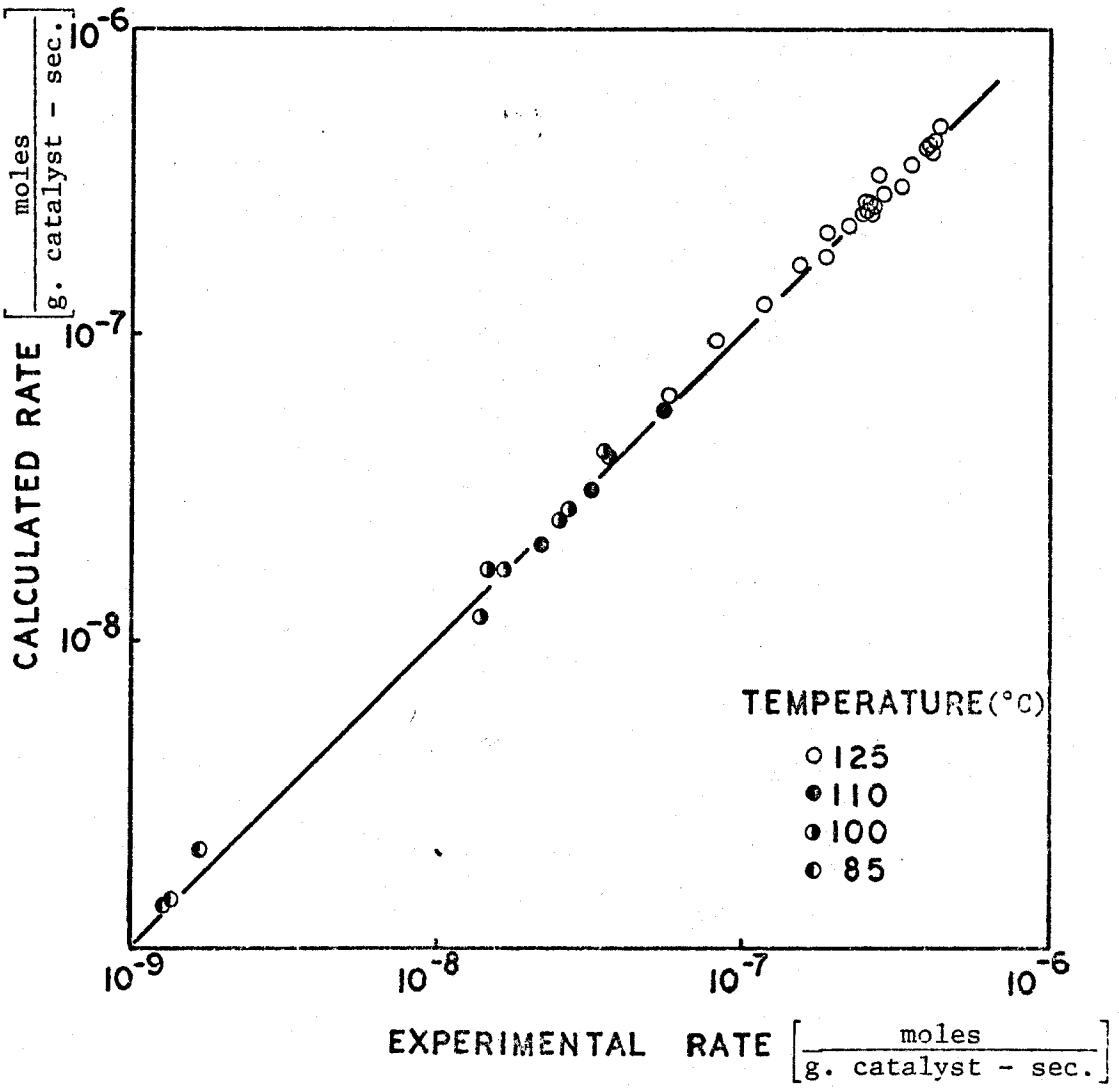

Figure 4-2: Comparison of Experimental and Calculated Rates of n-Butane Hydrogenolysis (Equation 4-1)

TABLE 4-2

Rate Constants for n-Butane Hydrogenolysis

Temperature (°C)	Rate Constant $\left[\frac{\text{mole-torr}^{0.44}}{\text{g. catalyst - sec.}}\right]$
145	2.76×10^{-4}
125	5.44×10^{-5}
110	5.42×10^{-6}
100	9.43×10^{-7}
85	5.85×10^{-8}

in Figure 4-3. The value at 145°C was determined from data taken at this temperature but not used in the kinetic analysis. Thiele modulus calculations predict that pore diffusion resistances are rate limiting at this temperature and therefore the observable activation energy should be decreased. The value of the rate constant at 145°C is in good agreement with that predicted and the rate constants at the other temperatures are linearly related.

The rate data were also fitted to Equation 4-2. In this case the five parameters were estimated using nonlinear regression analysis by Rosenbrock search technique (Appendix B.2). Initial values of the parameters were determined by linear regression analysis of the transformed equation at one temperature at a time. These values were then improved by searching over all the data simultaneously using the equation in the nonlinear form. The results of these calculations are in Table 4-3. The apparent activation energy was nearly the same as for the analysis of Equation 4-1 and the adsorption of the hydrocarbon was endothermic, ΔH = 1.1 kcal. per mole. The value of α corresponds to a loss of 5 to 6 hydrogen atoms on the dissociative adsorption of n-butane. The observed and predicted rates are compared in Figure 4-4 and the agreement is good, but not significantly better than that obtained from the analysis of Equation 4-1.

To test the rate equation further, experiments were taken at total pressures of 1100 and 1400 torr and 125°C (Table D-3).. The change in total pressure greatly increased the range of hydrogen partial pressures and was a severe test of the rate equations. According to

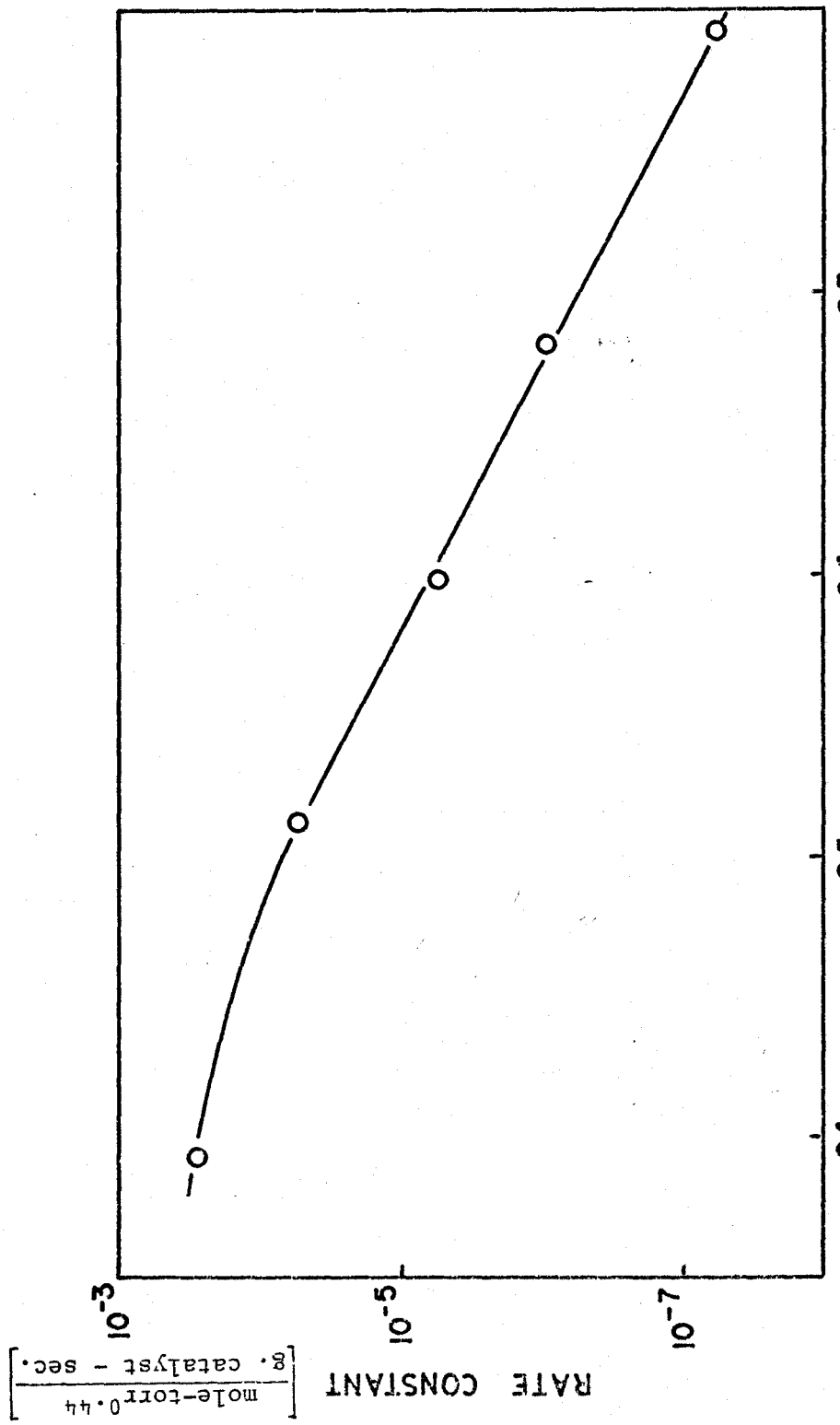

Figure 4-3: Arrhenius Plot for n-Butane Hydrogenolysis

TABLE 4-3

Analysis of n-Butane Rate Data Using Equation 4-2

Number of Observations:	41
Residual Degrees of Freedom:	36
Residual Sum of Squares:	47.9
Residual Root Mean Square:	1.15

Parameter	Estimated Value	
α (or $n/2$)	2.80	
A	1.80×10^{22}	(mole-torr$^{0.8}$/g. catalyst - sec.)
E	46.2	(kcal./mole)
K	7.41×10^{5}	(torr$^{1.8}$)
ΔH	1.11	(kcal./mole)

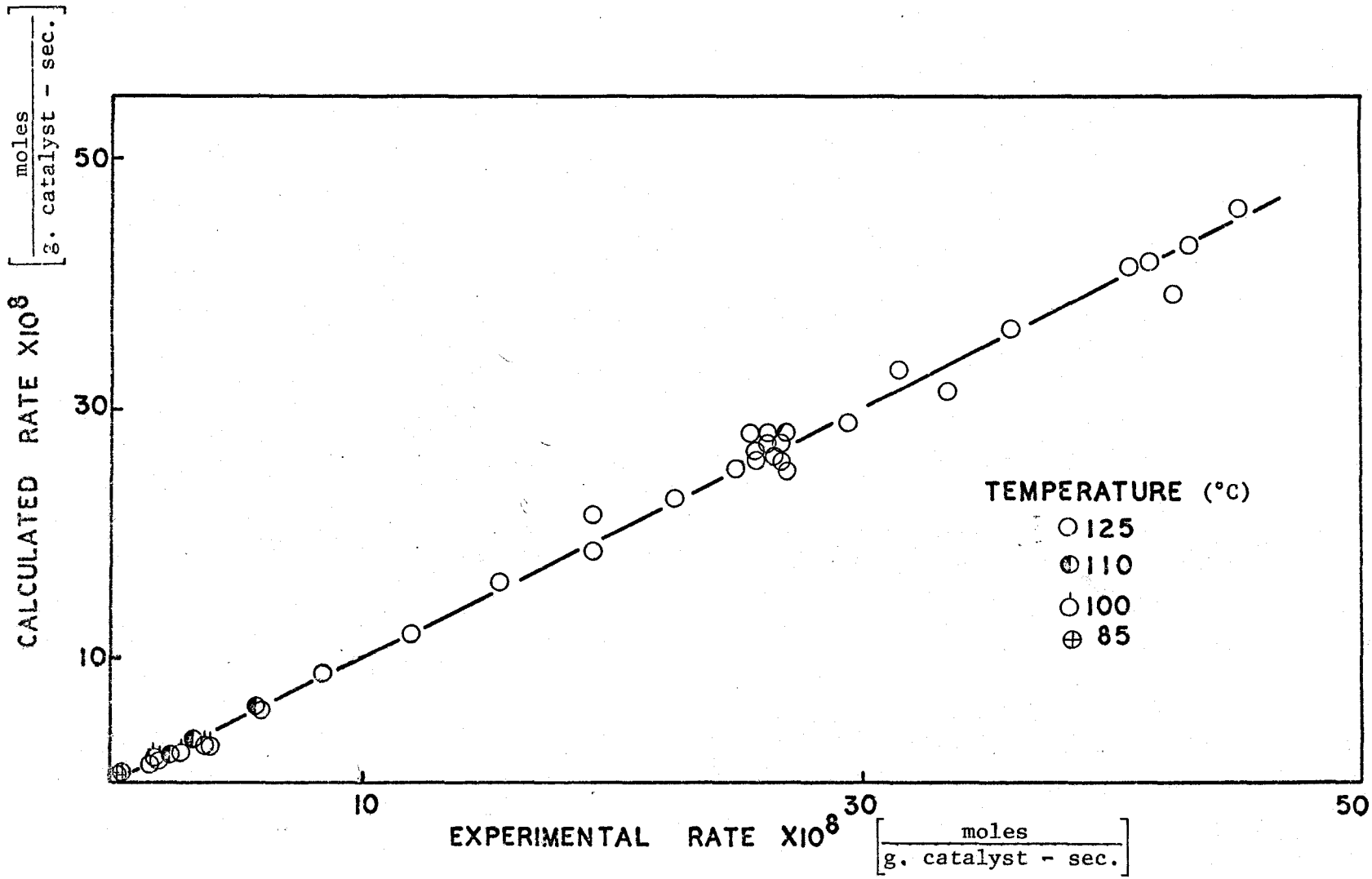

Figure 4-4: Comparison of Experimental and Calculated Rates of n-Butane Hydrogenolysis (Equation 4-2)

the analysis of data at 800 torr, the rate should decrease with increasing pressure. This decrease was observed; however, the rates at 1100 and 1400 torr were much lower (by a factor of four) than would be predicted from the previous analysis. Furthermore, an attempt to correlate all the data at 125°C and the three pressure levels by either Equation 4-1 or Equation 4-2 failed due to a lack of fit and correlation of the error with the total pressure. Therefore a more complex mechanistic model was proposed.

Kemball has described the application of the basic Langmuir equation to the dissociative adsorption of hydrogen and saturated hydrocarbons (9). If the majority of the surface is covered by hydrogen atoms and hydrocarbon species which are only slightly dissociated, the fractional surface coverage by hydrogen will be

$$\theta_H = \frac{K_H P_H^{\frac{1}{2}}}{(1 + K_H P_H^{\frac{1}{2}} + K_{HC} P_C / P_H^{\frac{1}{2}})} \qquad (4\text{-}4)$$

where: θ_H - fractional surface coverage by hydrogen atoms

K_H, K_{HC} - adsorption equilibrium constants

P_H - partial pressure of hydrogen

P_C - partial pressure of hydrocarbons

It has been assumed that the competitive effects of all the hydrocarbon species for surface sites are similar enough that they can be gathered into a single factor, P_C, which is the sum of the partial pressures of all the hydrocarbons present.

If the reactive adsorbed C_4 species has lost n hydrogen atoms on adsorption, then its fractional surface coverage will be

$$\theta_{C_4} = \frac{K P_{C_4} / P_H^{n/2}}{(1 + K_H P_H^{\frac{1}{2}} + K_{HC} P_C / P_H^{\frac{1}{2}})} \qquad (4\text{-}5)$$

where: θ_{C_4} - fractional coverage of reactive C_4 species

K - adsorption equilibrium constant

P_{C_4} - butane partial pressure

Assuming that the surface cracking reaction involves the interaction of an adsorbed hydrogen atom and hydrocarbon species, the rate is given by

$$r = k' \theta_H \theta_{C_4} \qquad (4\text{-}6)$$

By substituting Equation 4-4 and Equation 4-5, the overall rate becomes

$$r = \frac{k P_{C_4} P_H^{\frac{1-n}{2}}}{(1 + K_H P_H^{\frac{1}{2}} + K_{HC} P_C / P_H^{\frac{1}{2}})^2} \qquad (4\text{-}7)$$

Equation 4-7 was fitted to the data given in Table D-3 and also the data at 125°C and 800 torr by nonlinear regression analysis. The equation was first linearized by inversion and examined using linear regression analysis to formulate initial estimates of the parameters. These were then improved using the equation as it appears and searching by Rosenbrock technique.

The results of these calculations appear in Table 4-4. The

TABLE 4-4

Analysis of n-Butane Rate Data at Various Total Pressures

Number of Observations:	41
Residual Degrees of Freedom:	37
Residual Sum of Squares:	139
Residual Root Mean Square:	1.94

Parameter	Estimated Value	
k	25.4	(mole-torr^2/g. catalyst - sec.)
K_H	0.0685	(torr$^{-0.5}$)
K_{HC}	0.133	(torr$^{-0.5}$)
n	7.06	

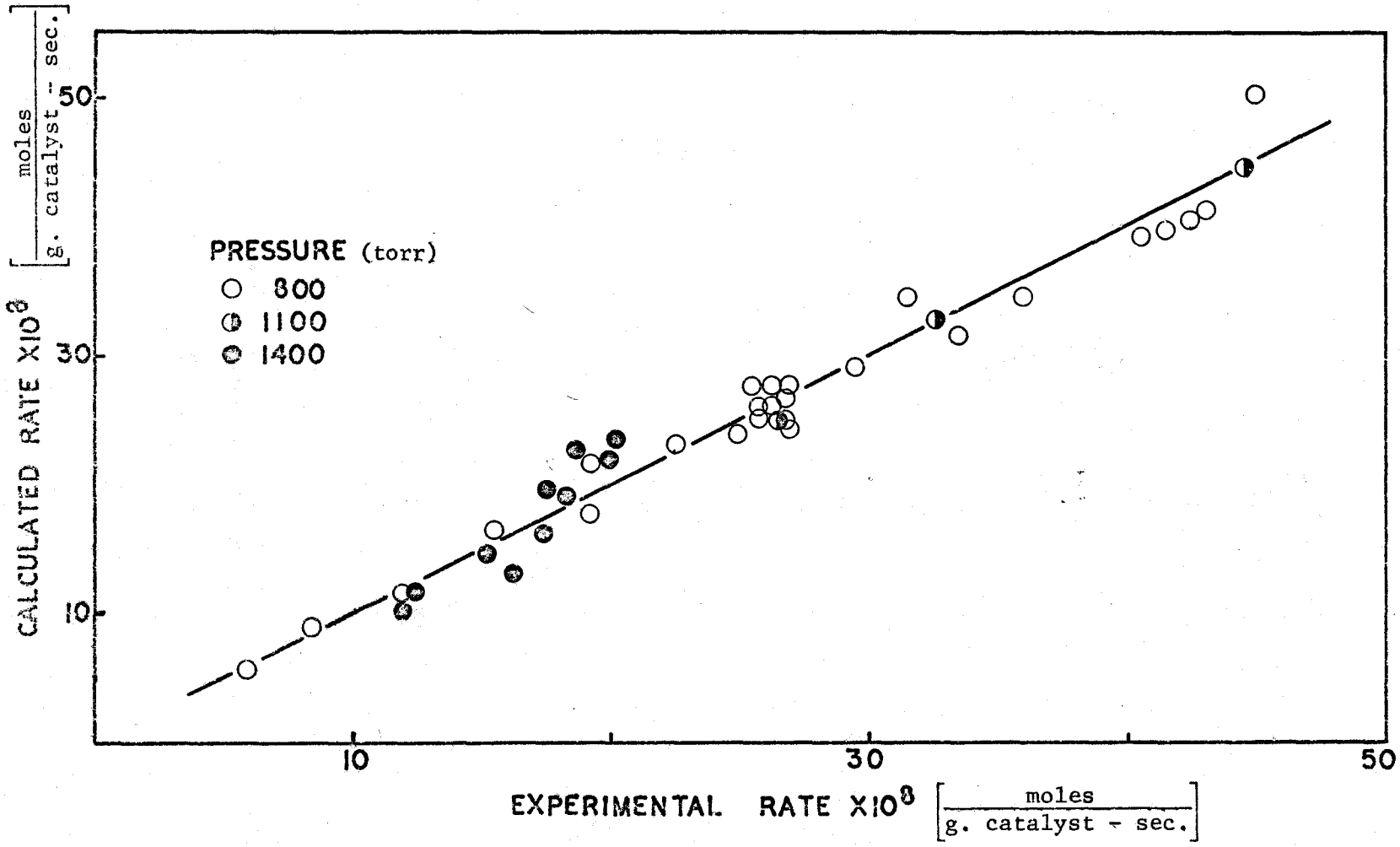

Figure 4-5: Comparison of Experimental and Calculated Rates of n-Butane Hydrogenolysis at Various Total Pressures

values of the equilibrium constants indicate that the surface was mostly covered with hydrogen but with significant amounts of adsorbed hydrocarbons also present. The value of n corresponds to the loss of seven hydrogen atoms on adsorption. The calculated and experimental rates are in good agreement at all total pressure levels (Figure 4-5).

4.4 Isobutane

The data for isobutane hydrogenolysis were taken at a total pressure of 800 torr and over the following range of experimental variables (Table D-4):

Temperature:	105°, 115°, 125°, 130°C
Hydrogen Pressure:	480 to 780 torr
Butane Pressure:	5 to 150 torr
Butane Conversion:	5 to 75%
Hydrogen/Hydrocarbon:	30/1 to 1.5/1

Due to a failure of the bearings in the system, it was necessary to change the catalyst charge after five experiments. The second batch of catalyst had an activity much greater than the first but this was accounted for by including a step change of activity in the rate correlation (see Equation 4-8). This change in activity took the form of an increased rate constant. Other small changes in activity were corrected for by using standard runs.

Two experiments for which the isobutane concentrations were very large (greater than 175 torr) evidenced abnormally low rates of reaction. These activity changes were reversible and after treatment in flowing hydrogen the catalytic behavior returned to normal. Possibly,

this deactivation was due to deposition of carbonaceous material on the catalyst as has been reported by Hahn and Petersen (71), and Anderson and Avery (15). Neither of these experiments was used in the kinetic analysis.

The data were fitted to the following rate equation.

$$\log r = \log A - \frac{E}{2.303RT} + a \log P_H + b \log P_{iC_4} + \Delta \phi \qquad (4\text{-}8)$$

where: ϕ - dummy variable for activity change having a value 1 for the first charge and 0 for the second charge

Δ - parameter corresponding to the size of the change in activity

The results of this linear regression analysis are listed in Table 4-5. The activation energy was much smaller than for n-butane and the reaction orders were also slightly different with the butane exponent positive but smaller and the hydrogen exponent negative and also diminished. The overall rate of reaction was approximately an order of magnitude less than that for n-butane. The experimental and calculated rates are compared in Figure 4-6.

At each temperature an average rate constant was calculated using the correlation. These values appear in Table 4-6 and Figure 4-7.

The rate data were also fitted to Equation 4-2 using the method outlined in the section on n-butane. The best estimates of the five parameters are shown in Table 4-7. The value of α corresponds to 4 to 5 hydrogen atoms lost on the adsorption of isobutane, slightly less than for n-butane. The activation energy was slightly less than for the

TABLE 4-5

Analysis of Isobutane Rate Data Using Equation 4-8

Number of Observations:	35
Residual Degrees of Freedom:	30
Total Sum of Squares:	2.46
Residual Sum of Squares:	0.030
Residual Root Mean Square:	0.032

Parameter	Estimated Value	95% Confidence Interval
log A	13.63	±0.60 (mole-torr$^{-0.08}$/g. catalyst - sec.)
E	36.2	±0.9 (kcal./mole)
a	-0.66	±0.19
b	0.74	±0.03
Δ	-0.631	±0.022

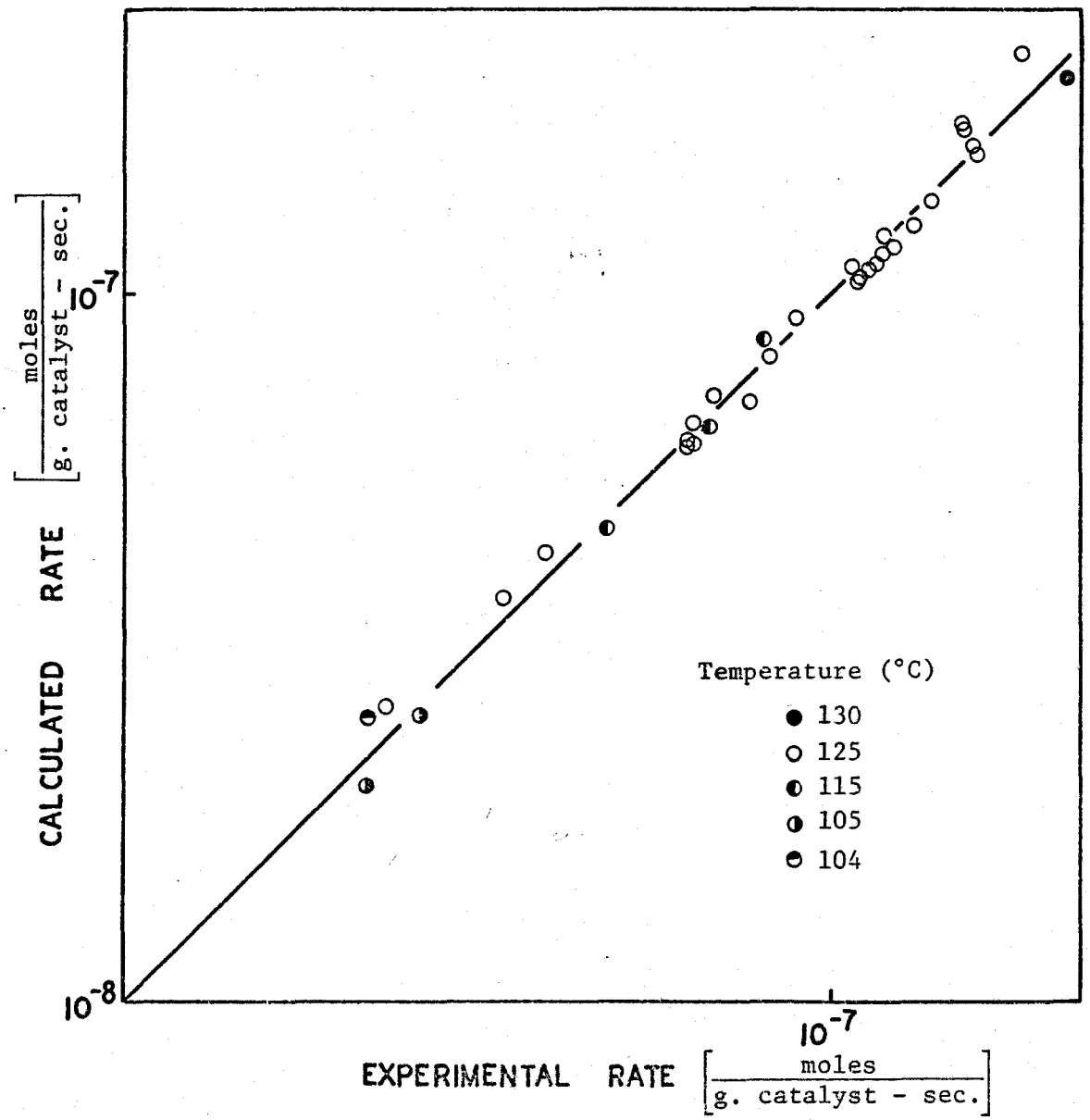

Figure 4-6: Comparison of Experimental and Calculated Rates of Isobutane Hydrogenolysis (Equation 4-8)

TABLE 4-6

Rate Constants for Isobutane Hydrogenolysis

Temperature (°C)	$\left[\frac{\text{Rate Constant}}{\text{mole-torr}^{-0.08}}{\text{g. catalyst - sec.}}\right]$
130	1.06×10^{-6}
125	5.63×10^{-7}
115	1.77×10^{-7}
105	5.43×10^{-8}
104	3.89×10^{-8}

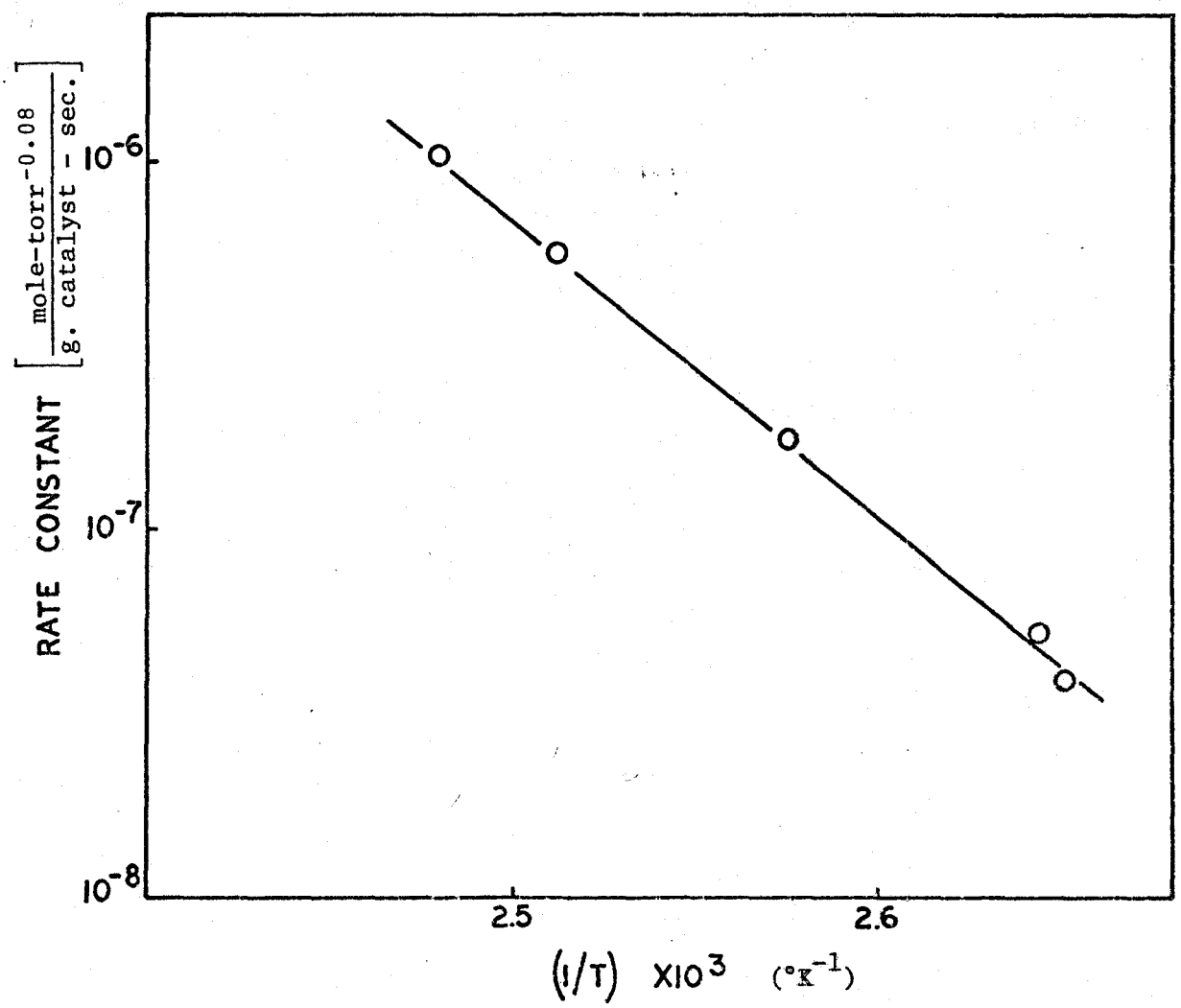

Figure 4-7: Arrhenius Plot for Isobutane Hydrogenolysis

TABLE 4-7

Analysis of Isobutane Rate Data Using Equation 4-2

Number of Observations:	30
Residual Degrees of Freedom:	25
Residual Sum of Squares:	11.8
Residual Root Mean Square:	0.69

Parameter	Estimated Value	
α (or $n/2$)	2.34	
A	7.05×10^{14}	(mole-torr$^{0.34}$/g. catalyst - sec.)
E	35.4	(kcal./mole)
K	8.95×10^{4}	(torr$^{1.34}$)
ΔH	0.50	(kcal./mole)

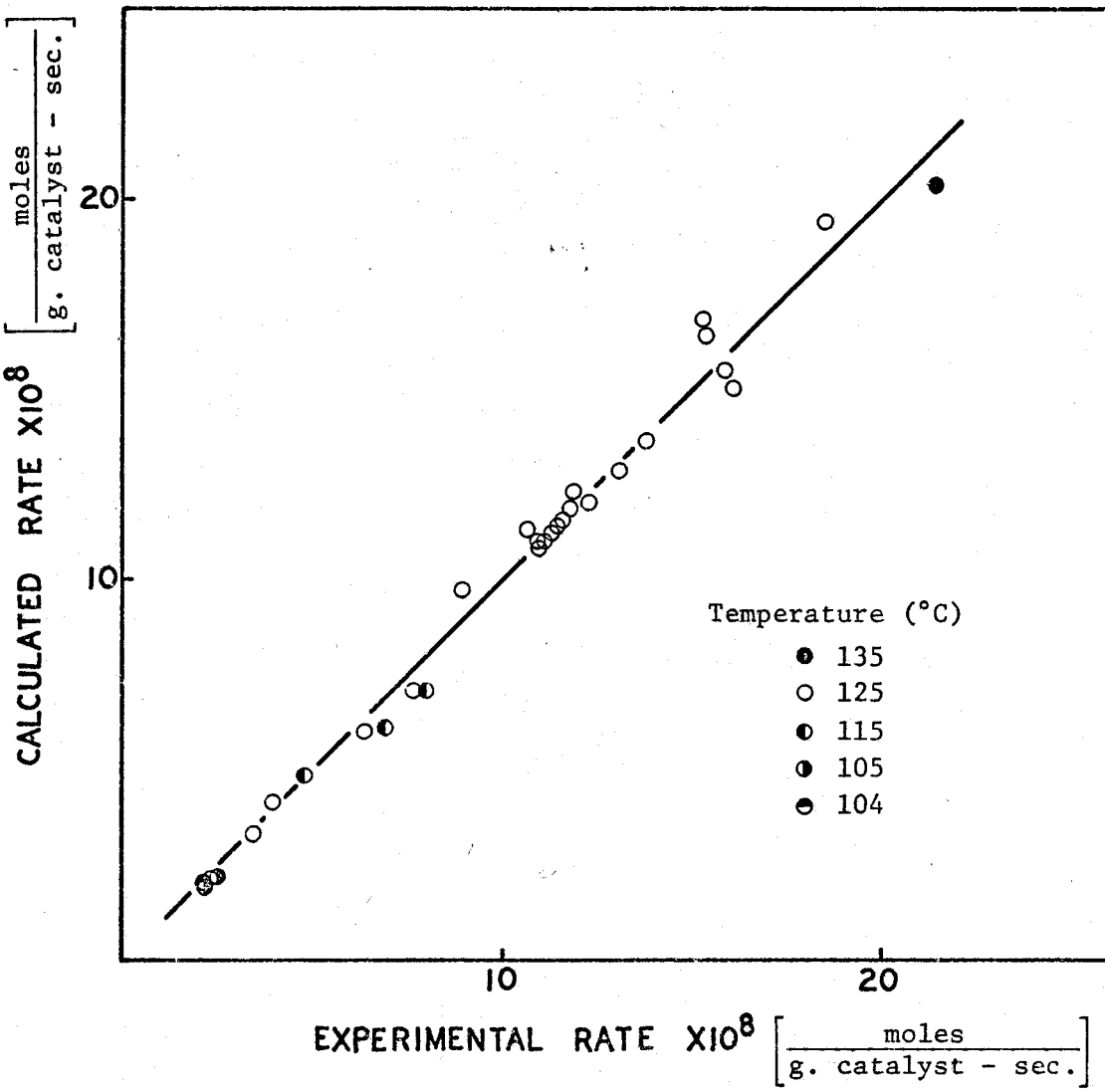

Figure 4-8: Comparison of Experimental and Calculated Rates of Isobutane Hydrogenolysis (Equation 4-2)

power-function rate equation and the adsorption equilibrium was endothermic, ΔH = 0.5 kcal. per mole. The calculated and observed rates are compared in Figure 4-8.

4.5 Isopentane

The rate data for isopentane cracking were mostly taken at a total pressure of 800 torr but with a few experiments at 850 torr to give a wider variation in hydrogen partial pressures. The following range of experimental variables was covered:

Temperature:	90°, 100°, 109°, 110°, 120°C
Hydrogen Pressures:	500 to 800 torr
Isopentane Pressure:	20 to 110 torr
Isopentane Conversion:	5 to 75%
Hydrogen/Hydrocarbon:	25/1 to 2/1

The data are presented in Table D-5.

Standard runs were performed intermittently throughout the experimental program with n-butane as the reactant. Using the correlation for rate already presented for n-butane (Table 4-1), the rate constants were calculated and these were subsequently used to correct the isopentane rates to a constant activity. The catalytic activity remained very nearly constant throughout the experimental period so that few corrections were required and these were nearly always small, less than 5%. The activity of the catalyst sample used in these tests was approximately four times larger than that of the sample used for the n-butane experiments.

TABLE 4-8

Analysis of Isopentane Rate Data Using Equation 4-1

Number of Observations:	29
Residual Degrees of Freedom:	25
Total Sum of Squares:	3.54
Residual Sum of Squares:	0.026
Residual Root Mean Square:	0.032

Parameter	Estimated Value	95% Confidence Interval
log A	19.59	±0.58 (mole-torr$^{0.39}$/g. catalyst - sec.)
E	43.2	±0.9 (kcal./mole)
a	-1.07	±0.19
b	0.68	±0.04

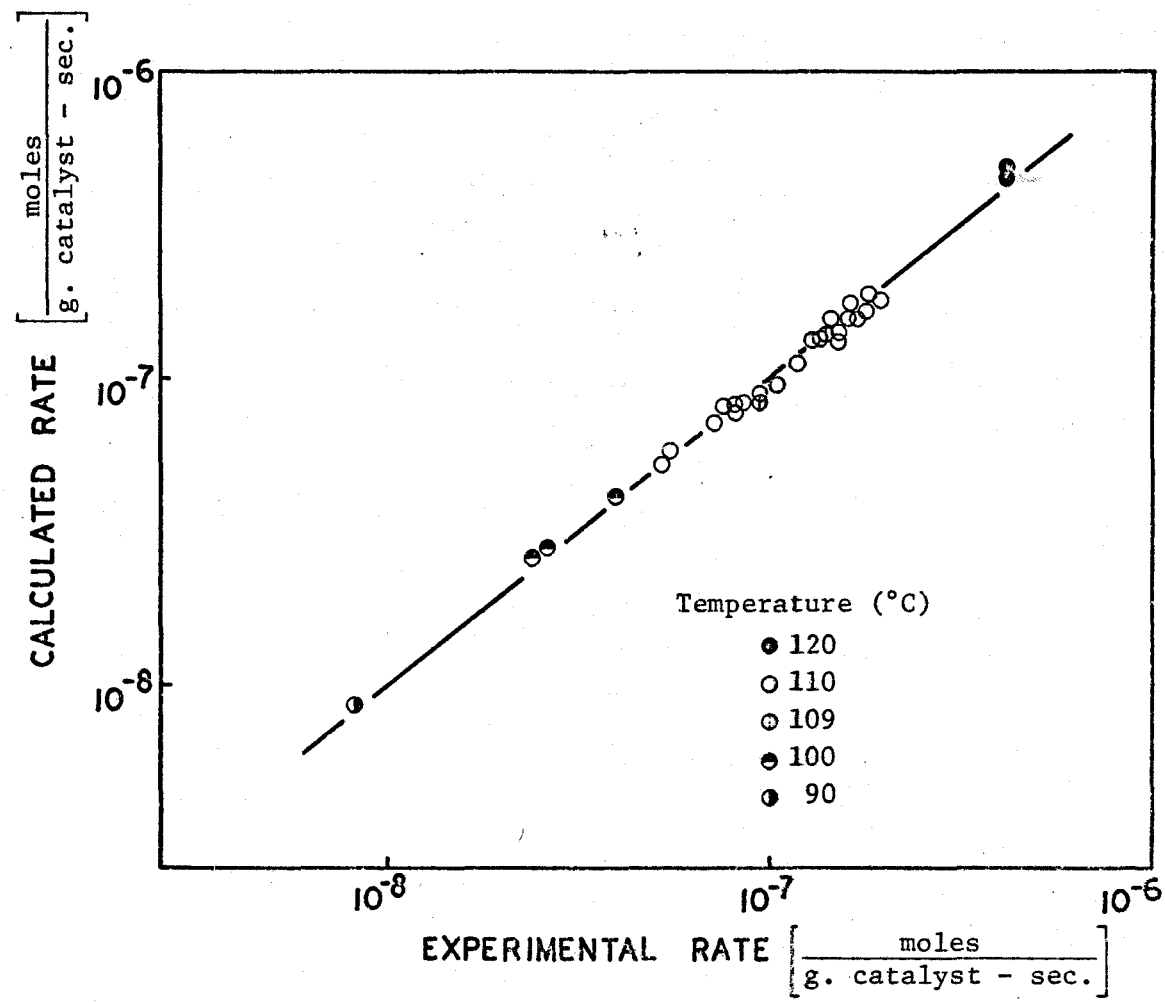

Figure 4-9: Comparison of Experimental and Calculated Rates of Isopentane Hydrogenolysis (Equation 4-1)

TABLE 4-9

Rate Constants for Isopentane Hydrogenolysis

Temperature (°C)	$\left[\frac{\text{Rate Constant}}{\text{mole-torr}^{0.39}}\right]$ $\left[\text{g. catalyst - sec.}\right]$
120	3.23×10^{-5}
110	8.74×10^{-6}
109	7.79×10^{-6}
100	1.78×10^{-6}
90	3.64×10^{-7}

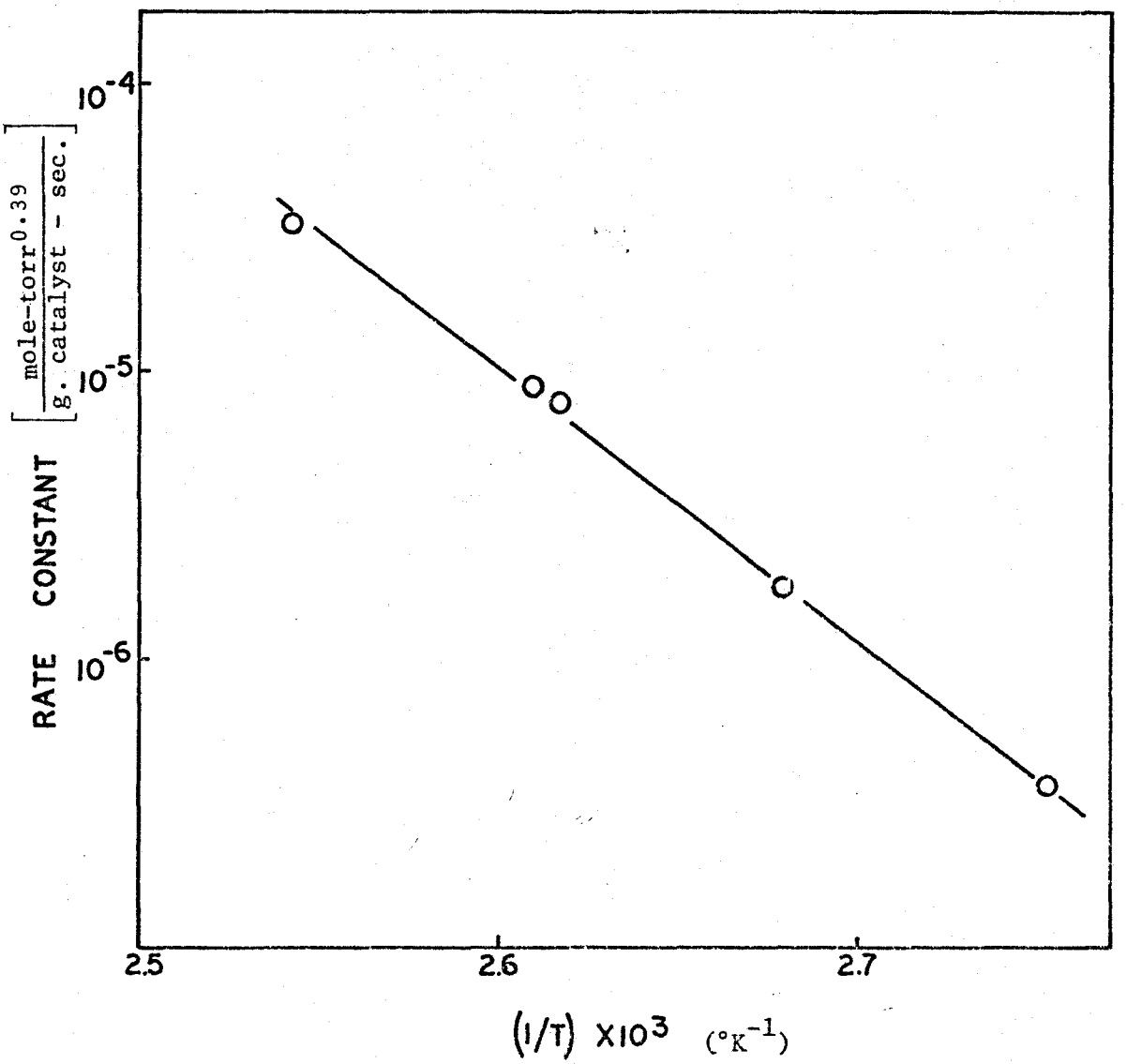

Figure 4-10: Arrhenius Plot for Isopentane Hydrogenolysis

TABLE 4-10

Analysis of Isopentane Rate Data Using Equation 4-2

Number of Observations:	29
Residual Degrees of Freedom:	24
Residual Sum of Squares:	20.6
Residual Root Mean Square:	0.93

Parameter	Estimated Value	
α (or $^{n}/2$)	3.16	
A	7.45×10^{18}	(mole-torr$^{1.16}$/g. catalyst - sec.)
E	37.2	(kcal./mole)
K	4.1×10^{5}	(torr$^{2.16}$)
ΔH	-2.3	(kcal./mole)

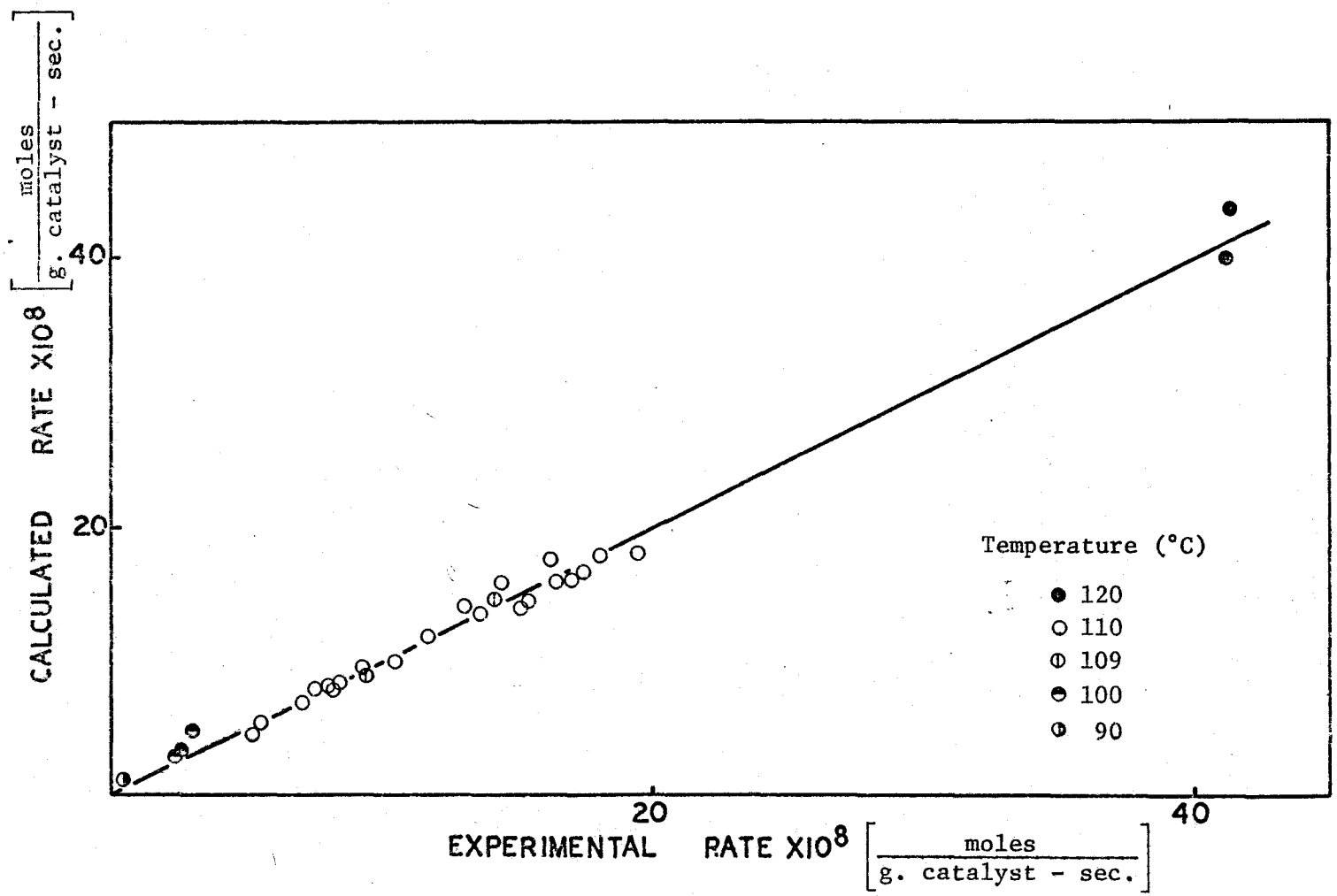

Figure 4-11: Comparison of Experimental and Calculated Rates of Hydrogenolysis of Isopentane (Equation 4-2)

The data have been fitted to Equation 4-1 by linear least squares analysis. The results of these calculations are listed in Table 4-8, and Figure 4-9 is a comparison of the observed and calculated rates. Again, the hydrocarbon exponent was positive and the hydrogen exponent was negative. Both the hydrogen order and the activation energy were intermediate in value between the n-butane and isobutane values. For each temperature, an average rate constant was calculated using the above correlation. The Arrhenius plot appears in Figure 4-10 and the data in Table 4-9.

Equation 4-2 was also examined with this data using a Rosenbrock search technique to locate the best estimates of the parameters. The results of these calculations are presented in Table 4-10. The α value corresponds to six hydrogen atoms being lost on adsorption of isopentane. The activation energy was significantly lower than for Equation 4-1 and the adsorption equilibrium was exothermic by 2.3 kcal. per mole. The experimental and calculated rates are compared in Figure 4-11.

4.6 Neopentane

The hydrogenolysis of neopentane was slow compared to the hydrocarbons previously studied and therefore higher temperatures were required. The following range of experimental conditions was used:

Total Pressure:	800 torr
Temperature:	125°, 135°, 145°, 150°, 155°C
Hydrogen Pressure:	115 to 780 torr
Neopentane Pressure:	5 to 55 torr
Neopentane Conversion:	10 to 75%

TABLE 4-11

Analysis of Neopentane Rate Data Using Equation 4-1

Number of Observations:	28
Residual Degrees of Freedom:	24
Total Sum of Squares:	5.46
Residual Sum of Squares:	0.037
Residual Root Mean Square:	0.039

Parameter	Estimated Value	95% Confidence Interval
log A	16.94	±0.40 (mole-torr$^{-0.02}$/g. catalyst - sec.)
E	43.5	±0.8 (kcal./mole)
a	-0.87	±0.04
b	0.89	±0.02

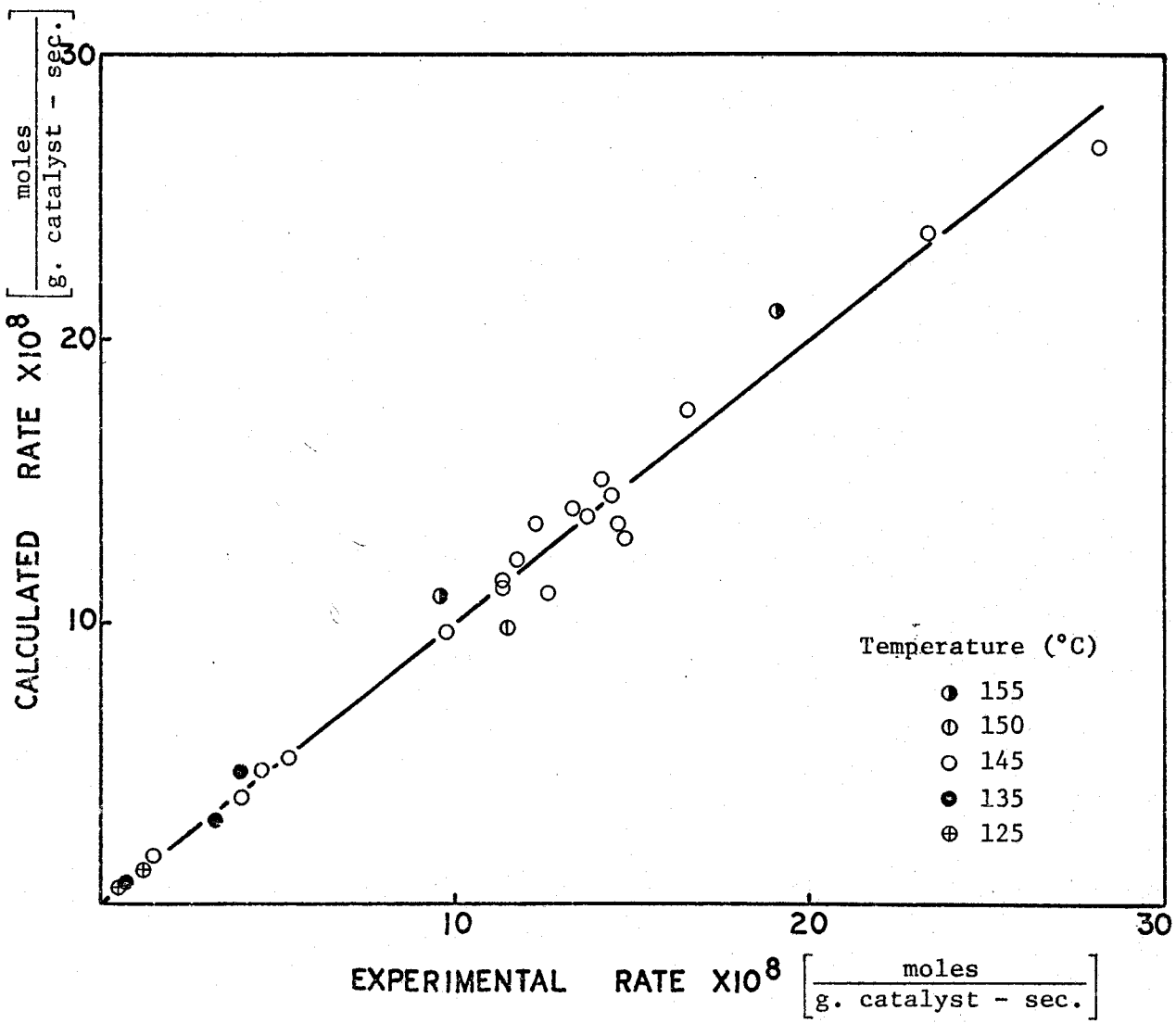

Figure 4-12: Comparison of Experimental and Calculated Rates of Neopentane Hydrogenolysis (Equation 4-1)

TABLE 4-12

Rate Constants for Neopentane Hydrogenolysis

Temperature (°C)	$\left[\frac{\text{Rate Constant}}{\text{mole-torr}^{-0.02}}\right]$
155	4.75×10^{-6}
150	3.39×10^{-6}
145	1.58×10^{-6}
135	4.22×10^{-7}
125	1.14×10^{-7}

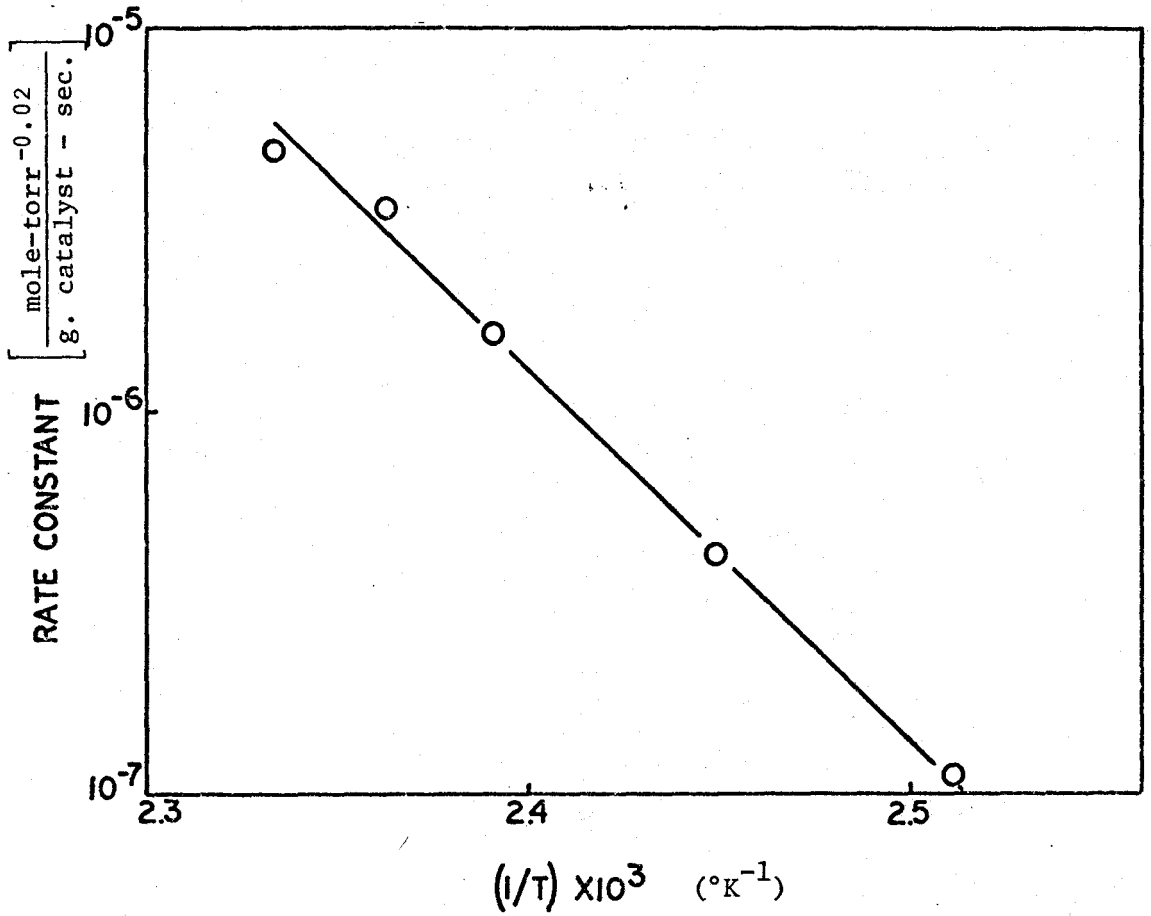

Figure 4-13: Arrhenius Plot for Neopentane Hydrogenolysis

TABLE 4-13

Analysis of Neopentane Rate Data Using Equation 4-2

Number of Observations:	28
Residual Degrees of Freedom:	23
Residual Sum of Squares:	24.9
Residual Root Mean Square:	1.04

Parameter	Estimated Value	
α (or $^{n}/2$)	1.91	
A	9.40×10^{16}	(mole-torr$^{-0.09}$/g. catalyst - sec.)
E	43.7	(kcal./mole)
K	3.67	(torr$^{0.91}$)
ΔH	1.12	(kcal./mole)

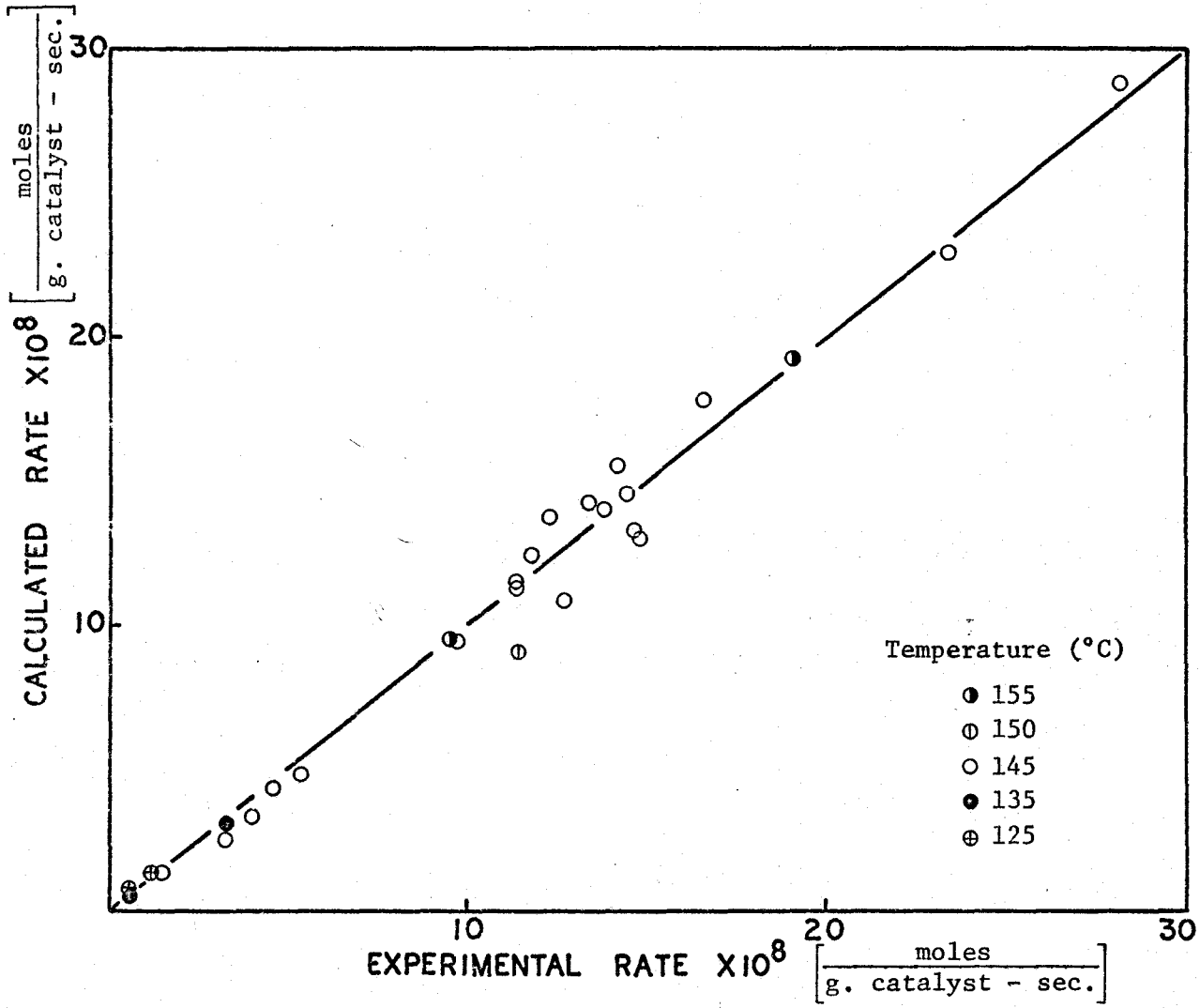

Figure 4-14: Comparison of Experimental and Calculated Rates of Neopentane Hydrogenolysis (Equation 4-2)

Hydrogen/Hydrocarbon: 35/1 to 0.2/1

The data are given in Table D-6.

Equation 4-1 was used to correlate the data by linear least squares analysis and the results of these calculations appear in Table 4-11. The activation energy was nearly the same as for isopentane and the reaction orders followed the usual pattern with the hydrocarbon exponent being positive but less than unity while the hydrogen exponent was negative. Figure 4-12 is a comparison of the calculated and observed rates; the equation was able to correlate the data very well.

For each temperature an average rate constant was calculated using the rate expression and the experimental data. These are in Table 4-12 and Figure 4-13.

Equation 4-2 was also examined with this data using nonlinear least squares analysis as outlined in the section on n-butane. The results of these calculations are tabulated in Table 4-13. The apparent activation energy was nearly the same as for the power-function equation and the adsorption of neopentane was endothermic, ΔH = 1.1 kcal. per mole. The value of α corresponds to about 4 hydrogen atoms being lost on adsorption. A comparison of the observed and calculated rates is shown in Figure 4-14. The fit is good and the parameter values are similar to those estimated for the hydrogenolysis of the other hydrocarbons.

4.7 Order of Reactivity of Hydrocarbons

The preceeding experimental data were collected using several batches of catalyst which had varying activities, and therefore it was

necessary to compare reaction rates over the same catalyst sample to obtain an accurate evaluation of the relative reactivity of the hydrocarbons. Because each of the hydrocarbons obeys a different kinetic expression, i.e., the rates do not vary in exactly the same manner with reactor conditions, unique values of the relative reactivities cannot be determined. However, as an approximation, the ratios of rates have been determined for the following conditions: 600 torr of hydrogen, 30 torr of feed hydrocarbon, and 125°C.

Several experiments were performed with pairs of hydrocarbons over a single catalyst sample; because the effluent concentration could not easily be set at the standard conditions, the data were corrected to these conditions using the correlations of Equation 4-1 previously reported. For ethane the correlation of Sinfelt (4) has been accepted. The relative reactivities based on propane as unity are listed in Table 4-14; propane has been used as a datum level because it appears either as a product or a reactant in all of the experimental studies.

The order of reactivity generally increases with the length of the carbon chain, but the reactivity is decreased somewhat by the presence of branched groups. Neopentane seems to be particularly inactive.

The same order of reactivity has been reported for the deuterium exchange reactions of these hydrocarbons over most transition metals (1) and this order is also similar to those reported by Anderson and Avery for hydrogenolysis over nickel and rhodium films (6).

TABLE 4-14

Relative Rates of Hydrogenolysis

Hydrocarbon	Reactivity
Ethane	0.02
Propane	1.
n-Butane	10.
Isobutane	0.8
Isopentane	9.5
Neopentane	0.04

This scale is based on a propane reactivity of unity.

4.8 Summary and Discussion

The kinetics of hydrogenolysis reactions have usually been reported in terms of the reaction orders with respect to hydrogen and hydrocarbon, and the activation energy (2, 15). Fitting Equation 4-1 to the data for each hydrocarbon has simultaneously estimated these parameters; a summary of the results is presented in Table 4-15.

In each case, the hydrocarbon order was positive and had a value between 0.7 and 1.0, indicating a low surface coverage by the adsorbed hydrocarbon species (72). The hydrogen orders were negative with values ranging between -0.66 and -1.5. Because the adsorption of the hydrocarbons is dissociative, an increase in the hydrogen partial pressure shifts the adsorption equilibrium of the hydrocarbons so that fewer reactive species exist on the surface (73). In this way, the rate of hydrogenolysis is retarded by increased hydrogen concentration.

The mechanism proposed by Cimino, Boudart, and Taylor (16) implies a fundamental significance to the hydrogen and hydrocarbon orders. According to their development, the number of hydrogen atoms lost by the adsorbing hydrocarbon is given by

$$n = 2(1 - a) / b \qquad (4\text{-}9)$$

where: n - number of hydrogen atoms lost

a, b - hydrogen and hydrocarbon orders

The calculated values of n appear in Table 4-15. For the straight chain hydrocarbons (isopentane is included in this group because 85% of the cracking occurred at the carbon-carbon bond far removed from the branched

TABLE 4-15

Summary of Parameters from the Analysis of Equation 4-1

Hydrocarbon	Temperature (°C)	Pre-exponential Factor (Log A)	Activation Energy (kcal./mole)	Reaction Orders		Hydrogen Atoms Lost (n)
				Hydrogen	Hydrocarbon	
Propane	125	—	—	-1.5	1.	5.
n-Butane	85-125	22.17	48.1	-1.35	0.91	5.2
Isobutane	105-130	13.63	36.2	-0.66	0.74	4.4
Isopentane	90-120	19.59	43.2	-1.07	0.68	6.0
Neopentane	125-155	16.94	43.5	-0.87	0.89	4.2

group - see Section 5.5), the number of hydrogen atoms lost was between five and six, but for the branch-chain hydrocarbons this number was near four. For a ruthenium catalyst, ethane has been reported to lose six hydrogen atoms on adsorption (4), and propane to lose five (33). The similarity of the reaction orders for ethane, propane, and n-butane hydrogenolysis strongly suggests that a common intermediate exists for these reactions. Since, in the case of ethane, a loss of six hydrogen atoms must produce a carbon structure devoid of hydrogen, possibly propane and n-butane also adsorb at two adjacent carbon atoms and these carbons are stripped of their hydrogens, i.e., approximately five hydrogen atoms are lost. Under this supposition, isobutane would be able to give up four hydrogen atoms (the predicted value from kinetics is 4.4), while neopentane is unable to adsorb at two adjacent carbons, explaining its unusually low rate of cracking. This simple picture seems to fit the observations but is far from conclusive.

The activation energies were between 35 and 50 kcal. per mole. There appears to be a relationship between the activation energies and the hydrogen exponent for the series of hydrocarbons (Figure 4-15); the data of Tajbl for the hydrogenolysis of ethane and propane over supported ruthenium shows the same behavior (33). A similar trend has also been reported for the hydrogenolysis of ethane over supported copper, cobalt, nickel, and platinum (20). The apparent activation energy is composed of the energy required to rupture the carbon-carbon bond in the rate-limiting step and the heat of adsorption. Sinfelt has proposed that the adsorption of the hydrocarbon is endothermic, and that the endothermicity

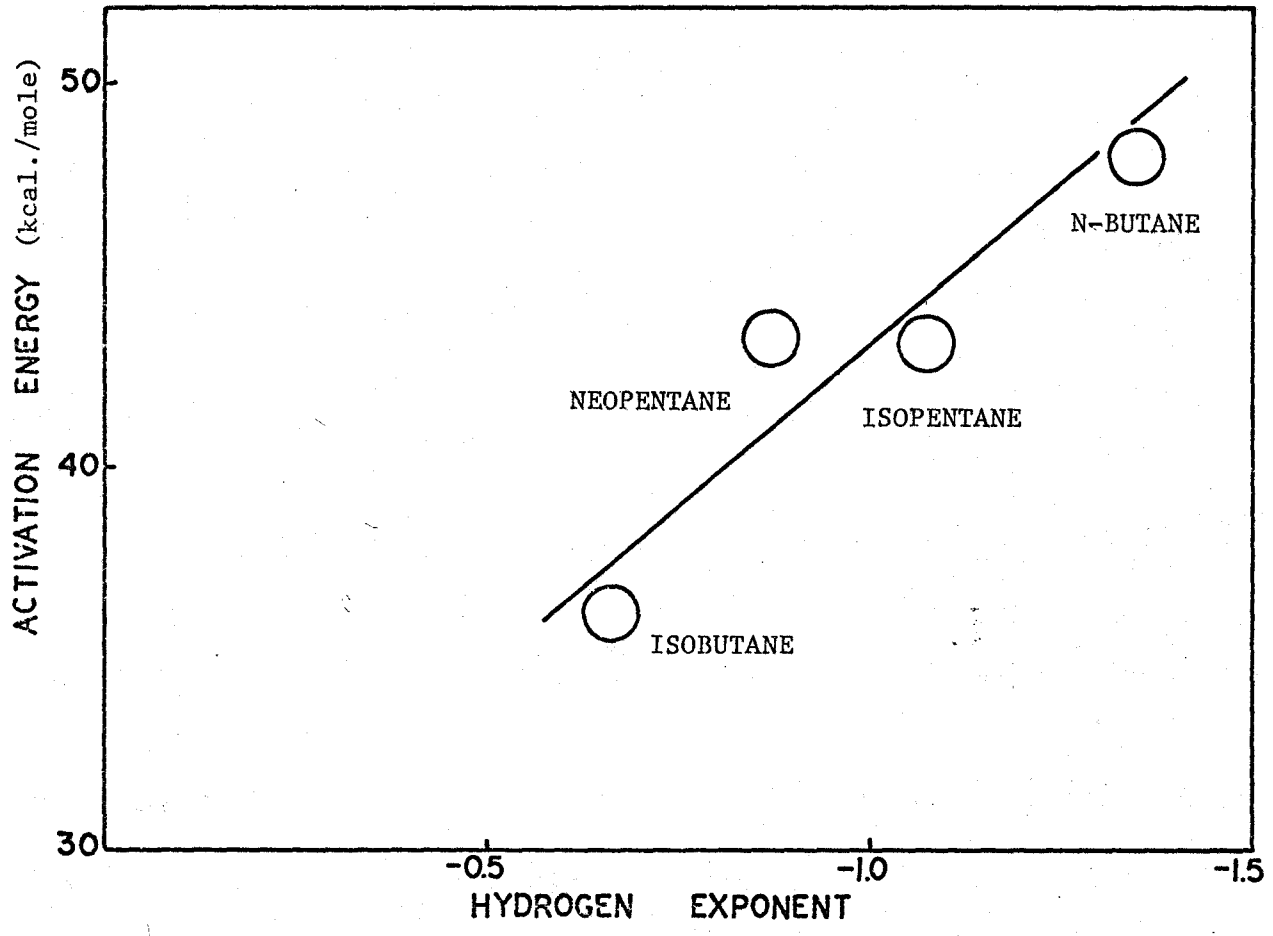

Figure 4-15: The Relationship Between the Activation Energy and the Hydrogen Exponent

increases as the hydrogen exponent becomes more negative.

The relative reactivities of the hydrocarbons can be examined in light of the parameter values. As has previously been described, the order of reactivity was

n-Butane, Isopentane > Propane, Isobutane > Ethane, Neopentane

For the straight-chain hydrocarbons, the rate of hydrogenolysis increased with increasing length of the chain, reflecting a decrease in the strength of the carbon-carbon bonds broken in the rate-limiting step. Ethane, propane, and n-butane have carbon-carbon strengths of 83, 82, and 79 kcal. per mole, respectively (74). The work of Tajbl indicates that the increase in reactivity from ethane to propane was due to a decrease in the activation energy and that the pre-exponential factor remained nearly constant (33). The bond strength of the carbon-carbon bonds in the branch-chain hydrocarbons are lower than those for straight-chain hydrocarbons and the activation energies were also lower (Table 4-15). With neopentane the decrease in activation energy was not as great as with isobutane because neopentane cannot adsorb at two adjacent carbons and the concerted effect of weakening the carbon-carbon bond by adsorption on the catalyst is not as great. There was no corresponding increase in reactivity with decreasing activation energies for the branch-chain hydrocarbons because the pre-exponential factors also decreased. This effect was most obvious for isobutane which had a pre-exponential factor lower by a factor of 10^9 than that of n-butane, presumably due to some steric effect which may have interfered with adsorption of the hydrocarbon or with the interaction of the adsorbed species and hydrogen.

With isopentane the decrease in the pre-exponential factor was not as great because most of the cracking occurred at the carbon-carbon bond far from the branched group (see Section 5.5). The neopentane pre-exponential factor was greater than that for isobutane, indicating that α-γ adsorption was not as greatly hindered by branched groups; however, the hydrogenolysis rate was much lower due to a larger activation energy. The order of reactivity is qualitatively accounted for in terms of the strength of the carbon-carbon bonds and steric effects.

The order of reactivity can also be examined in a manner analogous to that proposed by Voge and Adams for the catalytic oxidation of olefins (75). They used partial rate factors to calculate the overall rate as the product of individual factors for segments of the molecule. These factors were dependent upon whether the allylic carbon atoms were primary, secondary or tertiary. For the hydrogenolysis reaction, partial rate factors can be defined for the addition of hydrocarbon groups to lengthen the carbon chain; the addition of secondary, tertiary, and quaternary carbons corresponds to rate factors of 50, 40, and 2.5, respectively. These factors must be modified to account for the original length of the carbon chain as is obvious from the observation that propane reacts 50 times faster than ethane but decane reacts only 1.5 times faster than octane (76). For two-carbon and three-carbon chains the rate factors must be divided by 1 and 5, respectively, to give a good fit to the order of reactivity. Now, beginning with ethane which was assumed to have a reactivity of unity, the reactivity of the other hydrocarbons can be estimated by multiplying the appropriate partial

rate factors. The addition of secondary, tertiary, and quaternary carbon groups to form propane, isobutane, and neopentane increases the reactivity by factors of 50, 40, and 2.5. The addition of secondary and tertiary carbon groups to propane to form n-butane and isopentane further increases the reactivity by factors of 10 and 8 (Table 4-16). Although this treatment is highly speculative, a pattern has been found which may prove useful when more hydrocarbons have been studied.

The application of the kinetic data to Equation 4-2 was an effort to examine a theoretical rather than empirical rate equation. Although no significant improvement was observed in the correlation of the reaction rates, the parameter estimates for the series of hydrocarbons were interesting (Table 4-17). The value of the parameter α is directly related to the number of hydrogen atoms lost on the adsorption of the hydrocarbon. The estimates shown in Table 4-17 are very close to those values previously determined from fitting the power-function equation. The apparent activation energies and the pre-exponential factors are also quite similar to those estimated from the analysis of Equation 4-1. The heats of adsorption of the hydrocarbon were small but these parameters were very difficult to estimate accurately due to the functional form of the equation and the nature of the data. The pre-exponential factors for the adsorption equilibrium constant were approximately equal except for neopentane, which may reflect the fact that neopentane cannot adsorb in an α-β manner. The overall values of the adsorption equilibrium constants suggest that the hydrocarbon is only weakly adsorbed.

TABLE 4-16

Order of Reactivity of Hydrocarbons

Hydrocarbon	Experimental Reactivity	Estimated Reactivity
Ethane	1*	1*
Propane	50	50
n-Butane	500	500
Isobutane	40	40
Isopentane	475	400
Neopentane	2.5	2.5

* These scales are based on an ethane reactivity of unity.

TABLE 4-17

Summary of Parameters from the Analysis of Equation 4-2

Hydrocarbon	Hydrogen Atoms Lost on Adsorption	A	Activation Energy (kcal./mole)	K	ΔH (kcal./mole)
n-Butane	5.6	1.8×10^{22}	46.2	7.4×10^{5}	1.1
Isobutane	4.6	7.0×10^{14}	35.4	9.0×10^{4}	0.5
Isopentane	6.3	7.5×10^{18}	37.2	4.1×10^{5}	-2.3
Neopentane	3.8	9.4×10^{16}	43.7	3.7	1.1

The experimental study for n-butane hydrogenolysis at higher total pressures proved that Equations 4-1 and 4-2 could not be extrapolated to higher pressures. Equation 4-7 was developed from consideration of the equilibrium adsorption of the hydrocarbons and hydrogen. This equation was completely satisfactory in correlating the results at several total-pressure levels. Once again the number of hydrogen atoms lost by n-butane on adsorption could be estimated and the value was seven.

Chapter 5

PRODUCT DISTRIBUTION FROM HYDROGENOLYSIS REACTIONS

5.1 Introduction

The hydrogenolysis of paraffins over ruthenium results in a mixture of smaller saturated hydrocarbons. The distribution of these compounds changes with experimental conditions and the form of this change is directly related to the reaction mechanism. Thus, examination of the product distribution is a powerful tool for further elucidation of the nature of the process.

For each of the hydrocarbons studied (propane, n-butane, isobutane, isopentane, and neopentane), the effluent concentrations were measured as a function of conversion of the feed hydrocarbon, temperature, and hydrogen partial pressure. These data have been reported in terms of selectivities, where the selectivity for any particular product is defined as the ratio of the moles of that product formed to the moles of the feed hydrocarbon consumed. Further explanation of this term and its calculation from primary experimental data are given in Appendix B.1.

Because the initial fragments (excluding the C_1 species) from the feed hydrocarbon can crack further to create still smaller products, the selectivities are a function of the extent of reaction. The extent of reaction is measurable in the form of the conversion of the initial hydrocarbon. Higher conversions favour the formation of smaller

paraffins (methane, ethane, etc.); product distributions at very low conversions are representative of the hydrogenolysis of the feed hydrocarbon alone. Reaction networks with both consecutive and parallel reaction paths were proposed and applied to the selectivity versus conversion data.

The reaction networks include the reversible adsorption-desorption of each hydrocarbon and the irreversible splitting of the carbon-carbon bonds of the adsorbed hydrocarbon species to give two smaller adsorbed species. The deuterium exchange reactions of these hydrocarbons substantiate the reversibility of the adsorption-desorption step (1) and the cracking reaction is so highly favoured thermodynamically at these temperatures that it will be essentially irreversible (73). All of the steps of the process were coupled, i.e., no single rate-determining step was assumed. An overall hydrogenolysis reaction in which two or more carbon-carbon bonds are broken (14) can occur if the adsorbed product from a first reaction undergoes a second carbon-carbon bond rupture before desorbing. The frequency of this occurrence depends on the relative rates of desorption and cracking of the adsorbed hydrocarbon species.

Reaction networks in chain destruction processes are in general simpler than those for chain growth processes, i.e., polymerization, because there is a limit to how far the reaction will proceed (methane is the smallest possible product); therefore, fewer simplifying assumptions are required. The networks were solved analytically to develop selectivity equations which were then regressed to the data for

each hydrocarbon using nonlinear least squares. The validity of the reaction mechanism can be determined from the goodness of the fit and the credibility of the estimated values of the parameters.

The product distribution can also be influenced by temperature because the elementary reactions may have different activation energies. A wide variation in the magnitude of this temperature dependence was observed for the various hydrocarbons; however, the direction of change was constant - higher temperatures favoured the formation of smaller products, i.e., more extensive cracking. Similar trends have been reported by Shephard (14), and Kikuchi et al. (36) for the hydrogenolysis of propane and n-pentane over nickel. Data were collected at a number of temperatures for each hydrocarbon and where feasible these data were incorporated into the overall reaction network analysis.

Minor effects of hydrogen pressure on the product distribution were detected but they were of the same order of magnitude as the experimental error involved in measuring the selectivities. Lower hydrogen partial pressures enhanced the formation of smaller products and in this way were similar to an increase in temperature. Presumably, a decrease in hydrogen pressure favoured the surface cracking reactions over desorption. Shephard (14), and Kikuchi and Morita (36) also observed these effects. The inclusion of terms to account for the hydrogen pressure effects met with some success but due to the small nature of the response, the fit was not always a significant improvement over that for reaction networks without hydrogen pressure effects.

In the following sections, each of the hydrocarbons is examined individually, and then the results are summarized in the final section.

5.2 Propane

Ethane and methane are the only possible hydrogenolysis products from propane and in this case, the maximum selectivities for ethane and methane are one and three, respectively. The data were collected at 125°C (Table D-7) and are plotted in Figure 5-1. Nearly equal amounts of each product were formed at low conversions; with increasing conversion, the fraction of methane increased as would be expected if some of the ethane formed were also cracking to methane.

A reaction network involving the reversible adsorption-desorption of each hydrocarbon and the irreversible surface cracking reaction of adsorbed propane and ethane has been proposed (Figure 5-2). This system is described further in Appendix C.2, and the analytical solution is

$$S_2 = \frac{\left[\frac{k_2'}{k_2^* + k_2'}\right]}{\left[1 + \frac{k_2''}{k_3''}\left[\frac{X_3}{1 - X_3}\right]\right]} \qquad (5\text{-}1)$$

$$2\,S_2 + S_1 = 3 \qquad (5\text{-}2)$$

where: S_2, S_1 - selectivity of ethane and methane

k - rate constants (see Figure 5-2)

X_3 - fractional conversion of propane

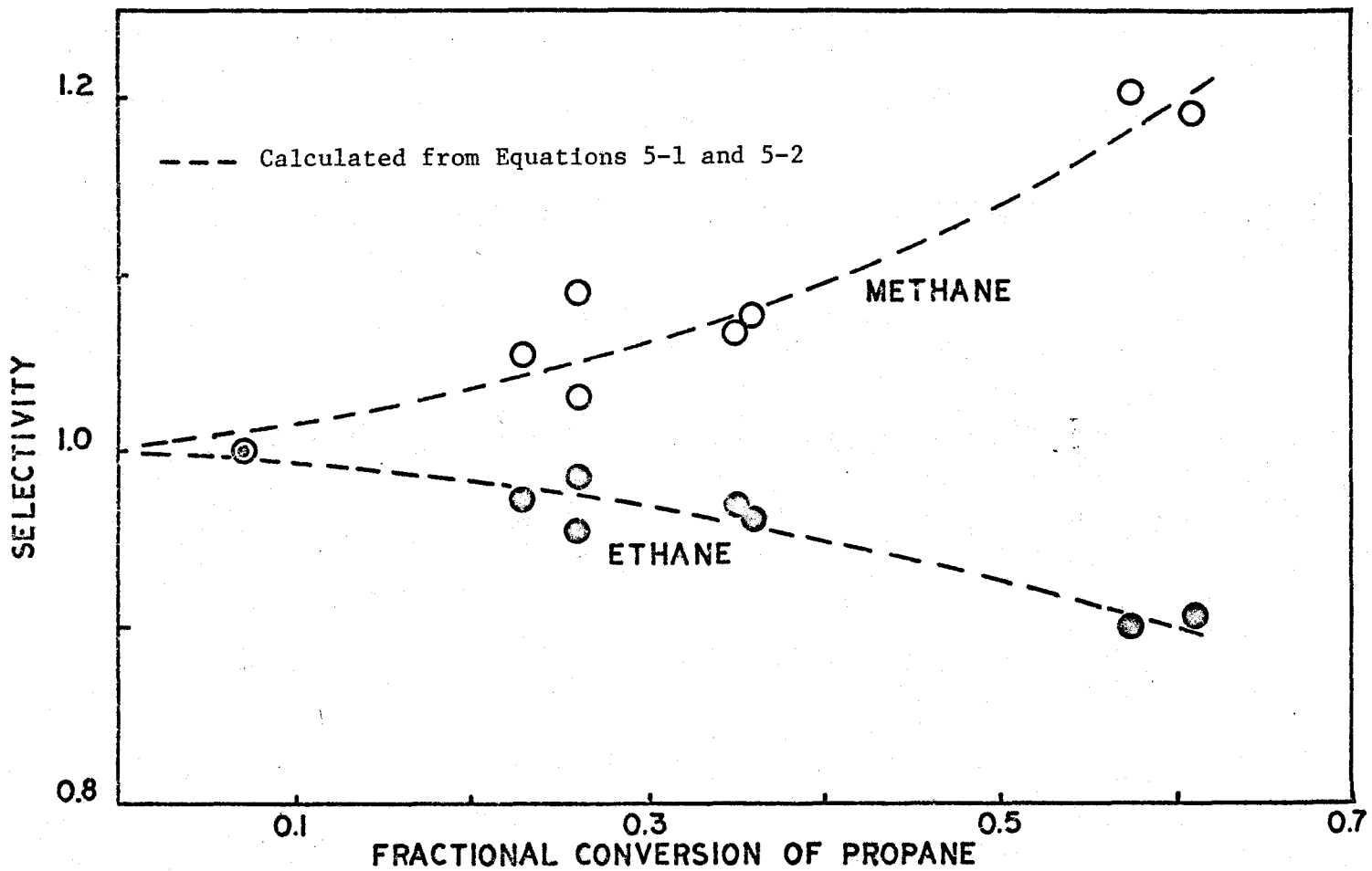

Figure 5-1: Product Distribution from Propane Hydrogenolysis

C_i - gaseous hydrocarbons

C_i^* - adsorbed hydrocarbon species

$$C_3 \underset{k_3'}{\overset{k_3}{\rightleftharpoons}} C_3^*$$

$$C_2 \underset{k_2'}{\overset{k_2}{\rightleftharpoons}} C_2^*$$

$$C_1 \underset{k_1'}{\overset{k_1}{\rightleftharpoons}} C_1^*$$

$$C_3^* \xrightarrow{k_3^*} C_2^* + C_1^*$$

$$C_2^* \xrightarrow{k_2^*} 2\,C_1^*$$

$$k_3'' = \left[\frac{k_3\, k_3^*}{k_3^* + k_3'}\right]$$

$$k_2'' = \left[\frac{k_2\, k_2^*}{k_2^* + k_2'}\right]$$

Figure 5-2:

PROPANE HYDROGENOLYSIS MECHANISM

Equation 5-1 was fitted to the experimental data by nonlinear regression analysis (Appendix B). The initial estimates of the parameters were determined by a grid search and then improved by the Rosenbrock optimization technique. The results of these calculations appear in Table 5-1. The methane selectivities were computed using Equation 5-2 along with the predicted ethane selectivities. The experimental and calculated selectivities are compared in Figure 5-1.

The physical significance of the parameters has been developed in Appendix C. The rate constant k_i'' applies to the overall hydrogenolysis reaction of hydrocarbon "i". Because all the reactions were assumed first order in hydrocarbon, the ratio of the two rate constants (k_i''/k_j'') represents the relative rates of hydrogenolysis of hydrocarbons "i" and "j". The value of the parameter (k_2''/k_3'') indicates that propane reacts 14 times faster than ethane. Similarly, the rate constants k_2' and k_2^* apply to the rates of desorption and cracking of the adsorbed C_2 fragment. The parameter estimate shows that k_2' is much greater than k_2^*, i.e., desorption of the C_2 species occurs much more rapidly than cracking. Therefore, the adsorption-desorption reaction of ethane is nearly at equilibrium.

5.3 n-Butane

Propane, ethane, and methane were formed by the hydrogenolysis of n-butane over ruthenium; no isobutane was observed. The absence of the isomerization reaction allowed each of the butanes to be examined independently without interference from non-cracking reactions.

TABLE 5-1

Propane Product Distribution Analysis

Number of Observations: 8

Temperature: 125°C

Equation 5-1

Residual Sum of Squares: 8.1×10^{-4}

Residual Root Mean Square: 1.2×10^{-2}

Parameter	Estimated Value	95% Confidence Interval
$\left[\frac{k_2'}{k_2^* + k_2'}\right]$	1.0	±0.01
$\frac{k_2''}{k_3''}$	0.07	±0.02

All of the products can be formed directly from the rupture of a single carbon-carbon bond in the n-butane chain. There are two types of carbon-carbon bonds; splitting the central bond produces two ethane molecules and breaking of either terminal bond creates methane and propane. The maximum possible selectivities for propane, ethane, and methane are one, two, and four, respectively.

The product distribution was examined extensively at 125°C and 110°C and 800 torr total pressure (Tables D-8, D-9 and Figures 5-3, 5-4). At low conversions, nearly equal amounts of ethane and methane were formed along with slightly smaller amounts of propane. As the conversion increased, the methane and ethane selectivities increased at the expense of propane, but at very high conversions (90%) the ethane selectivity leveled out.

Experimental results at various other temperatures and total pressures are listed in Tables D-10 and D-11, and plotted in Figure 5-5. A comparison of these data with those previously described shows that the effects of temperature and pressure on the product distribution were minor.

The variation in selectivities with conversion was due to the consecutive reaction of propane and ethane to create still smaller alkanes. However, the product distribution corresponding to the primary cracking of n-butane alone can be examined by extrapolating the curves of selectivity versus conversion to zero conversion. The results are plotted in Figure 5-6. The catalyst was too active to allow low conversion experiments at 125°C but the extension of the selectivity

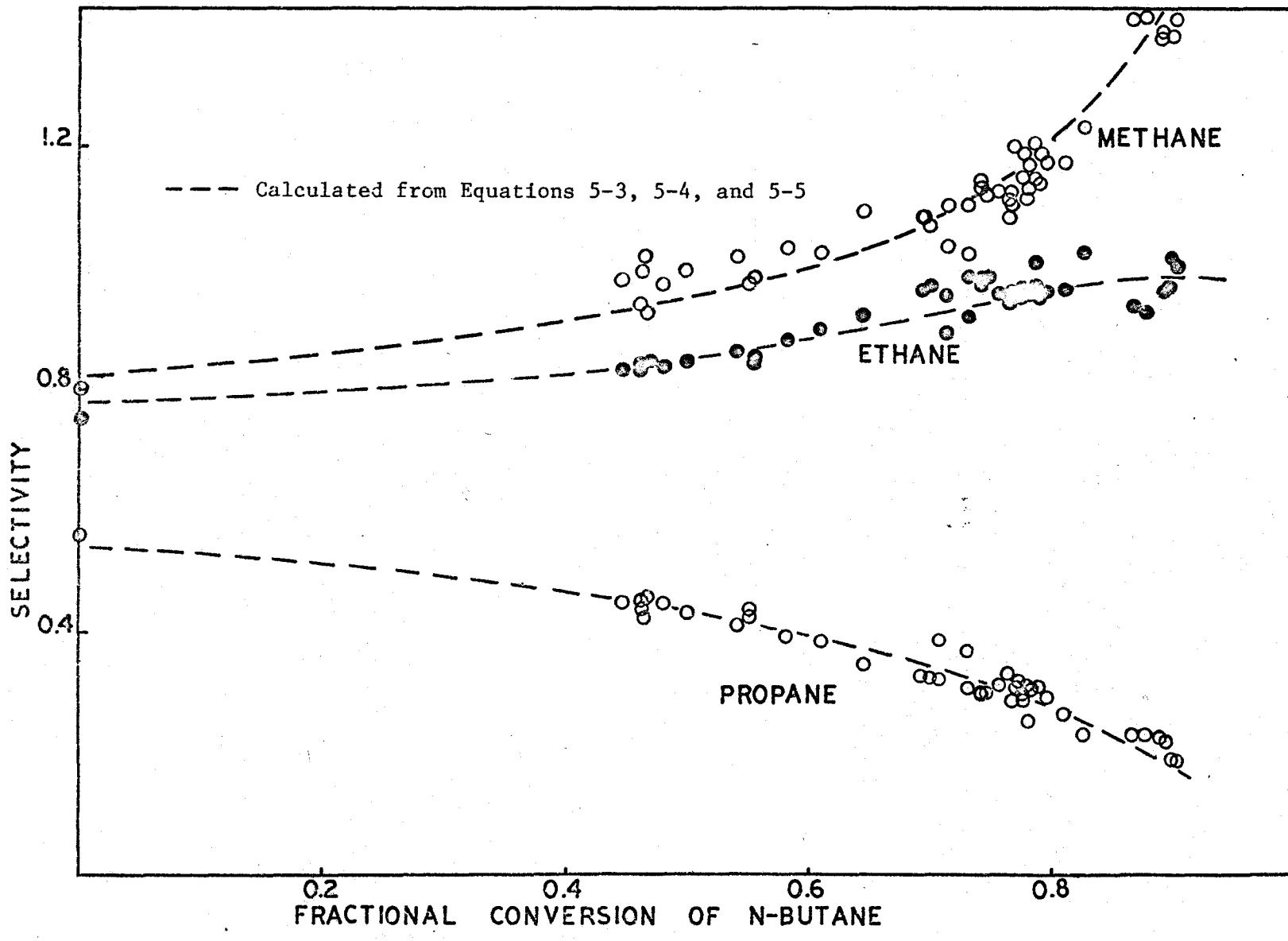

Figure 5-3: Product Distribution from n-Butane Hydrogenolysis (125°C)

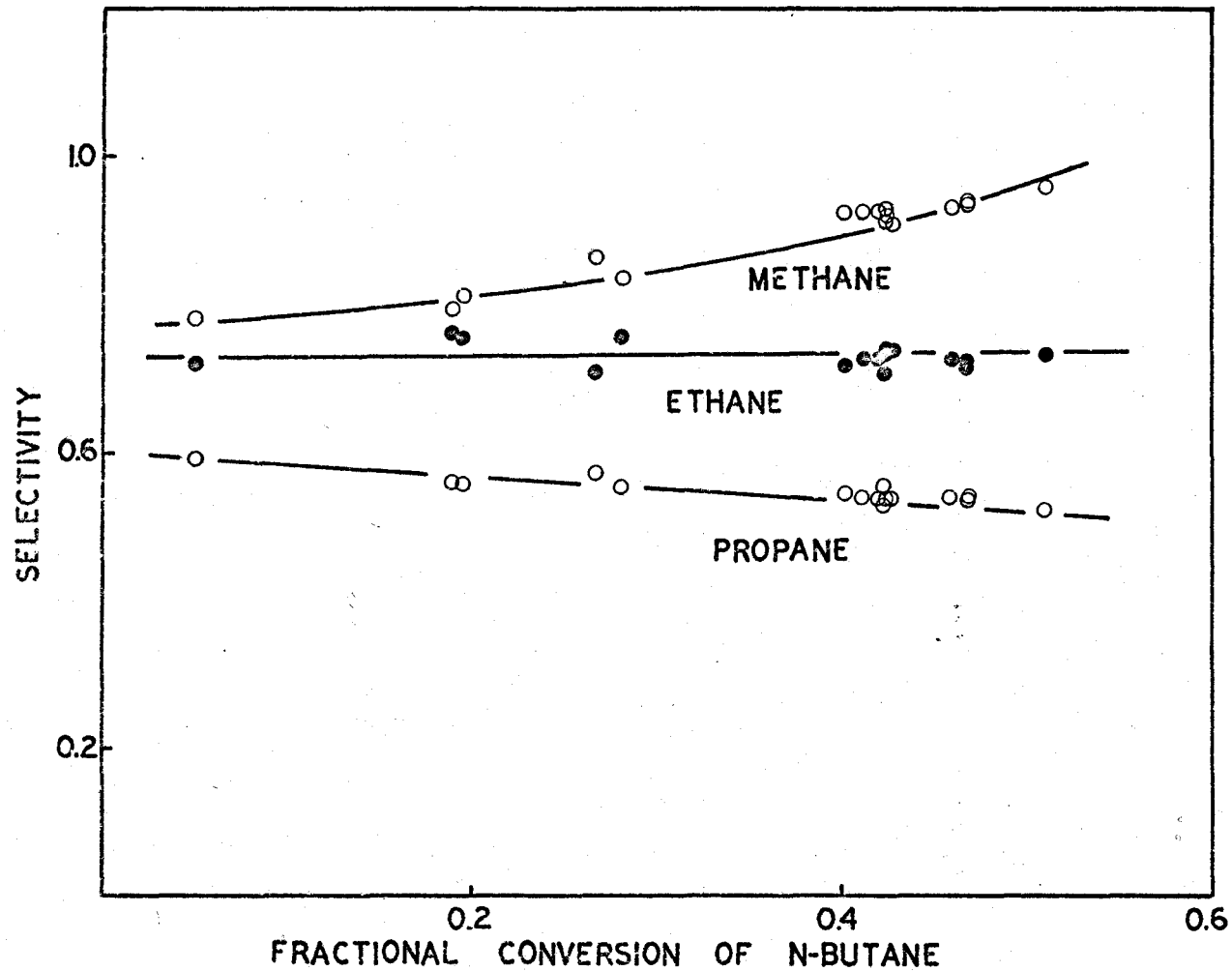

Figure 5-4: Product Distribution from n-Butane Hydrogenolysis (110°C)

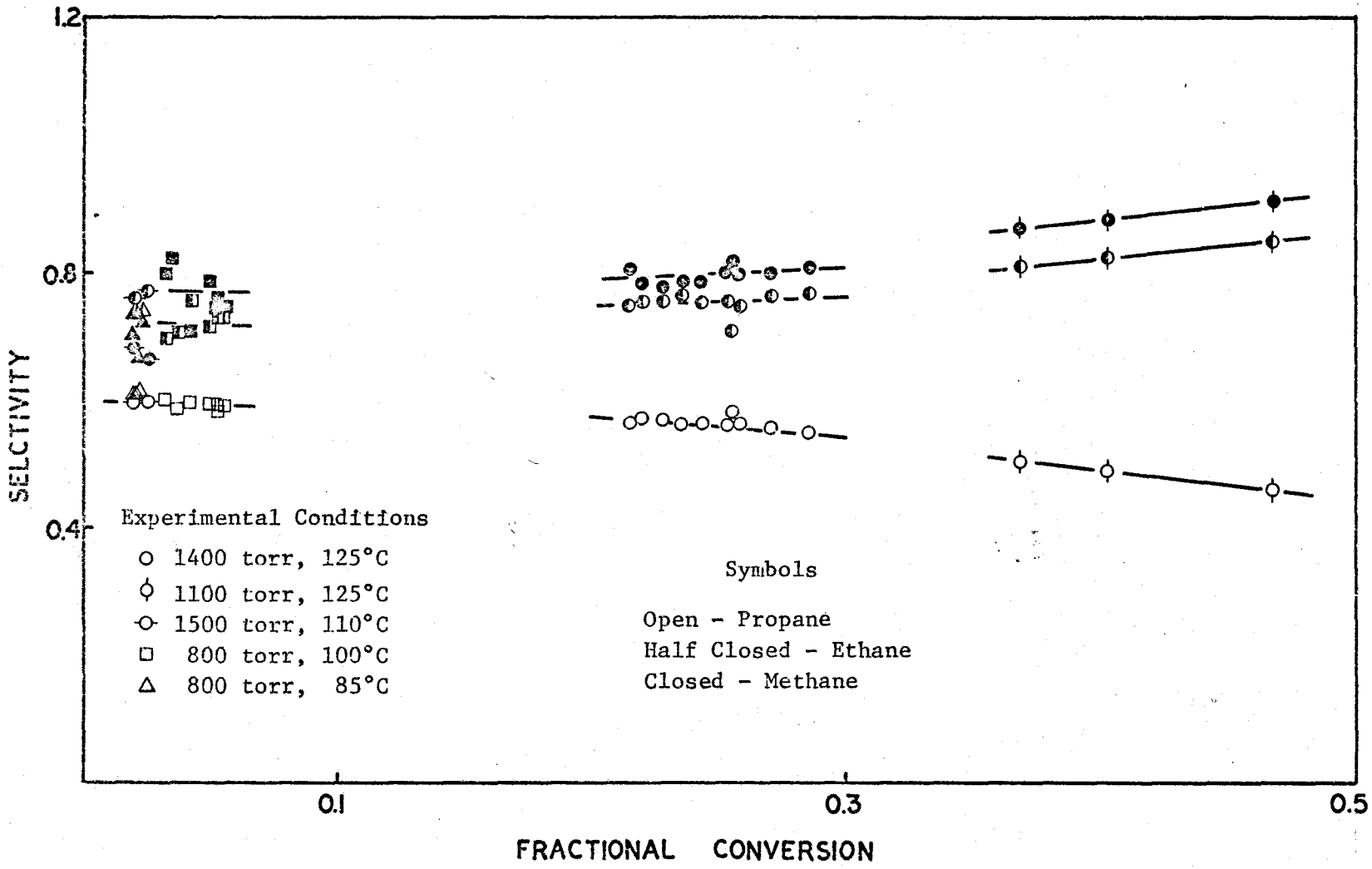

Figure 5-5: Product Distribution from n-Butane Hydrogenolysis

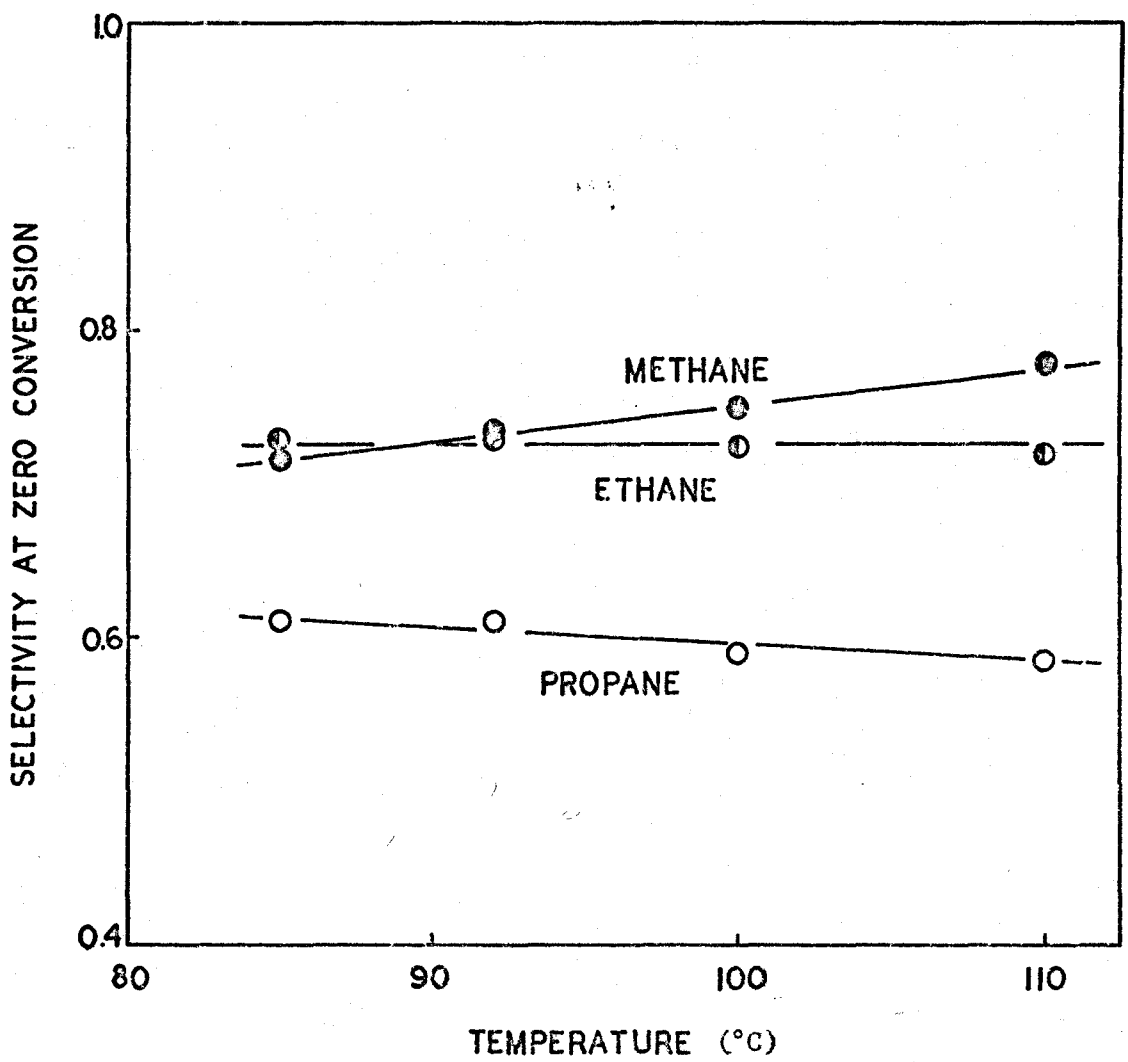

Figure 5-6: Product Distribution at Zero n-Butane Conversion

versus temperature data to 125°C gave very reasonable values (see Figure 5-3). The product distribution was only slightly dependent upon temperature over the range examined, with increasing temperature favouring the formation of methane.

The reaction network proposed for the analysis of n-butane hydrogenolysis is similar to that for propane except that the adsorption-desorption and irreversible cracking reactions for n-butane are included. The reaction steps and the pertinent rate constants are shown in Figure 5-7. The n-butane molecule can break at either of two different types of carbon-carbon bonds. The factor F represents the fraction of butane molecules breaking at the central bond and the remaining fraction, (1-F), must crack at one of the two terminal bonds. The fractional split factor was assumed to remain constant with conversion. This network has been analysed (Appendix C.3) and proved to conform to the following equations:

$$S_3 = \frac{(1-F)\left[\dfrac{k_3'}{k_3^* + k_3'}\right]}{\left[1 + \dfrac{k_3''}{k_{n4}''}\left[\dfrac{X_4}{1 - X_4}\right]\right]} \qquad (5\text{-}3)$$

$$S_2 = \frac{(1+F-S_3)\left[\dfrac{k_2'}{k_2^* + k_2'}\right]}{\left[1 + \dfrac{k_2''}{k_{n4}''}\left[\dfrac{X_4}{1 - X_4}\right]\right]} \qquad (5\text{-}4)$$

$$S_1 + 2\,S_2 + 3\,S_3 = 4 \qquad (5\text{-}5)$$

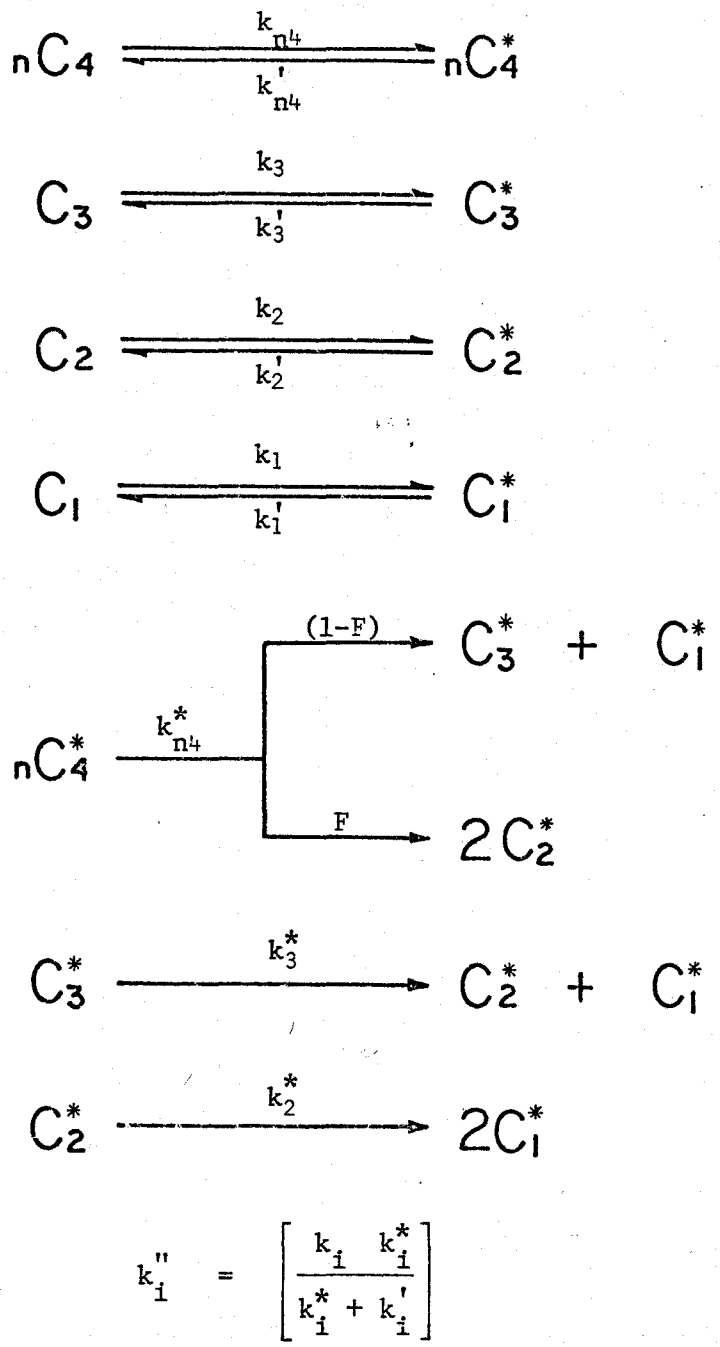

$$k_i'' = \left[\frac{k_i \; k_i^*}{k_i^* + k_i'} \right]$$

where: i - may be n4, 3 or 2

Figure 5-7:
N-BUTANE HYDROGENOLYSIS MECHANISM

where: S_3, S_2, S_1 - selectivity for propane, ethane, methane

X_4 - fractional conversion of butane

k - rate constants (Figure 5-7)

The first two equations result from a mass balance for propane and ethane over the reactor and the final equation is merely a carbon balance. These expressions are in the form of selectivity versus conversion and can be applied directly to the experimental data. Equation 5-3 was fitted to the propane selectivities at 125°C and 800-torr total pressure using nonlinear least squares analysis. Then, Equation 5-4 was fitted to the ethane selectivity data at the same conditions using the predicted propane selectivities from the previous analysis. Finally, Equation 5-5 and the predicted values of ethane and propane selectivities were used to determine the methane selectivities. The results of this analysis are presented in Table 5-2 and the calculated selectivities are compared with the experimental values in Figure 5-3.

The estimated values of the parameters reflect the properties of the reaction mechanism. The value of F corrresponds to one-third of the n-butane molecules breaking at the central bond and two-thirds at the terminal bonds. Thus, we can conclude that each carbon-carbon bond has about the same probability of being broken, i.e., the reaction is not selective with respect to bond type. Once again, the predicted desorption rates of the adsorbed hydrocarbons are greater than the surface cracking rates (k_3' and k_2' are greater than k_3^* and k_2^*), suggesting that the rupture of the carbon-carbon bonds in the adsorbed

TABLE 5-2

N-Butane Product Distribution Analysis (125°C)

Number of Observations: 49

Temperature: 125°C

Total Pressure: 800 torr

Equation 5-3

Residual Sum of Squares: 2.2×10^{-2}

Residual Root Mean Square: 2.2×10^{-2}

Parameter	Estimated Value	95% Confidence Interval
$\left[\frac{k_3'}{k_3^* + k_3'}\right]$ (1-F)	0.53	±0.02
$\frac{k_3''}{k_{n4}''}$	0.21	±0.02

Equation 5-4

Residual Sum of Squares: 3.5×10^{-2}

Residual Root Mean Square: 2.8×10^{-2}

Parameter	Estimated Value	95% Confidence Interval
F	0.32	±0.02
$\left[\frac{k_2'}{k_2^* + k_2'}\right]$	1.0	±0.01

TABLE 5-2 (continued)

Parameter	Estimated Value	95% Confidence Interval
$\frac{k_2''}{k_{n4}''}$	0.015	±0.004

Derived Data

$$\left[\frac{k_3'}{k_3^* + k_3'}\right] = 0.78$$

hydrocarbons is the slowest step. The ratios of the hydrogenolysis rate constants indicate that n-butane reacts approximately five times as fast as propane and sixty-five times as fast as ethane.

The selectivity analysis was extended to encompass all of the data at 800 torr and various temperatures (85°, 100°, 110°, 125°C) by including the temperature dependence of the rate constants. Because the propane selectivities at zero conversion did not vary greatly with temperature, the numerator of Equation 5-3 was assumed to be constant. The hydrogenolysis rate constants were assumed to vary according to an Arrhenius relationship and therefore the ratio (k_3''/k_{n4}'') becomes

$$\frac{k_3''}{k_{n4}''} = A_{3n4}^{-\Delta E_{3n4}/RT} \tag{5-6}$$

where: A_{3n4} - ratio of pre-exponential factors for propane and n-butane hydrogenolysis

ΔE_{3n4} - difference in activation energies between propane and n-butane hydrogenolysis reactions

Substituting this into Equation 5-3 yields

$$S_3 = \frac{(1-F)\left[\frac{k_3'}{k_3^* + k_3'}\right]}{\left[1 + A_{3n4}e^{-\frac{\Delta E_{3n4}}{RT}}\left[\frac{X_4}{1 - X_4}\right]\right]} \tag{5-7}$$

Equation 5-4 was insensitive to the parameter k_2''/k_{n4}'' (the denominator had a value near unity for all experimental conversions) and

therefore a similar analysis for ethane selectivity failed to give significant parameter estimates.

The results of the nonlinear regression analysis of Equation 5-7 using the data contained in Tables D-8, D-9, and D-10 are listed in Table 5-3. Figure 5-8 demonstrates that the fit was good at all temperature levels. The estimated difference in activation energy between the propane and n-butane hydrogenolysis reactions was 20 kcal. per mole, but this value is very approximate.

For the previous analyses, the effects of the hydrogen pressure on the elementary steps in the reaction network have been assumed constant and incorporated into the corresponding rate constant. This postulate was justified by the fact that the hydrogen pressure did not vary over a great range and also the rate constants always appeared in ratios so an effect in one was balanced by a similar effect in the other. However, by including the hydrogen effects in an explicit form, some of the groups of rate constants were separated and more detailed information was obtained. The drawback to this procedure was that the hydrogen pressure effects were small and therefore the parameter estimates were poor.

If the surface cracking reaction is one-half order in hydrogen and the desorption reaction is second order in hydrogen, then the overall hydrogen order for the hydrogenolysis reaction will be -1.5. This value is in good agreement with the kinetics reported for n-butane and propane. Substitution of these terms into the selectivity equations (Appendix C.3) yields

TABLE 5-3

N-Butane Product Distribution Analysis at Various Temperatures

Number of Observations: 72

Temperature: 85°, 100°, 110°, 125°C

Total Pressure: 800 torr

Equation 5-7

Residual Sum of Squares: 3.7×10^{-2}

Residual Root Mean Square: 2.3×10^{-2}

Parameter	Estimated Value
$\left[\frac{k_3'}{k_3^* + k_3'}\right](1-F)$	0.58
A_{3n4}	5.1×10^{10}
ΔE_{3n4}	20 kcal./mole

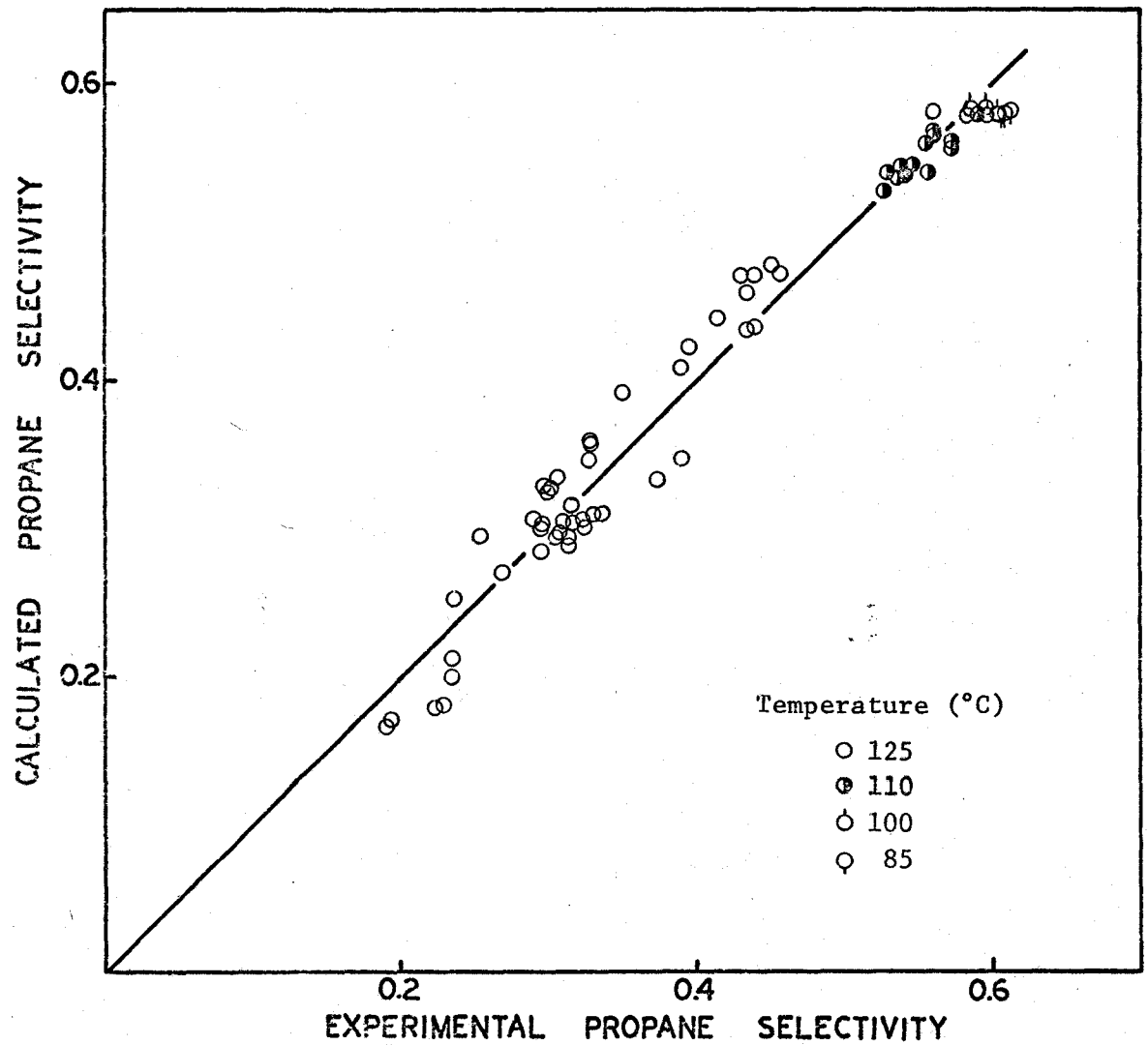

Figure 5-8: Comparison of Experimental and Calculated Propane Selectivities from n-Butane Hydrogenolysis at Various Temperatures

$$S_3 = \frac{(1-F)}{\left[1 + \frac{h_3^*}{h_3'} P_H^{-1.5} + \left[\frac{h_3^* h_3}{h_3' h_{n4}}\right] P_H^{-1.5} \left[1 + \frac{h_{n4}'}{h_{n4}^*} P_H^{1.5}\right] \left[\frac{X_4}{1 - X_4}\right]\right]} \quad (5\text{-}8)$$

$$S_2 = \frac{(1+F-S_3)}{\left[1 + \frac{h_2^*}{h_2'} P_H^{-1.5} + \left[\frac{h_2^* h_2}{h_2' h_{n4}}\right] P_H^{-1.5} \left[1 + \frac{h_{n4}'}{h_{n4}^*} P_H^{1.5}\right] \left[\frac{X_4}{1 - X_4}\right]\right]} \quad (5\text{-}9)$$

where: P_H - partial pressure of hydrogen

h - rate constants with hydrogen pressure effects explicit

The initial parameter estimates were determined by fitting the linearized equations. These estimates were then improved by nonlinear regression analysis using the Rosenbrock search technique. The application of the equations to the data at 800-torr total pressure and 125°C yielded the results in Table 5-4. The residual sum of squares has been lowered significantly by the inclusion of the hydrogen pressure terms (see Table 5-2). The parameter values show that propane and ethane adsorb more slowly than n-butane and that desorption of the adsorbed C_2 and C_3 species are more rapid than cracking. The estimated values of the fractional split factor are in good agreement with the previous analysis. One important feature of this analysis is that it affords a determination of the parameter $(k_{n4}'/k_{n4}^* + k_{n4}')$. At an average hydrogen pressure of 600 torr, the value was calculated to be 0.98 from the propane selectivities and 0.96 from the ethane selectivities. These values are close to unity and therefore a confirmation of

TABLE 5-4

N-Butane Product Distribution Analysis with Hydrogen Pressure Effects

Number of Observations: 49

Temperature: 125°C

Total Pressure: 800 torr

Equation 5-8

Residual Sum of Squares: 1.1×10^{-2}

Residual Root Mean Square: 1.6×10^{-2}

Parameter	Estimated Value
F	0.27
h_3^*/h_3'	6.7×10^3 torr$^{1.5}$
h_3/h_{n4}	0.011
h_{n4}^*/h_{n4}'	3.3×10^2 torr$^{1.5}$

Equation 5-9

Residual Sum of Squares: 2.2×10^{-2}

Residual Root Mean Square: 2.2×10^{-2}

Parameter	Estimated Value
F	0.31
h_2^*/h_2'	12.1 torr$^{1.5}$
h_2/h_{n4}	0.70
h_{n4}^*/h_{n4}'	6.0×10^2 torr$^{1.5}$

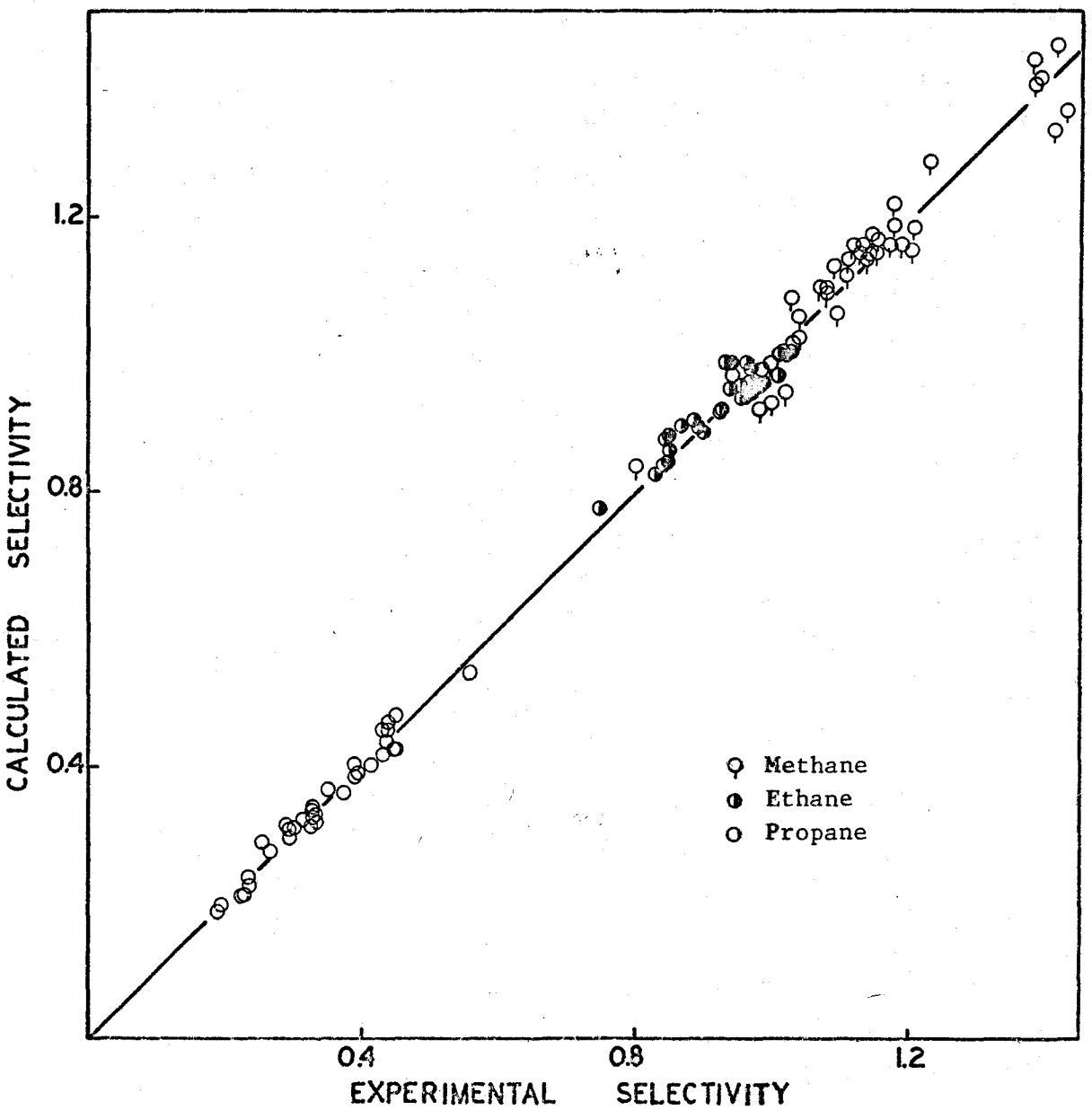

Figure 5-9: Comparison of Experimental and Calculated Selectivities from the Analysis of n-Butane Data with Hydrogen Pressure Effects

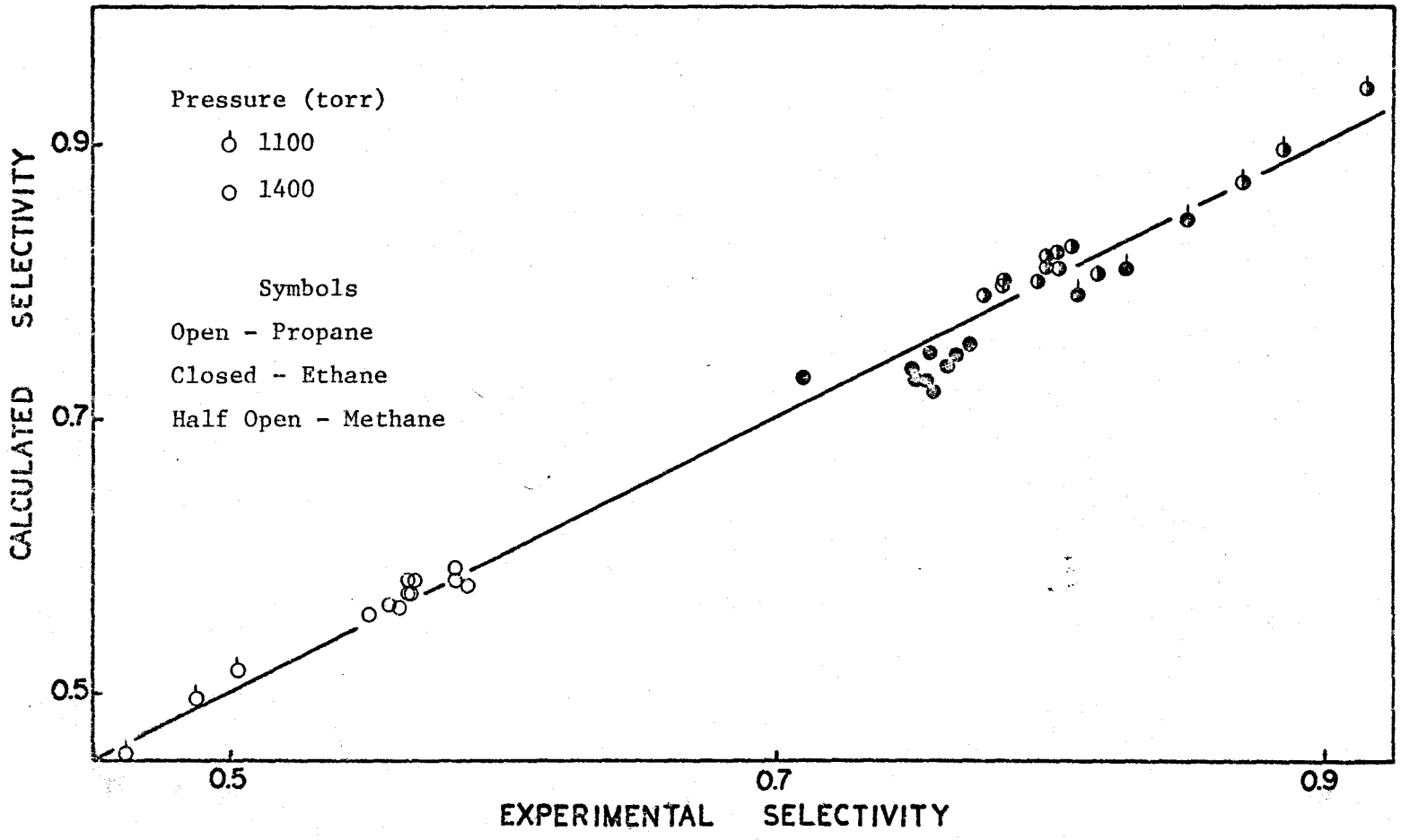

Figure 5-10: Comparison of Experimental and Calculated Selectivities from n-Butane Hydrogenolysis at Higher Total Pressures

the proposal that the surface cracking reaction is the rate-limiting step for the hydrogenolysis of n-butane. A comparison of the experimental and calculated selectivities appears in Figure 5-9. The data acquired at higher total pressures, 1100 and 1400 torr (Table D-11), were predicted using the estimated parameters from the foregoing analysis. The results (Figure 5-10) show that the regressed equations (Equations 5-8, 5-9) can be extrapolated outside the range of original data with good accuracy. This is another indication of the validity of the reaction network.

5.4 Isobutane

The products of isobutane hydrogenolysis were propane, ethane, and methane - all in significant amounts; no evidence of isomerization to n-butane was observed. The majority of the data was obtained at 125°C and over a range of conversions from 5 to 75% (Table D-12, Figure 5-11). Supplemental data taken at various other temperatures are given in Table D-13 and Figure 5-12.

Unlike n-butane, isobutane has only one type of carbon-carbon bond which ruptures to form methane and propane. Ethane cannot be created as a primary product except by the rupture of more than one carbon-carbon bond to produce ethane and two methane molecules. The latter type of reaction has been reported by Shephard (14) for the hydrogenolysis of propane over nickel.

At 125°C, the selectivity for ethane was substantial even at conversions as low as 5% where the value was 0.3. The corresponding selectivity of methane was large (greater than one mole per mole of

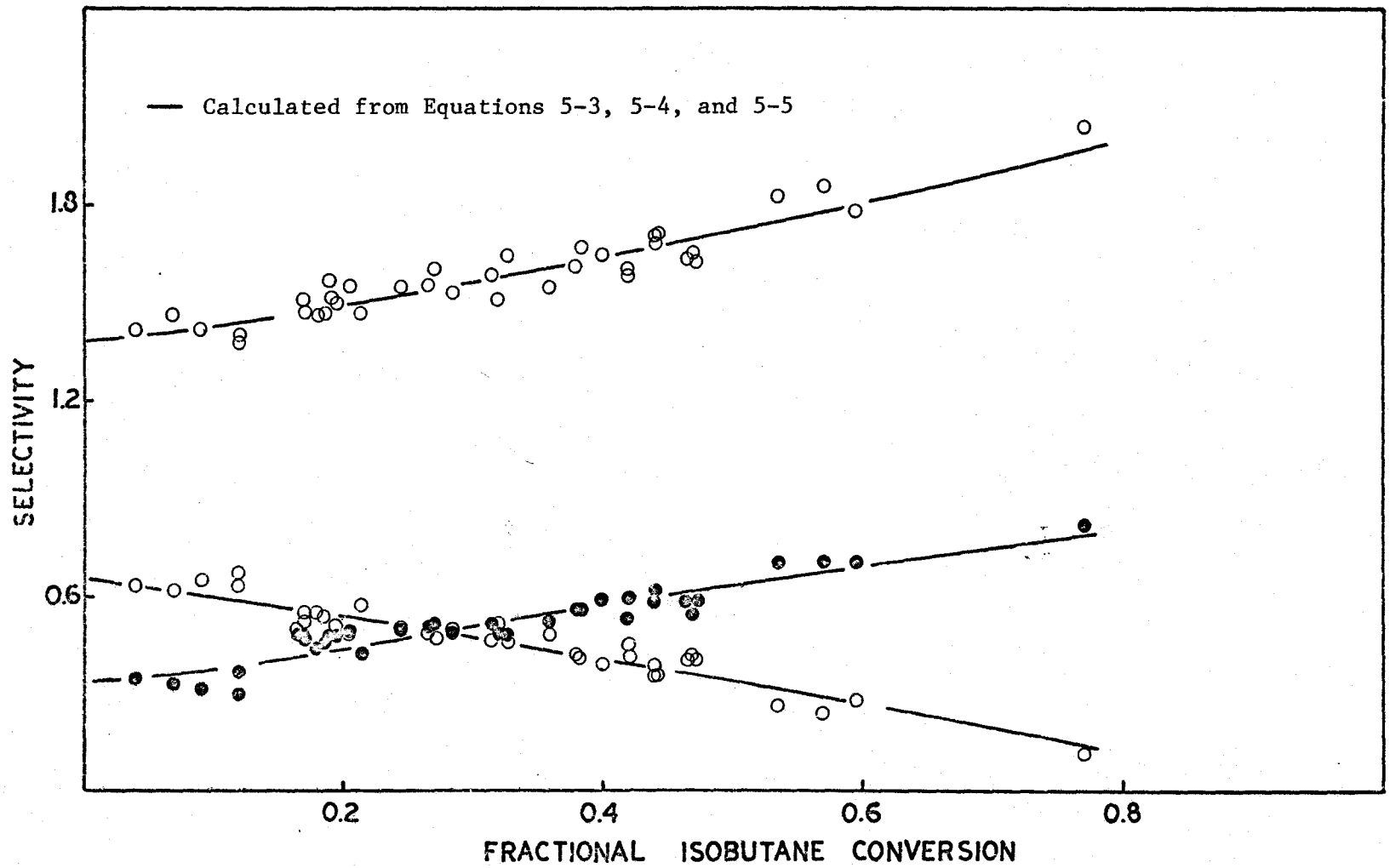

Figure 5-11: Product Distribution from Isobutane Hydrogenolysis (125°C)

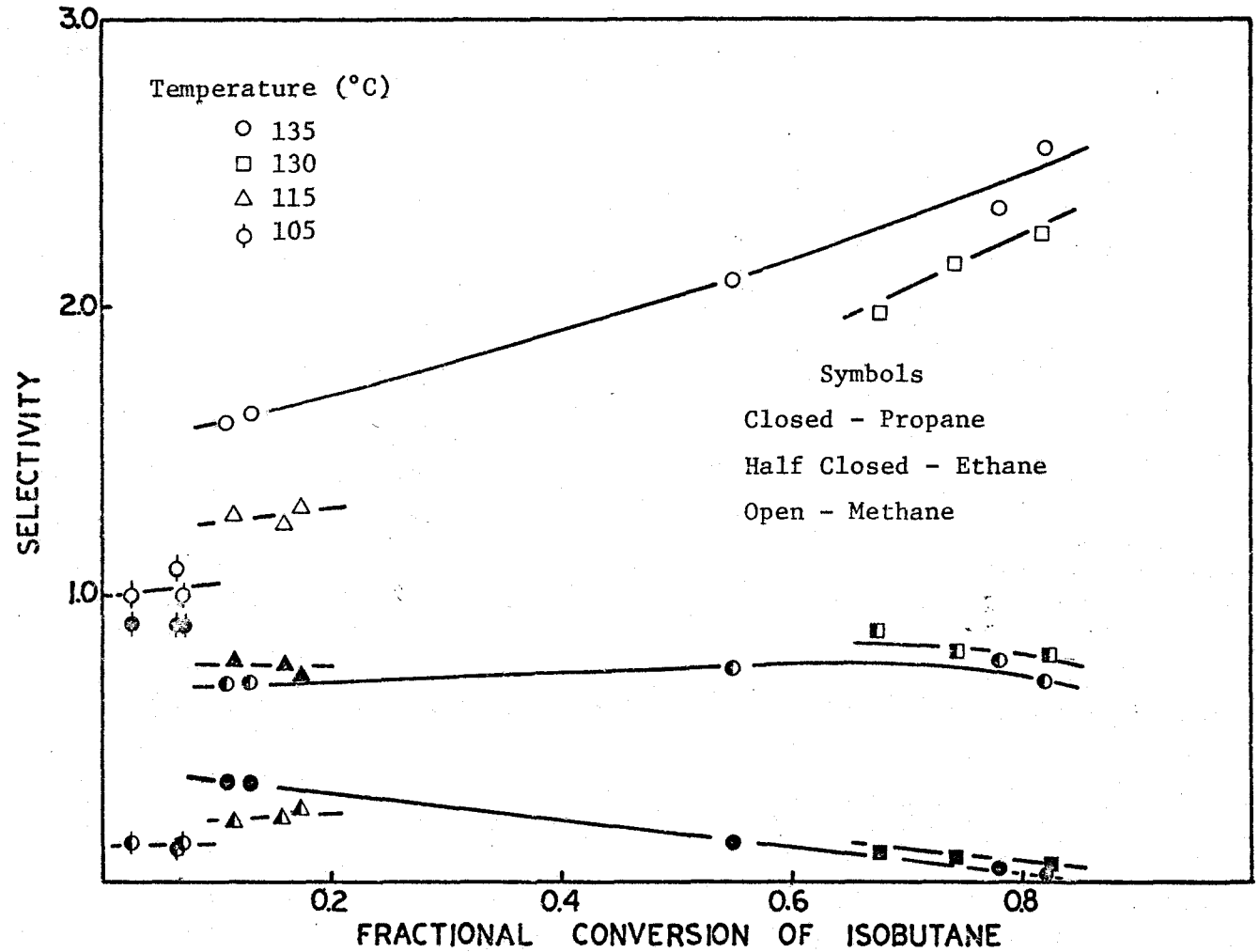

Figure 5-12: Product Distribution from Isobutane Hydrogenolysis at Other Temperatures

isobutane reacted) and that of propane was 0.6. With increasing conversion, the amounts of methane and ethane increased at the expense of propane. This trend is the same as that observed for n-butane hydrogenolysis and is due to the cracking of the primary products (particularly propane) to smaller hydrocarbons. The product distributions at other temperatures (105°, 115°, 130°, 135°C) were different. However, the same type of changes were observed with increasing conversion.

The primary product distribution was estimated by extrapolation of the selectivity-conversion data to zero conversion (Figure 5-13). In direct contrast to the n-butane reaction, the selectivities were strongly dependent upon temperature. At the lower temperatures, the propane and methane selectivities approached unity and that of ethane became small. In this case, one of the carbon-carbon bonds in the adsorbed iC_4 species must have ruptured and the resultant fragments desorbed without further cracking. At higher temperatures, there was an increase in the amount of ethane and methane formed corresponding to a situation in which the initially formed C_3 fragments cracked again before desorbing. In this way, ethane and two methane molecules were formed as primary products. Since higher temperatures favoured this latter process, the activation energy for rupture of the carbon-carbon bonds must be larger than that for desorption. This is in good agreement with the observation that hydrogenolysis reactions have larger activation energies than exchange reactions (1).

The reaction network proposed for the analysis of isobutane

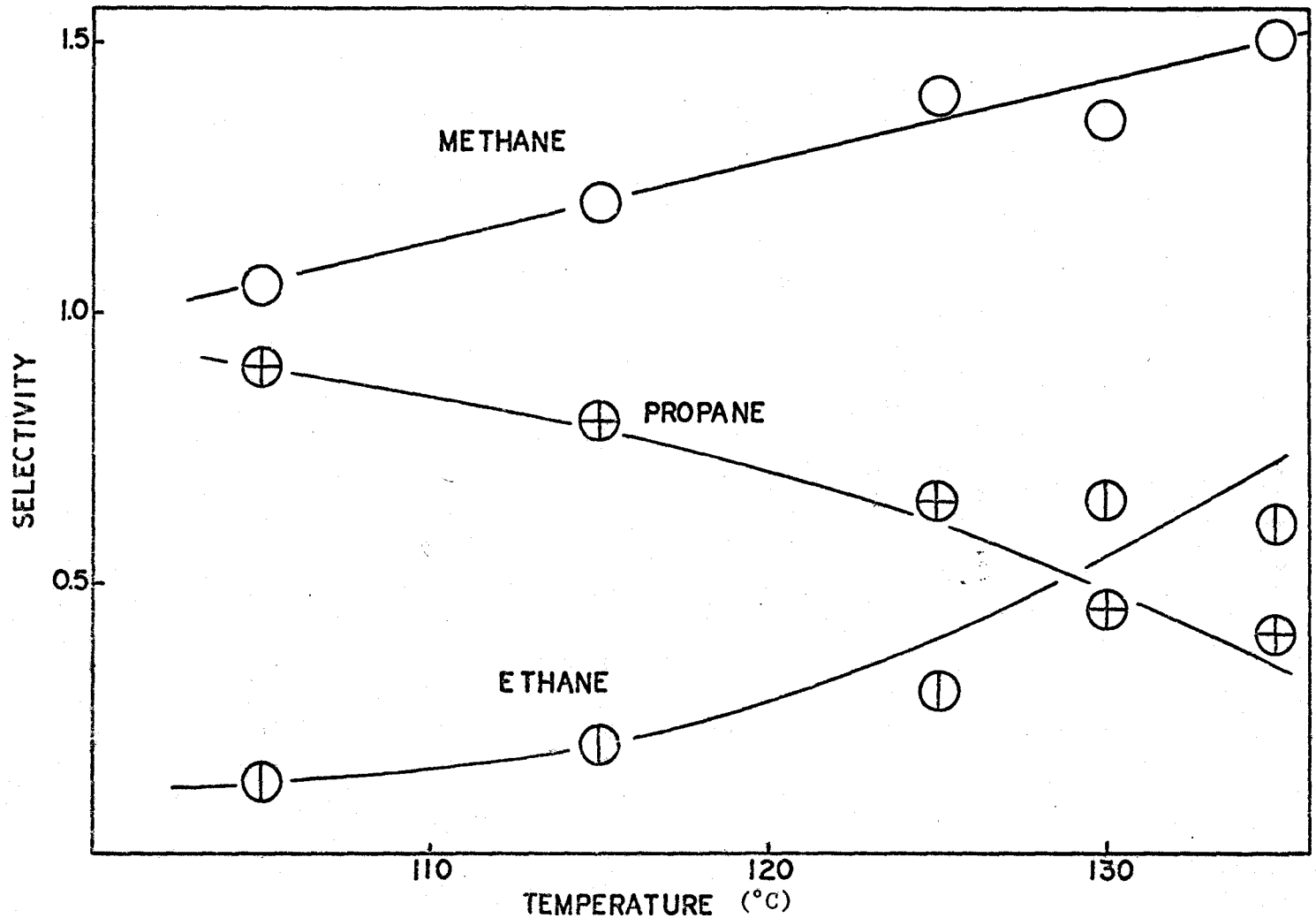

Figure 5-13: Product Distribution at Zero Isobutane Conversion

product distribution is exactly the same as that described in Section 5.3. The results of nonlinear regression analysis of Equations 5-3 and 5-4 using the data at 125°C are reported in Table 5-5 and the calculated selectivities are compared with the experimental values in Figure 5-11.

The value of the fractional split factor F was very small. Because there is no single carbon-carbon bond in isobutane which can be broken to produce ethane, the expected value for this parameter is zero and therefore the analysis is consistent with theoretical restrictions to this extent. The estimated parameters also show that the desorption rates of the adsorbed C_3 and C_2 species are greater than the surface cracking rates at this temperature. Isobutane cracks at approximately the same rate as propane.

Simultaneous analysis of the data at different temperatures is a more complex problem because the product distribution at zero conversion varied widely with temperature. The value of F was set at zero. The temperature dependence of the rate constant group $(k_3'/(k_3^* + k_3'))$ in the numerator of Equation 5-3 is very complicated but was assumed to be linear over the temperature range examined; the corresponding term in Equation 5-4 was found to be approximately invariant with temperature. In a similar manner to the n-butane analysis, the rate constant ratios in the denominator of these equations were assumed to obey an Arrhenius relationship. The transformed temperature dependent equations are

TABLE 5-5

Isobutane Product Distribution Analysis (125°C)

Number of Observations: 38
Temperature: 125°C
Total Pressure: 800 torr

Equation 5-3

Residual Sum of Squares: 5.8×10^{-2}
Residual Root Mean Square: 4.0×10^{-2}

Parameter	Estimated Value	95% Confidence Interval
$\left[\frac{k_3'}{k_3^* + k_3'}\right](1-F)$	0.67	±0.02
$\frac{k_3''}{k_{i4}''}$	0.98	±0.12

Equation 5-4

Residual Sum of Squares: 6.4×10^{-2}
Residual Root Mean Square: 4.3×10^{-2}

Parameter	Estimated Value	95% Confidence Interval
F	0.02	±0.02
$\left[\frac{k_2'}{k_2^* + k_2'}\right]$	0.93	±0.04

TABLE 5-5 (continued)

Parameter	Estimated Value	95% Confidence Interval
$\frac{k_2''}{k_{i4}''}$	0.005	±0.03

Derived Data

$$\left[\frac{k_3'}{k_3^* + k_3'}\right] = 0.68$$

$$S_3 = \frac{A - BT}{\left[1 + A''_{3i4}\, e^{-\Delta E_{3i4}} \left[\frac{X_4}{1 - X_4}\right]\right]} \qquad (5\text{-}10)$$

$$S_2 = \frac{(1-S_3)\left[\frac{k_2'}{k_2^* + k_2'}\right]}{\left[1 + A''_{2i4}\, e^{-\Delta E_{2i4}} \left[\frac{X_4}{1 - X_4}\right]\right]} \qquad (5\text{-}11)$$

where: S_3, S_2 - selectivity of propane and ethane

A, B - parameters

T - temperature (°K)

A''_{3i4}, A''_{2i4} - ratios of pre-exponential factors

ΔE_{3i4}, ΔE_{2i4} - difference in activation energies between propane and isobutane, and ethane and isobutane hydrogenolysis reactions

X_4 - fractional conversion of isobutane

These equations were fitted to the data in Tables D-12 and D-13. Initial estimates of the parameters were determined by a grid search and then improved by Rosenbrock optimization; the results are located in Table 5-6. The values of A and B were such that the rate constant group $(k_3'/(k_3^* + k_3'))$ varied from near unity at 105°C to 0.4 at 135°C. The qualitative behavior of ΔE_{3i4} and ΔE_{2i4} was as expected (6), i.e., ΔE_{2i4} was greater than ΔE_{3i4} which was greater than ΔE_{3n4}

TABLE 5-6

Isobutane Product Distribution Analysis at Various Temperatures

Number of Observations: 52

Equation 5-10

Residual Sum of Squares:	6.2×10^{-2}
Residual Root Mean Square:	3.6×10^{-2}

Parameter	Estimated Value
A	5.17
B	0.0113
A''_{3i4}	4.6×10^{26}
ΔE_{3i4}	49 kcal./mole

Equation 5-11

Residual Sum of Squares:	8.7×10^{-2}
Residual Root Mean Square:	4.2×10^{-2}

Parameter	Estimated Value
$\left[\frac{k_2'}{k_2^* + k_2'}\right]$	0.97
A''_{2i4}	1.4×10^{34}
ΔE_{2i4}	66 kcal./mole

(Table 5-3). The values seemed excessively large, but the form of the equations being fitted allowed only a very approximate estimate of these parameter values. A comparison of the experimental and calculated selectivities (Figure 5-14) demonstrates that the data were well correlated over the entire temperature range.

The product distribution from isobutane hydrogenolysis was also analysed by inserting hydrogen pressure terms into the rate equations. The rates of rupture of the carbon-carbon bonds in the adsorbed hydrocarbons were assumed to be one-half order in hydrogen and the rates of desorption were assumed to be $^3/2$ order for isobutane and second order for propane. These values correspond to an overall hydrogen order of -1.0 and -1.5 for isobutane and propane hydrogenolysis. The selectivity equation for propane transforms to (Appendix C.3)

$$S_3 = \frac{1}{\left[1 + \frac{h_3^*}{h_3'} P_H^{-1.5} + \left[\frac{h_3^* h_3}{h_3' h_{i4}}\right] P_H^{-1.5} \left[1 + \frac{h_{i4}'}{h_{i4}^*} P_H\right] \left[\frac{X_4}{1 - X_4}\right]\right]} \qquad (5\text{-}12)$$

where: h_i - rate constants with hydrogen pressure effects explicit

P_H - hydrogen partial pressure

The analysis of the ethane selectivity data in a similar manner resulted in insignificant parameter estimates.

Equation 5-12 was linearized and fitted to the data at 125°C (Table D-12). The parameter estimates were improved by nonlinear least squares analysis and the results are listed in Table 5-7. The parameter estimates indicate that propane adsorbs more slowly than isobutane and

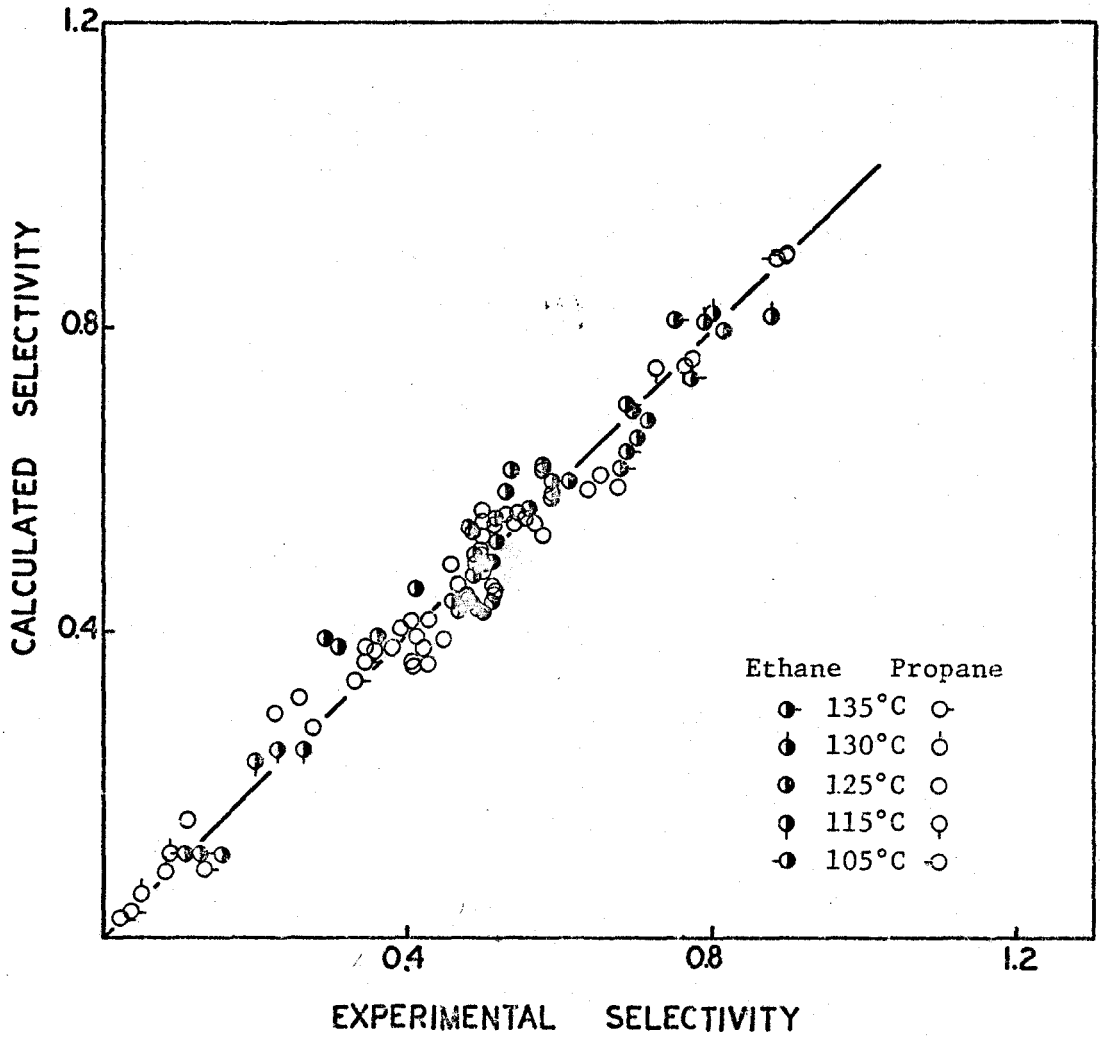

Figure 5-14: Comparison of Experimental and Calculated Selectivities for Isobutane Hydrogenolysis at Various Temperatures

TABLE 5-7

Isobutane Product Distribution With Hydrogen Pressure Effects

Number of Observations:	38
Temperature:	125°C
Total Pressure:	800 torr

Equation 5-12

Residual Sum of Squares:	4.6×10^{-2}
Residual Root Mean Square:	4.2×10^{-2}

Parameter	Estimated Value
$\frac{h_3^*}{h_3'}$	9.6×10^3 torr$^{1.5}$
$\frac{h_3}{h_{i4}}$	0.44
$\frac{h_{i4}^*}{h_{i4}'}$	1.4×10^2 torr

that the surface cracking reactions are slower than desorption reactions. The value of $(k'_{i4}/(k^*_{i4} + k'_{i4}))$ was estimated to be about 0.84 for a hydrogen pressure of 600 torr. This term could not be estimated from the analysis without hydrogen pressure effects. The value is near unity, strongly suggesting a mechanism for isobutane hydrogenolysis in which the rupture of the carbon-carbon bond is the slowest step.

5.5 Isopentane

The products from isopentane hydrogenolysis were n-butane, isobutane, propane, ethane, and methane. Once again, no isomerization reactions were observed. There are three distinguishable carbon-carbon bonds in isopentane.

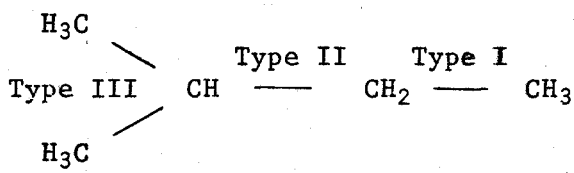

The rupture of Type I carbon-carbon bonds produces methane and isobutane; the rupture of Type II bonds produces ethane and propane; and the rupture of Type III bonds produces methane and n-butane. Therefore, each of the observable products can be formed directly from isopentane.

The hydrogenolysis reaction occurred readily and the majority of the experiments was carried out at slightly lower temperatures than for the butanes. The selectivity data at 110°C (Table D-14, Figure 5-15) were obtained over a range of conversions from 5 to 75%. The major products were methane and isobutane, both with selectivities slightly less than unity at low conversions, indicating a preponderance of

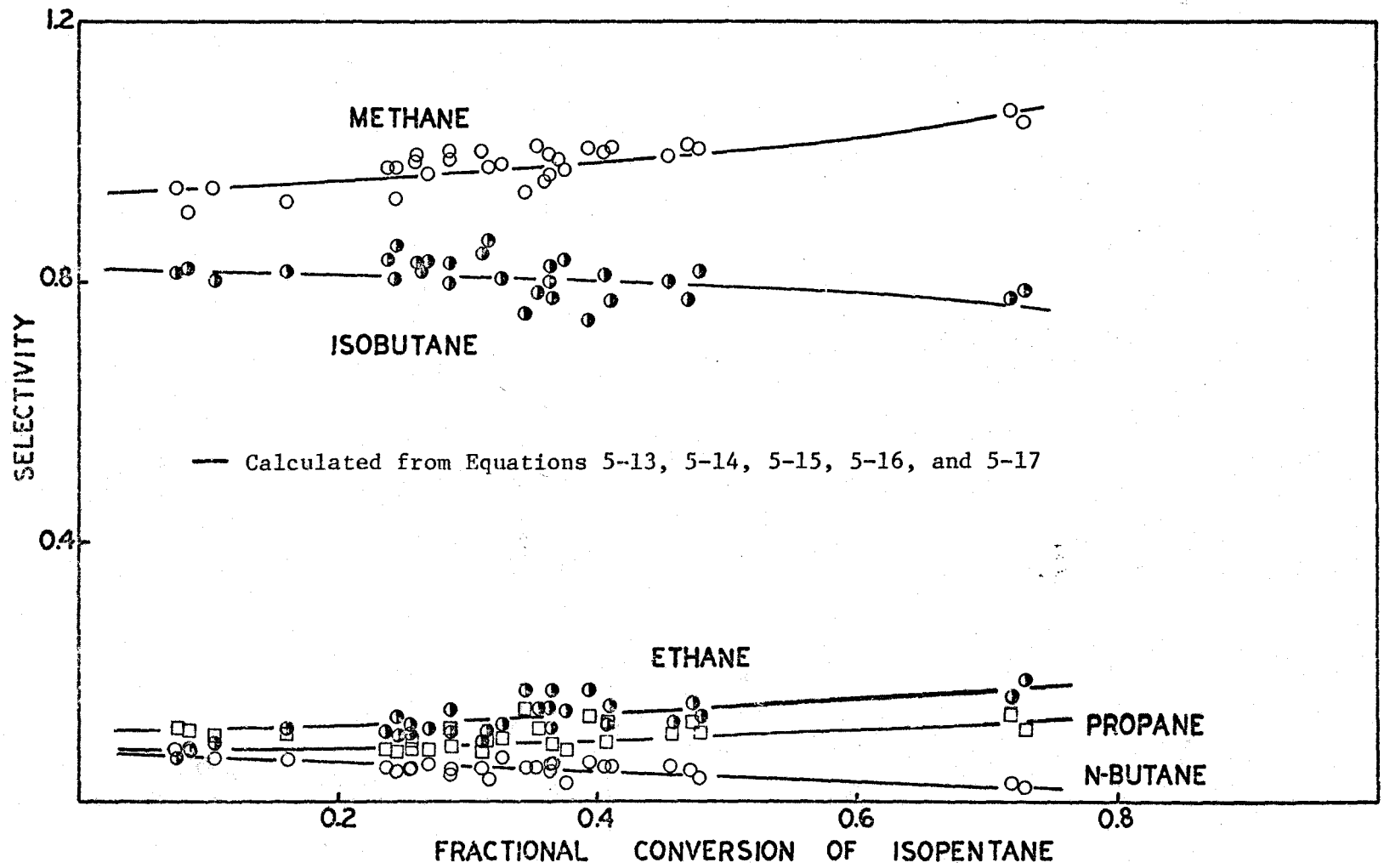

Figure 5-15: Product Distribution from Isopentane Hydrogenolysis (110°C)

cracking at bond Type I. Propane, ethane, and n-butane were produced in nearly equal amounts (selectivities up to 0.2) but significantly smaller quantities than methane and isobutane. With increasing conversion the selectivities of n-butane and isobutane decreased while those of the other products increased; however, this change was not as marked as was observed for the n-butane and isobutane hydrogenolysis reactions. The experimental results at various other temperatures are listed in Table D-15 and plotted in Figure 5-16.

The effect of temperature on product distribution was not great. At the lower temperatures, the data were extrapolated to zero conversion to obtain a value for the product distribution from the primary reaction. The results are given in Figure 5-17. There were only small changes in the product distribution with temperature similar to the results for n-butane cracking.

The reaction network proposed for the explanation of these data is similar to that for the butanes except that the adsorption-desorption and irreversible cracking reactions of isopentane are included (Figure 5-18). The method of analysis is therefore completely analogous and only the degree of complexity is increased. Once again, each of the hydrocarbons undergoes reversible adsorption-desorption processes to form adsorbed surface species. Each of these species (excepting C_1 fragments) crack irreversibly to form smaller adsorbed fragments. The isopentane molecule can break at any one of three different types of carbon-carbon bonds. Two fractional split factors were defined so that f and f' represent the fraction of isopentane molecules cracking

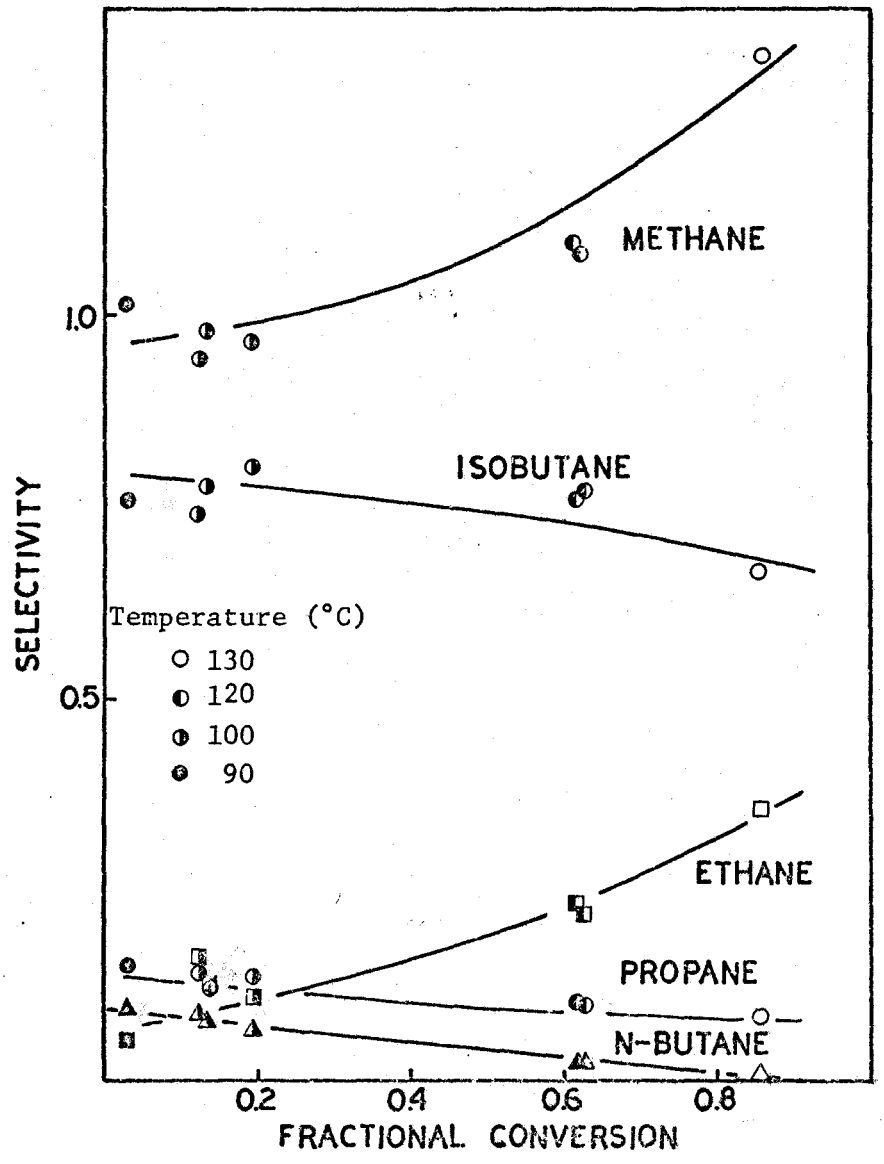

Figure 5-16: Product Distribution from Isopentane Hydrogenolysis at Other Temperatures

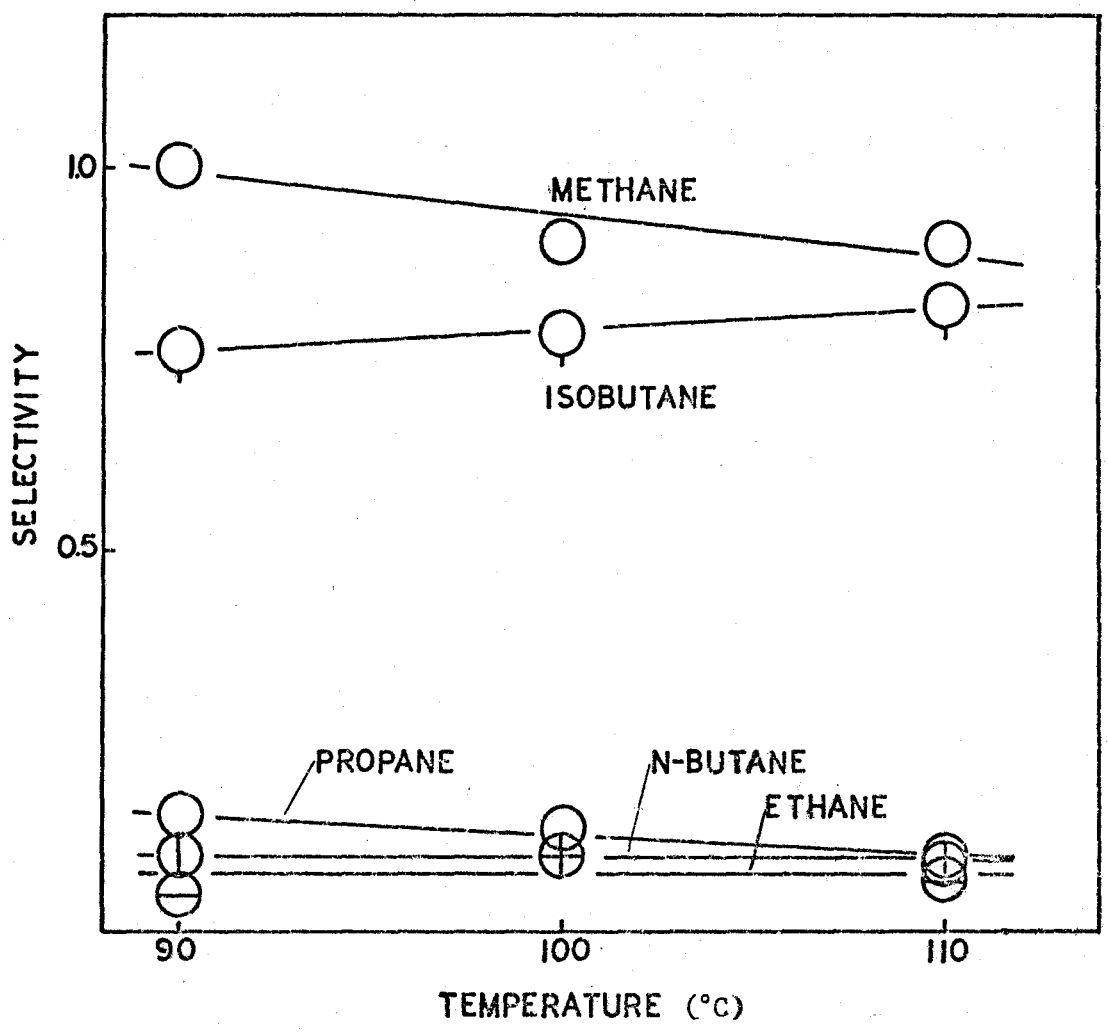

Figure 5-17: Product Distribution at Zero Isopentane Conversion

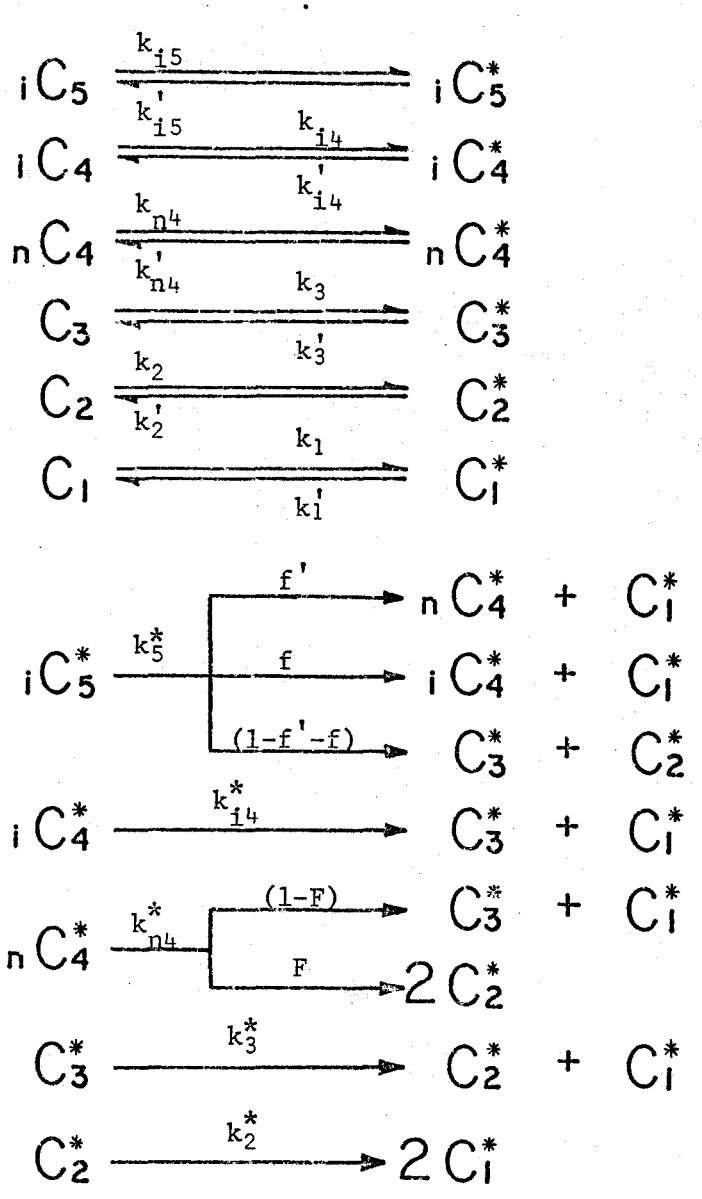

$$k_i'' = \left[\frac{k_i \; k_i^*}{k_i^* + k_i'}\right]$$

where: i - may be i5, n4, i4, 3, or 2

Figure 5-18:
ISOPENTANE HYDROGENOLYSIS MECHANISM

at bond Types I and III, respectively. The remaining fraction (1-f-f') applies to the rupture of Type II bonds to form ethane and propane. Similarly, the n-butane can break either at the central or terminal bonds. The fractional split factor F describes this phenomena (see n-butane analysis). The reaction network has been analysed (Appendix C.4) and proved to conform to the following equations:

$$S_{n4} = \frac{f' \left[\frac{k'_{n4}}{k^*_{n4} + k'_{n4}}\right]}{\left[1 + \frac{k''_{n4}}{k''_{i5}} \left[\frac{X_5}{1 - X_5}\right]\right]} \tag{5-13}$$

$$S_{i4} = \frac{f \left[\frac{k'_{i4}}{k^*_{i4} + k'_{i4}}\right]}{\left[1 + \frac{k''_{i4}}{k''_{i5}} \left[\frac{X_5}{1 - X_5}\right]\right]} \tag{5-14}$$

$$S_3 = \frac{(1 - f'F - S_{i4} - (1-F)\, S_{n4}) \left[\frac{k'_3}{k^*_3 + k'_3}\right]}{\left[1 + \frac{k''_3}{k''_{i5}} \left[\frac{X_5}{1 - X_5}\right]\right]} \tag{5-15}$$

$$S_2 = \frac{(2 - f' - f + Ff' - S_{i4} - (1+F)\, S_{n4} - S_3) \left[\frac{k'_2}{k^*_2 + k'_2}\right]}{\left[1 + \frac{k''_2}{k''_{i5}} \left[\frac{X_5}{1 - X_5}\right]\right]} \tag{5-16}$$

$$S_1 + 2S_2 + 3S_3 + 4(S_{i4} + S_{n4}) = 5 \qquad (5\text{-}17)$$

where: S_{n4}, S_{i4}, S_3, S_2, S_1 - selectivity for n-butane, isobutane propane, ethane, methane

X_5 - fractional conversion of isopentane

k - rate constants (Figure 5-18)

These expressions are in the form of selectivity versus conversion and therefore can be applied directly to the experimental data. Equations 5-13 and 5-14 were fitted to the data at 110°C by nonlinear least squares. First estimates of the parameters were developed from a grid search and then improved by Rosenbrock search technique. Equation 5-15 was examined in a similar manner using the previously estimated values for the n-butane and isobutane selectivities. Because the ethane selectivities were very small, Equation 5-16 was substituted into Equation 5-17 to obtain a relationship between methane selectivity and conversion. This equation was then fitted to the data by nonlinear least squares analysis using the methane selectivities as the independent variable. The ethane selectivities were subsequently calculated from Equation 5-17. This method gave an improved fit to the data.

The results of these calculations are listed in Table 5-8 and the predicted selectivities are compared with the experimental results in Figure 5-15. The values of the fractional split factors for isopentane indicate that about 82% of the molecules split at the Type I carbon-carbon bond, 8% crack at Type III, and the remainder at Type II. This is consistent with the observation that n-butane reacts about an

TABLE 5-8

Isopentane Product Distribution Analysis (110°C)

Number of Observations: 29

Temperature: 110°C

Total Pressure: 800 torr

Equation 5-13

Residual Sum of Squares: 2.7×10^{-3}

Residual Root Mean Square: 1.0×10^{-2}

Parameter	Estimated Value	95% Confidence Interval
$\left[\frac{k'_{n4}}{k^*_{n4} + k'_{n4}}\right] f'$	0.072	±0.006
$\frac{k''_{n4}}{k''_{i5}}$	0.64	±0.24

Equation 5-14

Residual Sum of Squares: 2.2×10^{-2}

Residual Root Mean Square: 2.8×10^{-2}

Parameter	Estimated Value	95% Confidence Interval
$\left[\frac{k'_{i4}}{k^*_{i4'} + k'_{i4}}\right] f$	0.82	±0.02
$\frac{k''_{i4}}{k''_{i5}}$	0.03	±0.03

TABLE 5-8 (continued)

Equation 5-15

Residual Sum of Squares: 9.9×10^{-3}

Residual Root Mean Square: 2.0×10^{-2}

Parameter	Estimated Value	95% Confidence Interval
$f'F$	0.025	±0.015
F	0.31	±0.26
$\left[\frac{k_3'}{k_3^* + k_3'}\right]$	0.85	±0.10
$\frac{k_3''}{k_{i5}''}$	0.10	±0.15

Equations 5-16 and 5-17

Residual Sum of Squares: 1.1×10^{-2}

Residual Root Mean Square: 2.2×10^{-2}

Parameter	Estimated Value	95% Confidence Interval
$f'+f-f'F$	0.85	±0.02
F	0.41	±0.34
$\left[\frac{k_2'}{k_2^* + k_2'}\right]$	0.84	±0.10
$\frac{k_2''}{k_{i5}''}$	0.003	±0.08

TABLE 5-8 (continued)

Derived Data

$$f' = 0.08$$

$$f = 0.82$$

$$\left[\frac{k'_{n4}}{k^*_{n4} + k'_{n4}}\right] = 0.9$$

$$\left[\frac{k'_{i4}}{k^*_{i4} + k'_{i4}}\right] = 1.$$

order of magnitude more quickly than isobutane. The estimates of factor F for the rupture of the nC_4 fragment are in good agreement with the values calculated from the n-butane hydrogenolysis data despite the fact that the isopentane data are insensitive to this parameter. The ratios of the hydrogenolysis rate constants predict that isopentane reacts more readily than any of its products. The ratios of its hydrogenolysis rate with respect to n-butane, isobutane, propane,and ethane were 1.6, 33, 10 and about 330, respectively.

An analysis of the selectivity data at several temperatures failed due to the small amount of data taken at the other temperatures. However, Figure 5-17 demonstrates that the effect of temperature was small.

The inclusion of hydrogen dependency terms into the reaction network was also unsuccessful and resulted in insignificant estimates of the parameters, probably due to the fact that the isopentane data was taken over a smaller range of hydrogen pressure than the other hydrocarbons. Also, the n-butane, propane, and ethane selectivities were too small to show accurately any change in selectivity with hydrogen pressure.

5.6 Neopentane

The products from neopentane hydrogenolysis were isobutane, propane, ethane, and methane. No evidence of isomerization to the other pentanes was observed; this is in agreement with Boudart and Ptak (35) who have studied the isomerization reaction of neopentane over a number of supported metals including ruthenium. Normal butane

might also have been expected as a product if rearrangement of the carbon chain could occur simultaneously with the cracking reaction (isobutane does not isomerize to n-butane over this catalyst). To check this eventuality some preliminary experiments were performed solely to analyse for n-butane production. The regular chromatographic analysis system would not separate neopentane and n-butane; therefore, a column of 5A molecular sieve (this column would separate n-butane from all other components) was used in parallel with the original system. No n-butane was observed for experiments at 125°C and 135°C, and conversions between 2 and 40%. The analysis for n-butane was therefore discontinued and its selectivity was assumed to be zero in all cases.

Only one type of carbon-carbon bond is present in the neopentane molecule, the rupture of which creates isobutane and methane. Propane can be formed by the hydrogenolysis of the isobutane, and ethane can be formed by subsequent cracking of the propane. Therefore, the hydrocracking mechanism is one of successive demethylation with no possibility of parallel cracking reactions for any adsorbed species.

The neopentane had a relatively slow rate of hydrogenolysis and therefore the temperature range examined was higher than for the previous hydrocarbons. Most of the data were taken at 145°C; these are listed in Table D-16 and plotted in Figure 5-19. The production of methane was extensive with selectivities ranging from 3.5 to 5 depending upon conversion (the maximum possible selectivity is 5). The next most prominent hydrocarbon was ethane (selectivities around 0.4) while the

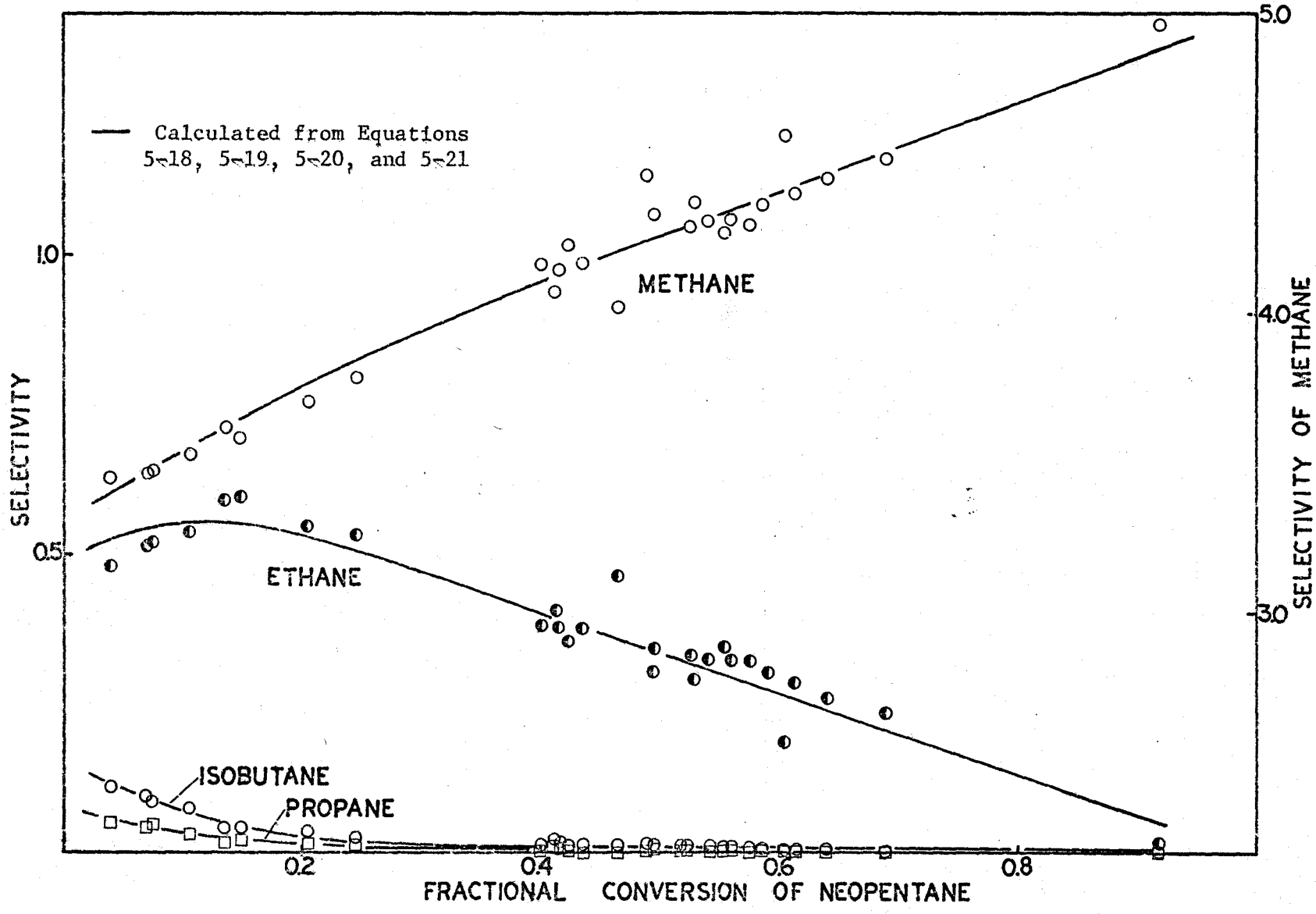

Figure 5-19: Product Distribution from Neopentane Hydrogenolysis (145°C)

yield of isobutane and propane was almost negligible. With increasing conversion, the selectivity of methane increased and those of isobutane and propane decreased, indicating that the consecutive cracking steps have more effect as the severity of the reactor conditions increases. The ethane selectivities passed through a maximum at about 10 to 20% conversion and then decreased to almost a zero at 90% conversion.

Additional data taken at other temperatures between 125° and 155°C are given in Table D-17 and Figure 5-20. These data showed a similar pattern of behavior to those at 145°C.

The selectivity versus conversion data were extrapolated to zero conversion at each temperature to obtain a relationship between the initial hydrogenolysis products and temperature (Figure 5-21). The intercepts were very difficult to determine because there were rapid changes in the selectivities at low conversions; therefore, the values are only approximate. The product distribution was fairly constant with only the ethane and methane selectivities varying appreciably. Increased temperature favoured the formation of smaller products, i.e., more extensive cracking.

The reaction network proposed for the analysis of neopentane hydrogenolysis is depicted in Figure 5-22. This network has been examined analytically and proved to conform to the following set of equations (Appendix C.4):

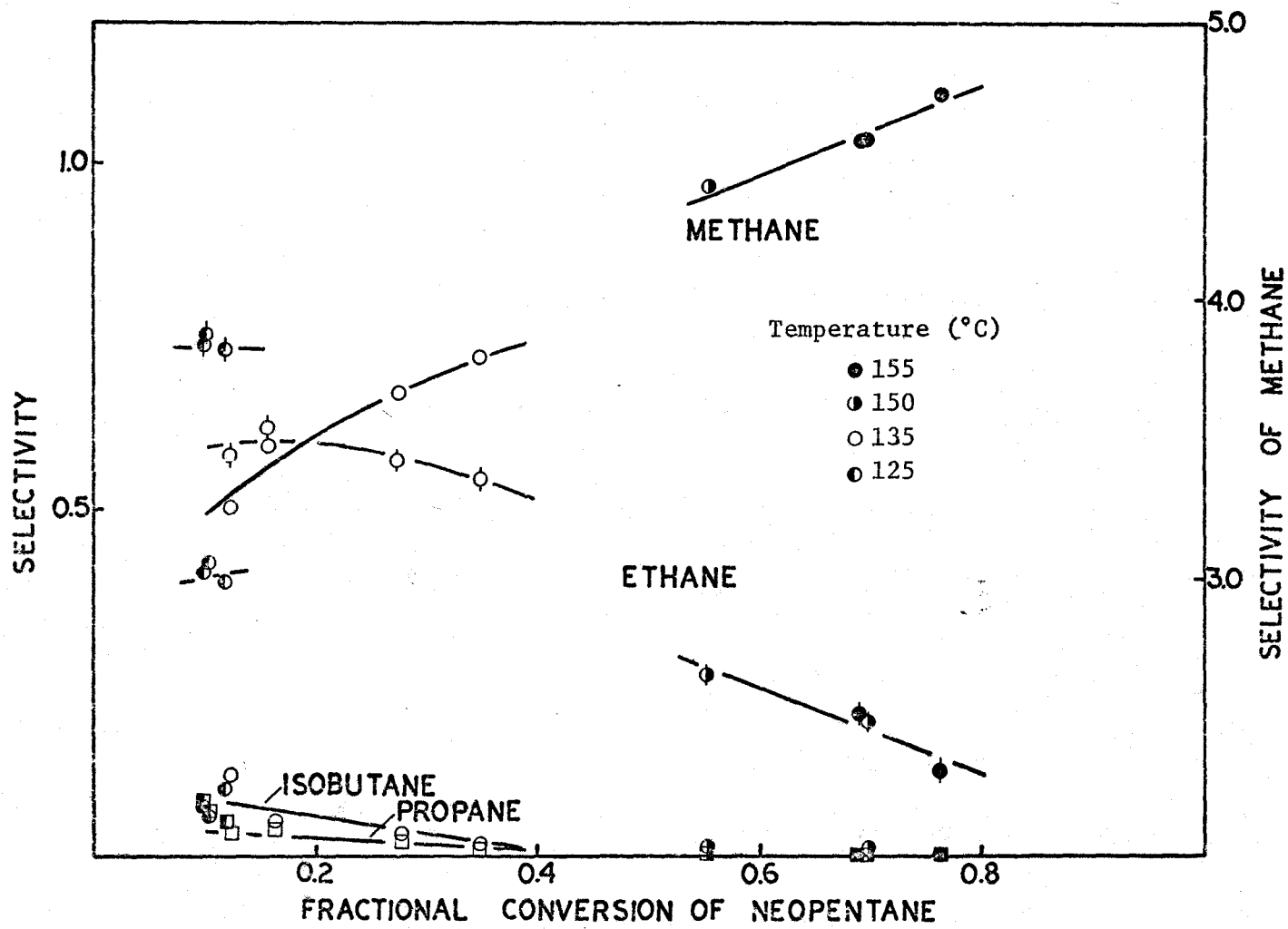

Figure 5-20: Product Distribution from Neopentane Hydrogenolysis at Other Temperatures

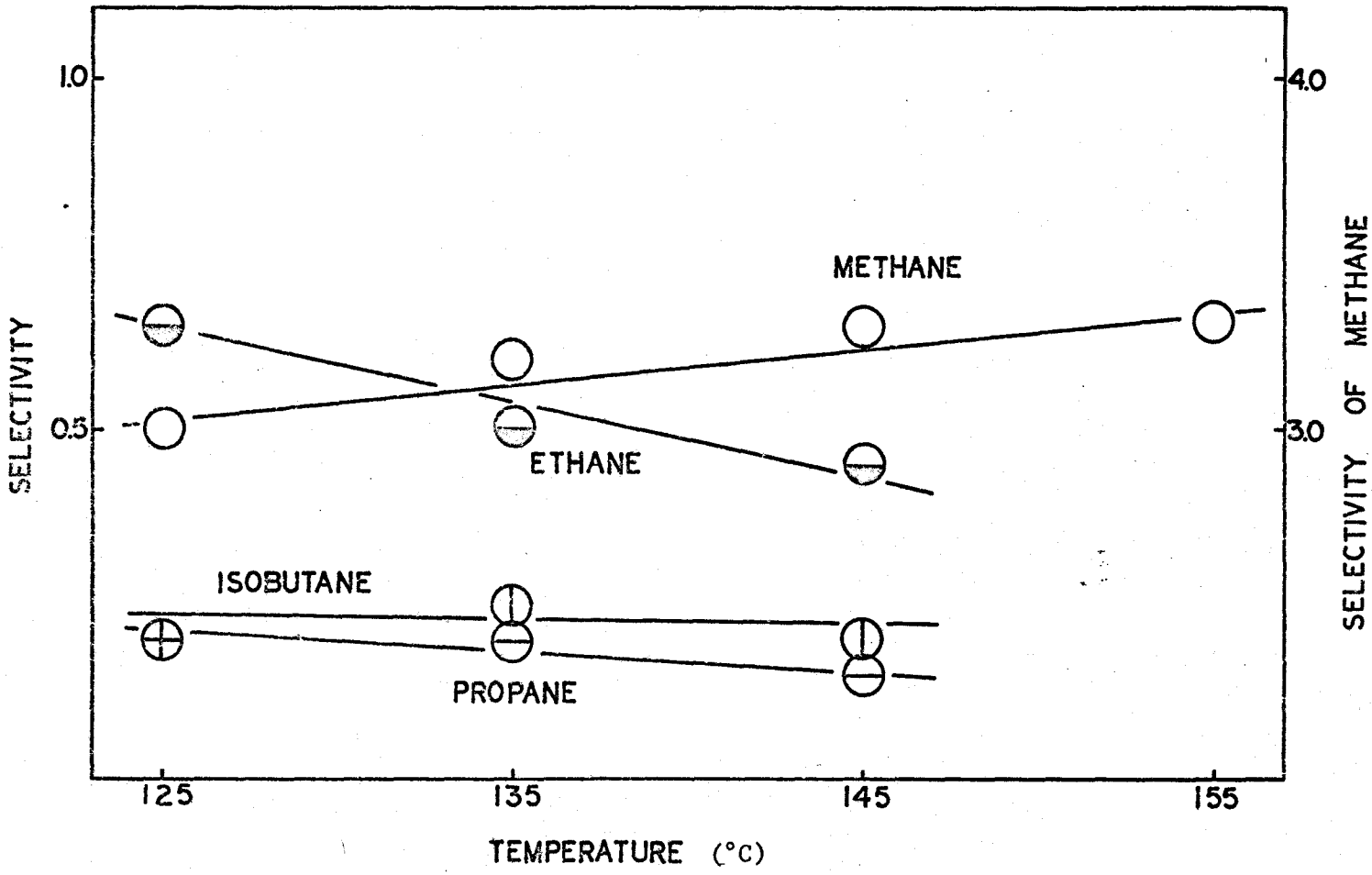

Figure 5-21: Product Distribution at Zero Neopentane Conversion

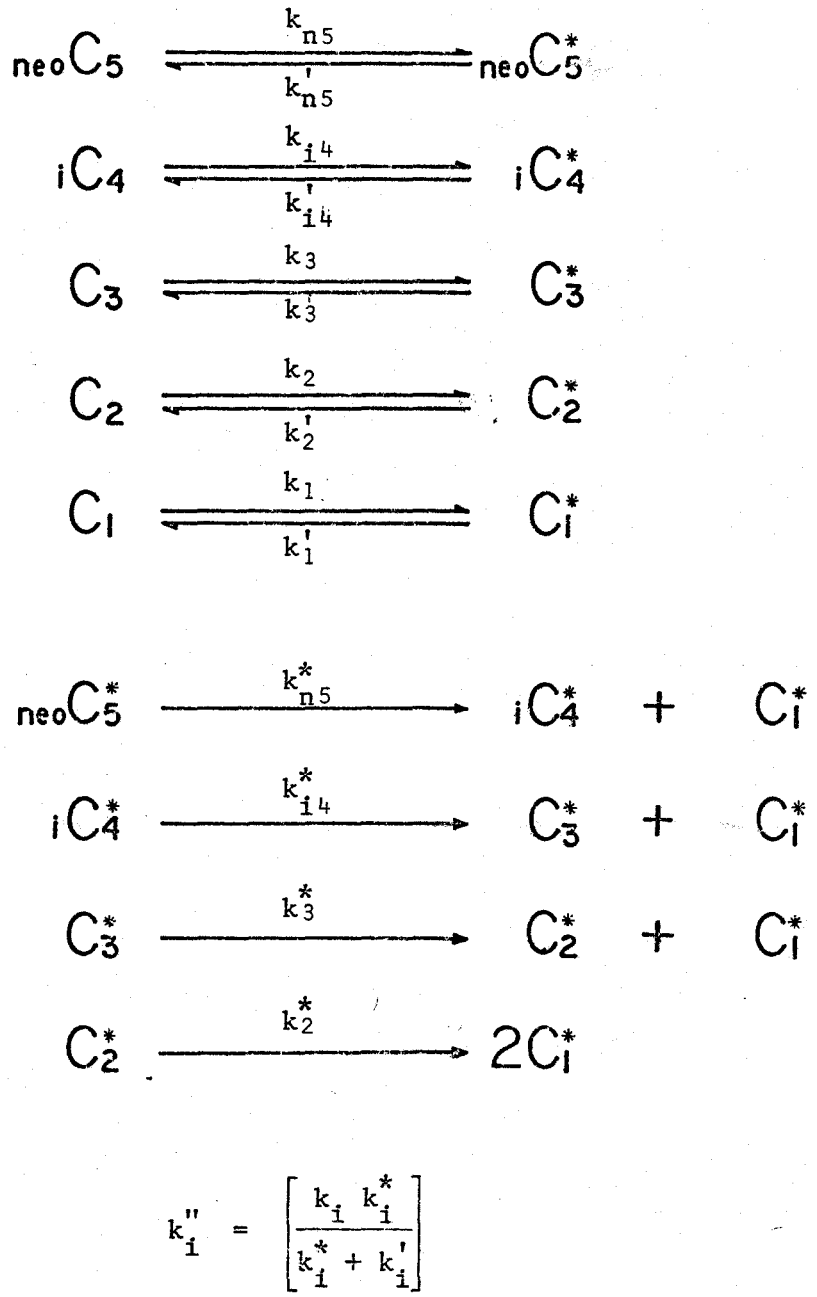

$$k_i'' = \left[\frac{k_i\, k_i^*}{k_i^* + k_i'}\right]$$

where: i - may be n5, i4, 3, or 2

Figure 5-22:
NEOPENTANE HYDROGENOLYSIS MECHANISM

$$S_{i4} = \frac{\left[\frac{k'_{i4}}{k^*_{i4} + k'_{i4}}\right]}{\left[1 + \frac{k''_{i4}}{k''_{n5}}\left[\frac{X_5}{1 - X_5}\right]\right]} \qquad (5\text{-}18)$$

$$S_3 = \frac{(1 - S_{i4})\left[\frac{k'_3}{k^*_3 + k'_3}\right]}{\left[1 + \frac{k''_3}{k''_{n5}}\left[\frac{X_5}{1 - X_5}\right]\right]} \qquad (5\text{-}19)$$

$$S_2 = \frac{(1 - S_{i4} - S_3)\left[\frac{k'_2}{k^*_2 + k'_2}\right]}{\left[1 + \frac{k''_2}{k''_{n5}}\left[\frac{X_5}{1 - X_5}\right]\right]} \qquad (5\text{-}20)$$

$$S_1 + 2\,S_2 + 3\,S_3 + 4\,S_{i4} = 5 \qquad (5\text{-}21)$$

where: k - rate constants as shown in Figure 5-22

S_{i4}, S_3, S_2, S_1 - selectivity for isobutane, propane, ethane, and methane

X_5 - conversion of neopentane

The first three equations were determined from a mass balance of isobutane, propane, and ethane around the reactor and the final equation is merely a carbon balance. These expressions are in the form of

selectivity versus conversion and can be applied directly to the experimental data.

Equation 5-18 was fitted to the isobutane selectivity data by nonlinear least squares analysis. The initial parameter estimates were determined by grid search and then Rosenbrock optimization was used to determine the best parameter estimates. Using the predicted values for isobutane selectivity, Equation 5-19 was fitted by nonlinear least squares and similarly Equation 5-20 was also examined. The methane selectivities were then calculated using the carbon balance equation (Equation 5-21) and the predicted selectivities for the other products.

The results of this regression analysis are presented in Table 5-9; Figure 5-19 is a comparison of the experimental and calculated selectivities. The estimated parameter values suggest that the neopentane reacts 18 times slower than isobutane, 21 times slower than propane, and at approximately the same rate as ethane. The large hydrogenolysis rates of the initial products are a partial explanation for the extensive formation of methane. The predicted desorption rates of isobutane and propane are smaller than the rates of cracking of the adsorbed species; these values are in agreement with the trend of the parameters with increasing temperature as calculated from the product distributions for the cracking of the other hydrocarbons (see Section 5.7).

The inclusion of the hydrogen pressure effects in the reaction network improved the prediction of the selectivity data. However, the isobutane and propane selectivities were too small to show the effects

TABLE 5-9

Neopentane Product Distribution Analysis (145°C)

Number of Observations: 28
Temperature: 145°C
Total Pressure: 800 torr

Equation 5-18

Residual Sum of Squares: 6.9×10^{-4}
Residual Root Mean Square: 5.2×10^{-3}

Parameter	Estimated Value	95% Confidence Interval
$\left[\frac{k'_{i4}}{k^*_{i4} + k'_{i4}}\right]$	0.20	±0.02
$\frac{k''_{i4}}{k''_{n5}}$	17.5	±2.

Equation 5-19

Residual Sum of Squares: 2.6×10^{-4}
Residual Root Mean Square: 3.2×10^{-3}

Parameter	Estimated Value	95% Confidence Interval
$\left[\frac{k'_3}{k^*_3 + k'_3}\right]$	0.12	±0.01
$\frac{k''_3}{k''_{n5}}$	21.0	±3.

TABLE 5-9 (continued)

Equation 5-20

Residual Sum of Squares: 5.4×10^{-2}

Residual Root Mean Square: 4.5×10^{-2}

Parameter	Estimated Value	95% Confidence Interval
$\left[\frac{k_2'}{k_2^* + k_2'}\right]$	0.67	±0.07
$\frac{k_2''}{k_{n5}''}$	0.94	±0.3

of hydrogen pressure and therefore only the analysis of ethane selectivities was successful. Ethane and neopentane were assumed to acquire four and three hydrogens on desorption as these values generated the correct overall hydrogen order for hydrogenolysis. Equation 5-20 becomes (Appendix C.4)

$$S_2 = \frac{(1 - S_{i4} - S_3)}{\left[1 + \frac{h_2^*}{h_2'} P_H^{-1.5} + \left[\frac{h_2^* h_2}{h_2' h_{n5}}\right] P_H^{-1.5} \left[1 + \frac{h_{n5}'}{h_{n5}^*} P_H\right]\left[\frac{X_5}{1 - X_5}\right]\right]} \quad (5\text{-}22)$$

The equation was linearized for the initial parameter estimates; these were improved using nonlinear least squares analysis. The data at 145°C and 800 torr were analysed and the results are listed in Table 5-10. The rate constant group $(k_{n5}'/(k_{n5}^* + k_{n5}'))$ can be estimated since the inclusion of the hydrogen pressure terms allows the separation of the neopentane rate constants. The value at a hydrogen partial pressure of 600 torr was 0.80. This value supports the idea that under these conditions the adsorption-desorption reactions of neopentane are near equilibrium while the rupture of the carbon-carbon bonds is the slowest step. The comparison of the experimental and calculated ethane selectivities appears in Figure 5-23; the residual sum of squares was lowered considerably by the inclusion of the hydrogen pressure terms in the rate equations.

5.7 Summary and Discussion

For each of the hydrocarbons studied, the product distribution data were applied to reaction networks (Appendix C) containing reactions

TABLE 5-10

Neopentane Product Distribution Analysis with Hydrogen Pressure Effects

Number of Observations:	28
Temperature:	145°C
Total Pressure:	800 torr

Equation 5-22

Residual Sum of Squares:	3.8×10^{-2}
Residual Root Mean Square:	3.9×10^{-2}

Parameter	Estimated Value
$\frac{h_2^*}{h_2'}$	1.4×10^4 torr$^{1.5}$
$\frac{h_2}{h_{n5}}$	0.22
$\frac{h_{n5}^*}{h_{n5}'}$	1.6×10^2 torr

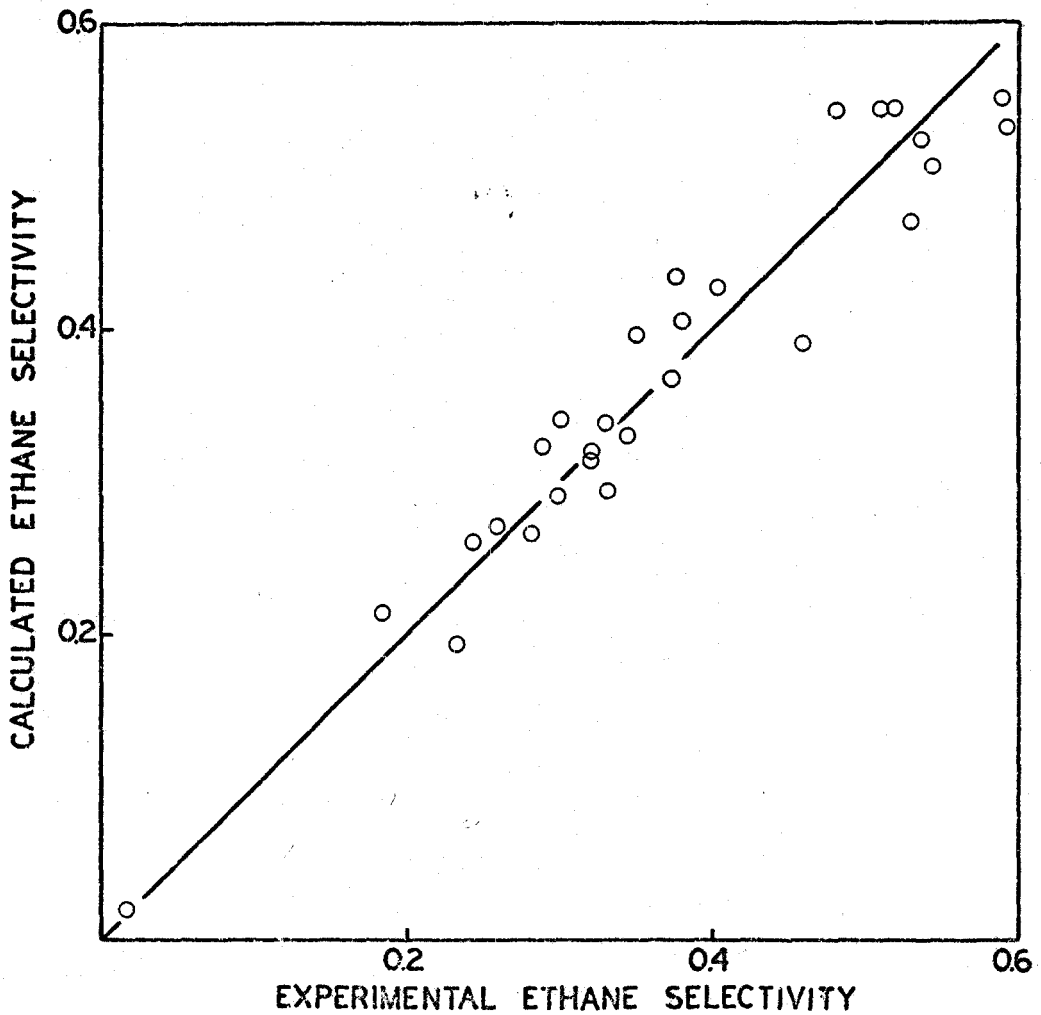

Figure 5-23: Comparison of Experimental and Calculated Ethane Selectivities from the Analysis of Neopentane Data with Hydrogen Pressure Effects

both in series and in parallel. The proposed elementary steps included the reversible adsorption-desorption of all the hydrocarbons and also the irreversible rupture of the carbon-carbon bonds in the adsorbed species to form smaller adsorbed fragments; no assumptions were made concerning the rate-limiting step. Analytical solution of these networks, assuming the reactions were first order with respect to the hydrocarbons, produced selectivity equations which were fitted directly to the data. In the initial analysis, hydrogen partial pressure effects were assumed constant and only isothermal data were considered. However, where the data warranted, terms were also incorporated into the selectivity equations to account for variations in temperature and the effects of hydrogen on the desorption and surface cracking reactions.

There are two criteria for the rejection of the mechanism. First, an inability to explain the data as evidenced by a large residual sum of squares or a correlation of the error with some variable, and second, an unreasonable value of one or more of the estimated parameters, i.e., negative rate constants, fractional split factors greater than unity, etc. Comparisons of the observed and calculated selectivities have demonstrated that the postulated reaction mechanism was capable of fitting the experimental data (Figures 5-1, 5-3, 5-11, 5-15, and 5-19). A discussion of the parameter estimates follows.

There are three distinct types of parameters arising from the derivation of the selectivity equations. First, there are groups appearing in the form $(k_j'/(k_j^* + k_j'))$, where the subscript "j" refers to the particular hydrocarbon being considered. This parameter corresponds

to the relative rates of desorption and cracking of the adsorbed species. The second is the fractional split factors (F, f, and f') which were defined to account for the possibility of isopentane and n-butane splitting at more than one kind of carbon-carbon bond. Finally, there are ratios of rate constants (k''_i/k''_j) which represent the relative overall rates of hydrogenolysis of hydrocarbons "i" and "j". The parameter values for each of these types are discussed individually in the following paragraphs. Fortunately, some of the parameters of the first two types were estimated in more than one way or from more than one set of data, thereby providing an internal check on the consistency of the mechanism. The estimated values for the ratios of hydrogenolysis rate constants can also be checked because they have been independently determined from rate data (Section 4.7). The applicability of the reaction network is dependent upon the validity of the parameter estimates.

For ethane, propane, n-butane, isobutane, and neopentane, the parameter relating to the relative rates of desorption and surface reaction can be determined. These parameters are in the form ($k'_j/(k^*_j + k'_j)$), where k'_j is the desorption rate constant and k^*_j is the rate constant for rupture of the carbon-carbon bonds in the adsorbed species. Because both reactions were assumed first order in the concentration of the adsorbed hydrocarbon, the rates of desorption and cracking vary directly with the values of the rate constants. The parameter must have a value between unity and zero depending upon the relative values of k'_j and k^*_j; the nonlinear regression analysis always

yielded values in this range. When desorption rates are much greater than surface reaction rates, the rupture of the carbon-carbon bonds must be the slowest step; this mechanism has been proposed by Sinfelt (2), and Kikuchi and Morita (36) for the hydrogenolysis of ethane over ruthenium and n-pentane on nickel.

The ethane parameter was estimated from the data for propane at 125°C, n-butane and isobutane at a series of temperatures, and isopentane and neopentane at 110°C and 145°C, respectively. The propane parameter was also estimated from all of these except the propane data. The isobutane parameter could be obtained from the data for isobutane at 125°C, isopentane at 110°C, and neopentane at 145°C. The n-butane parameter was calculated from the n-butane data and the isopentane data, and the neopentane parameter could only be estimated from the neopentane data.

Figure 5-24 shows the parameter values plotted as a function of temperature. The parameter estimates are self consistent despite the fact that they originate from a number of completely independent sets of product distribution data, confirming the acceptability of the reaction network.

The individual rate constants are a strong function of temperature according to an Arrhenius relationship and therefore, in a region where k_j' and k_j^* are comparable in value, the parameter $(k_j'/(k_j^* + k_j'))$ will also be a function of temperature. A general trend of decreasing parameter values was observed with increasing temperature, indicating that the activation energy for rupture of the carbon-carbon bonds is

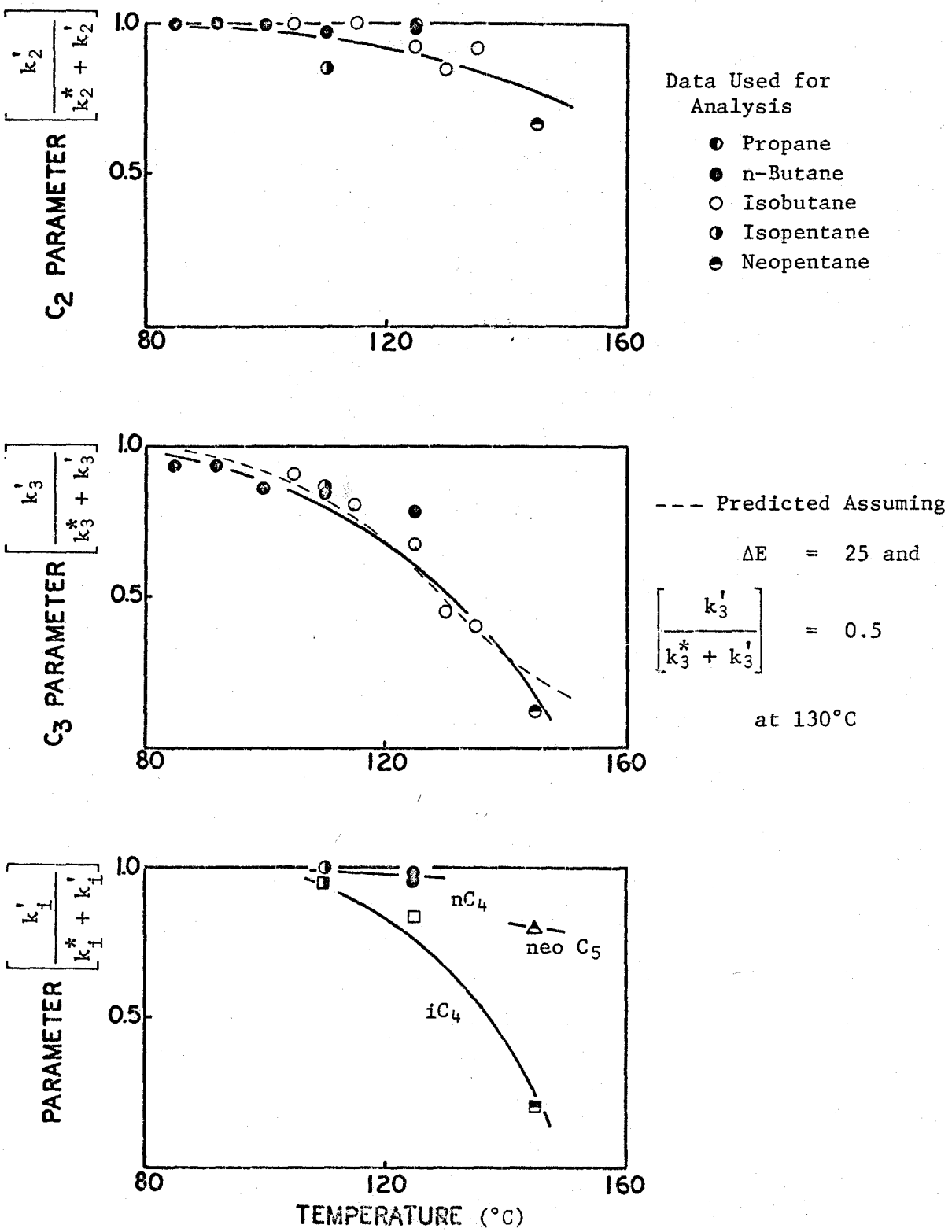

Figure 5-24: Desorption-Cracking Parameters

greater than that for desorption, i.e., k_j^* increases more rapidly with temperature than k_j'. This conclusion compares favourably with previous investigations; for ethane over ruthenium, the activation energy for hydrogenolysis is much greater than that for deuterium exchange (4, 17).

The predicted variation in the parameter corresponding to the adsorbed C_3 species was calculated assuming a difference in activation energies between the cracking and desorption reactions equal to 25 kcal. per mole and a parameter value of 0.5 at 130°C (see Figure 5-24). There is good agreement, suggesting that the activation energy difference is in the order of 25 kcal. per mole.

Certain parameters have been defined to account for the fact that n-butane and isopentane have more than one type of carbon-carbon bond and that parallel cracking reactions can occur. The split factor F represents the fraction of n-butane molecules breaking at the central bond, and f and f' represent the fraction of isopentane cracking to produce isobutane and n-butane, respectively. These parameters are subject to the mathematical constraint that they must lie between zero and unity.

The fractional split factors were estimated from a number of selectivity equations (Table 5-11) and the estimated values were very nearly constant. The n-butane factor F corresponds to one-third of the n-butane molecules splitting at the central carbon-carbon bond and two-thirds at the terminal bonds in the chain. Because there are twice as many terminal bonds as central bonds, we can conclude that the hydrogenolysis reaction is not selective with respect to bond type in

TABLE 5-11

Estimated Fractional Split Factors

Hydrocarbon Data Used	Equation Analysed	Parameter F	Parameter f'	Parameter f
n-Butane	5-4	0.32	—	—
	5-8	0.27	—	—
	5-9	0.31	—	—
Isopentane	5-13	—	∿0.07	—
	5-14	—	—	∿0.82
	5-15	0.31	0.08	—
	5-16	0.41	—	0.80

the n-butane chain. However, the isopentane split factors show that the terminal carbon-carbon bond far from the branched group ruptures about one order of magnitude faster than the carbon-carbon bonds attached to the tertiary carbon. This result is in good agreement with the observation that n-butane reacts ten times faster than isobutane.

The analysis of the selectivity equations also allows the determination of parameters in the form (k_i''/k_j'') where, k_i'' and k_j'' are the rate constants for hydrogenolysis of hydrocarbons "i" and "j". Because the elementary steps in the reaction were assumed first order in the hydrocarbon species concerned, these ratios of rate constants are the relative rates of hydrogenolysis. From analysis of the product distribution for each hydrocarbon, the hydrogenolysis rate of each of the products was determined relative to the feed hydrocarbon. These ratios have been converted by assuming that propane has a reactivity of unity (propane is the largest hydrocarbon occurring in each of the studies). The relative rates of hydrogenolysis of the hydrocarbons have also been determined by measurement of the reaction rates (Section 4.7). These data are compared in Table 5-12. The estimated rates from the analysis of the selectivity equations agree with those determined from rate measurement - another confirmation of the validity of the reaction mechanism.

TABLE 5-12

Estimated Relative Rates of Hydrogenolysis

Source of Data (Feed Hydrocarbon)	Hydrogenolysis Rate for					
	Ethane	Propane	n-Butane	Isobutane	Isopentane	Neopentane
Kinetics	0.02	1	10	0.8	9.5	0.04
Propane	0.07	1	—	—	—	—
n-Butane	0.07	1	5	—	—	—
Isobutane	0.01	1	—	1.0	—	—
Isopentane	0.03	1	6	0.3	10	—
Neopentane	0.05	1	—	0.8	—	0.05

Note: all rates based on a propane rate of unity.

Chapter 6

CONCLUSIONS

A continuous stirred-tank catalytic reactor was constructed and tested to insure that physical transport limitations were negligible for this kinetic study. The reactor was particularly suited to the investigation of hydrogenolysis reactions because the catalyst activity was nearly constant, the reaction occurred readily at low temperatures (80° to 150°C), and the reaction was clean, i.e., uncomplicated by extraneous byproducts.

The catalyst, 0.5 weight percent ruthenium supported on γ-alumina, was examined by the adsorption of nitrogen at 77°K and hydrogen at 20°C, and by electron microprobe analysis to determine its physical properties, including the total surface area, the pore-radius distribution, the ruthenium surface area, and the ruthenium concentration gradient.

The hydrogenolysis reactions of a series of paraffins (propane, n-butane, isobutane, isopentane, and neopentane) were studied and found to have hydrocarbon orders varying from 0.7 to 1.0 and hydrogen orders between -0.66 and -1.5. These orders favour a mechanism in which the dissociative adsorption-desorption of the hydrocarbons is at equilibrium and the rupture of the carbon-carbon bonds in the adsorbed species is the rate-limiting step. The number of hydrogen atoms lost on adsorption of the hydrocarbons was calculated according to the mechanism of Cimino et al. (16) and discussed in terms of α-β adsorbed species. The

activation energies were fairly large, ranging between 36 and 48 kcal. per mole.

The order of reactivity was

n-Butane, Isopentane > Propane, Isobutane > Ethane, Neopentane

The reactivity of the straight chain hydrocarbons increased with the chain length but the presence of branched groups retarded the reactivity by about an order of magnitude. The reactivity of neopentane was particularly low.

The analysis of the product distribution from the reaction of each hydrocarbon yielded a consistent description of the reaction mechanism in which the hydrocarbons adsorb reversibly and the adsorbed species react irreversibly on the surface by rupture of carbon-carbon bonds. The desorption of the adsorbed hydrocarbons was faster than the cracking reaction at the temperatures used for the kinetic studies; at higher temperatures, the surface reaction can become comparable in rate. This series of hydrocarbons provided a wide coverage of the possible relative reactivities of the feed hydrocarbon and its products. For propane, n-butane, and isopentane, the products reacted much slower than the original hydrocarbon; for neopentane, the products cracked more quickly and for isobutane, the products reacted at about the same rate. From the product distribution analysis, the order of reactivity was predicted with good accuracy.

REFERENCES

1. Bond, G.C., "Catalysis by Metals", Academic Press, New York, 1962.

2. Sinfelt, J.H., Catalysis Reviews 3, 175 (1969).

3. Newham, J., Chemical Rev. 63, 123 (1963).

4. Sinfelt, J.H., and Yates, D.J.C., J. Catalysis 8, 82 (1967).

5. Carberry, J.J., Ind. Eng. Chem. 56, 39 (1964).

6. Anderson, J.R., and Baker, B.G., Proc. Roy. Soc. A271, 402 (1963).

7. Wright, P.G., Ashmore, P.G., and Kemball, C., Trans. Far. Soc. 54, 1692 (1958).

8. Galwey, A.K., Proc. Roy. Soc. A271, 218 (1963).

9. Kemball, C., Disc. Faraday Soc. 41, 190 (1966).

10. Morikawa, K., Benedict, W.S., and Taylor, H.S., J. Am. Chem. Soc. 58, 1795 (1936).

11. Morikawa, K., Trenner, N.R., and Taylor, H.S., J. Am. Chem. Soc. 59, 1103 (1937).

12. Taylor, E.H., and Taylor, H.S., J. Am. Chem. Soc. 61, 503 (1939).

13. Kemball, C., and Taylor, H.S., J. Am. Chem. Soc. 70, 345 (1948).

14. Shephard, F.E., J. Catalysis 14, 148 (1969).

15. Anderson, J.R., and Avery, N.R., J. Catalysis 5, 446 (1966).

16. Cimino, A., Boudart, M., and Taylor, H.S., J. Phys. Chem. 58, 796 (1954).

17. Anderson, J.R., and Kemball, C., Proc. Roy. Soc. A223, 361 (1954).

18. Kemball, C., Proc. Roy. Soc. A223, 377 (1954).

19. Hougen, O.A., and Watson, K.M., "Chemical Process Principles, Part III", John Wiley and Sons, New York, 1947.

20. Sinfelt, J.H., Ind. Eng. Chem. 58, 18 (1966).

21. Sinfelt, J.H., and Taylor, W.F., Trans. Faraday Soc. 64, 3086 (1968).

22. Sinfelt, J.H., and Yates, D.J.C., J. Catalysis 10, 362 (1968).

23. Yates, D.J.C., Sinfelt, J.H., and Taylor, W.F., Trans. Far. Soc. 61, 2044 (1965).

24. Sinfelt, J.H., Taylor, W.F., and Yates, D.J.C., J. Phys. Chem. 69, 95 (1965).

25. Yates, D.J.C., and Sinfelt, J.H., J. Catalysis 14, 182 (1969).

26. Taylor, W.F., Yates, D.J.C., and Sinfelt, J.H., J. Phys. Chem. 68, 2962 (1964).

27. Sinfelt, J.H., J. Phys. Chem. 68, 344 (1964).

28. Taylor, W.F., Sinfelt, J.H., and Yates, D.J.C., J. Phys. Chem. 69, 3857 (1965).

29. Yates, D.J.C., and Sinfelt, J.H., J. Catalysis 8, 348 (1967).

30. Yates, D.J.C., Taylor, W.F., and Sinfelt, J.H., J. Am. Chem. Soc. 86, 2996 (1964).

31. Carter, J.L., Cusumano, J.A., and Sinfelt, J.H., J. Phys. Chem. 70, 2257 (1966).

32. Tajbl, D.G., Can. J. Chem. Eng. 47, 154 (1969).

33. Tajbl, D.G., Ind. Eng. Chem. Proc. Des. Dev. 8, 364 (1969).

34. Anderson, J.R., and Avery, N.R., J. Catalysis 7, 315 (1967).

35. Boudart, M., and Ptak, L.D., J. Catalysis 16, 90 (1970).

36. Kikuchi, E., and Morita, Y., J. Catalysis 15, 217 (1969).

37. Anderson, R.B., "Experimental Methods in Catalytic Research", Academic Press, New York, 1968.

38. Satterfield, C.N., and Sherwood, T.K., "The Role of Diffusion in Catalysis", Addison-Wesley Pub. Co., Mass., 1963.

39. Tajbl, D.G., Simons, J.B., and Carberry, J.J., Ind. Eng. Chem. Fund. 5, 171 (1966).

40. Brisk, M.L., Day, R.L., Jones, M., and Warren, J.B., Trans. Instn. Chem. Engrs. 46, T3 (1968).

41. Carberry, J.J., Catalysis Reviews 3, 61 (1969).

42. Blakemore, J.W., and Hoerl, A.E., Chem. Eng. Prog. Symp. Ser. No. 42, 59, 14 (1963).

43. Weller, S., A. I. Ch. E. J. 2, 59 (1956).

44. Boudart, M., A. I. Ch. E. J. 2, 62 (1956).

45. Mezaki, R., and Happel, J., Catalysis Reviews 3, 241 (1969).

46. Draper, N.R., and Smith, H., "Applied Regression Analysis", John Wiley and Sons, New York, 1966.

47. Bard, Y., and Lapidus, L., Catalysis Reviews 2, 67 (1968).

48. Kittrell, J.R., Mezaki, R., and Watson, C.C., British Chem. Eng. 11, 15 (1966).

49. Kittrell, J.R., Hunter, W.G., and Watson, C.C., A. I. Ch. E. J. 11, 1051 (1965).

50. Kittrell, J.R., Mezaki, R., and Watson, C.C., Ind. Eng. Chem. 57, 19 (1965).

51. Brunauer, S., "The Adsorption of Gases and Vapors - Physical Adsorption", Princeton, 1942.

52. De Boer, J.H., and Lippens, B.C., J. Catalysis 3, 38 (1964).

53. Brunauer, S., Emmett, P.H., and Teller, E., J. Am. Chem. Soc. 60, 309 (1938).

54. Lippens, B.C., "Structure and Texture of Aluminas", Thesis, Delft, 1961.

55. Gregg, S.J., and Sing, K.S.W., "Adsorption, Surface Area, and Porosity", Academic Press, New York, 1967.

56. Lippens, B.C., and De Boer, J.H., J. Catalysis 4, 319 (1965).

57. Lippens, B.C., Linsen, B.G., and De Boer, J.H., J. Catalysis 3, 32 (1964).

58. Broekhoff, J.C.P., and De Boer, J.H., J. Catalysis 9, 8 (1967).

59. Broekhoff, J.C.P., and De Boer, J.H., J. Catalysis 9, 15 (1967).

60. Shaw, I.D., "Pore Distribution Calculations", Student Report, McMaster, 1970.

61. Anderson, R.B., J. Catalysis 3, 50 (1964).

62. Brooks, C.S., and Christopher, G.L.M., J. Catalysis 10, 211 (1968).

63. Boudart, M., Adv. in Catalysis 20, 153 (1969).

64. Bond, G.C., Plat. Metals Rev. 12, 100 (1968).

65. "The Electron Probe Microanalyser", McMaster University, 1969.

66. Levenspiel, O., "Chemical Reaction Engineering", John Wiley and Sons, New York, 1962.

67. Coughanowr, D.R., and Koppel, L.B., "Process Systems Analysis and Control", McGraw-Hill, New York, 1965.

68. DeAcetis, J., and Thodos, G., Ind. Eng. Chem. 52, 1003 (1960).

69. Petersen, E.E., "Chemical Reaction Analysis", Prentice-Hall, New Jersey, 1965.

70. Prater, C.D., Chem. Eng. Sci. 8, 284 (1958).

71. Hahn, J.L., and Petersen, E.E., Can. J. Chem. Eng. 48, 147 (1970).

72. Sinfelt, J.H., Ind. Eng. Chem. 62, 22 (1970).

73. Germain, J.E., "Catalytic Conversion of Hydrocarbons", Academic Press, New York, 1969.

74. Morrison, R.T., and Boyd, R.N., "Organic Chemistry", Allyn and Bacon, Boston, 1965.

75. Voge, H.H., and Adams, C.R., Advances in Catalysis 17, 151 (1967).

76. Kochloefl, K., and Bazant, V., J. of Catalysis 10, 140 (1968).

77. Rosenbrock, H.H., Computer J. 3, 175 (1960).

78. Pang, K.H., "Simulation of the Dynamic Behavior and Control Studies of a Liquid-liquid Extraction Column", Ph.D. Thesis, McMaster, 1970.

79. Pang, K.H., Yau, A.Y., and Johnson, A.I., "Application of Hooke and Jeeves' and Rosenbrock's Hill Climbing Techniques", Computer Application Report, McMaster University, 1969.

80. Boudart, M., "Kinetics of Chemical Processes", Prentice-Hall, New Jersey, 1968.

81. Denbigh, K., "The Principles of Chemical Equilibrium", Cambridge University Press, London, 1964.

A P P E N D I X A

ANALYSIS BY GAS CHROMATOGRAPHY

A.1 Description of Apparatus

A model 90P-3 Varian Aerograph chromatograph was used in conjunction with a 125 microlitre gas-sampling valve and a servo/riter one mv. scale recorder to measure the composition of the effluent stream from the reactor. The system separated hydrogen and all of the various saturated hydrocarbons from methane to the pentanes.

Maximum sensitivity is obtained using a carrier gas with a thermal conductivity which differs from that of the components in the sample by as much as possible. However, the molecules to be analysed had such a wide range of conductivities that there was no wholly satisfactory carrier gas. The best compromise was helium, which has a thermal conductivity close to hydrogen, because hydrogen was always the largest portion of the sample.

The column assembly (Figure A-1) was constructed in such a way that both sides of the thermal conductivity cell were used for detection. The first column, which separated the hydrocarbons between ethane and pentane, was 18.2% propylene carbonate supported on 80/100 mesh P-chromosorb and packed in 25 feet of ¼ inch O.D. copper tubing. The column was conditioned in flowing helium for twenty hours at 60°C before use and maintained at 40°C during analysis. Hydrogen and methane were not separated but came through the first column as a single peak - the

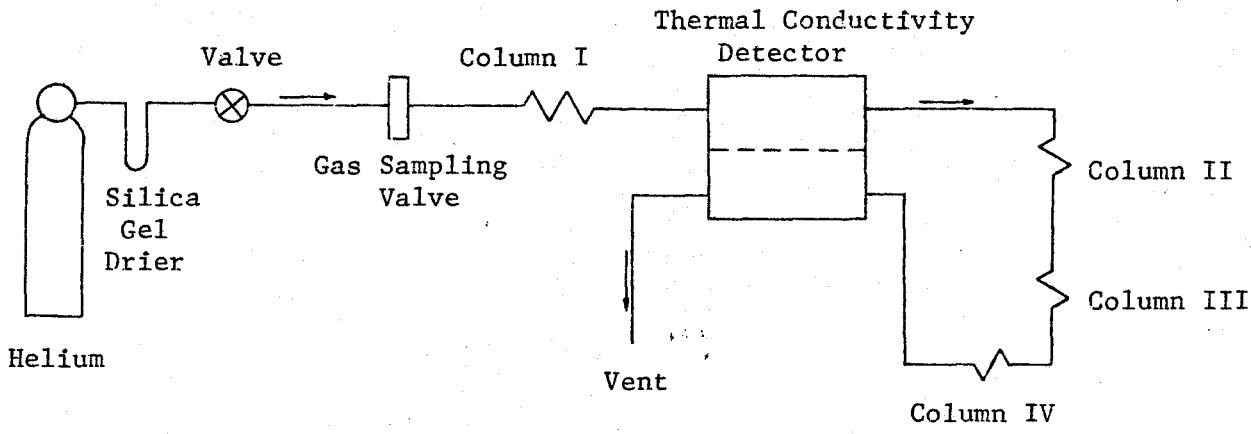

Column I: 25 feet of 18.2% propylene carbonate on 80/100 mesh P-chromosorb

Column II: empty tubing

Column III: 2 feet of 10X molecular sieve, 30/50 mesh

Column IV: 4 feet of 5A molecular sieve, 60/80 mesh

Figure A-1: Gas Chromatograph Schematic

first components to appear. Empty copper tubing was placed directly downstream from the detector to provide a time delay so that no components would arrive at the second side of the detector until all were completely through the first side. Next, two feet of ¼ inch copper tubing packed with 30/50 mesh 10X molecular sieve was used to detain the larger hydrocarbons (isobutane, isopentane, and neopentane) almost indefinitely so that these components were never detected on the second side of the detector. The last column was four feet of 60/80 mesh 5A molecular sieve in ¼ inch copper tubing maintained at about 55°C. This column was responsible for the separation of hydrogen and methane, and also retained ethane, propane, and n-butane so that they did not appear at the second side of the detector. The molecular sieve columns were dehydrated in flowing helium at 350°C for approximately twelve hours before use and the helium carrier gas was dried over silica gel to keep them from being deactivated.

The residence times of the various components are listed in Table A-1. Neopentane and n-butane were not separated; however, they never occurred together in a sample - the reaction of neopentane produced no n-butane (Section 5.6). The hydrogen and methane residence times could be altered by changing the length of the time delay.

A polarity reversal switch was used so that all of the peaks could be plotted in the positive direction. After the hydrocarbons had been eluted from the first column, the polarity was reversed and the hydrogen and methane peaks from the molecular-sieve columns also appeared in a positive direction.

TABLE A-1

Residence Times for Components (min.)

Hydrogen and Methane	8.2
Ethane	8.9
Propane	9.8
Isobutane	11.2
Normal Butane	12.5
Neopentane	12.7
Isopentane	16.2
Normal Pentane	18.2
Polarity Reversed	
Hydrogen	21.2
Methane	27.6

The overall conditions under which the chromatographic system was operated are listed in Table A-2. These conditions were found to give maximum resolution and accuracy.

A.2 Calibration of the Chromatograph

The interpretation of the chromatograms required a correlation between concentration and signal response for each component. Because the sampling valve injected a constant volume, the sample size could be varied by changing the pressure. The sample valve was evacuated; an individual pure component was added up to a desired pressure; the sample was injected; and the corresponding area was recorded. Between fifteen and twenty samples were examined for each component over the range projected for experimental use. The components calibrated in this manner were hydrogen, methane, ethane, propane, and n-butane. Isobutane, isopentane, and neopentane were calibrated using standard mixtures of propane, hydrogen, and the component to be examined. The response of the component was compared to that of propane and the hydrogen was used merely as a diluent.

Intermittent checks of the calibration using standard mixtures produced in a gas cylinder demonstrated that there was no change over the experimental period.

The calibration results are plotted in Figures A-2 and A-3. The data for each component were regressed using linear least squares analysis (Appendix B) of the following equation:

$$P = m S + b \qquad \text{(A-1)}$$

TABLE A-2

Gas Chromatograph Operating Conditions

Temperature of column I:	40°C
Temperature of columns II and III:	room temperature
Temperature of column IV:	55°C
Injector temperature:	70°C
Detector temperature:	70°C
Carrier gas:	helium
Carrier gas flow rate:	40 ml./min.
Filament Current:	200 ma.
Chart Speed:	½ inch per minute
Attenuation:	variable between 1 and 512
Polarity:	variable (negative or positive)

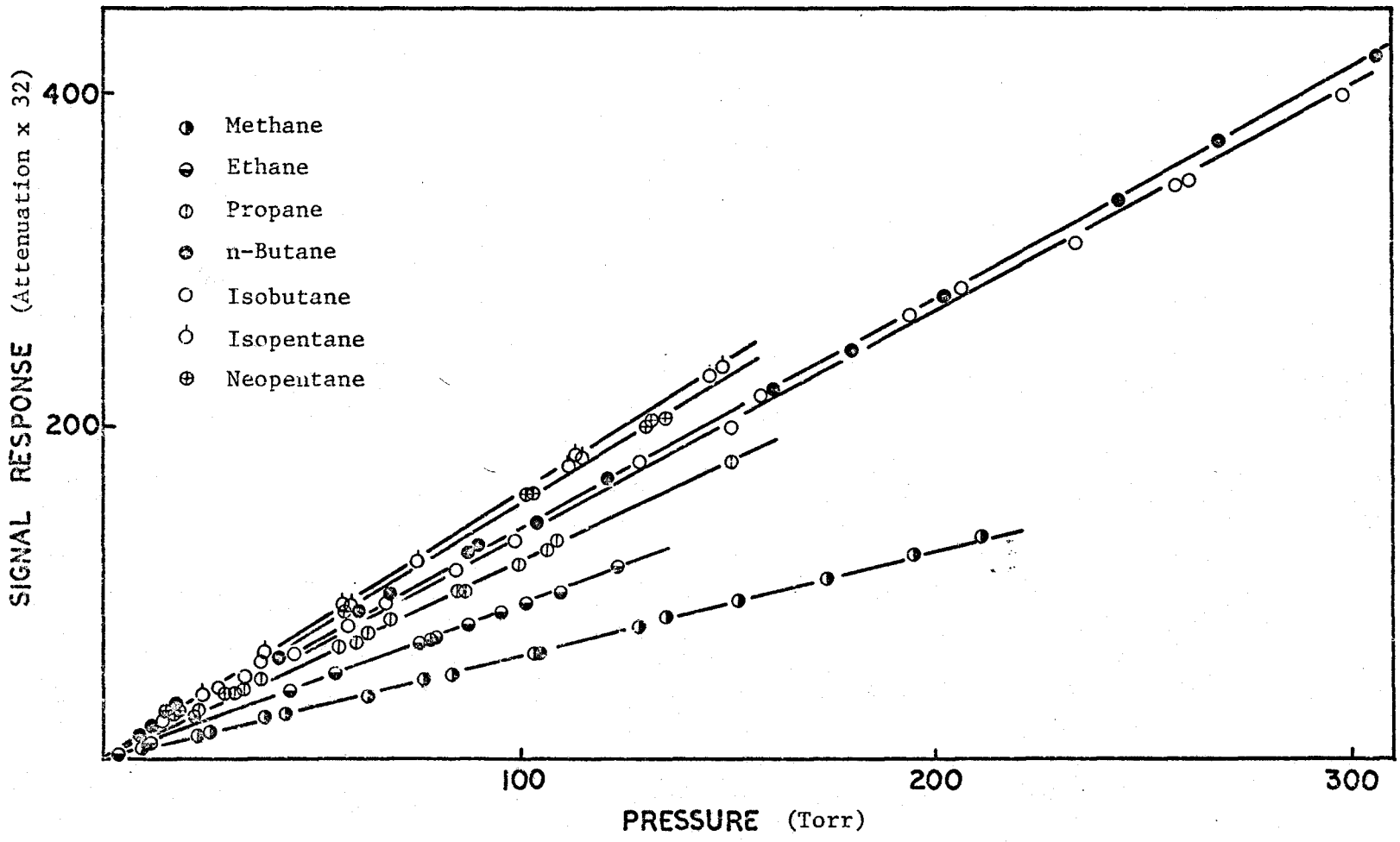

Figure A-2: Chromatographic Calibrations for Hydrocarbons

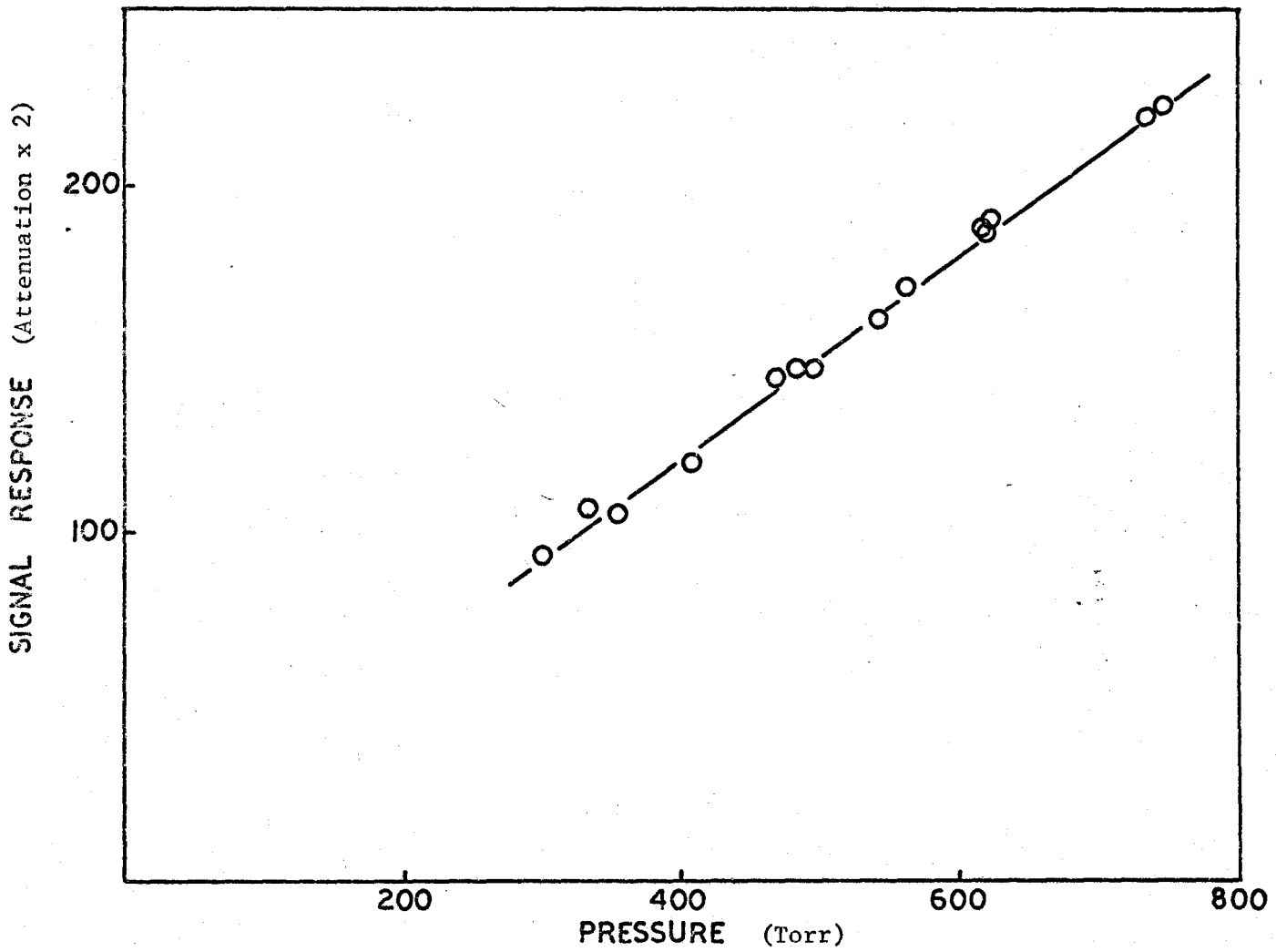

Figure A-3: Hydrogen Chromatographic Calibration

where: P - partial pressure of component (torr)

S - signal intensity in area counts

m, b - parameters

For the hydrocarbons, the intercept "b" was not significantly different from zero at a 95% confidence level and so it was omitted from the correlation. Table A-3 contains the estimated values of the parameters and also the root mean square of the residuals. Because an average sample contained 25 torr of hydrocarbon and 600 torr of hydrogen, the analysis had an error of about 5%. The correlations were used directly to calculate partial pressures and mole fractions from the chromatograms.

TABLE A-3

Chromatographic Calibration Results

	Slope (m)	Intercept (b)	Residual Root Mean Square (torr)
Isopentane	0.6316	-	1.2
Neopentane	0.6511	-	1.0
n-Butane	0.7228	-	2.0
Isobutane	0.7418	-	2.0
Propane	0.8416	-	1.3
Ethane	1.0871	-	1.2
Methane	1.6010	-	1.9
Hydrogen	3.4637	-20.83	10

Note: All hydrocarbon signal intensities were corrected to an attenuation of 32.

Hydrogen signal intensities were corrected to an attenuation of 2.

A P P E N D I X B

CALCULATION PROCEDURES

B.1 Calculation of Conversion, Selectivity, and Rate of Reaction

For each experiment, the reactor temperature and total pressure, and the effluent flow rate and composition were the measured variables. Because the reactor was at steady state and ideally mixed, the effluent properties were representative of the entire system and differential rates and product distributions could be calculated.

Partial pressures for each component in the effluent were determined from the chromatographic-calibration equations (Appendix A) and assuming ideal gas behavior, mole fraction compositions were calculated.

The conversion, defined as the moles of feed hydrocarbon consumed divided by the moles supplied to the reactor, was calculated according to the following equation:

$$X_n = \frac{\sum_{1}^{n-1} j\, Y_j}{\sum_{1}^{n} j\, Y_j} \qquad \text{(B-1)}$$

where: n - the number of carbon atoms per molecule of the feed hydrocarbon

j - series of integer numbers 1, 2, ... n, representing the number of carbon atoms per molecule for the hydrocarbons

X_n - conversion of the feed hydrocarbon

Y_j - mole fraction of hydrocarbon "j" in effluent

The selectivity of the reaction for any particular product was defined as the moles of that product formed divided by the moles of the feed hydrocarbon consumed. The selectivities were calculated from the equation:

$$S_i = \frac{n\, Y_i}{\sum_{1}^{n-1} j\, Y_j} \qquad \text{(B-2)}$$

where: S_i - selectivity of hydrocarbon "i"

The hydrogenolysis rates were normally reported per unit weight of catalyst. These values can easily be transformed to other units such as per surface area or per weight of ruthenium by using the catalyst properties reported in Chapter 2. To calculate the rate of reaction, the following equation was used:

$$r = \frac{F}{W} \cdot \frac{\sum_{1}^{n-1} j\, Y_j}{n} \qquad \text{(B-3)}$$

where: r - rate (moles/g. catalyst - sec.)

F - effluent flow rate (moles/sec.)

W - weight of catalyst in the reactor (g.)

Computer programs were written for each hydrocarbon to perform these calculations.

B.2 Estimation of Parameters in Kinetic Equations

B.2.1 Linear Least Squares Analysis

The most common rate equation for hydrogenolysis kinetics has been a power function with an Arrhenius temperature dependence of the rate constant.

$$r = Ae^{-E/RT} P_H^a P_{HC}^b \qquad \text{(B-4)}$$

where: r - rate of reaction

A - pre-exponential factor

E - activation energy

P_H - hydrogen partial pressure

P_{HC} - hydrocarbon partial pressure

a, b - reaction orders

A mechanistic derivation of this equation as it applies to the hydrogenolysis of small paraffins was originally presented by Cimino et al. (16). This equation can be linearized with respect to the parameters by taking logarithms.

$$\log r = \log A - \frac{E}{2.303\ RT} + a \log P_H + b \log P_{HC} \qquad \text{(B-5)}$$

Best estimates of the parameters, i.e., those values which correspond to a minimum sum of squares of the residual between the experimental and predicted value of the logarithm of the rate, can be determined by linear least squares analysis.

(i) Theory

The general linear relationship can be expressed as:

$$\underline{y} = \underline{X}\,\underline{\theta} + \underline{\varepsilon} \qquad \text{(B-6)}$$

where: $\underline{y}$ - vector of observations

$\underline{X}$ - matrix of constants (functionally dependent upon the operating conditions)

$\underline{\theta}$ - vector of constants to be estimated

$\underline{\varepsilon}$ - vector of experimental errors

The errors are assumed to be normally distributed with a mean of zero and a variance σ^2 which is independent of the observations. For the linearized power-function equation (Equation B-5), the dependent variable is the logarithm of the rate. No experimental tests were made to ensure that the error variance in the logarithm of the rate was constant. As proof of the robustness of the parameter estimates to this assumption, Equation B-4 was examined using the data for n-butane hydrogenolysis by nonlinear least squares, i.e., the error variance in the rate itself was assumed constant; the parameter estimates were well within the 95% confidence intervals of the parameter estimates from linear regression analysis of Equation B-5.

From linear least squares theory (46), the maximum-likelihood unbiased estimates of the parameters are given by

$$\underline{\hat{\theta}} = (\underline{X}'\,\underline{X})^{-1}\,\underline{X}'\,\underline{y} \qquad \text{(B-7)}$$

where: $\underline{\hat{\theta}}$ - vector of best parameter estimates

The variance of these parameters is

$$V(\hat{\underline{\theta}}) = (\underline{X}' \underline{X})^{-1} \sigma^2 \qquad \text{(B-8)}$$

where: $V(\hat{\underline{\theta}})$ - variance-covariance matrix

The 95% confidence intervals were computed using the value of the "Students t" distribution corresponding to the appropriate number of degrees of freedom.

$$\underline{\theta} = \hat{\underline{\theta}} \pm t^{n}_{0.95} [(\underline{X}' \underline{X})^{-1} \sigma^2]^{\frac{1}{2}} \qquad \text{(B-9)}$$

To complete this calculation the value of the variance σ^2 was estimated from a number of replicate experiments for n-butane hydrogenolysis (see Section (ii)).

The linear regression analysis calculations were made using a SHARE library program (SDA #3497) entitled "Linear Least-Squares Curve Fitting Program". This program would transform the data to the form required for fitting and then perform the calculations, printing out detailed lists of statistical information.

(ii) Estimation of Error Variance in Log Rate

Replicate experiments were taken intermittently throughout the kinetic study of n-butane hydrogenolysis and used to estimate the error variance σ^2. The experimental conditions were 125°C, 520 torr of hydrogen, and 30 torr of n-butane. Because the effluent concentration could not be set exactly at these values, the observed rates were corrected slightly using the overall correlation determined for n-butane hydrogenolysis (Table 4-1). In all cases these corrections were very small (less than 1.5%). The data are located in Table B-1.

TABLE B-1

Replicate Experiments for n-Butane Hydrogenolysis

Temperature: 125°C

Hydrogen Partial Pressure: 520 torr

n-Butane Partial Pressure: 30 torr

Run Number	Rate X 10^8 $\left[\frac{\text{moles}}{\text{g. catalyst - sec.}}\right]$
1	26.68
2	27.91
3	27.38
4	25.18
5	27.66
6	26.60
7	26.94
8	26.11
9	26.68
10	25.24

The error variance was calculated according to the equation:

$$V(\log r) = \frac{\Sigma(\log r)^2 - \frac{1}{n}(\Sigma \log r)^2}{n-1} \qquad \text{(B-10)}$$

The variance was 3×10^{-4} and this value was used in determining the confidence intervals of the parameter estimates for the linearized form of the power-function rate equation.

B.2.2 Nonlinear Least Squares Analysis

(i) Parameter Estimation

Most equations describing heterogeneous kinetics are nonlinear in the parameters and therefore require the more general parameter estimation techniques (47). The nonlinear form can be represented by

$$\underline{y} = f(\underline{X}, \underline{\theta}) + \underline{\varepsilon} \qquad \text{(B-11)}$$

where: $\underline{y}$ - vector of observations

$\underline{X}$ - matrix of constants (functionally dependent upon the operating conditions)

$\underline{\theta}$ - vector of parameters

$\underline{\varepsilon}$ - vector of errors

$\partial f/\partial\theta$ - dependent upon the parameter values

If the errors are assumed normally distributed and independent, then the parameter values which minimize the residual sum of squares will also be the maximum-likelihood estimates (46).

$$S(\underline{\theta}) = \Sigma(\underline{y} - f(\underline{X}, \underline{\theta}))^2 \qquad \text{(B-12)}$$

where: $S(\theta)$ - residual sum of squares

The problem of finding the vector $\hat{\theta}$ which minimizes this function is nearly always a search problem and in this investigation direct search methods were used.

The simplest to use but least efficient of these methods is the grid search; values of the residual sum of squares are calculated for various discrete grid points in parameter space and the process is repeated with decreasing grid spacing in the region of minimum $S(\underline{\theta})$ until a minimum (according to some appropriate criterion) is located.

Rosenbrock has developed a much more efficient search method consisting of a trial and error method in which all of the parameter estimates are varied simultaneously (77). The effect of the trial parameters on the objective function determines how the parameters are changed on the next trial with respect to step size and direction. The search therefore moves in a direction in parameter space corresponding to the best success.

All searching techniques require the selection of initial values of the parameters. The number of iterations required to attain a minimum, and also whether convergence is to a local or global minimum are heavily dependent on these initial parameter estimates (50). In this work, the initial estimates were determined either by linearization of the equation and linear least squares analysis or by a grid search.

An executive program was written to receive and transfer input and output information and to control the calculation order when more than one equation was being examined. The subroutine which does the Rosenbrock optimization was written by H. Pang (78) and was called by

the executive program. An object subroutine received the trial parameter values from the Rosenbrock subroutine and, after testing to insure that the values were inside the constraints, the residual sum of squares corresponding to these parameters was determined and returned to the Rosenbrock subroutine. A complete description of the optimization program and its order of calculation is found in the following reference: (79).

The search area was constrained to those values of the parameters which had physical meaning, i.e., rate constants which were positive, etc. The object program adjusted the residual sum of squares upwards whenever one of the trial parameters was beyond a restraint so that this type of trial would always be a failure.

The program was assumed to have converged when the residual sum of squares and best estimate parameter values did not change appreciably with further trials. The best parameter values were then used to calculate the regressed values of the independent variable.

(ii) Confidence Intervals

The 100 (1-α)% confidence contours can be approximated by choosing the values of the parameter vector which satisfy

$$S(\underline{\theta}) = S(\underline{\hat{\theta}}) \left[1 + \frac{P}{n-p} F\ (p,\ n-p,\ 1-\alpha) \right] \qquad \text{(B-13)}$$

where: $S(\underline{\theta})$ - residual sum of squares

$S(\underline{\hat{\theta}})$ - minimum residual sum of squares

n - number of observations

p - number of parameters

F - value of F-distribution corresponding to "p" and "n-p" degrees of freedom and $100(1-\alpha)\%$ confidence level

This approximation is dependent upon the assumption that the linearized form of the model is valid around $\underline{\hat{\theta}}$. The individual confidence intervals were determined using this expression and varying the parameters one at a time while holding the other parameters at their best-estimate value. These intervals are not joint-confidence-region estimates, but for the selectivity equations, the parameters were found to be relatively uncorrelated so that the intervals are representative of the uncertainty in the parameter estimates.

APPENDIX C

THE DEVELOPMENT OF THE EQUATIONS FOR PREDICTING SELECTIVITY

C.1 Introduction

For each of the hydrocarbons examined, the hydrogenolysis reaction created a number of smaller saturated hydrocarbons as products. Usually, all of the alkanes that could be formed by splitting of carbon-carbon bonds without isomerization were observed, although occasionally in small quantities. The relative amounts of these products varied widely with the experimental conditions.

The data have been reported in terms of selectivities. The selectivity for any particular hydrocarbon is defined as the moles of this product formed divided by the moles of feed hydrocarbon consumed. A further discussion of this term and a description of the method of calculation appears in Appendix B.1.

The product distributions depend upon the extent of reaction, i.e., the conversion of the feed hydrocarbon, because every product (excepting methane) can crack again to produce still smaller alkane molecules. Any reaction network proposed to explain the product distribution must take this consecutive reaction scheme into account and must also allow for the parallel hydrogenolysis of any hydrocarbon with more than one type of carbon-carbon bond. The entire reaction scheme is too complex for exact solution and requires some simplifying assumptions.

Nevertheless, a high degree of generality is still retained because no rate-limiting step is assumed and all possible hydrocarbon reactions are considered.

The proposed reaction networks for each hydrocarbon are very similar and vary only in degree of complexity as larger hydrocarbons are treated. The major assumptions are discussed in general before the individual derivations are described.

Each of the hydrocarbons was assumed to adsorb and desorb reversibly to produce reactive species on the metal surface. This type of behavior is well substantiated by deuterium exchange reactions of saturated hydrocarbons (17). The adsorbed species were assumed to react irreversibly via the rupture of one carbon-carbon bond to produce smaller adsorbed fragments; the hydrogenolysis reaction is so highly favoured thermodynamically (73) that the reverse reaction (chain growth) does not occur. Where more than one type of carbon-carbon bond existed in an adsorbed species, a fractional split factor was assigned to each bond type to represent the probability of the hydrogenolysis occurring at that bond. These factors were assumed to be invariant with conversion. No isomerization reactions were considered because isomerization of the feed hydrocarbon was never observed.

Each of the reactions was assumed to be first order in the hydrocarbon involved. This assumption is reasonable; hydrogenolysis reactions have always been reported to be nearly first order with respect to the hydrocarbon (2).

Hydrogen can also reversibly adsorb and desorb on the surface and probably takes part in the surface cracking reaction. However, the effects of the hydrogen partial pressure were assumed to be nearly constant and incorporated into the rate constants. This assumption is justified by the observation that the product distributions observed over a wide range of total pressures (800, 1100, and 1400 torr) for n-butane hydrogenolysis were nearly unaffected by changes in hydrogen pressure. Also, the final form of the selectivity equations (e.g. Equation C-17) is always such that the parameters occur as ratios of rate constants. Thus, any error of incorporating hydrogen pressure effects into a rate constant is minimized by dividing by another rate constant with a similar error.

Equations including terms for the effect of hydrogen on product distribution have been developed by making a reasonable estimate of the hydrogen contribution to the rate constants. Whenever feasible, the data have been analysed using these more complete selectivity equations.

C.2 Propane

The reaction network proposed for the hydrogenolysis of propane appears in Figure C-1. All of the hydrocarbons can adsorb to form a surface species which desorbs reversibly to produce the gaseous hydrocarbon. The adsorbed C_3 species ruptures irreversibly at one carbon-carbon bond to create adsorbed C_2 and C_1 fragments; the C_2 species cracks to produce two adsorbed C_1 species. Each reaction was assumed to be first order in the concentration of the hydrocarbon involved and the corresponding rate constants are shown in the figure.

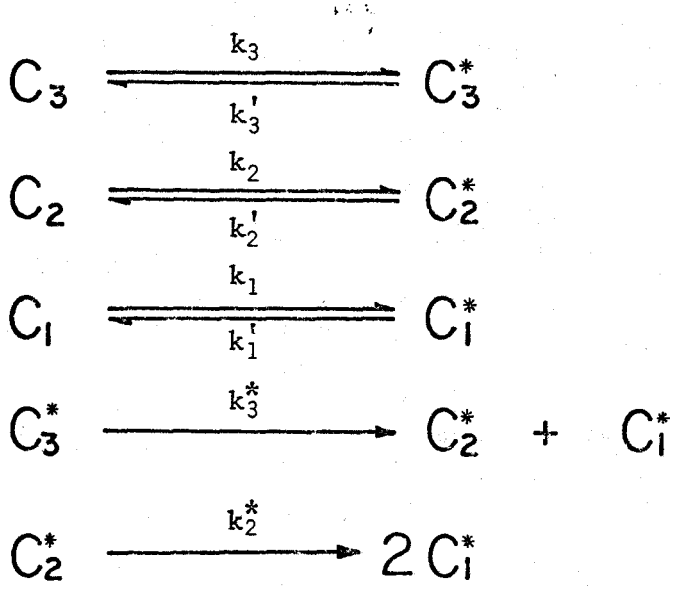

C_3, C_2, C_1 - gaseous propane, ethane, and methane

C_3^*, C_2^*, C_1^* - adsorbed hydrocarbon species

k_i - adsorption rate constant

k_i' - desorption rate constant

k_i^* - cracking rate constant

Figure C-1:
PROPANE HYDROGENOLYSIS MECHANISM

This reaction network can be solved by invoking the steady state approximation (80) for the adsorbed species. The rate equations can then be applied to a mass balance for a continuous stirred-tank reactor to obtain a solution for selectivity as a function of the conversion of the feed hydrocarbon.

From the reaction network, the overall rate of formation of propane is given by

$$R_3 = - k_3 C_3 + k_3' A_3 \qquad (C\text{-}1)$$

$$R_3 = - k_3^* A_3 \qquad (C\text{-}2)$$

where: R_3 - overall rate of formation of propane (per unit volume of reactor)

C_3 - gaseous concentration of propane

A_3 - fractional coverage of catalyst surface by adsorbed C_3 species

The combination of these two equations to eliminate A_3 yields

$$-R_3 = \left[\frac{k_3 k_3^*}{k_3^* + k_3'} \right] C_3 \qquad (C\text{-}3)$$

$$-R_3 = k_3'' C_3 \qquad (C\text{-}4)$$

where: k_3'' - defined as the group of rate constants in Equation C-3

A propane mass balance was made over the reactor; the propane entering in the feed stream either reacts or leaves in the effluent stream. Hydrogenolysis reactions are equimolar (one mole of hydrogen and one of

hydrocarbon combine to form two moles of hydrocarbon) and therefore, there is no change in flow rate between the inlet and effluent streams. The mathematical description of this process is

$$F\,C_3^\circ = F\,C_3 + V\,k_3''\,C_3 \qquad \text{(C-5)}$$

$$C_3^\circ = C_3 + \tau\,k_3''\,C_3 \qquad \text{(C-6)}$$

where: C° - propane concentration in inlet stream

C - propane concentration in reactor and effluent

τ - reactor residence time (V/F)

F - inlet and effluent flow rate

V - reactor volume

Rearrangement of this equation yields

$$\frac{C_3}{C_3^\circ} = \frac{1}{1 + k_3''\,\tau} \qquad \text{(C-7)}$$

and from the definition of conversion

$$X_3 = 1 - \frac{C_3}{C_3^\circ} \qquad \text{(C-8)}$$

where: X_3 - fractional conversion of propane

the following equations are computed:

$$X_3 = \frac{k_3''\,\tau}{1 + k_3''\,\tau} \qquad \text{(C-9)}$$

$$\tau = \frac{X_3}{k_3''\,(1-X_3)} \qquad \text{(C-10)}$$

The overall rate of formation of ethane can be deduced from the reaction network.

$$R_2 = k_2 C_2 - k_2' A_2 \qquad \text{(C-11)}$$

$$R_2 = - k_2^* A_2 + k_3^* A_3 \qquad \text{(C-12)}$$

where: R_2 - overall rate of formation of ethane

C_2 - gaseous concentration of ethane

A_2 - fractional coverage of catalyst surface by adsorbed C_2 species

The amalgamation of these two equations to eliminate A_2 and substitution of Equations C-4 and C-2 gives

$$-R_2 = k_2'' C_2 - \left[\frac{k_2' k_3''}{k_2^* + k_2'}\right] C_3 \qquad \text{(C-13)}$$

where: $k_2'' = \left[\frac{k_2 k_2^*}{k_2^* + k_2'}\right]$

A mass balance over the reactor for ethane reveals that all the ethane which is produced must leave in the exit stream (there is no ethane in the feed stream).

$$0 = C_2 + \tau \left[k_2'' C_2 - \left[\frac{k_2' k_3''}{k_2^* + k_2'}\right] C_3 \right] \qquad \text{(C-14)}$$

Substitution of Equations C-7, C-9, and C-10 yields

$$\frac{C_2}{C_3^\circ} = \frac{\left[\frac{k_2'}{k_2^* + k_2'}\right] X_3}{\left[1 + \frac{k_2''}{k_3''}\left[\frac{X_3}{1 - X_3}\right]\right]} \qquad \text{(C-15)}$$

The definition of selectivity is

$$S_2 = \frac{C_2}{C_3^\circ X_3} \qquad \text{(C-16)}$$

and substitution into Equation C-15 produces

$$S_2 = \frac{\left[\frac{k_2'}{k_2^* + k_2'}\right]}{\left[1 + \frac{k_2''}{k_3''}\left[\frac{X_3}{1 - X_3}\right]\right]} \qquad \text{(C-17)}$$

The last equation is a relationship between the selectivity for ethane and the conversion of propane, and contains two parameters which are essentially complex groups of rate constants. The expression can be applied directly to the data by means of nonlinear regression analysis to obtain the best estimates for these parameters.

The first parameter, $[k_2'/(k_2^* + k_2')]$, corresponds to the relative rates of desorption and cracking of the adsorbed C_2 species. When k_2' is much greater than k_2^*, the parameter value is unity indicating that desorption is much faster than cracking. Under these conditions, the rupture of the carbon-carbon bond is the rate-limiting step for ethane hydrogenolysis.

The second parameter (k_2''/k_3'') is a ratio of rate constants. By examination of Equation C-4, it can be seen that k_3'' is the rate constant corresponding to the overall rate of hydrogenolysis of propane and similarly an examination of Equation C-13 for C_3 equal to zero, i.e., no propane in the system, reveals that k_2'' corresponds to the overall rate of hydrogenolysis of ethane. Because the system is assumed to be first order in all hydrocarbons the ratio of these rate constants represents the relative hydrogenolysis rate of ethane and propane.

Once the ethane selectivity is determined the methane selectivity is automatically fixed by a carbon balance according to

$$2S_2 + S_1 = 3 \qquad \text{(C-18)}$$

because there is only one independent stoichiometric equation in this system as can be easily shown by the method of Denbigh (81).

C.3 Butanes

The reaction network for the hydrocracking of butanes and subsequent cracking of the products (Figure C-2) is similar to the reaction network described for propane. Again, all the hydrocarbons adsorb and desorb reversibly, and the surface species crack irreversibly but, in this case, adsorbed C_4 species can crack to produce C_3 and C_1 fragments or to produce a pair of C_2 species. A fractional split factor, F, was defined to represent the fraction of butane cracking to produce two-carbon radicals. Propane and ethane have only one type of carbon-carbon bond to be broken and methane does not undergo any cracking reactions.

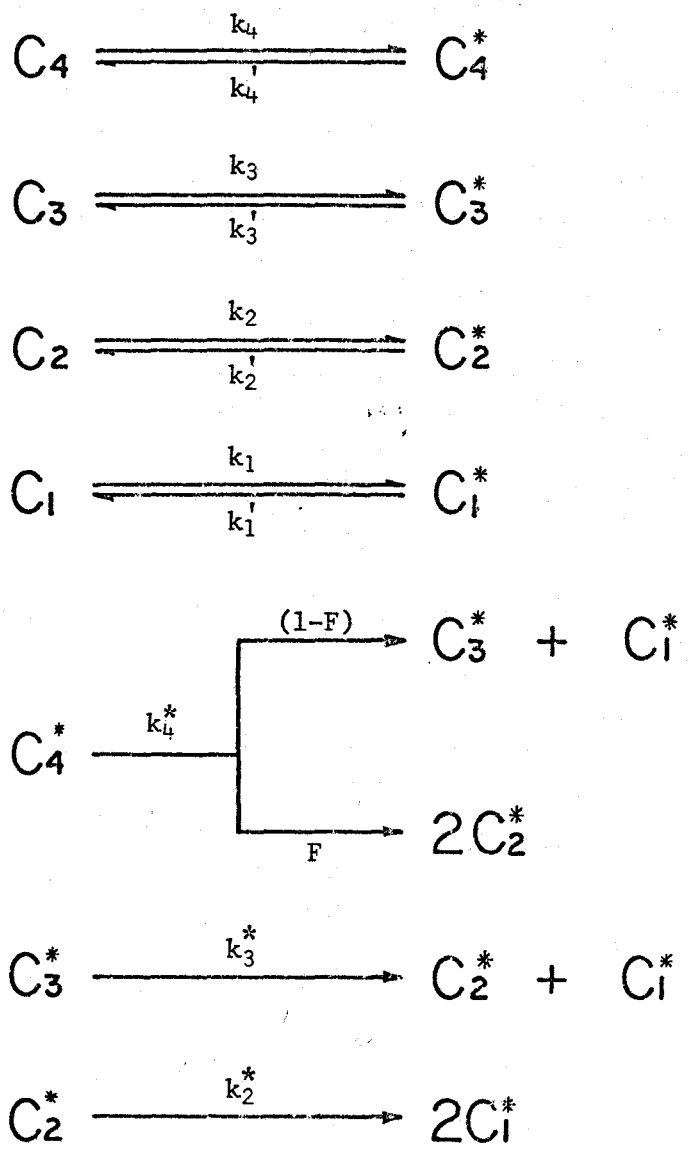

C_4, C_3, C_2, C_1 - gaseous butane, propane, ethane, and methane

C_4^*, C_3^*, C_2^*, C_1^* - adsorbed hydrocarbon species

k_i - adsorption rate constant

k_i' - desorption rate constant

k_i^* - cracking rate constant

Figure C-2:
BUTANE HYDROGENOLYSIS MECHANISM

The reaction network applies equally well for either n-butane or isobutane except that in the case of isobutane the expected value of F is zero.

According to the reaction network, the overall rate of formation of butane is

$$R_4 = - k_4 C_4 + k_4' A_4 \qquad \text{(C-19)}$$

$$R_4 = - k_4^* A_4 \qquad \text{(C-20)}$$

where: R_4 - overall rate of formation of butane

C_4 - gaseous concentration of butane

A_4 - fractional surface area covered by C_4 species

The rearrangement of these two equations to eliminate A_4 yields

$$-R_4 = k_4'' C_4 \qquad \text{(C-21)}$$

where: $$k_4'' = \left[\frac{k_4 k_4^*}{k_4^* + k_4'}\right]$$

A mass balance for butane over the reactor creates a set of equations completely analogous to Equations C-7, C-9, and C-10.

$$\frac{C_4}{C_4^\circ} = \frac{1}{1 + k_4'' \tau} \qquad \text{(C-22)}$$

$$X_4 = \frac{k_4'' \tau}{1 + k_4'' \tau} \qquad \text{(C-23)}$$

$$\tau = \frac{X_4}{k_4'' (1 - X_4)} \qquad \text{(C-24)}$$

where: X_4 - fractional conversion of butane

C_4° - inlet concentration of butane

C_4 - butane concentration in the reactor

τ - reactor residence time

The overall rate of formation of propane is:

$$R_3 = - k_3 C_3 + k_3' A_3 \qquad \text{(C-25)}$$

$$R_3 = - k_3^* A_3 + k_4^* (1 - F) A_4 \qquad \text{(C-26)}$$

where: F - fractional split factor

Substitution of Equations C-20 and C-21 into Equation C-26 and combination with Equation C-25 yields

$$-R_3 = k_3'' C_3 - \left[\frac{k_3' k_4''}{k_3^* + k_3'}\right] (1 - F) C_4 \qquad \text{(C-27)}$$

where: $k_3'' = \left[\frac{k_3 k_3^*}{k_3^* + k_3'}\right]$

A mass balance for propane about the reactor and substitution of Equations C-22, C-23, and C-24 along with the definition of selectivity ($S_3 = C_3 / C_4^\circ X_4$) yields an equation which is completely analogous to Equation C-17.

$$S_3 = \frac{(1 - F)\left[\frac{k_3'}{k_3^* + k_3'}\right]}{\left[1 + \frac{k_3''}{k_4''}\right]\left[\frac{X_4}{1 - X_4}\right]} \qquad \text{(C-28)}$$

An analysis of the reaction network for the overall rate of ethane formation results in the following equations:

$$R_2 = - k_2 C_2 + k_2' A_2 \qquad \text{(C-29)}$$

$$R_2 = - k_2^* A_2 + 2k_4^* FA_4 + k_3^* A_3 \qquad \text{(C-30)}$$

Substitution of the necessary equations to eliminate A_2, A_3, and A_4 yields

$$-R_2 = k_2'' C_2 - \left[\frac{k_2' k_3''}{k_2^* + k_2'}\right] C_3 - \left[\frac{k_2' k_4''}{k_2^* + k_2'}\right] \left[C_4 (1 + F) - \left[\frac{k_3'}{k_3^* + k_3'}\right] (1 - F) \right] \qquad \text{(C-31)}$$

A mass balance for ethane about the reactor and simplification by means of substitution of the equations for selectivity and conversion produces the final equation

$$S_2 = \frac{(1 + F - S_3) \left[\frac{k_2'}{k_2^* + k_2'}\right]}{\left[1 + \frac{k_2''}{k_4''} \left[\frac{X_4}{1 - X_4}\right]\right]} \qquad \text{(C-32)}$$

The number of independent stoichiometric equations in the butane system is two and therefore once the propane and ethane selectivities are determined the methane selectivity is fixed by a carbon balance.

$$S_1 + 2S_2 + 3S_3 = 4 \qquad \text{(C-33)}$$

Equations C-28 and C-32 are relationships between the propane and ethane selectivities and the butane conversion, and can be applied directly to the data to calculate the appropriate parameters. From Equation C-28,

$$(1 - F)\left[\frac{k_3'}{k_3^* + k_3'}\right] \quad \text{and} \quad \frac{k_3''}{k_4''}$$

can be estimated. The first parameter has a complex depending upon the fractional split factor and the relative rates of desorption and surface cracking of propane. The second parameter has a more direct significance; it is the ratio of the rates of hydrogenolysis of propane and butane. The analysis of Equation C-32 affords values for F,

$$\left[\frac{k_2'}{k_2^* + k_2'}\right] \quad \text{and} \quad \frac{k_2''}{k_4''} \quad .$$

The fractional split factor is evaluated independently of the other parameters along with an estimate of the relative rates of desorption and surface cracking for ethane, and a ratio of the rates of hydrogenolysis of ethane and propane. The values of all these parameters provide an insight into the nature of the reaction mechanism.

In the previous development, the hydrogen pressure effects were incorporated into the rate constants. To include the hydrogen pressure effects explicitly, all of the surface cracking reactions were assumed to be one-half order in hydrogen, corresponding to an interaction with one hydrogen atom. The desorption reactions were $(n/2)^{th}$ order in hydrogen, where n represents the number of hydrogen atoms acquired by the adsorbed species on desorption. The adsorption rate was considered

to be independent of the presence of hydrogen. The rate constants can therefore be replaced by a similar rate constant multiplied by the appropriate hydrogen pressure term (the rate constant nomenclature has been changed from "k" to "h" when the hydrogen pressure terms are explicit). Equation C-28 becomes

$$S_3 = \frac{(1 - F)\left[\dfrac{h_3' P_H^{n/2}}{h_3^* P_H^{\frac{1}{2}} + h_3' P_H^{n/2}}\right]}{\left[1 + \dfrac{\left[\dfrac{h_3 h_3^* P_H^{\frac{1}{2}}}{h_3^* P_H^{\frac{1}{2}} + h_3' P_H^{n/2}}\right]}{\left[\dfrac{h_4 h_4^* P_H^{\frac{1}{2}}}{h_4^* P_H^{\frac{1}{2}} + h_4' P_H^{m/2}}\right]}\left[\dfrac{X_4}{1 - X_4}\right]\right]} \qquad \text{(C-34)}$$

where: h - rate constants with hydrogen pressure effects explicit

n,m - number of hydrogen atoms lost by propane and butane on adsorption

P_H - hydrogen partial pressure

On rearrangement this equation transforms to

$$S_3 = \frac{(1 - F)}{\left[1 + \dfrac{h_3^*}{h_3'} P_H^{\frac{1-n}{2}} + \left[\dfrac{h_3^* h_3}{h_3' h_4}\right] P_H^{\frac{1-n}{2}} \left[1 + \dfrac{h_4'}{h_4^*} P_H^{\frac{m-1}{2}}\right]\left[\dfrac{X_4}{1 - X_4}\right]\right]} \qquad \text{(C-35)}$$

Similarly Equation C-32 rearranges to

$$S_2 = \frac{(1 + F - S_3)}{\left[1 + \dfrac{h_2^*}{h_2'} P_H^{\frac{1-v}{2}} + \left[\dfrac{h_2^* h_2}{h_2' h_4}\right] P_H^{\frac{1-v}{2}} \left[1 + \dfrac{h_4'}{h_4^*} P_H^{\frac{m-1}{2}}\right]\left[\dfrac{X_4}{1 - X_4}\right]\right]} \qquad \text{(C-36)}$$

where: v - number of hydrogen atoms lost by ethane on adsorption

The value of the hydrogen orders for the desorption reaction was fixed by choosing values for n, m, and v which would produce an overall hydrogen dependency most closely approximating the hydrogen orders obtained in the kinetic studies (analysis of Equation 4-1). The parameters could then be estimated by nonlinear regression analysis. The net result of including the hydrogen terms is to permit the calculation of certain rate constant ratios (e.g. (h_4'/h_4^*), (h_3/h_4), etc.) which previously existed only in complex inseparable groups. However, these estimates were often poor because the effects of hydrogen pressure on product distribution were about the same order of magnitude as the experimental error.

C.4 Pentanes

The reaction network for the hydrogenolysis of the pentanes is one more step in complexity from that of butanes because the adsorption-desorption and cracking reaction of pentane must now be considered. The system is depicted in Figure C-3. The pentane can split to form nC_4 and C_1 adsorbed species, or iC_4 and C_1, or C_3 and C_2. Two fractional split factors have been defined to cover these possibilities. The factor f' refers to n-butane production; f refers to isobutane production; and the remaining fraction $(1-f'-f)$ applies to the production of propane and ethane. The fractional split factor F for n-butane has been retained. This reaction network applies equally well for isopentane and neopentane except that for neopentane the value of

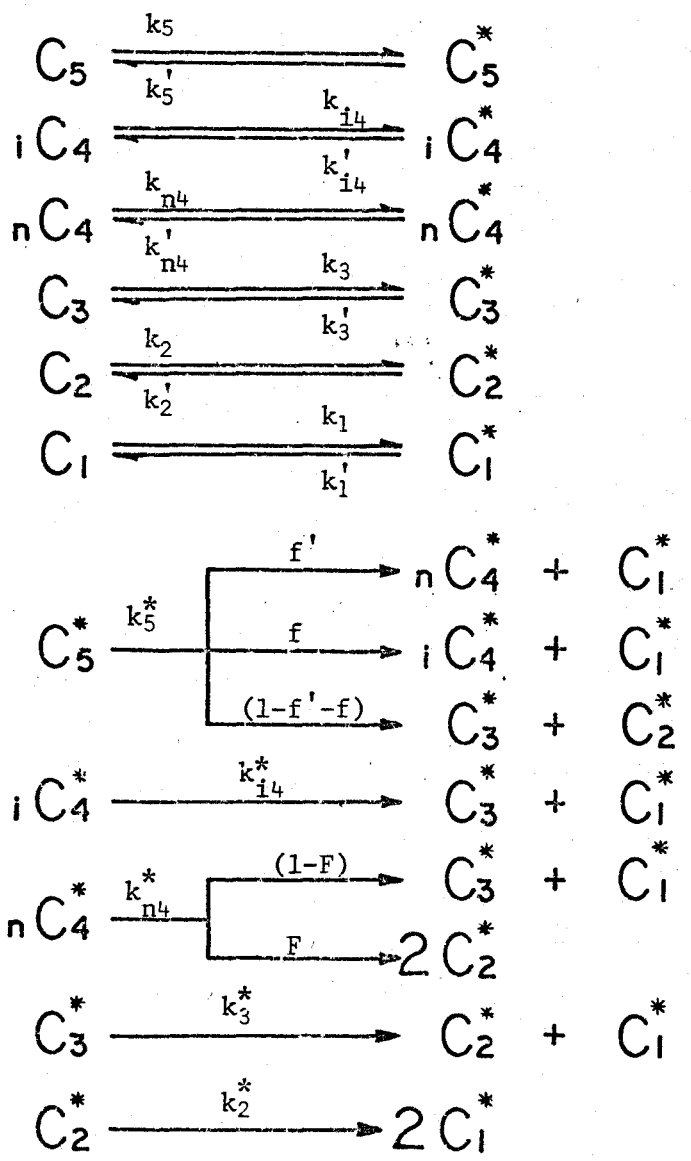

k_i - adsorption rate constant

k_i' - desorption rate constant

k_i^* - cracking rate constant

Figure C-3:
PENTANE HYDROGENOLYSIS MECHANISM

f' must be unity and the nC_4 species is not formed. The complete system is analysed first and then simplifying assumptions are added to obtain the specific equations to be applied to the neopentane data.

The overall rate of formation of pentane can be deduced from the reaction network.

$$R_5 = - k_5 C_5 + k_5' A_5 \tag{C-37}$$

$$R_5 = k_5^* C_5 \tag{C-38}$$

where: R_5 - overall rate of formation of pentane

C_5 - gaseous concentration of pentane

A_5 - fractional surface area covered by C_5 species

The amalgamation of these two equations to eliminate A_5 yields

$$-R_5 = k_5'' C_5 \tag{C-39}$$

where: $$k_5'' = \left[\frac{k_5 k_5^*}{k_5^* + k_5'}\right]$$

The mass balance for pentane about the reactor is derived in exactly the same way as for the propane analysis and gives

$$\frac{C_5}{C_5^\circ} = \frac{1}{1 + k_5'' \tau} \tag{C-40}$$

$$X_5 = \frac{k_5'' \tau}{1 + k_5'' \tau} \tag{C-41}$$

$$\tau = \frac{X_5}{k_5'' (1-X_5)} \qquad \text{(C-42)}$$

where: X_5 - fractional conversion of pentane

C_5° - feed concentration of pentane

C_5 - reactor concentration of pentane

τ - reactor residence time

The overall rate of formation of isobutane is

$$R_{i4} = - k_{i4} C_{i4} + k_{i4}' A_{i4} \qquad \text{(C-43)}$$

$$R_{i4} = - k_{i4}^* A_{i4} + k_5^* f A_5 \qquad \text{(C-44)}$$

where: R_{i4} - overall rate of formation of isobutane

C_{i4} - gaseous concentration of isobutane

A_{i4} - fractional coverage of catalyst surface by iC_4 species

f - fractional split factor

Substitution of Equations C-38 and C-39 into Equation C-44 and combination with C-43 to eliminate A_{i4} yields

$$-R_{i4} = k_{i4}'' C_{i4} - \left[\frac{k_{i4}' k_5''}{k_{i4}^* + k_{i4}'}\right] f C_5 \qquad \text{(C-45)}$$

where: $k_{i4}'' = \left[\frac{k_{i4} k_{i4}^*}{k_{i4}^* + k_3'}\right]$

A mass balance for isobutane over the reactor is given by

$$0 = C_{i4} + k''_{i4} C_{i4} \tau - \left[\frac{k'_{i4} k''_5}{k^*_{i4} + k'_{i4}}\right] f \tau C_5 \qquad \text{(C-46)}$$

Rearrangement and substitution of Equation C-40, C-41, and C-42 gives

$$\frac{C_{i4}}{C^\circ_5} = \frac{f \left[\frac{k'_{i4}}{k^*_{i4} + k'_{i4}}\right] X_5}{\left[1 + \frac{k''_{i4}}{k''_5} \left[\frac{X_5}{1 - X_5}\right]\right]} \qquad \text{(C-47)}$$

The definition of selectivity of isobutane is

$$S_{i4} = \frac{C_{i4}}{C^\circ_5 X_5} \qquad \text{(C-48)}$$

and substitution into Equation C-47 produces

$$S_{i4} = \frac{f \left[\frac{k'_{i4}}{k^*_{i4} + k'_{i4}}\right]}{\left[1 + \frac{k''_{i4}}{k''_5} \left[\frac{X_5}{1 - X_5}\right]\right]} \qquad \text{(C-49)}$$

In considering n-butane, a completely analogous equation can be developed.

$$S_{n4} = \frac{f' \left[\frac{k'_{n4}}{k^*_{n4} + k'_{n4}}\right]}{\left[1 + \frac{k''_{n4}}{k''_5} \left[\frac{X_5}{1 - X_5}\right]\right]} \qquad \text{(C-50)}$$

where: S_{n4} - selectivity of n-butane

$$k''_{n4} = \left[\frac{k_{n4}\, k^*_{n4}}{k^*_{n4} + k'_{n4}}\right]$$

f' - fractional split factor

According to the reaction network, the overall rate of formation of propane is

$$R_3 = - k_3 C_3 + k'_3 A_3 \qquad \text{(C-51)}$$

$$R_3 = - k^*_3 A_3 + k^*_5 (1-f'-f) A_5 + k^*_{i4} A_{i4} + k^*_{n4} (1-F) A_{n4} \qquad \text{(C-52)}$$

Substitution of the necessary equations to eliminate A_3, A_5, A_{i4}, and A_{n4} yields

$$-R_3 = k''_3 C_3 - \left[\frac{k'_3}{k^*_3 + k'_3}\right] \left[k''_{i4} C_{i4} + k''_{n4} (1-F) C_{n4} + k''_5 C_5 \left[- \left[\frac{k'_{i4}}{k^*_{i4} + k'_{i4}}\right] f - \left[\frac{k'_{n4}}{k^*_{n4} + k'_{n4}}\right] f' (1-F) + (1-F f') \right] \right] \qquad \text{(C-53)}$$

The propane mass balance around the continuous stirred-tank catalytic reactor is

$$0 = C_3 - R_3 \tau \qquad \text{(C-54)}$$

Substitution of Equation C-53 and the definitions for selectivity and conversions (Equations C-40, C-41, C-42) produces

$$S_3 = \frac{\left[\frac{k'_3}{k^*_3 + k'_3}\right] (1-f' F - S_{i4} - S_{n4} (1-F))}{\left[1 + \frac{k''_3}{k''_5} \left[\frac{X_5}{1 - X_5}\right]\right]} \qquad \text{(C-55)}$$

An analysis of the reaction network for ethane yields

$$R_2 = - k_2 C_2 + k_2' A_2 \tag{C-56}$$

$$R_2 = - k_2^* A_2 + k_5^* (1-f'-f) A_5 + 2 k_{n_4} F A_{n_4} + k_3 A_3 \tag{C-57}$$

Substitution of the necessary equations to eliminate A_2, A_3, A_{n_4}, and A_{i_4} results in

$$\begin{aligned} -R_2 = {} & k_2'' C_2 - \left[\frac{k_2'}{k_2^* + k_2'}\right] \left(k_3'' C_3 + k_{i_4}'' C_{i_4} \left[1 - \left[\frac{k_3'}{k_3^* + k_3'}\right]\right] \right. \\ & + k_{n_4}'' C_{n_4} \left[(1 + F) - \left[\frac{k_3'}{k_3^* + k_3'}\right] (1 - F)\right] + k_5'' C_5 \left[2 \right. \\ & - f' - f + F f' - \left[\frac{k_{i_4}'}{k_{i_4}^* + k_{i_4}'}\right] f - (1 + F) f' \\ & \left[\frac{k_{n_4}'}{k_{n_4}^* + k_{n_4}'}\right] + \left[\frac{k_3'}{k_3^* + k_3'}\right] \left[\left[\frac{k_{i_4}'}{k_{i_4}^* + k_{i_4}'}\right] f + \left[\frac{k_{n_4}'}{k_{n_4}^* + k_{n_4}'}\right] \right. \\ & \left. \left. \left. f' (1 - F) - (1 - F f') \right] \right] \right) \end{aligned} \tag{C-58}$$

The ethane mass balance is

$$0 = C_2 - R_2 \tau \tag{C-59}$$

The substitution of Equation C-58 along with the definition of selectivity and conversion produces

$$S_2 = \frac{\left[\frac{k_2'}{k_2^* + k_2'}\right] (2-f-f' + F\,f' - S_{i4} - S_{n4}\,(1+F) - S_3)}{\left[1 + \frac{k_2''}{k_5''}\left[\frac{X_5}{1 - X_5}\right]\right]} \qquad \text{(C-60)}$$

Equations C-49, C-50, C-55, and C-60 are the four expressions which relate the product selectivities to pentane conversion and can therefore be applied directly to the isopentane data. The methane selectivity is again fixed by a carbon balance

$$S_1 + 2\,S_2 + 3\,S_3 + 4\,S_{i4} + 4\,S_{n4} = 5 \qquad \text{(C-61)}$$

The hydrogenolysis of neopentane is a special case of the complete reaction network for pentane cracking. Due to the structure of the neopentane molecule, n-butane, propane, and ethane cannot be formed as primary products. Therefore, the factor f is unity and f' has a value of zero. Because no isomerization reactions are being considered, the selectivity for n-butane must be zero (this was experimentally observed). The selectivity equations may be simplified to

$$S_{i4} = \frac{\left[\frac{k_{i4}'}{k_{i4}^* + k_{i4}'}\right]}{\left[1 + \frac{k_{i4}''}{k_5''}\left[\frac{X_5}{1 - X_5}\right]\right]} \qquad \text{(C-62)}$$

$$S_3 = \frac{(1 - S_{i_4}) \left[\frac{k_3'}{k_3^* + k_3'}\right]}{\left[1 + \frac{k_3''}{k_5''} \left[\frac{X_5}{1 - X_5}\right]\right]} \qquad \text{(C-63)}$$

$$S_2 = \frac{(1 - S_{i_4} - S_3) \left[\frac{k_2'}{k_2^* + k_2'}\right]}{\left[1 + \frac{k_2''}{k_5''} \left[\frac{X_5}{1 - X_5}\right]\right]} \qquad \text{(C-64)}$$

$$S_1 + 2\,S_2 + 3\,S_3 + 4\,S_4 = 5 \qquad \text{(C-65)}$$

The physical significance of each parameter is similar to those for the propane and butane analyses. The isopentane data affords a direct calculation of the fractional split factors f and f'. The relative rates of hydrogenolysis of the various hydrocarbons, and of desorption and cracking of the adsorbed species are also determined.

The hydrogen pressure dependencies of the desorption and surface cracking reactions can also be added similarly to the way in which the butane equations were altered (Equations C-35 and C-36). This method was used to calculate some rate constants which previously existed in inseparable groups.

A P P E N D I X D

TABLES OF EXPERIMENTAL DATA

TABLE D-1

Propane Hydrogenolysis Rate Data

Temperature: 125°C

Total Pressure: 800 torr

Partial Pressure (torr)				Rate (X 10^8) $\left[\frac{\text{moles}}{\text{g. catalyst - sec.}}\right]$
Hydrogen	Propane	Ethane	Methane	
777	13.3	4.8	5.0	2.35
723	48.1	14.0	15.2	8.86
720	38.2	20.0	22.0	6.50
747	30.5	10.5	12.3	4.85

TABLE D-2

n-Butane Hydrogenolysis Rate Data

Total Pressure: 800 torr

Temperature (°C)	Partial Pressure (torr) Hydrogen	n-Butane	Propane	Ethane	Methane	Rate (X 10^8) $\left[\frac{\text{moles}}{\text{g. catalyst - sec.}}\right]$
125	516	30.8	34.4	101	118	26.8
125	584	24.8	26.9	76.9	87.4	19.3
125	659	19.2	19.6	48.4	53.8	12.0
125	520	29.4	32.7	100	118	26.8
125	457	29.9	34.3	128	151	33.4
125	510	27.5	32.0	104	127	27.0
125	357	34.2	38.7	168	202	45.0
125	517	29.7	32.3	100	121	26.6
125	728	10.6	10.4	23.6	27.4	5.88
125	515	32.0	34.2	100	119	26.3
125	517	29.1	32.1	102	121	26.4
125	662	36.0	19.6	38.2	44.2	19.3
125	604	42.6	25.8	59.8	68.1	29.5
125	736	16.8	9.1	17.6	20.2	8.42
125	536	49.8	31.7	83.5	98.8	42.4
125	523	32.6	32.3	97.5	115	25.6
125	516	30.2	31.3	101	122	26.3

TABLE D-2 (continued)

Temperature (°C)	Partial Pressure (torr) Hydrogen	n-Butane	Propane	Ethane	Methane	Rate (X 10^8) $\left[\frac{\text{moles}}{\text{g. catalyst - sec.}}\right]$
125	714	30.3	11.0	20.4	24.0	15.6
125	681	40.2	15.2	29.1	34.5	22.6
125	637	54.5	20.4	40.1	48.4	31.5
125	508	31.2	31.7	102	127	26.9
125	520	29.4	30.2	99.1	122	25.8
125	521	30.6	29.4	97.6	122	25.8
125	530	29.7	30.8	95.0	114	25.0
125	452	35.4	32.2	128	153	35.9
125	454	43.6	37.3	122	143	43.1
125	457	42.4	37.5	123	140	41.5
125	462	42.6	36.9	120	139	40.7
110	705	62.7	8.6	11.5	12.4	3.29
110	723	41.9	9.1	12.4	13.5	2.26
110	643	105	13.8	18.8	19.7	5.79
100	660	129	3.4	4.3	4.0	1.44
100	561	213	7.5	9.3	9.3	2.55
100	613	168	5.5	6.8	6.9	1.73
100	545	235	5.4	6.5	7.5	2.79
100	465	302	9.5	11.4	12.5	3.71

TABLE D-2 (continued)

Temperature (°C)	Partial Pressure (torr) Hydrogen	n-Butane	Propane	Ethane	Methane	Rate (X 10^8) $\left[\frac{\text{moles}}{\text{g. catalyst} - \text{sec.}}\right]$
100	617	171	3.4	3.9	4.5	1.52
100	472	295	9.4	11.9	12.2	3.77
85	592	199	2.7	3.3	3.3	0.13
85	587	203	3.0	3.6	3.2	0.14
85	530	261	3.1	3.8	3.6	0.18

TABLE D-3

n-Butane Hydrogenolysis Rates at Higher Pressures

Reactor Temperature: 125°C

Total Pressure (torr)	Partial Pressure (torr)					Rate ($X 10^8$) $\left[\frac{\text{moles}}{\text{g. catalyst - sec.}}\right]$
	Hydrogen	n-Butane	Propane	Ethane	Methane	
1100	652	152	61.5	113	122	44.5
1100	756	139	45.5	77.1	82.4	32.6
1100	824	122	35.7	57.4	61.6	26.6
1400	995	256	39.9	52.8	56.6	18.7
1400	962	255	48.5	65.2	69.1	20.2
1400	1006	221	45.7	62.6	65.4	18.3
1400	963	236	52.2	72.8	76.5	19.9
1400	1023	229	39.7	53.8	55.2	17.7
1400	1084	183	36.9	44.7	51.5	15.3
1400	1129	156	30.8	40.9	43.3	12.5
1400	1076	204	32.5	43.1	44.7	17.5
1400	1112	171	31.1	41.6	44.0	16.3
1400	1169	142	24.0	31.8	32.7	12.0

TABLE D-4

Isobutane Hydrogenolysis Rate Data

Total Pressure: 800 torr

Temperature (°C)	Partial Pressure (torr) Hydrogen	Isobutane	Propane	Ethane	Methane	Rate (X 10^8) $\left[\frac{\text{moles}}{\text{g. catalyst - sec.}}\right]$
		(Second Catalyst Charge)				
125	568	49.6	15.3	46.3	121	16.1
125	578	52.9	15.5	42.7	111	15.9
125	702	38.0	9.9	12.9	37.4	11.6
125	698	35.5	10.6	15.2	40.7	11.0
125	771	9.4	2.5	4.3	13.1	3.46
125	661	64.1	13.6	15.1	46.6	15.4
125	780	5.9	2.2	2.8	8.6	2.35
125	698	41.9	11.2	12.1	36.4	11.9
125	697	37.4	9.7	14.6	41.2	11.5
125	677	67.6	10.9	10.6	33.9	15.3
125	724	38.3	7.6	7.4	23.2	10.7
125	653	89.0	11.4	11.1	35.7	18.5
125	761	18.2	4.3	4.1	12.7	6.35
125	691	48.3	10.9	11.3	38.5	13.8
125	687	34.0	12.4	17.6	49.3	10.9

TABLE D-4 (continued)

Temperature (°C)	Partial Pressure (torr) Hydrogen	Isobutane	Propane	Ethane	Methane	Rate ($X 10^8$) $\left[\frac{\text{moles}}{\text{g. catalyst - sec.}}\right]$
125	686	10.3	3.9	28.5	71.3	3.95
125	764	21.9	3.4	2.4	8.6	7.70
125	690	38.7	12.4	14.7	44.4	11.8
125	690	36.0	10.7	16.5	47.1	11.3
125	658	28.1	11.5	28.9	73.9	8.96
125	686	35.0	12.3	17.5	49.4	11.1
125	678	39.1	10.9	18.9	52.9	12.3
125	686	43.3	10.9	15.1	44.9	13.1
130	510	29.8	7.2	68.5	184	21.4
115	641	123	12.3	3.2	20.4	8.03
115	675	87.7	12.7	3.9	20.9	6.88
115	713	58.4	8.9	3.3	16.1	4.84
105	654	127.2	7.9	1.0	9.7	2.62
105	687	97.3	6.6	1.0	8.1	2.22
104	642	150.3	3.5	0.6	3.9	2.22
		(First Catalyst Charge)				
125	626	111	13.8	11.8	37.5	6.30
125	574	149	16.4	14.5	45.8	8.19
125	591	130	16.4	15.1	47.7	6.99
125	617	119	14.3	11.4	37.6	6.41
125	627	109	12.6	12.3	38.7	6.27

TABLE D-5

Isopentane Hydrogenolysis Rate Data

Temperature (°C)	Partial Pressure (torr)						Rate (X 10^8) $\left[\frac{\text{moles}}{\text{g. catalyst - sec.}}\right]$
	Hydrogen	Isopentane	n-Butane	Isobutane	Propane	Ethane	Methane	
110	653	76.1	1.8	29.1	2.7	3.3	34.5	17.1
110	691	49.9	1.5	23.6	2.5	3.4	28.4	11.7
110	723	35.0	1.2	16.0	2.0	2.9	19.4	8.54
110	663	77.9	1.7	24.0	2.3	3.3	27.9	16.3
110	691	39.6	2.0	26.7	3.5	4.1	33.1	10.5
110	654	60.0	2.4	33.4	3.8	5.0	41.1	13.1
110	731	32.2	1.3	13.8	1.9	2.4	17.6	8.18
110	756	18.6	1.0	8.9	1.6	2.0	12.1	5.19
110	731	27.8	1.4	15.0	2.4	2.8	19.4	7.16
110	708	31.8	1.9	22.0	3.3	4.1	28.5	8.05
110	669	65.2	2.9	25.4	2.8	3.6	30.8	15.4
110	641	91.5	2.6	26.8	2.4	3.5	31.9	19.5
110	664	82.8	2.3	21.6	2.0	2.6	25.0	17.5
110	683	64.0	2.0	21.4	2.1	2.5	25.5	15.2
110	603	29.0	2.2	60.6	10.6	11.7	83.1	9.26
110	567	79.7	2.9	59.8	7.4	9.5	73.4	18.1
110	518	41.7	2.6	88.0	12.4	21.0	116.8	13.7

TABLE D-5 (continued)

Temperature (°C)	Partial Pressure (torr) Hydrogen	Isopentane	n-Butane	Isobutane	Propane	Ethane	Methane	Rate (X 10^8) $\left[\frac{\text{moles}}{\text{g. catalyst - sec.}}\right]$
110	699	81.9	2.9	26.2	3.6	4.3	32.0	14.4
110	771	37.8	1.8	14.9	2.7	3.4	18.9	7.62
110	796	24.1	1.4	10.2	2.4	2.4	13.9	5.47
110	687	96.8	3.3	25.4	3.3	3.6	30.6	16.3
120	600	41.6	1.7	55.6	7.4	15.6	77.8	41.6
120	619	38.8	1.6	48.9	6.7	14.8	70.6	41.4
109	662	83.2	1.3	23.3	2.1	2.8	25.2	14.2
109	695	41.6	0.8	24.5	2.2	4.2	31.8	9.41
100	715	65.8	2.0	6.7	1.2	1.3	8.4	2.59
100	665	101	3.0	12.2	1.8	1.8	15.1	3.97
100	718	54.3	0.5	11.3	0.9	1.3	13.3	2.39
90	680	111	2.3	2.6	0.5	0.1	3.4	0.83

TABLE D-6

Neopentane Hydrogenolysis Rate Data

Total Pressure: 800 torr

Temperature (°C)	Partial Pressure (torr)						Rate (X 10^8) $\left[\frac{\text{moles}}{\text{g. catalyst} - \text{sec.}}\right]$
	Hydrogen	Neopentane	Isobutane	Propane	Ethane	Methane	
145	593	37.1	0.5	0.2	11.0	158	14.2
145	654	35.9	0.4	0.1	9.1	100	12.3
145	398	48.1	0.5	0.2	13.7	339	28.2
145	742	14.0	0.2	0.1	4.0	40.1	5.39
145	758	9.9	0.1	0.1	2.7	29.3	3.98
145	537	31.1	0.3	0.1	14.0	217	13.4
145	572	30.0	0.3	0.1	12.7	185	14.9
145	431	32.0	0.3	0.1	16.5	320	16.6
145	742	7.4	0.04	0.02	3.8	46.8	3.33
145	656	11.2	0.2	0.1	7.1	126	4.62
145	751	4.0	0.04	0.02	2.6	42.1	1.53
145	577	34.2	0.3	0.2	13.1	175	14.5
145	591	33.4	0.4	0.2	10.8	164	13.8
145	115	12.4	0.02	0.0	2.3	670	23.4
145	570	31.4	0.3	0.2	14.2	184	14.7

TABLE D-6 (continued)

Temperature (°C)	Partial Pressure (torr) Hydrogen	Neopentane	Isobutane	Propane	Ethane	Methane	Rate ($X 10^8$) $\left[\frac{\text{moles}}{\text{g. catalyst} \cdot \text{sec.}}\right]$
145	622	29.0	0.3	0.1	10.7	138	11.4
145	615	26.8	0.3	0.1	10.9	147	12.7
145	637	24.2	0.3	0.1	10.4	128	9.81
145	658	29.6	0.3	0.1	11.6	101	11.4
145	657	32.5	0.3	0.1	8.4	101	11.8
150	648	12.5	0.1	0.1	5.7	133	11.5
155	578	13.2	0.1	0.1	5.2	203	19.1
155	709	7.8	0.05	0.03	3.5	79.7	9.55
135	707	50.6	0.5	0.4	6.3	35.5	3.97
135	717	31.1	0.4	0.3	6.9	44.0	3.31
135	780	6.0	0.1	0.1	1.8	12.2	0.64
125	764	24.8	0.2	0.2	2.2	8.9	0.63
125	724	53.1	0.4	0.5	4.3	17.9	1.20

TABLE D-7

Product Distribution for Propane Hydrogenolysis

Temperature: 125°C

Total Pressure: 800 torr

Conversion of Propane (%)	Selectivity Ethane	Methane
7.3	1.002	0.996
23.0	0.973	1.054
26.7	0.955	1.091
26.7	0.985	1.030
35.2	0.968	1.065
36.1	0.962	1.076
57.6	0.899	1.203
61.1	0.906	1.189

TABLE D-8

Product Distribution for n-Butane Hydrogenolysis (125°C)

Temperature: 125°C

Total Pressure: 800 torr

Conversion of n-Butane (%)	Selectivity Propane	Ethane	Methane
0*	0.56	0.75	0.80
44.6	0.451	0.833	0.981
46.2	0.457	0.843	0.944
46.2	0.440	0.841	0.997
46.5	0.430	0.845	1.020
48.0	0.449	0.841	0.973
49.8	0.434	0.849	0.999
54.1	0.415	0.867	1.021
55.1	0.440	0.850	0.979
55.5	0.437	0.852	0.985
58.1	0.397	0.886	1.036
60.9	0.389	0.902	1.028
64.4	0.351	0.926	1.095
69.5	0.329	0.966	1.081
69.7	0.329	0.966	1.081
69.9	0.329	0.971	1.070
71.3	0.328	0.955	1.106
71.3	0.392	0.893	1.038
73.1	0.306	0.989	1.104
73.2	0.375	0.924	1.027
74.1	0.299	0.979	1.145

* by extrapolation of selectivity versus temperature data

TABLE D-8 (continued)

Conversion of n-Butane (%)	Selectivity Propane	Ethane	Methane
74.2	0.301	0.982	1.131
74.6	0.301	0.988	1.122
75.7	0.317	0.960	1.129
76.3	0.336	0.938	1.114
76.4	0.334	0.956	1.087
76.5	0.334	0.943	1.111
76.7	0.324	0.949	1.129
76.8	0.290	0.964	1.203
77.0	0.311	0.958	1.152
77.3	0.297	0.959	1.191
77.4	0.325	0.953	1.118
77.6	0.300	0.965	1.171
77.7	0.295	0.960	1.185
77.9	0.309	0.960	1.154
78.0	0.314	0.963	1.132
78.1	0.255	1.013	1.208
78.3	0.306	0.967	1.148
78.4	0.314	0.954	1.148
78.8	0.315	0.956	1.144
79.6	0.297	0.967	1.176
81.0	0.269	0.967	1.176
82.7	0.206	1.029	1.232
86.7	0.236	0.940	1.411
87.7	0.237	0.930	1.429
89.0	0.230	0.964	1.383
89.3	0.224	0.968	1.392
89.8	0.193	1.020	1.383
90.2	0.191	1.007	1.414

TABLE D-9

Product Distribution for n-Butane Hydrogenolysis (110°C)

Temperature: 110°C

Total Pressure: 800 torr

Conversion of n-Butane (%)	Selectivity Propane	Ethane	Methane
5	0.59	0.72	0.78
19.0	0.560	0.762	0.795
19.6	0.559	0.755	0.812
26.7	0.573	0.709	0.862
28.1	0.555	0.756	0.823
40.2	0.547	0.718	0.924
41.1	0.539	0.729	0.925
42.0	0.540	0.727	0.925
42.3	0.530	0.740	0.931
42.3	0.557	0.709	0.912
42.4	0.539	0.733	0.919
42.7	0.539	0.737	0.909
45.9	0.541	0.724	0.929
46.7	0.537	0.725	0.940
46.7	0.543	0.717	0.937
50.9	0.527	0.732	0.957

TABLE D-10

Product Distribution for n-Butane Hydrogenolysis at Other Temperatures

Total Pressure: 800 torr

Conversion of n-Butane (%)	Selectivity Propane	Ethane	Methane
	Temperature: 100°C		
3.2	0.602	0.697	0.800
3.7	0.587	0.708	0.822
4.2	0.596	0.756	0.701
5.0	0.594	0.717	0.784
5.2	0.596	0.732	0.747
5.2	0.584	0.744	0.762
5.6	0.594	0.738	0.743
	Temperature: 85°C		
1.9	0.607	0.739	0.700
2.2	0.603	0.735	0.721
2.3	0.613	0.747	0.666

TABLE D-11

Product Distribution for n-Butane Hydrogenolysis at Higher Pressures

Total Pressure (torr)	Temperature (°C)	Conversion of n-Butane (%)	Selectivity		
			Propane	Ethane	Methane
1100	125	36.8	0.503	0.810	0.870
1100	125	40.2	0.488	0.827	0.884
1100	125	46.7	0.462	0.849	0.916
1400	125	21.6	0.566	0.749	0.803
1400	125	21.9	0.570	0.754	0.783
1400	125	22.8	0.570	0.757	0.776
1400	125	23.6	0.564	0.763	0.783
1400	125	24.3	0.564	0.754	0.799
1400	125	25.3	0.562	0.756	0.802
1400	125	25.5	0.587	0.710	0.818
1400	125	25.8	0.567	0.752	0.796
1400	125	27.1	0.558	0.765	0.798
1400	125	28.6	0.551	0.769	0.808
1500	110	2.1	0.600	0.760	0.681
1500	110	2.7	0.598	0.772	0.662

TABLE D-12

Product Distribution for Isobutane Hydrogenolysis (125°C)

Temperature: 125°C

Total Pressure: 800 torr

Conversion of Isobutane (%)	Selectivity Propane	Ethane	Methane
4.2	0.627	0.352	1.415
7.3	0.623	0.332	1.466
9.2	0.653	0.311	1.420
11.7	0.634	0.361	1.374
11.7	0.676	0.292	1.387
16.6	0.498	0.501	1.505
17.1	0.545	0.499	1.466
17.2	0.529	0.468	1.476
17.8	0.554	0.441	1.455
18.7	0.539	0.460	1.462
18.8	0.498	0.488	1.530
19.1	0.467	0.515	1.568
19.6	0.516	0.477	1.500
20.5	0.494	0.481	1.554
21.3	0.577	0.411	1.446
24.5	0.495	0.484	1.547
26.6	0.483	0.501	1.548
27.1	0.456	0.512	1.608
28.4	0.500	0.486	1.530
31.4	0.463	0.514	1.583
31.8	0.510	0.484	1.505

TABLE D-12 (continued)

Conversion of Isobutane (%)	Selectivity Propane	Ethane	Methane
32.7	0.466	0.481	1.641
36.0	0.475	0.515	1.544
38.0	0.427	0.557	1.606
38.3	0.404	0.561	1.667
40.0	0.391	0.586	1.654
41.8	0.447	0.529	1.599
41.8	0.413	0.590	1.581
43.8	0.381	0.588	1.681
43.8	0.345	0.588	1.709
44.1	0.354	0.613	1.713
46.4	0.407	0.576	1.629
46.9	0.428	0.535	1.646
47.2	0.408	0.578	1.620
53.4	0.256	0.703	1.826
56.7	0.236	0.714	1.863
59.6	0.277	0.695	1.780
77.3	0.112	0.814	2.036

TABLE D-13

Product Distribution for Isobutane Hydrogenolysis at Other Temperatures

Total Pressure: 800 torr

Temperature (°C)	Conversion of Isobutane (%)	Selectivity Propane	Ethane	Methane
135	10.8	0.345	0.687	1.592
135	13.0	0.332	0.689	1.626
135	54.7	0.137	0.749	2.091
135	78.2	0.038	0.771	2.343
135	82.3	0.025	0.687	2.550
130	67.7	0.091	0.876	1.977
130	74.2	0.084	0.800	2.149
130	82.6	0.053	0.794	2.252
115	11.5	0.773	0.202	1.277
115	16.0	0.762	0.232	1.250
115	17.5	0.724	0.263	1.303
105	2.6	0.895	0.158	0.999
105	6.5	0.895	0.109	1.096
105	7.1	0.883	0.129	1.091

TABLE D-14

Product Distribution for Isopentane Hydrogenolysis (110°C)

Temperature: 110°C

Total Pressure: 800 torr

Conversion of Isopentane (%)	Selectivity				
	n-Butane	Isobutane	Propane	Ethane	Methane
7.7	0.080	0.815	0.117	0.069	0.943
8.6	0.080	0.821	0.111	0.078	0.909
10.3	0.069	0.801	0.103	0.091	0.947
16.1	0.067	0.819	0.104	0.108	0.926
23.8	0.055	0.835	0.081	0.109	0.977
24.6	0.049	0.859	0.077	0.104	0.928
24.6	0.049	0.805	0.113	0.130	0.986
26.1	0.053	0.835	0.081	0.109	0.977
26.1	0.052	0.816	0.095	0.127	0.987
27.0	0.060	0.833	0.078	0.114	0.967
28.7	0.053	0.830	0.086	0.106	1.000
28.7	0.044	0.797	0.117	0.147	0.989
31.2	0.052	0.843	0.078	0.094	1.000
31.7	0.036	0.861	0.075	0.105	0.979

TABLE D-14 (continued)

Conversion of Isopentane (%)	Selectivity				
	n-Butane	Isobutane	Propane	Ethane	Methane
32.7	0.071	0.804	0.092	0.122	0.981
34.5	0.055	0.750	0.147	0.185	0.968
35.4	0.057	0.783	0.114	0.144	1.010
36.4	0.051	0.824	0.089	0.118	0.995
36.4	0.061	0.799	0.101	0.145	0.966
36.6	0.060	0.775	0.119	0.173	0.956
37.7	0.032	0.843	0.080	0.144	0.971
39.3	0.067	0.742	0.135	0.177	1.008
40.7	0.058	0.812	0.093	0.121	0.999
41.2	0.058	0.771	0.126	0.149	1.008
45.7	0.059	0.802	0.105	0.124	0.994
47.2	0.054	0.775	0.123	0.152	1.012
47.9	0.039	0.818	0.101	0.131	1.005
71.9	0.029	0.778	0.136	0.160	1.067
72.8	0.024	0.788	0.111	0.188	1.045

TABLE D-15

Product Distribution for Isopentane at Other Temperatures

Temperature (°C)	Conversion of Isopentane (%)	Selectivity				
		n-Butane	Isobutane	Propane	Ethane	Methane
130	85.7	0.010	0.665	0.084	0.357	1.337
120	63.4	0.023	0.772	0.102	0.217	1.080
120	62.4	0.025	0.758	0.104	0.230	1.096
100	12.2	0.087	0.739	0.142	0.162	0.944
100	13.5	0.075	0.774	0.124	0.128	0.980
100	19.5	0.068	0.801	0.123	0.110	0.956
90	3.0	0.097	0.759	0.151	0.051	1.019

TABLE D-16

Product Distribution for Neopentane Hydrogenolysis (145°C)

Temperature: 145°C

Total Pressure: 800 torr

Conversion of Neopentane (%)	Selectivity			
	Isobutane	Propane	Ethane	Methane
4	0.11	0.05	0.48	3.45
7.1	0.096	0.043	0.512	3.464
7.5	0.085	0.049	0.519	3.474
10.7	0.075	0.033	0.536	3.528
13.6	0.037	0.017	0.589	3.622
14.9	0.041	0.021	0.595	3.584
20.5	0.038	0.018	0.545	3.706
24.6	0.026	0.016	0.530	3.787
40.2	0.015	0.005	0.380	4.167
41.3	0.022	0.012	0.404	4.067
41.7	0.019	0.008	0.376	4.147
42.4	0.013	0.005	0.352	4.231
43.7	0.017	0.005	0.374	4.168
46.6	0.012	0.004	0.461	4.020
48.8	0.011	0.004	0.243	4.461
49.5	0.012	0.005	0.302	4.332
52.7	0.010	0.004	0.330	4.290
52.9	0.010	0.004	0.288	4.374
54.2	0.008	0.005	0.322	4.309
55.4	0.009	0.003	0.345	4.266
56.0	0.008	0.004	0.321	4.313
57.7	0.008	0.004	0.331	4.296
58.6	0.008	0.003	0.299	4.361

TABLE D-16 (continued)

Conversion of Neopentane (%)	Selectivity			
	Isobutane	Propane	Ethane	Methane
60.5	0.006	0.003	0.185	4.596
61.4	0.006	0.003	0.284	4.397
64.2	0.006	0.002	0.259	4.452
68.9	0.004	0.001	0.233	4.516
91.8	0.000	0.000	0.017	4.965

TABLE D-17

Product Distribution for Neopentane Hydrogenolysis at Other Temperatures

Total Pressure: 800 torr

Temperature (°C)	Conversion of Neopentane (%)	Selectivity			
		Isobutane	Propane	Ethane	Methane
155	76.4	0.002	0.001	0.122	4.742
155	69.0	0.003	0.002	0.202	4.580
150	54.6	0.012	0.004	0.260	4.419
150	69.9	0.004	0.002	0.196	4.589
135	12.5	0.118	0.034	0.577	3.270
135	16.8	0.044	0.038	0.616	3.479
135	27.8	0.029	0.023	0.572	3.670
135	34.9	0.017	0.015	0.545	3.798
125	10.4	0.058	0.066	0.752	3.064
125	10.0	0.067	0.081	0.735	3.021
125	12.0	0.098	0.048	0.732	2.987

TABLE D-18

Mixing Test Number 1

Agitator Speed: 2000 r.p.m.

Nitrogen Pulse

Volumetric Flow: 7.19 ml./sec.

Dimensionless Time	Dimensionless Concentration
0.0	1.0
0.18	0.83
0.37	0.69
0.55	0.56
0.73	0.47
0.91	0.39
1.10	0.33
1.28	0.28
1.46	0.23
1.64	0.20
1.83	0.16
2.01	0.13

TABLE D-19

Mixing Test Number 2

Agitator Speed: 1500 r.p.m.
Butane Pulse
Volumetric Flow: 8.77 ml./sec.

Dimensionless Time	Dimensionless Concentration
0.0	1.0
0.23	0.80
0.45	0.64
0.68	0.50
0.91	0.40
1.14	0.32
1.36	0.25
1.59	0.20
1.82	0.16
2.04	0.13
2.27	0.10
2.50	0.09

TABLE D-20

Mixing Test Number 3

Agitator Speed: 1500 r.p.m.
Butane Pulse
Volumetric Flow: 5.10 ml./sec.

Dimensionless Time	Dimensionless Concentration
0.0	1.0
0.13	0.87
0.27	0.76
0.40	0.66
0.54	0.58
0.67	0.50
0.80	0.44
0.94	0.38
1.07	0.34
1.21	0.30
1.34	0.26
1.47	0.23
1.61	0.20
1.74	0.17
1.87	0.15
2.01	0.13
2.14	0.12
2.28	0.10
2.41	0.09

TABLE D-21

Mixing Test Number 4

Agitator Speed: 1500 r.p.m.
Butane Pulse
Volumetric Flow: 1.92 ml./sec.

Dimensionless Time	Dimensionless Concentration
0.0	1.0
0.09	0.91
0.18	0.83
0.27	0.75
0.36	0.68
0.45	0.62
0.54	0.56
0.63	0.51
0.73	0.46
0.82	0.42
0.91	0.38
1.00	0.35
1.09	0.32
1.18	0.29
1.27	0.26
1.36	0.24
1.45	0.22
1.54	0.20
1.63	0.18

TABLE D-22

Mixing Test Number 5

Agitator Speed: 1500 r.p.m.
Butane Pulse
Volumetric Flow: 0.679 ml./sec.

Dimensionless Time	Dimensionless Concentration
0.0	1.0
0.07	0.94
0.14	0.88
0.21	0.82
0.28	0.76
0.35	0.71
0.42	0.67
0.49	0.62
0.56	0.58
0.63	0.54
0.70	0.51
0.77	0.47
0.84	0.44
0.91	0.41
0.98	0.39
1.05	0.36
1.12	0.34
1.20	0.32
1.27	0.30
1.34	0.28
1.41	0.26